3D modeling of flow and sediment transport in tank with cavity

Yi Liu

UNIVERSITÉ DE STRASBOURG

ÉCOLE DOCTORALE MATHEMATIQUES SCIENCES DE L'INFORMATIQUE ET DE L'INGENIEUR

Laboratoire ICUBE - UMR 7357

THÈSE présentée par :

Yi LIU

soutenue le : **23 Juin 2017**

pour obtenir le grade de : **Docteur de l'université de Strasbourg**

Discipline/ Spécialité : Génie Civil

Modélisation 3D des écoulements et du transport solide dans un bassin à cavités

THÈSE dirigée par :

Abdellah GHENAIM	Professeur, INSA de Strasbourg

Co-directeur de thèse :

Abdelali TERFOUS	HDR, INSA de Strasbourg

RAPPORTEURS :

Denis DARTUS	Professeur,IMFT,INP-ENSEEIHT Toulouse
Abdellatif OUAHSINE	Professeur,UTCampiègne

AUTRES MEMBRES DU JURY :

Pierre-André GARAMBOIS	Maiître de conférences, INSA Strasbourg

Modélisation 3D des écoulements et du transport solide dans un bassin à cavités

Présentation des résultats majeurs de la thèse – Résumé étendu exigé pour une thèse rédigée en anglais

La gestion des eaux pluviales est un volet important en urbanisation. Le ruissellement des eaux pluviales véhicule en effet plusieurs types de polluants, y compris les nutriments, les matières solides, les métaux, le sel, les agents pathogènes, les pesticides, les hydrocarbures, etc. Les sédiments transportés ainsi transportés peuvent être évacués par les systèmes d'assainissement vers les milieux naturels. Selon un rapport du Département de la protection de l'environnement du Massachusetts (USA), les principaux facteurs contribuant à l'altération de la qualité de l'eau dans les cours d'eau, les rivières et les eaux marines sont les rejets des canalisations de drainage des eaux pluviales. En général, les problèmes causés par la dynamique des sédiments ne dépendent pas seulement du climat, de l'état des bassins versants et des réseaux de drainage, mais aussi de l'activité humaine. Avec le développement urbain progressif au cours des dernières décennies, les capacités des systèmes de drainage et des canalisations dans les bassins versants urbains et les voies navigables naturelles ont été largement dépassées et les problèmes de débordement relativement accentués. A l'heure où plus de 50% de la population vit dans les villes, les problèmes dus à la dynamique sédimentaire deviennent de plus en plus graves et demandent une solution rapide. Au cours des dernières décennies, il est apparu nécessaire de promouvoir une gestion des sédiments qui soit durable d'un point de vue environnemental, économique et social. L'étude des sédiments est un domaine relativement ancien et de nombreuses formules tentent de prédire la production, le mouvement et de dépôt des sédiments. En effet, elles permettent de dimensionner les réseaux d'assainissement pour les zones urbaines, dont l'optimisation est nécessaire pour la protection des biens et des personnes contre les inondations, pour prévenir la dispersion de sédiments contaminés dans le milieu naturel.

Une approche très utilisée pour la gestion des eaux pluviales est le système de décantation / rétention. Le dispositif principal est composé de bassins de retenue ou d'étangs. À l'origine, les bassins de décantation étaient conçus uniquement pour réguler les débits de crue maximaux mais ils peuvent également assurer une élimination satisfaisante des polluants selon les conditions. Les bassins de rétention

sont ainsi traditionnellement utilisés pour contrôler la dynamique du ruissellement et la qualité de l'eau.

Au cours des deux dernières décennies, l'amélioration de l'efficacité des bassins de rétention a été largement discutée dans la littérature scientifique. Habituellement, le fonctionnement des bassins de rétention est plus axé sur l'efficacité de dépôt des matières solides que des possibilités de leur élimination. En raison d'un manque de connaissances suffisant des mécanismes de transport de particules solides et des caractéristiques des écoulements, on considère le temps de séjour dans bassin comme le paramètre principal pour évaluer l'efficacité de l'élimination des matières solides.

Dans ce contexte, ce travail de thèse s'intéresse aux écoulements 3D et à la dynamique sédimentaire d'un bassin d'orage modélisé en laboratoire par un réservoir rectangulaire. Une nouvelle géométrie est ajoutée au fond du réservoir afin d'étudier l'effet de la présence d'une cavité sur l'écoulement et la sédimentation. Trois objectifs sont poursuivis :

- Améliorer la compréhension des écoulements 3D dans un bassin d'orage et identifier les paramètres influant sur la déposition de particules.
- Contribuer à la mise au point d'un outil pour modéliser l'efficacité de dépôt et la répartition spatiale des particules piégées dans un réservoir d'orage.
- Etudier l'effet de l'ajout d'une cavité au fond du réservoir rectangulaire sur les écoulements et le transport des sédiments.

Les études réalisées sont basées, à la fois, sur des expériences réalisées au laboratoire et sur des simulations numériques. Trois axes d'investigation principaux sont poursuivis :

- La simulation numérique de l'écoulement seul est réalisée pour trois géométries, y compris un réservoir court, un réservoir long et un réservoir long avec cavité.
- Le transport de sédiments dans le réservoir court et le réservoir long avec cavité est simulé par un couplage faible de la phase discrète et du calcul du fluide. Une condition de décantation basée sur le diagramme de Shields est implémentée.
- Des investigations expérimentales avec mesure des profils de vitesse découlement et du dépôt de sédiments sont menées dans un réservoir long avec cavité. le type de dépôt des sédiments est identifié pour deux niveaux d'eau dans le réservoir.

Les simulations numériques sont réalisées en utilisant 3 géométries différentes de réservoirs. Le réservoir court (ST ,Figure 1), le réservoir long (LT,Figure 2) et le réservoir long avec cavité (LTWC,Figure 3).

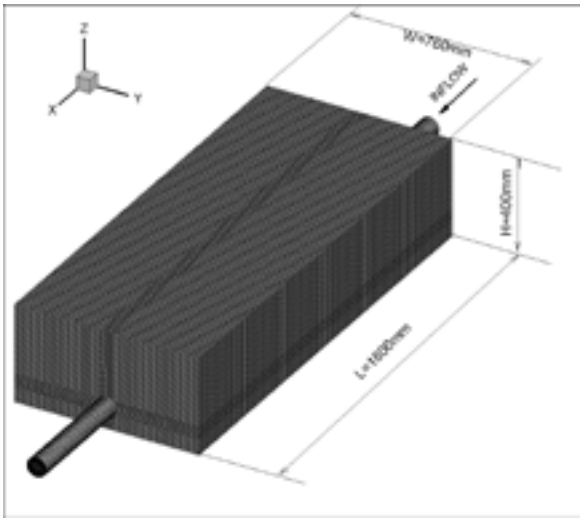

Figure 1 Géométrie détaillée et maillage du réservoir court (ST)

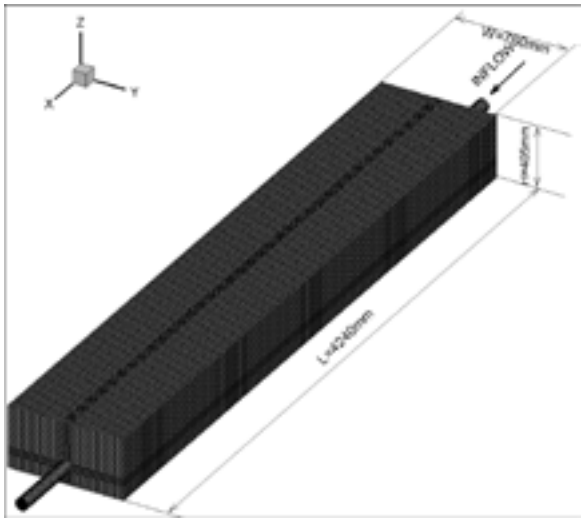

Figure 2 Géométrie détaillée et maillage de réservoir court (LT)

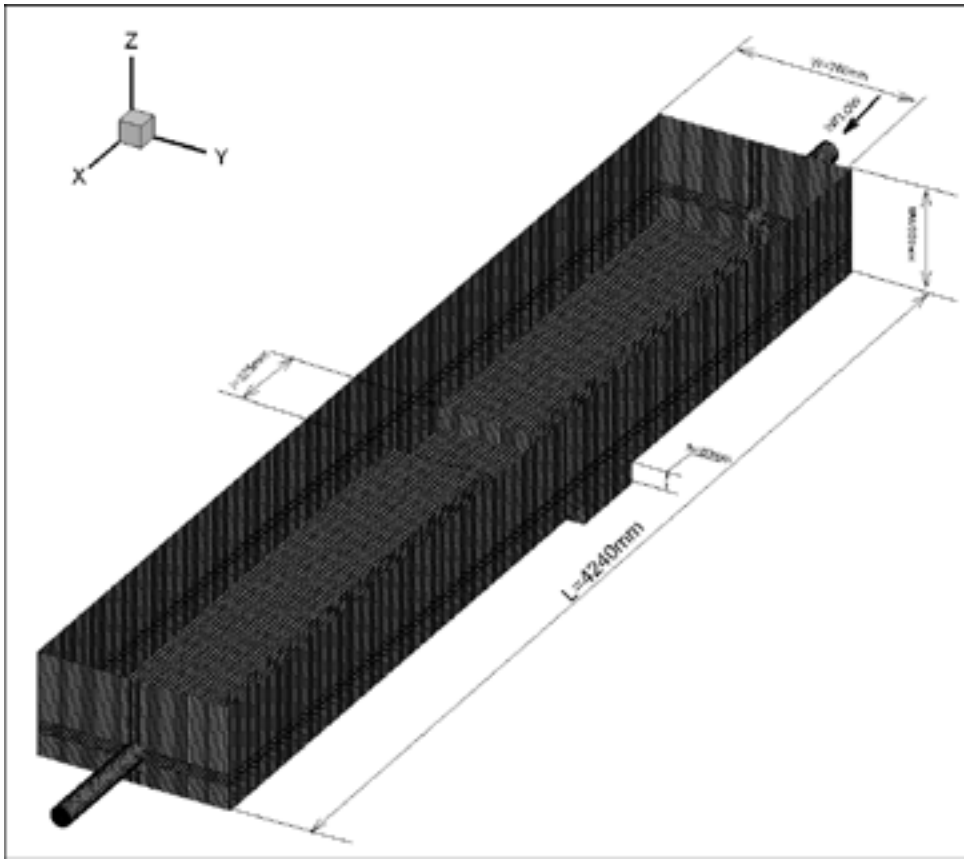

Figure 3 Géométrie détaillée et maillage du réservoir long avec cavité (LTWC)

Les équations de Navier Stokes en moyenne de Reynolds sont résolues avec un modèle de fermeture turbulente k-ε réalisable. À la suite du test de sensibilité au maillage, on choisit d'utiliser le même facteur de taille d'élément allant de 2.8 à 3.3 (défini par le ‘facteur de variable global’) pour discrétiser les différentes géométries. Cela suppose des caractéristiques d'écoulement similaires et des variabilités spatio-temporelles.

Simulation des écoulements

Les niveaux d'eau simulés varient de 11.5 cm à 30 cm pour des débits liquides entrants allant de 1 L/s à 5 L/s. Le niveau d'eau moyen est déterminé comme une moyenne spatiale des élévations d'interface, correspondant aux cellules où la fraction de volume d'eau est égale à 0.5 (Figure 4).

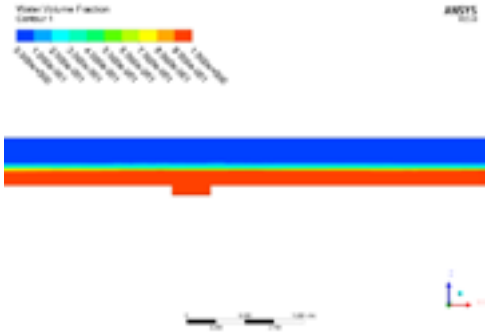

Figure 4 Fraction volumique de l'eau au débit volumique 1 L/s

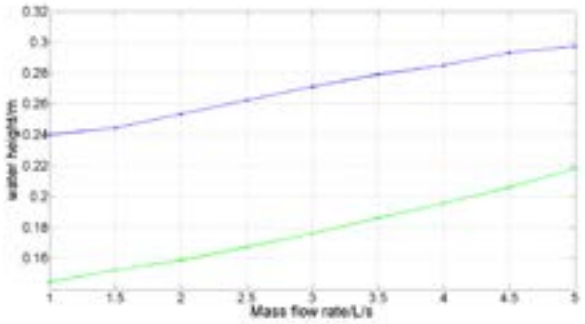

Figure 5 Niveau moyen de l'eau selon des débits d'entrée croissants

Des représentations 3D des lignes de courant et leur projection dans un plan horizontal moyen permettent d’investiguer l’aspect tridimensionnel et les symétries des écoulements pour les différentes géométries de réservoir et des conditions d’écoulement contrastées (figures 6 à 11).

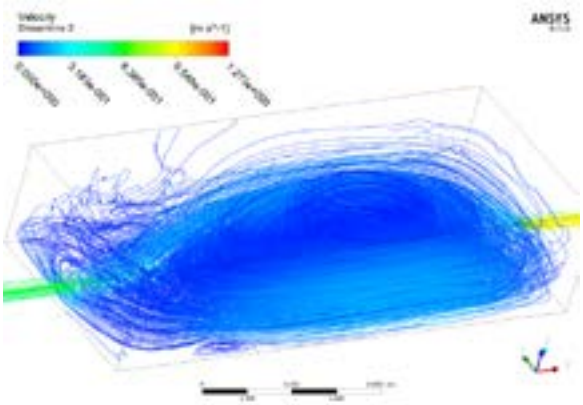

Figure 6 Streamlines 3D au débit volumétrique 3 L/s dans ST

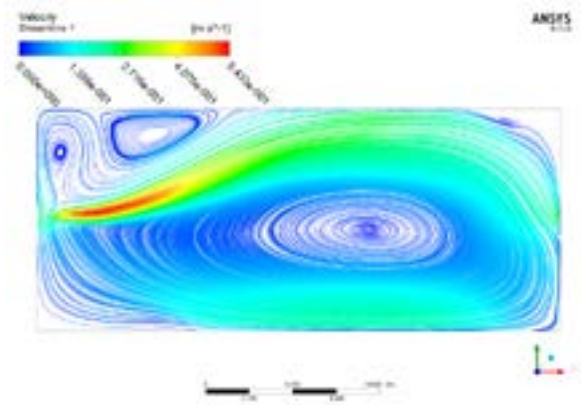

Figure 7 2D rationalise à Z = 0,04 m au débit volumique 3 L/s dans ST

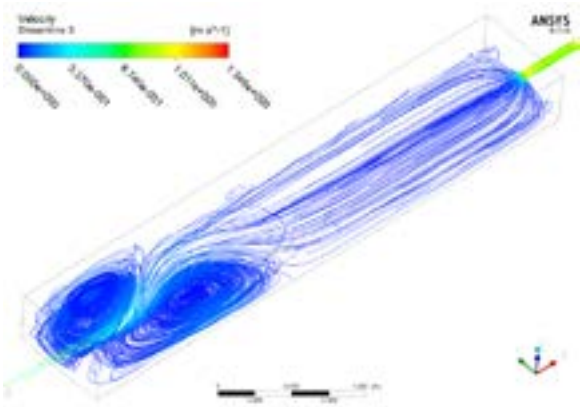

Figure 8 3D streamlines at volume flow rate 3 L/s dans LT

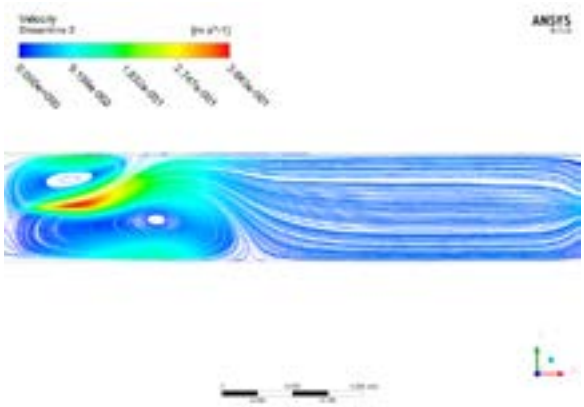

Figure 9 2D streamlines at Z = 0.04 m at volume flow rate 3 L/s dans LT

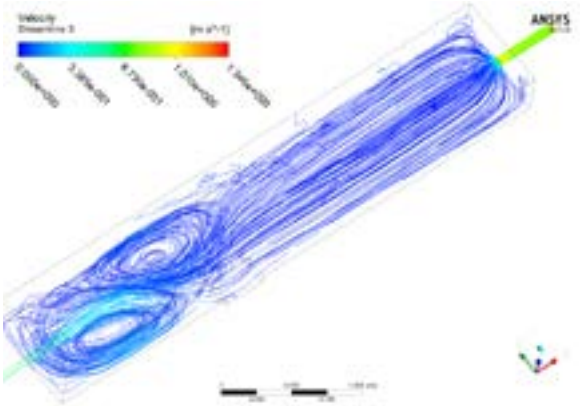

Figure 10 3D streamlines at volume flow rate 3 L/s dans LTWC

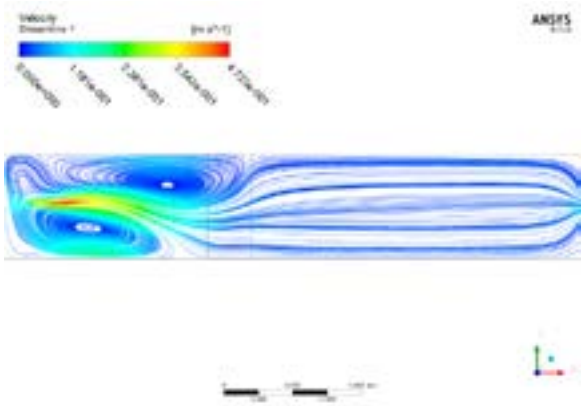

Figure 11 2D streamlines at Z = 0.04 m at volume flow rate 3 L/s dans LTWC

Dans le (ST), le motif d'écoulement est caractérisé par la taille et le centre des deux tourbillons. Pour un même débit d’entrée, le motif d'écoulement est influencé par les niveaux d’eau imposés par la condition limite aval. aval. aval.

Dans le cas des écoulements symétriques à faible débit, la taille des grands tourbillons est généralement plus grande pour les niveaux d'eau les plus grands. Dans le cas de motifs d'écoulements asymétriques, les deux tourbillons ont presque la même taille pour le niveau d'eau moyen, contrairement à la situation à faible niveau d'eau où un tourbillon est « repoussé » vers un coin du domaine coin.

Dans le réservoir long (LT), les structures d'écoulement sont principalement constituées de deux tourbillons à l'avant du réservoir et d'une partie d'écoulement assez uniforme à l'arrière du réservoir. Encore une fois, la taille et l'emplacement des tourbillons change avec l'augmentation des débits massiques et tend vers une dissymétrie du motif d'écoulement. À l'arrière du réservoir, l'écoulement est plus uniforme et la vitesse reste assez faible par rapport à la vitesse d'entrée. Les schémas d'écoulement symétriques n'existent pas lorsque le niveau de l'eau est faible, la raison en est que l'injection est proche de la surface libre, donc moins de pression d'eau agit sur le jet qui se développe avec moins de limites.

Les tourbillons dans le réservoir long n'existent que dans une région correspondant aux premiers 40% du réservoir le long de la direction d'écoulement, le reste du réservoir est rempli par un écoulement uniforme. Avec un niveau d'eau plus élevé dans le réservoir, le profil d'écoulement est plus susceptible d'être symétrique. Avec des débits d'entrée plus élevés, le motif d'écoulement à faible niveau d'eau est plus dissymétrique et tend à nouveau vers la symétrie avec des niveaux d'eau plus élevés.

Le champ d'écoulement dans LTWC est principalement dominé par deux tourbillons à l'avant et une partie d'écoulement uniforme à l'arrière, qui est similaire au champ d'écoulement dans le réservoir sans cavité. L'existence de la cavité ne peut pas changer le nombre de remous dans la partie avant, mais elle change leur distribution, emplacement et taille. La présence de la cavité peut même changer la symétrie du motif d'écoulement dans une certaine mesure et peut être influencée par le rapport longueur / largeur de la cavité.

Plusieurs caractéristiques générales d'écoulement ont été identifiées. Pour une géométrie donnée, le motif d'écoulement est sensible au débit massique d'entrée et à la profondeur de l'eau dans le réservoir. Avec un débit massique d'entrée croissant, le motif d'écoulement perd sa symétrie. Une augmentation de la profondeur de l'eau peut assurer un motif symétrique pour des débits d'entrée plus élevés dans une certaine mesure.

Pour une géométrie différente et la même plage de débit d'entrée que précédemment, les modes d'écoulement mettent en évidence une sensibilité au rapport de longueur /largeur. Pour le réservoir court avec un faible rapport de longueur/largeur, avec l'augmentation du débit massique d'entrée, le tourbillon remplira tout le réservoir. Mais pour un réservoir long (rapport élevé de longueur/largeur), le tourbillon occupe seulement les premiers 40% du réservoir, un écoulement uniforme se produisant ailleurs pour la plage de débits et le tirant d'eau.

L'existence de la cavité ne change pas radicalement le champ d'écoulement, la fonction de la cavité est de changer localement les paramètres d'écoulement et de créer une zone à faible valeur de contrainte de cisaillement et d'énergie cinétique turbulente pour favoriser le dépôt de sédiments. Dans le cas d'un faible débit, il n'y a qu'un seul tourbillon vertical dans la cavité. Dans le cas d'un débit élevé, deux tourbillons verticaux existent respectivement dans le coin avant et le coin arrière de la cavité.

Dans l'ensemble, le diagramme d'écoulement dans un réservoir rectangulaire est vraiment complexe et très sensible au débit massique d'entrée, au niveau de l'eau et à la géométrie du réservoir. Une petite variation de ces paramètres peut déclencher des varaitions significatives et non linéaires des motifs d'écoulement.

Simulation du transport de sédiments

Pour tous les cas avec un débit massique d'entrée différent et une profondeur d'eau variable dans le réservoir, la ligne de trajectoire des particules est également différente. La structure du flux est le facteur principal qui affectera la ligne de trajectoire de la particule. La figure 12 illustre l'évolution de l'advection de particules dans un cas donné.

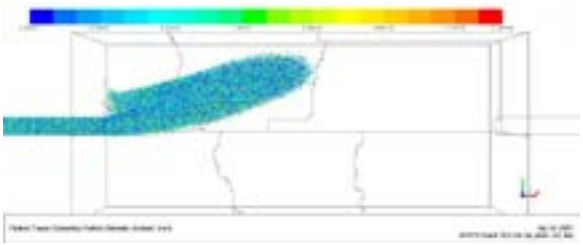

Trajectoire des particules à 3000 itérations

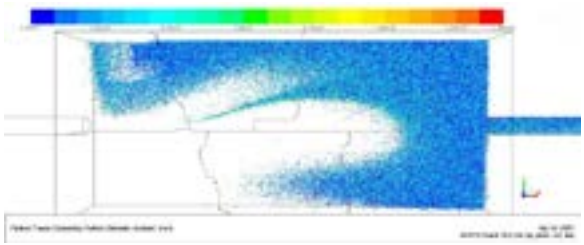

Trajectoire des particules à 15000 itérations

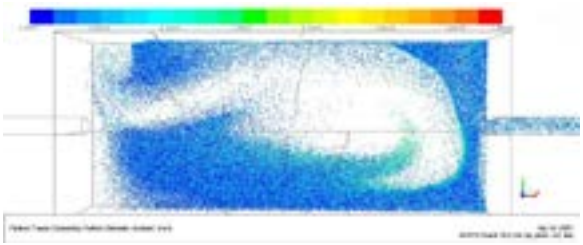

Trajectoire des particules à 25000 itérations

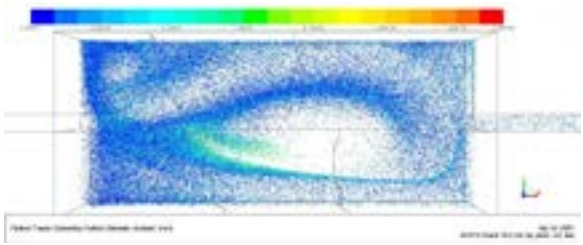

Trajectoire des particules à 35000 itérations

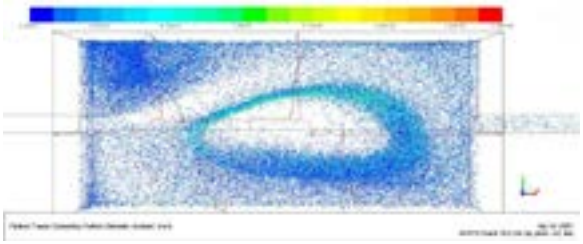

Trajectoire des particules à 45000 itérations

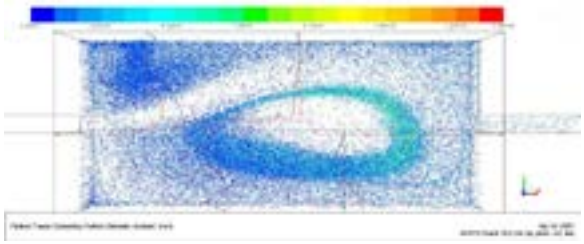

Trajectoire des particules à 50000 itérations

Figure 12 Trajectoire des particules à 3 L/s

Le tableau 1 montre la comparaison de l'efficacité du décantation entre la simulation et l'expérience, dans les cas où le débit massique d'entrée est faible, la prédiction de l'efficacité du décantation est proche des résultats de l'expérience, mais la différence augmente pour des débits massiques d'entrée croissants.

Tableau 1 Comparaison de l'efficacité du décantation entre la simulation et l'expérience

Décharges d'entrée (L/s)	Profondeur d'eau (cm)		Efficacité de décantation	
	Simulation	Expérience	Simulation	Expérience
1	11.48	8.3~8.6	77%	83%
1.5	11.98	12.0~12.2	74%	75%
2	12.37	13.2~13.4	70%	68%
2.5	13.35	14.5~14.9	72%	56%
3	14.49	14.7	64%	33%
3.5	15.91	14.9~15.2	53%	22%
4	17.39	15.8~16	56%	5%

La figure 13 montre la comparaison des zones de dépôt entre la simulation numérique et les résultats de l'expérience à 3 L/s.

Figure 13 La comparaison des zones de dépôt entre la simulation numérique et les résultats de l'expérience à 3 L/s

La figure 14 montre la comparaison de la distribution du dépôt de sédiments dans le réservoir long avec cavité et sans cavité. L'existence de la cavité crée une partie qui favorise le piégeage des sédiments. La comparaison du résultat de la simulation numérique en utilisant la condition de décantation mise en œuvre et l'expérience montrent un bon accord dans la prédiction de la zone de dépôt, l'efficacité totale de piégeage du dispositif est comparable à celle mesurée expérimentalement.

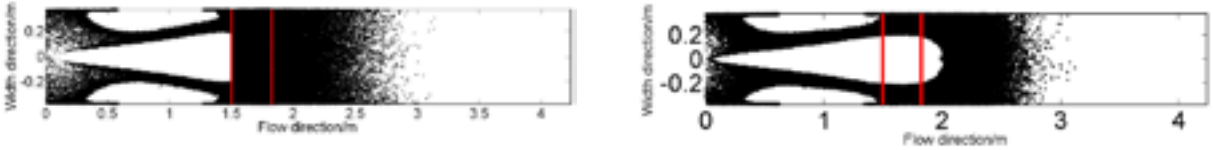

Figure 14 La comparaison de la distribution du dépôt de sédiments dans le réservoir long avec cavité et sans cavité à 3 L/s

La condition de «piège» dans les codes d'écoulment n'est qu'une description très simplifiée des processus physiques réels en jeu lors de la sédimentation. Elle conduit à une forte surestimation de l'efficacité du piège et une prévision inexacte des zones de dépôt. Afin d'améliorer la prédiction de la sédimentation des particules, une fonction définie par l'utilisateur basée sur la courbe de shields a été implémentée pour la condition limite au fond.

La condition de limite améliorée est plus précise dans les conditions avec un débit liquide d'entrée faible que pour des débits élevés. La raison en est que le mouvement des particules devient plus compliqué en raison de l'augmentation du débit liquide d'entrée conduisant à un écoulement plus turbulent. Des phénomènes de resuspension, non pris en compte, peuvent également avoir lieu.

La simulation du transport des sédiments la bassin court ST montre que le centre de la zone de dépôt est retrusif et l'incertitude mesurée le long de l'axe des X est beaucoup plus élevée que celle mesurée selon Y. Et la distribution du diamètre des particules déposées est du même type, bien que le débit d'entrée change.

Le processus de transport des sédiments est un processus aléatoire. Théoriquement, le critère de dépôt et de début de mouvement n'est pas le seul paramètre qui déterminera l'état de la particule. L'introduction de la méthode stochastique au critère pourrait être une idée utile pour améliorer la prédiction de l'efficacité de dépôt et de la zone de dépôt des sédiments.

Les particules déposées forment la nouvelle limite, la différence entre le lit des particules et le lit du réservoir signifie le changement des conditions de décantation, ce qui pourrait conduire à une mauvaise prédiction dans la simulation numérique.

Travaux expérimentaux

Le dispositif expérimental, utilisé dans le cadre de cette thèse, est représenté par la Figure 15. Le dispositif de mesure (transducteur) est basé sur l'analyse d’un signal ultrason rétrodiffusé par un nuage de particules. Le transducteur de mesure est fixé dans un support mobile sur le réservoir expérimental. Il peut se déplacer dans le sens de la longueur et le sens de la largeur du réservoir. L’eau pompée d’un réservoir de stockage est déversée dans le bassin expérimental. Les particules injectées dans le bassin sont mélangées dans l’unité d'injection. L'eau chargée de particules est déversée dans le bassin collecteur. les particules déversées sont colléctées en utilisant un filtre disposé en sortie de bassin.. le niveau d'eau dans le bassin expérimental est contrôlé par une vanne de réglage située à l’aval du bassin.

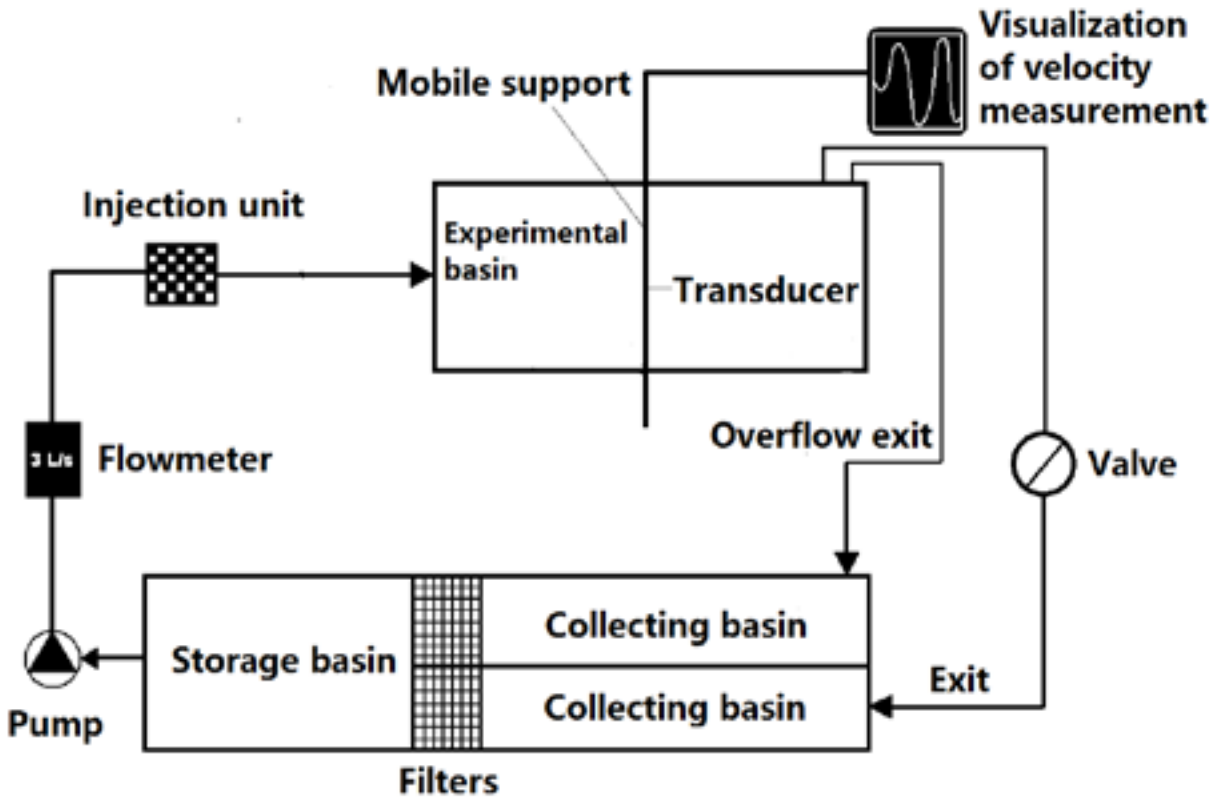

Figure 15 Schéma du dispositif expérimental

Pour chaque débit d'entrée, nous fixons 60 positions de mesure dans le réservoir, réparties sur toute la section du réservoir de telle sorte à construire des champs de vitesses représentatifs des écoulements crées.

Les expériences sont réalisées pour des niveaux d’eau faibles et des niveaux d’eau élevés. Il existe deux types de profil de vitesse verticale. Le premier est la répartition de la composante de la vitesse dans la direction X (sens de l'écoulement) dans le plan vertical, le plan est positionné à 0,3 m de l'entrée dans le sens de l'écoulement. Le second est la répartition de la composante de la vitesse dans la direction X selon la position Z des lignes verticales. Toutes les lignes sont positionnées à 0.3 m, 0.6 m, 0.9 m, 1.2 m, 1.5 m, 1.6 m, 1.7 m, 1.8 m, 2.1 m, 2.4 m, 2.7 m and 3 m de l'entrée du bassin.

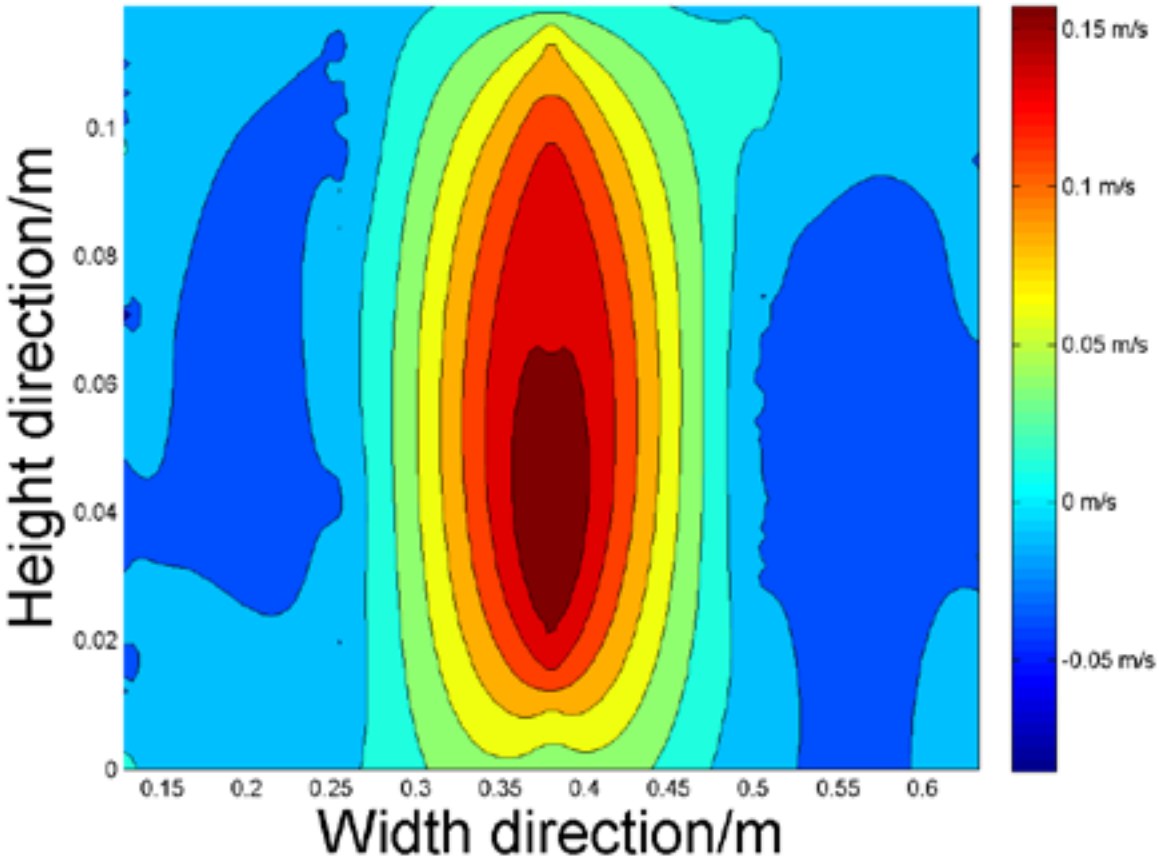

Figure 16 Profil vertical de la composante de la vitesse dans la direction de l'écoulement à X = 0,3 m pour un débit de 1 L/s à faible niveau d'eau

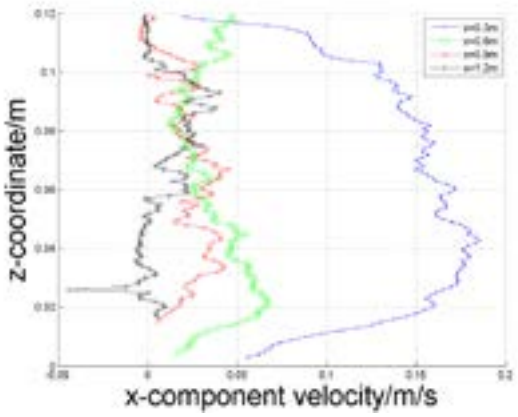

Figure 17 Distributions verticales de la vitesse (X= 0.3m-1.2m) pour un débit de 1 L/s

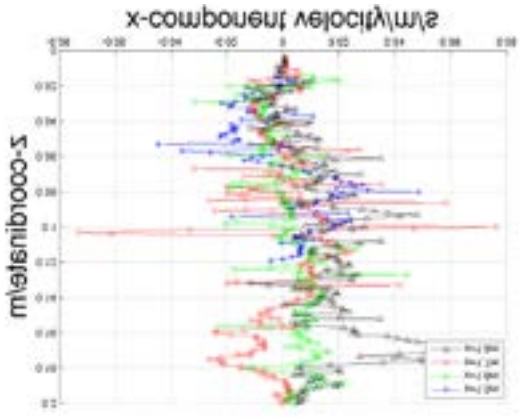

Figure 18 Distributions verticales de la vitesse (X = 1.5m-1.8m) pour un débit de 1 L/s

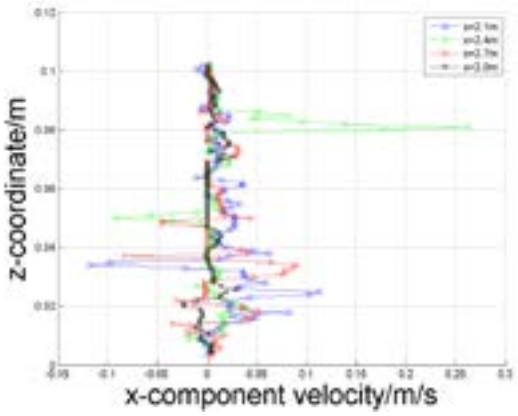

Figure 19 Distributions verticales de la vitesse (X = 2.1m-3m) pour un débit de 1 L/s

Le tableau 2 montre l'efficacité de dépôt dans différentes parties du réservoir, pour différentes conditions d'écoulement.

Tableau 2 Efficacités de sépôt dans différentes parties du réservoir.

Débits d'entrée (L/s)	Profondeur d'eau (cm)	Efficacités de dépôts			
		Avant	Cavité	Arrière	Total
1	11.8	60.16 %	30 %	9.85 %	100 %
1.5	12.5	25.84 %	44.1 %	29.56 %	99.5 %
2	12.5	16.97 %	38.48 %	42.22 %	97.67 %
2.5	12.5	8.58 %	17.58 %	56.14 %	82.3 %
3	12.5	2.63 %	11.48 %	41.92 %	56.03 %
3.5	12.6	7.91 %	2.76 %	31.78 %	42.45 %
4	13	1.75 %	1.06 %	18.83 %	21.64 %

4.5	13.5	1.2 %	0.3 %	0.5 %	1.8 %

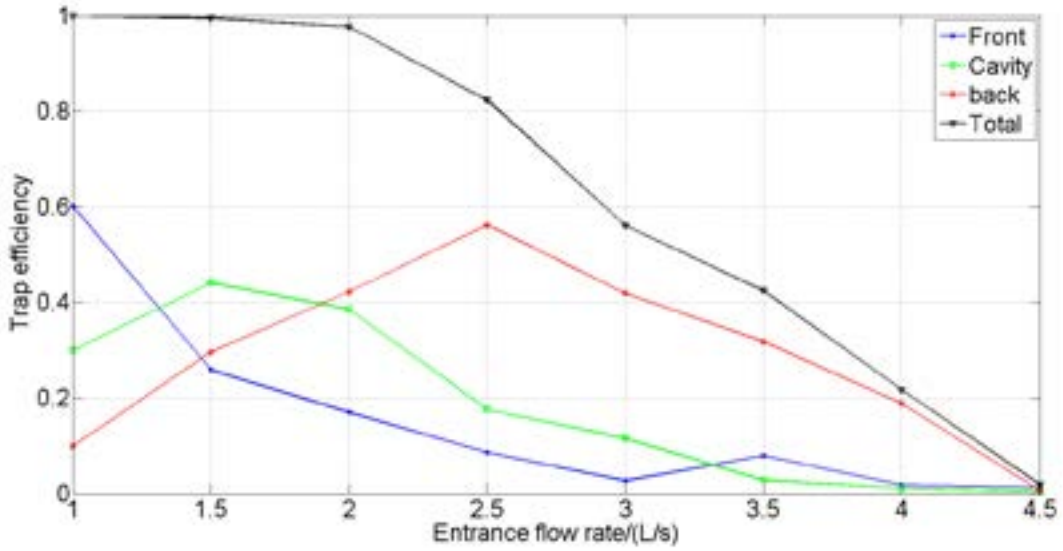

Figure 20 Efficacité de dépôt dans différentes parties du réservoir

L'efficacité totale de dépôt diminue quand le débit d'entrée augmente. Lorsque le débit est supérieur à 4.5 L/s, l'efficacité de dépôt est proche de 0. Une expérience démonstrative a montré que pour un débit de 5 L/s aucune particule injectée ne s'est déposée dans le réservoir. En général, l'efficacité de dépôt a tendance à diminuer avec l'augmentation du débit d'entrée dans les trois parties explorées du réservoir (avant, cavité et arrière).. Dans le cas où le débit est supérieur à 2 L/s, l'efficacité de dépôt dans la partie avant diminue de 10%. On observe une augmentation rapide de l'efficacité de dépôt dans la cavité lorsque le débit passe de 1 L/s à 1.5 L/s. Ensuite, l'efficacité de dépôt diminue en continu avec l'augmentation du débit,. L'efficacité du A l'arrière du réservoir, l'efficacité de dépôt augmente quand le débit varie de 1 L/s à 2.5 L/s puis diminue à partir de 2.5 L/s.

Par comparaison à la simulation numérique, l'expérience peut montrer beaucoup plus d'informations. La distribution de la vitesse verticale peut être divisée en deux types: la première est la zone proche du flux d'injection où la vitesse verticale augmente du fond vers le centre d'injection jusqu'à un pic puis diminue de l'injection centrale à la surface libre. La seconde est la zone éloignée de l'injection de flux, la vitesse verticale est plus uniforme. La structure de l'écoulement dans le cas où la profondeur de l'eau est inférieure à 13 cm est principalement dominée par deux tourbillons, où un

tourbillon est dans le coin près de l'entrée et l'autre est grand et étalé vers l'aval, le débit d'entrée peut modifier l'écart de L'injection du flux. La structure de l'écoulement dans le cas où la profondeur de l'eau est supérieure à 13 cm est également constituée par deux tourbillons, mais ces deux tourbillons sont principalement situés dans la partie amont de la cavité. A l'aval l'écoulement est uniforme.

La cavité présente de meilleures performances dans le piégeage des sédiments lorsque le débit d'entrée est inférieur à 3.0 L/s, avec un débit d'entrée plus élevé, l'efficacité de dépôt est assez faible. La profondeur de l'eau dans le réservoir rectangulaire est un facteur important pour l'efficacité de dépôt, en général, l'efficacité est beaucoup plus élevée avec une profondeur d'eau plus élevée dans le réservoir.

Mots clés: écoulements, transport de sédiments, simulation numérique, expérience, efficacité de dépôt, réservoir, cavité, système d'eaux pluviales.

Acknowledgements

Firstly, I want to express my sincere gratitude to my supervisors, Professor Abdallah Ghenaim and Associate Professor Abdelali Terfous for the attentive and diligent guide to my PhD investigation. In the past three and half years, Abdallah Ghenaim gave his support on the subject in the numerical simulation and especially the experimental measurements, Abdelali Terfous gave his guidance in the progress of this research, I'm really thankful to his advice and encouragement in the discussion.

I'm also grateful to Pierre-André Garambois , who put forward plenty of useful advices in my numerical simulation and his patience and conscientiousness in the modification of my manuscript.

I would like to thank Pierre François for his accompany and patient guidance in my experiment work, and also for his help on dealing with the raw experimental data.

I also want to thank all the members in the laboratory for their support during all my PhD career, and the help from the technician in INSA de Strasbourg and IMFS really means a lot in my experiment work.

I'm really grateful to China Scholarship Council for the financial supporting in the past three and half years, also I'd like to thank INSA de Strasbourg for providing me a wonderful research place.

At last not the least, I want to express my gratitude to my family, especially my father, my mother, my old sister and my brother in law, for their selfless support on my study career.

Table of contents

General introduction

Since the 4th century in Rome, the sediment problem becomes an issue that deserves to be attached importance to. As the sediment problem plays an important role in urban drainage system, which is in relation to the human daily life tightly, it will get more attention easily. Not only in the drainage system, sediment problem is also very common in the natural environment, rivers, seas or even in the air in the form of dust, smoke which leaves carbon spots on the wall or smog being a mixture of pollution and fog, as well as all chemical pollutants, all the process where the sediment problem is related prove the significance of the sediment problem without question. However, it is until the high development of urbanization that the sediment problem becomes more and more severe, which results in more and more attention being payed to by researchers and general public.

Stormwater management is one important part of the urbanization, in which the discharge runoff contains many kinds of pollutants, including nutrients, solids, metals, salt, pathogens, pesticides, hydrocarbon and so on. All the sediments discharged by stormwater runoff can be conveyed to all the near natural water area and sewer system. According to the report of Massachusetts Department of Environment Protection (MDEP, 1997), the largest contributors to water quality problems in the Commonwealth's stream, rivers and marine waters is the discharge from stormwater drain pipes and stormwater runoff. With progressive urban development in recent decades, the convey abilities of drain and pipe system in urbanized catchments and natural waterways has been increased significantly in quantities, water flow and rate, which leads to the urban flooding in the end. Research has shown that there has been a growing global trend of flood over last decades within the context of global climate change.

In general, the problem caused by sediment is not only variable and also is closely linked to the human being. With the continuously development of urbanization, the problem caused by sediment become more and more serious and demand prompt solution. In recent decades, growing public awareness of sediment problem has significantly emphasized the importance of environmental management of sediment problem. As mentioned above, the damage caused by sediment problems is

tremendous grievous not only in economy and also in common security. Many investigators and researchers devote to the investigation of sediment problem. For more than two centuries, workers in the sediment field attempted to formulate the conditions of incipient motion of sediment. In decades, the sediment transport in channels are processed in many research programs. Yalin (1963,1972), Yang (1972, 1973) and Vanoni (1984) find the extension. In this century, more than 50% of the population lives in the city, the portion will be even higher in the developed countries. A well operational urban water system will be significant to the daily life of the people living in the city. The sediment problem in urban water system will lead to city flood and contamination to the related aquatic habitats. In UK, a vegetated sustainable urban drainage system (SuDS) are constructed for flood risk management purposes. Up to 85% of the contaminants in the urban drainage system are conveyed to the stormwater system by absorption to fine sediment. The damage of the sediment in urban water system can be generally concluded as acceleration of maturing of the pipe, blocking the pipe path and so on.

Figure 1: Bedload sediment accumulation in sewerage and near inlet to pond (Snowmass, CO)

As a typical representative of sediment problem, stormwater management has its own difficulty and complexity. The purpose of stormwater management is to collect, treat and (re-)use runoff water, to restore the disturbed urban water cycle and to avoid contamination and destruction. The portion of impervious surfaces such as roofs in urbanized area and pavement has been increased due to the process of urbanization, which also leads to the increase of sediment entering the stormwater runoff, beacause those impervious surface prevent precipitation from soaking into the ground directly. The increasing load of stormwater runoff enters into drainage ditches, storm drains and sewer system rapidly, which cause problem as follow: stream bank erosion, Infrastructure damage, downstream flooding, contaminated streams, rivers and coastal water, combined sewer overflow.

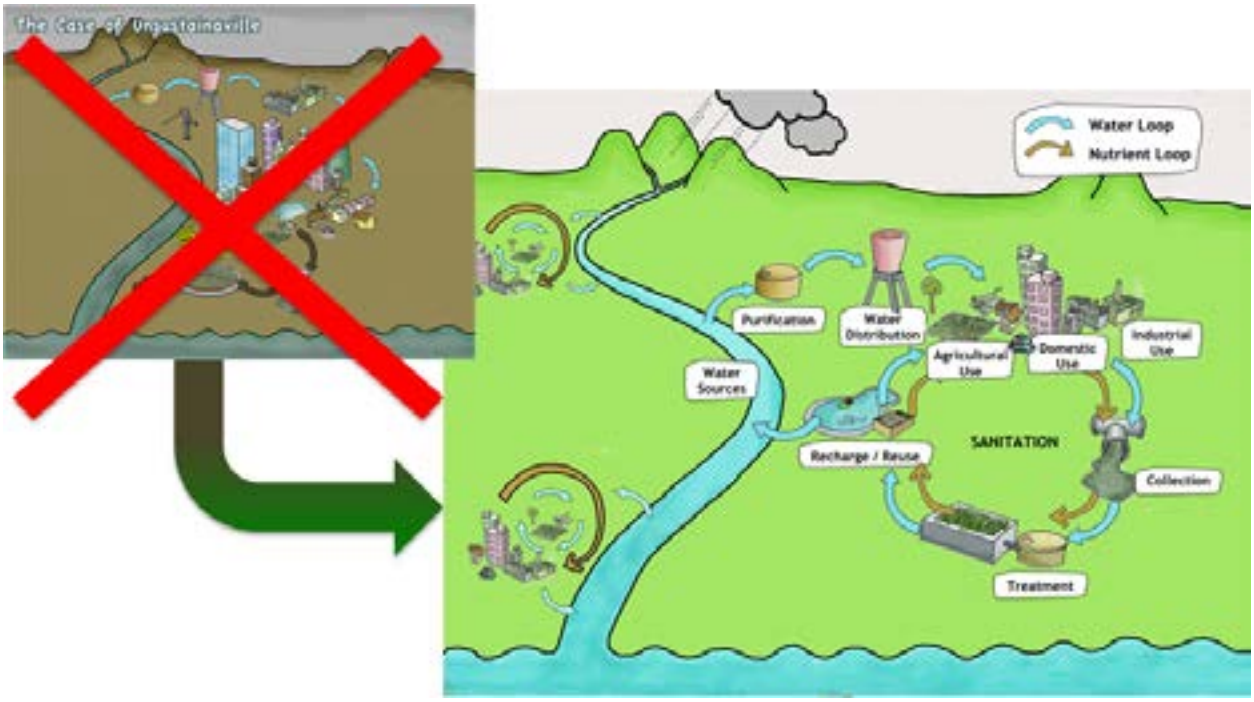

Figure 2: The purpose of stormwater management

Stormwater runoff can cause frequent flooding and contaminated natural water area by conveying the carrying contamination. The principle design for the stormwater management is identical, however the stormwater management varies depending on the local condition such as climate, topology and resources. Meanwhile, the stromwater management should vary depending on the age. Traditional stormwater management aims at collecting stormwater in pipe networks and transporting it off site safely, as for speed and economy, the method for stormwater management is to discharge the runoff to combined sewer systems flowing to a wastewater treatment

plant, or to rivers or streams, or to a large stormwater management infrastructure directly. However, the highly developing urbanization increases the quantities of stormwater runoff and alters the quality of the stormwater runoff, which is expected to convey to urban receiving waters. This variation makes traditional stormwater management hardly to fulfill the desire of general public to high quality of environment, which was designed to meet the community's need to minimize the threat of flood. So in the field of stormwater management, a need for not only greater information on managing the urban water cycle and additional design and assistance with implementation but also the quality of stormwater. Once the sediment enter the stormwater system, it will retain in the urban water system.

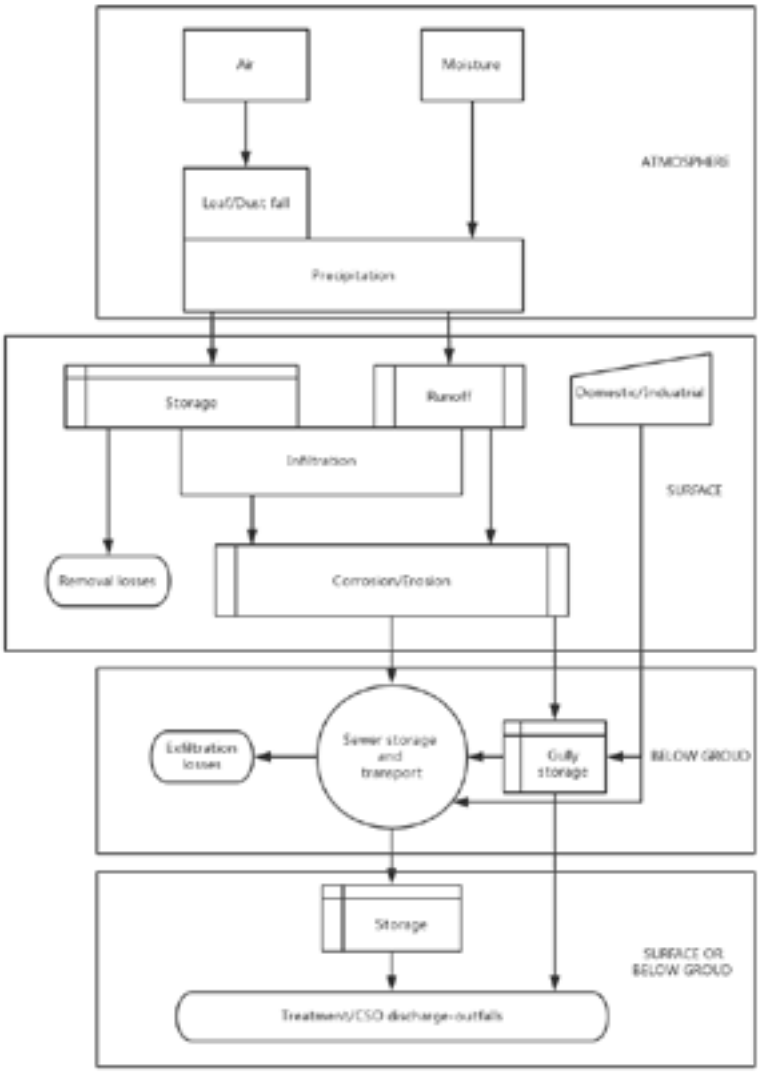

Figure 3: Pathways for sediment in urban water (Ashley, 2004)

The first approach used for stormwater management is detention/retention system, the main device is detention or retention basins or ponds. Originally, the detention basins were designed only for regulating the peak flow points. However, pollutant removal effect can be provided by the stormwater detention basins under the circumstance adequate settling time and sufficient size are available. Meanwhile, controlling discharge rate and reducing the flow velocity permit those facilities decrease the impact that urban development and impervious surface can have on water quality and aquatic habitats and reduce the possibilities of flood. Considering all those advantage the detention basins contain, more and more stormwater detention basins are used to control the quantity and quality of water. In 1970s, several researchers put forward an idea that using stormwater detention basins to fulfill dual purpose of mitigation of pollutant runoff load and flood control.

Though over past two decades the improvement in efficiencies of detention basins have been extensively discussed in the literature, both the basins designed for quantity and quality and the basins only for stormwater runoff peak discharge magnitude mitigation fail in perform the role to reduce stormwater runoff pollutant load. Usually the attention for detention basin is focused on increasing settling efficiency rather than limited possibilities in the removal of solid pollutant. Due to lack of enough acknowledge in pollutant particle transport and hydraulic characteristics of flow, the residence time of the detention basin is considered as the main way to evaluate the removal efficiency.

The dynamic nature of pollutant loads, the state of systems (temperature, water depth) and the entrance flow rate leads to the complexity of the stormwater detention system, however the detention basins are generally designed for the steady state. Nix et al (1985) stated that evaluating a stormwater detention system under steady state is inappropriate. Furthermore, it's hard to obtain the residence time of existing detention basins. Sediment characteristic and flow condition including residence time are main factor that can play influence on particle removal efficiency. Many experiment works and numerical simulations have been carried out on small scale model. Adamsson et al (2003) used a fixed bed shear stress boundary condition to model the sedimentation process. Dufresne carried out plenty of experiment to investigate the sediment transport. The experiment device used in the work of Dufresne was a simple rectangular tank, the dimension of which is $\mathbf{1800}\,\boldsymbol{mm} \times \mathbf{760}\,\boldsymbol{mm} \times \mathbf{400}\,\boldsymbol{mm}$, one cylinder pipe entrance and one cylinder pipe exit were included both with the diameter 80mm. Yan (2013) processed experimental work in a *situ* tank and run simulation of sediment transport in a small scale basin under steady and unsteady state, though improved the prediction of trap efficiency of the numerical simulation, the prediction of trap efficiency by numerical ways is still not satisfactory.

In general, there still exists problem in the simulation of sediment transport, the high prediction of trap efficiency and inaccurate prediction of spatial distribution of sedimentation zones. And the investigation on a simple rectangular tank can no longer fulfill the request of design of detention basin.

In this thesis, a new geometry is added to the bottom of a rectangular tank to investigate the effect of the new geometry on the flow and sedimentation. Also the research on how to use numerical simulation to model sediment transport is still necessary. Following works are finished:

- The numerical simulation of flow field is processed for three geometries, including short tank, long tank and long tank with cavity, where a volume of fluid model is applied to track the free-surface in the tank.
- The sediment transport in short tank and long tank with cavity is simulated by weak coupling of discrete phase and fluid calculation, a settling condition based on Shields diagram is implemented to the boundary condition.
- Velocity measurements of sediment transport in long tank with cavity are accomplished, the sediment deposition type in two water level is recorded.

There are three main objectives of this thesis. The first one is to understand the flow patterns in a storm tank in the 3D dimension, and to figure out the flow patterns is sensitive to which parameter. The second is to provide an effective ways for modeling the trap efficiency and spatial distribution of particles in a storm tank. The third is to investigate the effect of a cavity in a rectangular tank on the flow and sediment transport.

To realize these objectives, we organize our work in 4 chapters with a general introduction and a general conclusion.

The general introduction illustrates the importance and feasibility of the investigation, as well as the goal to achieve.

Chapter 1 presents a detailed literature review on numerical simulation and experiment works on flow and sediment transport in stormwater management field, and also gives an illustration on sediment investigation, including sediment source.

Chapter 2 presents the numerical simulation of flow patterns in rectangular tanks with different geometry, illustrates basic theory for the numerical method and the process of running a numerical simulation.

Chapter 3 processes the numerical simulation on the sediment transport, tests the default boundary condition in the Fluent codes and comes out a new boundary condition based on bed shear stress, and validates with experiment results.

Chapter 4 introduces the experiment works in the laboratory, the measurement mechanism is illustrated, the particle information is given, and the analysis of experiment results is shown.

The general conclusion presents all the results obtained in this thesis and point out the possibility for the future investigations.

1. Literature review

This chapter begins with a general description of sediment, the state of the sediment in the stormwater system and how to deal with the sediment problem in the sewer. Therefore, the theory for sediment transport process is been illustrated. In the end, numerical simulation and experiment works on sedimentation tanks by others researchers are presented.

1.1 Characteristic of sediment and stormwater system

1.1.1 General description of sediment

Essentially, sediments are solid fragments which originate from erosion of rocks by the physical and chemical disintegration. With the differences of origination, mineral composition, size and physical and chemical characteristics, the process of scour, transport and sedimentation of particles will be extraordinarily diverse. As the existence of sediment, the flow should be disposed as liquid-solid two phase flow, which means the sediment properties will be very critical to investigate the problem of sedimentation.

Particle size and density are the most important physical property of the sediment particle. It has a direct effect on the mobility of the particle and can range from great boulders, which are rolled only by mountain torrents, to fine clays, which once stirred uptake days to settle. Normally, the physical characteristic description of sediment can be classified as describing the size, shape and density.

According to the size of particles the sediment can be classified as many types, see the figure as follows: Figure 1.1 shows the relations in phi sizes, millimeter diameters, size classifications, ASTM and Tyler sieve sizes. The relations corresponding intermediate diameters, grains per milligram, settling velocity and threshold velocity for traction are described.

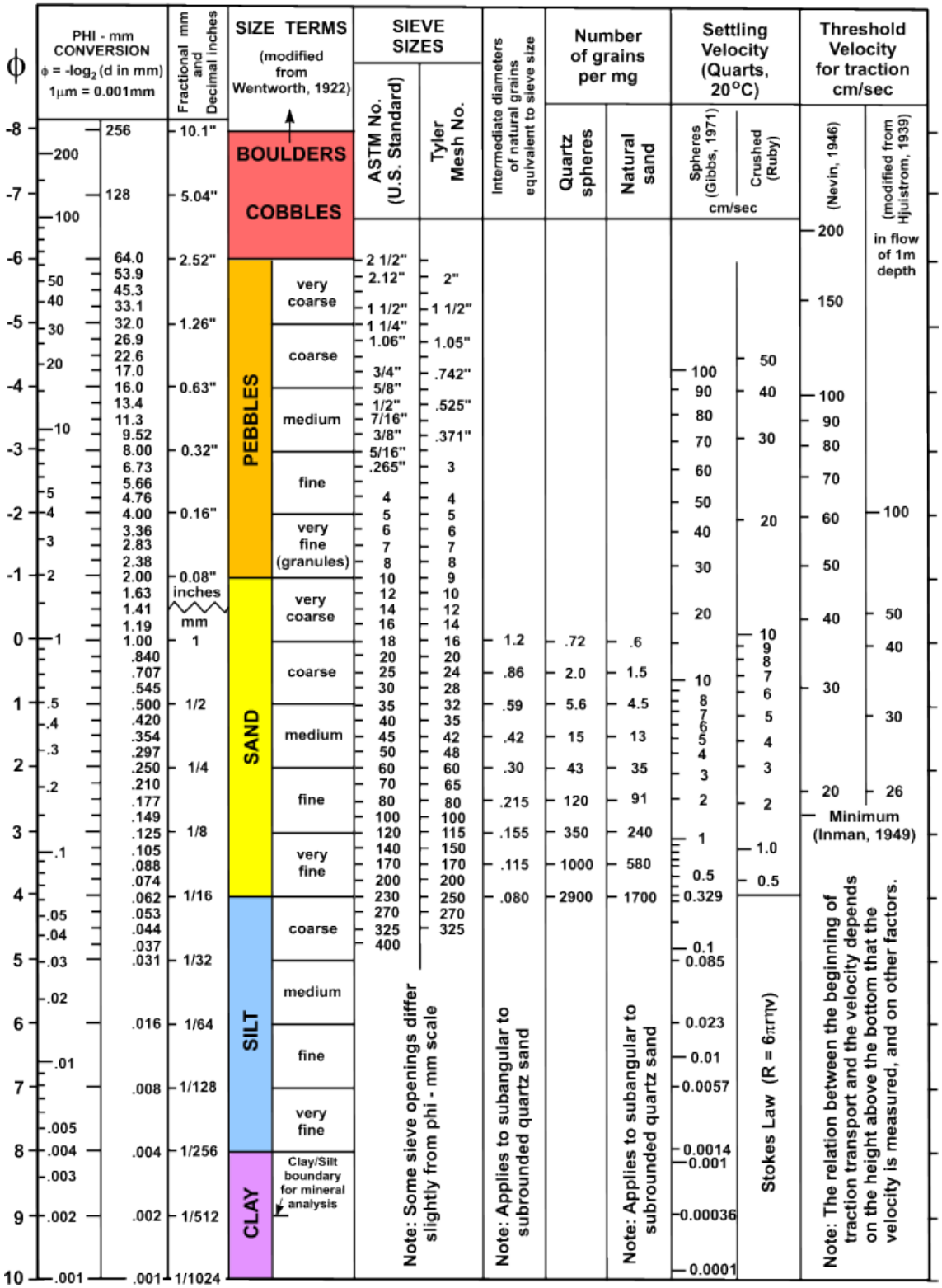

Figure 1.1 Size classifications of sediment particles (Widera,2011)

The size of sediment varies from micrometer up to centimeter when they are put under the spectrum, which make it challenge by classified the type by size due to so many variable value. However, there exist other methods to classify, for example classify by the shape or density. And there still exists a popular method for classification, which is based on the electrochemical interaction between sediment particles, where all the sediment is divided into two main groups, which are cohesive and non-cohesive sediment. The cohesive sediment always exists in the form of mixture with very fine sediment, such as organic material, clay and silt. Due to the existence of electrochemical processes, cohesive particles always attract each other to form into large object, which is so called “flocs”. In a flow field, the behavior of flocs and small particles are different, the flow pattern will be influenced by the flocs in a different way with small particles in a same volume. Due to the interaction between flocs and flow, flocs will break into smaller flocs. The flow properties and the material properties of small particles are the two main factors that determine the strength and size of flocs. The cohesive sediment transport is very complicated due to the breaking and complex patterns of floc creation, up till now the investigation only processed to a limited extent. The non-cohesive sediments are defined as particles where the electrochemical interaction can be neglected, and these particles will not form into flocs due to the material they are made of, their own mass and inertia. Due to the complexity of cohesive sediment transport, the particle mentioned in sediment transport is non-cohesive sediment.

The sediment particle ranges from great boulders to fine clays, due to which the size difference would be more than million times, and that’s why method of measurement is not unique. To substance like sediment particle without regular shape, it’s not sufficient to just obtain the size, used measure method and definition of the results should be detailed. The nominal diameter refers to the diameter of a sphere of same volume as the particle, usually measured by the displaced volume of a submerged particle. The sieve method is the most convenient way to determine the size of particles from boulder to fine sand. The sieve diameter is the minimum length of the square sieve opening through which a particle will fall. To the particle smaller than fine sand, the only method is the fall method. The fall diameter is the diameter of an equivalent sphere of specific gravity $\delta = 2.65$ having the same terminal settling velocity in water at 24°C.

Density is the most fundamental parameter and must be known. The particle density, ρ_s , is defined as its mass per unit volume when it’s inseparable. The particle specific weight, γ_s, corresponds to the solid weight per unit volume. Also the specific weight, γ_s , equals the product of the mass density of a solid particle, ρ_s , times the gravitational accelerating, thus:

$$\gamma_s = \rho_s \cdot g \tag{1.1}$$

Shape and roundness are other factors that do have an effect on sediment transport, though there is no direct quantitative way to measure shape, roundness and their effects. Generally, shape is the entire geometrical pattern of the particle and there are many modes to describe it. Wadell (1933) used sphericity to describe the shape, with the definition as follow:

$$\Lambda = A'/A \tag{1.2}$$

Where, Λ is the sphericity, A' is the superficial area of the sphere with the same volume of the particle, A is the superficial area of the particle. Current research has shown that the dynamic flow characteristic of two particles at the same sphericity would be identical practically.

Particle with different shape has different characteristics of transport and sedimentation. McNown (1951) suggested a shape factor $S.F. = c/\sqrt{ab}$, where c is the shortest of the three perpendicular axes (a,b,c) of the particle. The shape factor is always less than unity, and values of 0.7 are typical for naturally worn particles. Cailleux (1945) recommended a flatness elongation $F.E. = (a+b)/2c$.

Roundness is a parameter that represents the extent of blunt and tip of particle's edge. Wadell (1933) defined roundness as:

$$\Pi = \frac{(\sum_N r/R)}{N} \tag{1.3}$$

Where, R is the maximal radius of the inscribed circle on the maximal projective plane, r is the curvature radius of each edge on the same plane, N is the edge number of the particle.

In fact, it's very complex to measure the roundness of a particle. Krumbein (1938) calculated the roundness of some typical particles by the method of Wadell (1933) and made the results as figure, which could be treated as sample to decide the roundness of a specific particle. The actual application of this method had shown that it's approximately the same through comparison between a specific particle and the figure and calculation from the method of Wadell. And it should be known that with

the reduction of particle size and curvature radius, the measure accuracy would be abated significantly.

Settling velocity is another important parameter for the particles. For the solid portion, the settlement of particles is mainly resulted from the function of gravity. The particle will reach a constant velocity under the influence of the gravity, which is named terminal velocity. When the drag equals the terminal velocity, i.e. difference of the solid and fluid velocities, $v_s - v = w$, following equation is obtained:

$$w^2 = \frac{4}{3}\frac{1}{C_D} gd(\frac{\rho_s - \rho}{\rho}) \tag{1.4}$$

Where C_D is the drag coefficient, d is the particle diameter, ρ_s and ρ are the particle density and fluid density respectively and w is the settling velocity.

Thus, if the drag coefficient C_D is found, the problem of the particle in question is solved. For spherical particles of diameter d in a viscous fluid of dynamic viscosity , the drag coefficient can be defined. In laminar flow region, for $0.5 \leq \mathrm{Re} \leq 1.0$, where $Re = wd/v$, the Stokes' solution can be obtained:

$$F_D = 3\pi\mu dw \tag{1.5}$$

$$C_D = \frac{24}{Re} \tag{1.6}$$

Under two circumstances, the particle is very small or the viscosity of the fluid is very large, the Stokes' solution can be considered. The inertia terms is completely neglected in solving the general differential equation of Navier-Stokes in Stokes' solution. The first person who have successfully included the inertia terms, at least partly to the solution of the Navier-Stokes equation seems to by Oseen (1927), and the solution can be expressed as:

$$C_D = \frac{24}{Re}\left(1 + \frac{3}{16}Re\right) \tag{1.7}$$

A more complete solution for Oseen approximation provided by Goldstein (1929) can be formed as:

$$C_D = \frac{24}{Re}\left(1 + \frac{3}{16}Re - \frac{19}{1280}Re^2 + \frac{71}{20480}Re^3 + \cdots\right) \tag{1.8}$$

Where $Re \leq 0.2$

The level of the free stream turbulence rather than turbulence caused by the particle itself can strongly affect the value of drag coefficient. Also, whether or not the surface of the sphere is hydraulically smooth or rough can affect C_D .

When $Re \leq 800$, a formula suggested by Schiller and Naumann (1933) gives good results:

$$C_D = \frac{24}{Re}(1 + 0.150Re^{0.687}) \tag{1.9}$$

Combined with the equation of fall velocity, Schiller and Naumann also derived another formula:

$$C_D Re^2 = \frac{4}{3} g \frac{\rho_s - \rho}{\rho} \frac{d^3}{v^2} \tag{1.10}$$

For ≤ 100 , Olson (1961) put forward another equation where the drag coefficient can be well represented, the equation is in the form as follows:

$$C_D = \frac{24}{Re}(1 + 3/16\ Re)^{\frac{1}{2}} \tag{1.11}$$

1.1.2 Sediment in sewers

It seems that stormwater system and sewer system operate separately, however the stormwater will run into the sewer and cause problems. The integrity of the sewer system often gets intervention from illegal stormwater connections. During rainfall events, the stormwater will infiltration into the sewer, which makes the discharge peak

point occur and the overflow design of sewerage starts to operate. Both the stormwater system and sewer system have the necessary in using the detention basin for the treatment of peak discharge and sediment problems.

1.1.2.1 Sources of the sediment

The presence of solids in sewers can cause a variety of problems. Since the first sewer system was built in Rome in the 4th century BC, there existed the problems caused by solids consequently. It was because of the advent of industrial society and urbanization, the problems became acute. Solids entering sewer systems originate from a variety of sources. Five main sources are defined as:

- the atmosphere
- the surface of the catchment
- domestic sewage
- the environment and processes inside the drainage/sewer system
- industrial and commercial effluents and solids from construction sites.

The presence of solids may cause a variety of problems to the sewers. However, many reported problems do not have sufficient evidence so that they are regarded as anecdotal.

The composition and concentration of sediment in the sewage system will be different depending on the location. Though the concentration of sanitary solids in sewage is widely reported in the standard texts, the location or representiveness of the sample is not normally specified(e.g. source, in sewer or at the sewage treatment works). Similarity, these are assumed to be mean values, representative of the whole flow. Table 1.1 shows some typical international values. In this table SS represents suspended solids, BOD_5 is biochemical oxygen demand, COD means chemical oxygen demand.

Table 1.1 Averaged reported pollutant concentration in domestic (Ashley,2004)

Location	SS [h] (mg/l)	BOD_5 [i] (mg/l)	COD [j] (mg/l)	$NH_3 \cdot N$ [k] (mg/l)
Abu Dhabi [a]	198	228	600	35
Brussels(Blegium) [d]	290	325	670	35
Brazil(NE) [c]	392	240	570	38
Denmark [e]	120-450	150-350	214-740	12-50
France [f]	150-500	100-400	300-1000	20-80

Germany [g]		325	300-500	600	40-100(total)
Jordan [a]		900	770	1830	100
Kenya [a]		520	520	1120	33
USA [b]	weak	100	110	250	12
	medium	220	220	500	25
	strong	350	400	1000	50
UK [c]		80-195	143	40-517	20-90

[a] Horan (1990), [b] Metcalf and Eddy (1991), [c] Crabtree et al (1991), [d] Verbanck (1989), [e] Henze et al (1995), [f] Bertrand-Krajewski (1993), [g] averaged data from range of sources, [h]

1.1.2.2 Function of sedimentation tank

Sanitary system might be the closest way that contacts normal people to the sediment. With the development of urbanization both the quantity and quality of stormwater runoff delivered to urban water system have changed. In recent decades, people pay more and more attention to the pollutants, which is because of the importance of environment management of urban stormwater. As we all know, suspended solids and sediments are the main components of pollutants in sewer detention system, so the treatment of particles will become more and more important. Sedimentation is the last procedure before the effluent is discharged to the external, so it's crucial to make sedimentation tank to work effectively.

It's of great importance of sewage system in the process of urbanization, which also impels the treatment of sediment become more and more crucial. Sediments in the sewage system usually originates from five principal sources, which are atmosphere, the surface of the catchment, domestic sewage, the environment and processes inside the drainage/sewer system, industrial and commercial effluents and solids from construction sites. Without efficient management of those sediments unexpected result will happen, which may be very harmful to the environment and even to the human being.

Based on the purpose of collection, the sewer can be divided into combined, separate and above ground/underground sewer. Based on the purpose of transport, the sewer can be divided into gravity, pressure and vacuum sewer. In total, the type of the sewer system can be combined sewers, separate sewers, simplified sewers, solid free sewers, pressurised sewers, vacuum sewers and open channel drains. In those sewers, sedimentation tank can store water temporarily to regulate a flood.

The use of sediment tank is mainly for removing particles in the sanitary system. However the design of a sediment tank could not be obtained before it is constructed, which means the cost spent on constructing a tank will be wasted if the tank could not perform as it was supposed to be. With the development of computer science, it becomes possible to simulate flow in sediment tank with CFD codes, which is also called numerical computation.

There are two criterions for assessing the performance of sediment tank, one is the capacity of storage of water volume, the other is the maximum value of the pollution the tank can discharge. Flow condition in the sediment tank plays a very important role in the frame of mechanic fluid. As the fluid can not maintain a fix form independently, the flow conditions rely on not only the characteristics of the fluid and also the medium where the fluid move in.

Combined sewer overflow (CSO) control is recognized as a necessity (Ashley,2004). In France stormwater reservoirs serve many catchments, which is reported by Perez-Sauvagnat et al (1998) for the Seine st. Denis, by Faure et al (1998) for Nancy and by Charry and Lussagnet (1998) for Marseille. In Germany there are over 13,000 CSO control tanks working for the goal of capturing 80% of the settleable solids (Pitt, 2014). Detention-sedimentation basins are also widely used for water storage and improving the quality of the water. Table 1.2 shows the efficiency of detention basins and Table 1.3 shows the trap efficiency of detention basins in UK.

Table 1.2 Efficiency of detention basins (Nascimento, 1999)

	Ulis Sud [a] detention basin			Pollutant reduction after 2h of decantation(%)
	Yearly inflow load (kg/ha imp.)	Yearly outflow load (kg/ha imp.)	Yearly removal efficiency (kg/ha imp.)	
TSS	3902	387	90.1	88
BOD5	829	107	87.1	76
COD	2598	521	79.9	-
TKN	189	91	51.8	-
P total	44	22	50.6	-
Pb	0.893	0.054	94	65

Zn	5.12	0.66	87.1	77
Cd	0.031	0.0051	83.7	-
Cu	-	-	-	69
Hydrocarbons	65	4	94.2	-

Table 1.3 Trap efficiency of detention basins (Nascimento, 1999)

Pollutants	Imhoff settleability (24h)	Detention basin 2h removal (%)	Detention basin 6h removal (%)	Range
TSS	68	34	84	49-91
BOD5	32	13	48	14-53
Ptot	46	20	58	20-70
Pb	62	30	66	46-78
Oil/hydrocarbons	69	18	62	20-78
Total coliforms	71	60	72	47-73

1.2 Mechanism of sediment transport

The sediments problem involves with the mechanism of sediments eroding, transporting and depositing in the fluid, which happens in the nature world and human life frequently. Usually, the sediments problem could occur almost everywhere: in rivers, lakes, seas and hydraulic structures or even in the air. And sedimentation may always pertain to objects of various sizes, ranging from huge rocks to suspensions of fine particles. As indicated Yang et al (1996), there are many variables that affect the hydraulic of the flow and the nature of sediment transport in a natural stream. Unbelievable and extremely expensive example of sedimentation processes has happened in the whole world, which impels hydraulic researchers get knowledge about sediment transport. Sediment erosion, transport and deposition in fluvial system

are complex processes, however sediment and ancillary data are fundamental requirements for the proper management of river system, including the design of structures, the determination of aspects of stream behaviors, ascertaining the probable effect of removing an existing structure, estimation of bulk erosion, transport, and sediment delivery to the oceans, ascertaining the long-term usefulness of reservoirs and other public works, tracking movement of solid-phase contaminants, restoration of degraded or otherwise modified streams, and assistance in the calibration and validation of numerical models. Coarse material carried as bed load was focused on in the early study of sedimentation transport, other than suspended sediment. Bed load transport phase was better understood than the phase of suspension phase until 1925 when the problem of suspension was began to be dealt with. However, it's still not possible to predict the suspended-load discharge than bed load discharge with any greater certainty. For most engineering purposes, the study on sediment transport is to fulfill the certainty at a degree to predict the sediment discharge of an alluvial stream, which is still not possible though plenty volume of study was devoted to sedimentation mechanics.

In many situations sediment motion is of great importance. The estimated maximum flood level is a crucial factor to the cost of a flood control scheme, which in its turn may be seriously affected by the scour and subsequent downstream deposition of sediment, either temporarily during the course of a single flood, or as a part of a more permanent long-term process. The deposition of sediment may also reduce the storage capacity and therefore the value of reservoirs being used for some form of water supply. Similar deposition in harbors may require costly dredging or other measures for the continuous removal of banks and bars. Meanwhile, sediment also makes the environment contamination a critical social problem to the modern industrialization country. Pollutants discharged to the external environment from sewage system. According to Massachusettes Department of Environment Protection (MDEP,1997), stormwater runoff and the discharge from stormwater drain pipes were the largest contributors to water quality problems in the Common wealth’s rivers, streams, and marine waters.

Sediment transport with its attendant problems governs, therefore, a great many situations that are of major importance to civilized man. Indeed it is a major geological influence in the shaping of landforms, and the examples listed above are only short-term aspects of the long-term process. In dealing with these examples engineers are seeking to control this process(at least to a limited extent), and the task is formidable not only for its size but also for its complexity. In fact many features of sediment transport is still unkown, but progress continues to be made on the general problem by many investigator.

1.2.1 General

Usually referring to sediment transport, it means the motion of solid particles. The path of the sediment in the natural world can be concluded as erosion, transportation and sedimentation, which is presented in the Figure 3. In the natural world, this phenomenon is very common, and in the field of hydrology, water source engineering and hydraulic, it's a significant study object for the researchers. As mentioned in the general introduction, the problem caused by sediment transport can be severe and even expensive. Many experts start to investigate sediment transport since the awareness that sediment transport is in relation with a large variety of problems. A bed load equation with refinements and additions was developed by Yalin (1962, 1973), which is incorporating reasoning similar to Einstein (1942,1950).

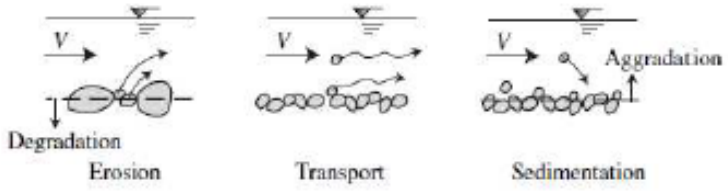

Figure 1.2 Process of erosion, transportation and sedimentation (Julien,2010)

Sediment transport is a very complicated process, normally it will be classified as two main types roughly:

- suspended load transport, the suspended particles are transported as suspended load transport. The fine silt brought into suspension from the catchment area rather than from bed material load in suspended load is called wash load.
- bed load transport, usually the transport where particles is in rolling, sliding and saltating motion is called bed load transport. When the value of bed-shear velocity just exceeds the critical value for initiation of motion, the bed material particles start rolling and/or sliding in continuous contact with the bed. Saltation happens when continuing increasing the bed shear velocity.

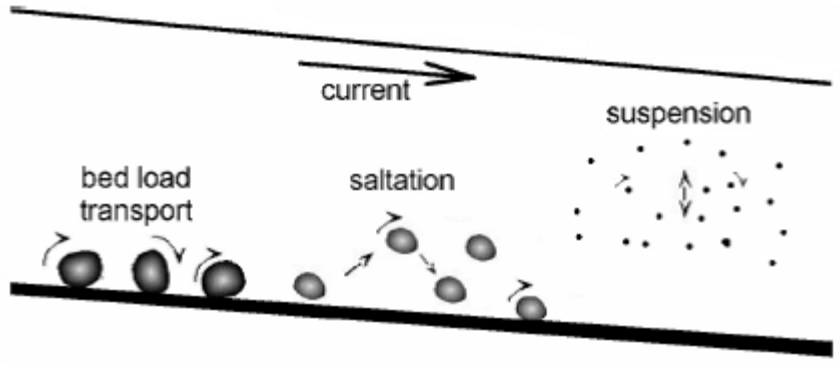

Figure 1.3 Pattern of particle motion

In this work, what should be focused on is the suspension and the settling condition for the particle, hence the bed load transport is not the emphasis.

1.2.2 Suspended load

The suspended load transport will be expressed as the concentration C in mass (kg/m^3) or in volume (m^3/m^3). A combination of convection, advection and turbulent diffusion can control the transport of suspended load. The advection-diffusion equation can be expressed as:

$$\frac{\partial C}{\partial t}+\frac{\partial uC}{\partial x}+\frac{\partial vC}{\partial y}+\frac{\partial wC}{\partial z} = D\left(\frac{\partial^2 C}{\partial x^2}+\frac{\partial^2 C}{\partial y^2}+\frac{\partial^2 C}{\partial z^2}\right)+\varepsilon_x\frac{\partial^2 C}{\partial x^2}+\varepsilon_y\frac{\partial^2 C}{\partial y^2}+\varepsilon_z\frac{\partial^2 C}{\partial z^2}+\dot{C} \quad (1.12)$$

Where D is the molecular diffusion coefficient and $\dot{C}$ is the term of phase change source.

The suspension of particles are the result of increasing the flow velocity, the particle is taken into eddies moving up and the velocity component in the upward is larger than the settling velocity of the particle, at the meantime the size of the eddy is much bigger than the particle. After long time impact on the particle by eddies, the particle will enter the main flow. As a word, the suspension of the particle is the result of large

scale turbulence. In contrary, the suspended particle will decrease the intensity of the turbulence.

1.2.3 Incipient motion of sediment

By increasing flow intensity gradually, the bed sediment will start move from static, which is called incipient motion of sediment, the relative critical flow condition in which the hydrodynamic acting on the sediment reached an exact value putting the sediment in motion is called as initial condition of sediment. The force resisting the incipient motion depends on the size and the type of particle, for coarse particles, the force resisting the incipient motion should be the gravity, as for finer sediment, cohesion should be the main factor of resisting incipient motion. However due to the complexity of cohesion, which depends on the composition of sediment and the environment the particle located, until now very few knowledge is obtained about cohesion, thus almost all the researchers choose non-cohesive particle as study object.

Determining critical condition for the sediment is of significant practice importance, an early work given by Lelliavsky (1955) reported a formula for critical velocity which was presented by Brahms (1753). Shear velocity and bed shear stress are two main parameter used popular for determine the critical condition.

1.2.3.1 Incipient drag force

In a uniform flow, the component in the flow direction of the drag force acted on the fluid per bed area can be expressed by:

$$\tau_0 = \gamma h J \tag{1.13}$$

Where γ is the specific weight of the fluid, h represents the water height and J is the descending slope. This expression can be also used in the non-uniform flow only if J is substituted by energy slope.

The dissipated energy by unit volume fluid per unit time can be formularized as:

$$w_s = \tau \frac{du}{dy} \tag{1.14}$$

If the water level is h , the total dissipated energy by the unit width fluid per unit time will be :

$$W_0 = \int_0^h \tau \frac{du}{dy} dy \tag{1.15}$$

The distribution of velocity along vertical direction can be expressed as:

$$u = Uf(y) \tag{1.16}$$

Where the mean vertical velocity $U = \frac{1}{h}\int_0^h Uf(y)dy$. Therefore, $\frac{1}{h}\int_0^h Uf(y)dy = 1$.

In a 2D flow, the vertical distribution of shear is :

$$\tau = \tau_0 \left(1 - {}^{y}/_{h}\right) \tag{1.17}$$

Thus the total energy will be :

$$W_0 = \int_0^h \tau_0(1 - y/h)U \frac{df(y)}{dy} dy = \tau_0 U \left[\int_0^h \frac{df(y)}{dy} dy - \frac{1}{h}\int_0^h \frac{df(y)}{dy} dy\right] \tag{1.18}$$
$$= \tau_0 U$$

In addition, the energy slop of the flow J_e physically equals to the dissipated energy of the fluid per unit weight in a distance per unit. Therefore, W_0 can also be expressed as:

$$W_0 = \gamma h U J_e \tag{1.19}$$

1.2.3.2 Shields's incipient curve

In 1936, Shields developed the incipient equation for uniform non-cohesive particles, based on the force balance exerted on the particle on the bed. The weight of a sphere particle is $W' = (\gamma_s - \gamma)\frac{\pi D^3}{6}$, the main force acting on the particle from the flow are drag force expressed as:

$$F_D = C_D a_1 d^2 \gamma \frac{u_0^2}{2g} \tag{1.20}$$

And lift force expressed as:

$$F_L = C_L a_2 d^2 \gamma \frac{u_0^2}{2g} \tag{1.21}$$

Where C_D and C_L are drag coefficient and uplift coefficient respectively, u_0 is the flow velocity acting on the particle.

When the bed is constituted by uniform particle, the vertical velocity distribution has the form as follows:

$$\frac{u}{U_*} = 5.75 \log 30.2 \frac{\chi y}{\alpha_1 d} \tag{1.22}$$

Where α_1 is approximately around 2 and χ is relevant to particle Reynolds number $\chi = f_1\left(\frac{U_* d}{\nu}\right)$.

The u_0 can be assigned as the velocity of $y = \alpha_2 d$, where α_2 is the coefficient near to 1.

Thus $u_0 = 5.75\, U_* \log 30.2 \frac{\alpha_2}{\alpha_1}\chi = U_* f_2\left(\frac{U_* d}{\nu}\right)$.

Then the critical condition of the particle starting slide is $F_D = f(W' - F_L)$, where f is the friction coefficient between the particles.

After the evolution,

$$\frac{\tau}{(\gamma_s-\gamma)d}=\frac{4}{3}\frac{f}{(C_D+fC_L)\left[f_2\left(\frac{U_*d}{\nu}\right)\right]^2} \tag{1.23}$$

The drag coefficient is relevant to the shape and Reynolds number, if the particle is close to sphere, the drag coefficient will be the function of Reynolds number:

$$C_D=f_3\left(\frac{u_0d}{\nu}\right)=f_1\left(\frac{U_*d}{\nu}\frac{u_0}{U_*}\right)=f_3\left[\frac{U_*d}{\nu}f_2\left(\frac{U_*d}{\nu}\right)\right]=f_4\left(\frac{U_*d}{\nu}\right) \tag{1.24}$$

To the uplift coefficient $\boldsymbol{C_L}$, a similar result will be obtained, at the end,

$$\frac{\tau}{(\gamma_s-\gamma)d}=f\left(\frac{U_*d}{\nu}\right) \tag{1.25}$$

And this is the so called Shields incipient drag force equation. The uplift force was not taken into account in the original derivation. In fact the basic form will not be changed neglecting the uplift force. The formula indicate the ratio of the flow drag force acting on the particle to the weight of particle should be the function of particle Reynolds number when the particle start to move.

The Shields curve was obtained by the experimental results from 4 kinds of particle with different specific weight. According to those point cloud and data from others research, a mean curve can be obtained.

The Shields curve provides the researchers a criterion to determine the incipient of particle motion. The Shields curve told us that the state when the particle Reynolds number equals to around 1.0, the value of $\frac{\tau}{(\gamma_s-\gamma)d}$ reach to the minimum and the thickness of the boundary layer is equal to the particle diameter, where the particle is most easily to start moving.

1.2.3.3 Initiation of suspension

The emphasis of suspension investigation is to determine the flow conditions when initiation of suspension will occur rather than the analysis of the main hydraulic parameters which influence the suspended load (Van Rjin, 1984). Bagnold (1966) pointed out that the condition for particle remaining in suspension is that the dominant vertical velocity components of the turbulent eddies exceeds the particle fall velocity (w_s). Assuming that the vertical velocity component (w') of the eddies are represented by the vertical turbulence intensity ($\overline{w}$), the critical value for initiation of suspension can be written as:

$$\overline{w} = \left[\overline{(w')^2}\right]^{0.5} > w_s \tag{1.26}$$

Suggested by the detailed studies on turbulence phenomena on boundary layer, the bed-shear velocity (u_*) and the maximum value of the vertical turbulence intensity ($\overline{w}$) share the same order. Therefore the critical bed-shear velocity ($u_{*,crs}$) for the initiation of suspension can be defined as:

$$\frac{u_{*,crs}}{w_s} = 1 \tag{1.27}$$

Which can be expressed as (see Figure1.4):

$$\theta_{crs} = \frac{u_{*,crs}^2}{(s-1)gd} = \frac{w_s^2}{(s-1)gd} \tag{1.28}$$

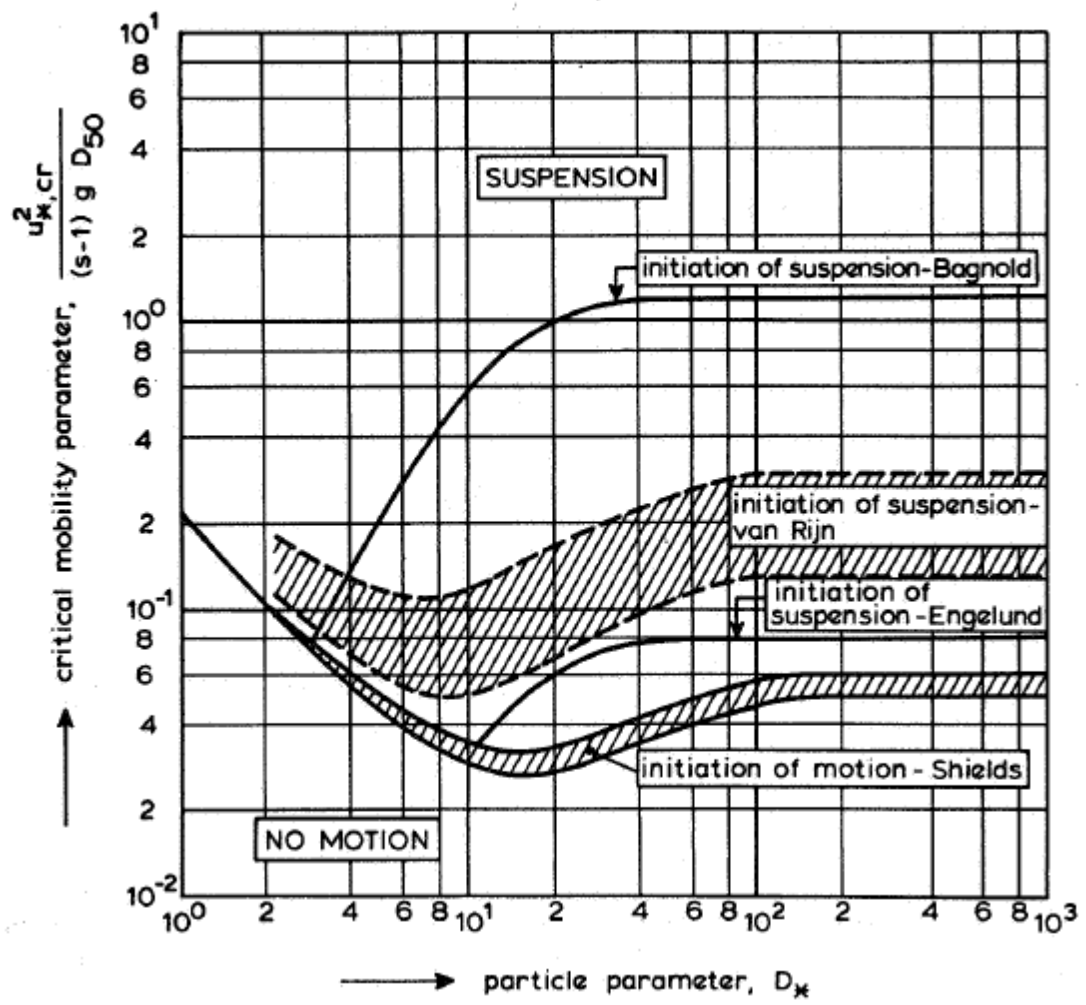

Figure 1.4 Initiation of motion and suspension(Van Rjin, 1984)

Based on a rather crude stability analysis, Engelund (1965) derived another criterion for initiation of suspension, which can be written as:

$$\frac{u_{*,crs}}{w_s} = 0.25 \tag{1.29}$$

At the end, the experimental results of Delft Hydraulics Laboratory are reviewed. Van Rjin (1984) determined the critical flow condition when instantaneous upward turbulent motions of the sediment particles (bursts) with jump lengths of the order of 100 particle diameters were observed (Delft hydraulics laboratory,1982). The experimental results can be represented by:

$$\frac{u_{*,crs}}{w_s} = \frac{4}{D_*}, for\ 1 < D_* \leq 10 \tag{1.30a}$$

$$\frac{u_{*,crs}}{w_s} = 0.4, for\ D_* > 10 \quad (1.30b)$$

Where $D_* = d\left[\frac{(s-1)g}{\nu^2}\right]^{\frac{1}{3}}$ is the particle parameter and $\boldsymbol{s}$ is the specific density.

Figure 1.4 shows the equations 1.28-1.30. To sum up, an upper limit is defined in the criterion of Bagnold when a concentration profile starts to develop, an intermediate stage is defined in the criterion of Van Rjin when locally turbulent bursts of sediment particles are lifted from the bed into suspension.

1.2.3.4 Incipient velocity

Also there are others criterion for the incipient of sediment motion, for example critical velocity and critical power. Table 1.4 shows some entrainment velocity equation of the investigation of the incipient of sediment motion by using the critical velocity.

Table 1.4 Formulas for entrainment velocity

Reference	Formulas	Remarks
Bogardi (1968)	$V_c = 0.000044u_* d^{\frac{1}{8}}\left(\frac{g}{\nu}\right)^{\frac{1}{12}}\left(\frac{h}{d}\right)^{\frac{1}{6}}$	d is the particle diameter in m
Novak and Nallun (1972)	$V_c = 0.20\sqrt{s-1}d^{0.38}$	d is the particle diameter in m and for open channel with loose boundary, $s = \rho_s/\rho$
Novak and Nallun (1975)	$V_c = 0.61\sqrt{g(s-1)d}\left(\frac{d}{R_h}\right)^{-0.38}$	R_h is the hydraulic radius of flow, d is the particle diameter in m
Novak and Nallun (1984)	$V_c = 0.54\sqrt{g(s-1)d}\left(\frac{d}{R_b}\right)^{-0.38}$	R_b is the hydraulic radius of related bed according to Einstein procedure, d is the particle diameter in m

1.2.4 Deposition

Deposition is another important process of the sediment transport. In many case, the deposition distribution is the emphasis to investigate. Adamsson (2003) applied a new boundary condition based on bed shear stress rather than the boundary condition in Fluent codes to simulate the spatial distribution of the deposition. Dufresne (2008) tested a fixed critical bed shear stress in the numerical simulation of a simple rectangular tank, and he also introduced bed turbulent kinetic energy as an criterion for the deposition, though the numerical results didn't fit the experimental results completely, a new concept in investigating the deposition has been found.

By taking water velocity and sediment particle size into consideration, Hjulström (1935) became the first researchers to determine the deposition by using velocity. The figure 1.5 shows published Hjulström curve, which reveals the relationships between particle transport, deposition and erosion.

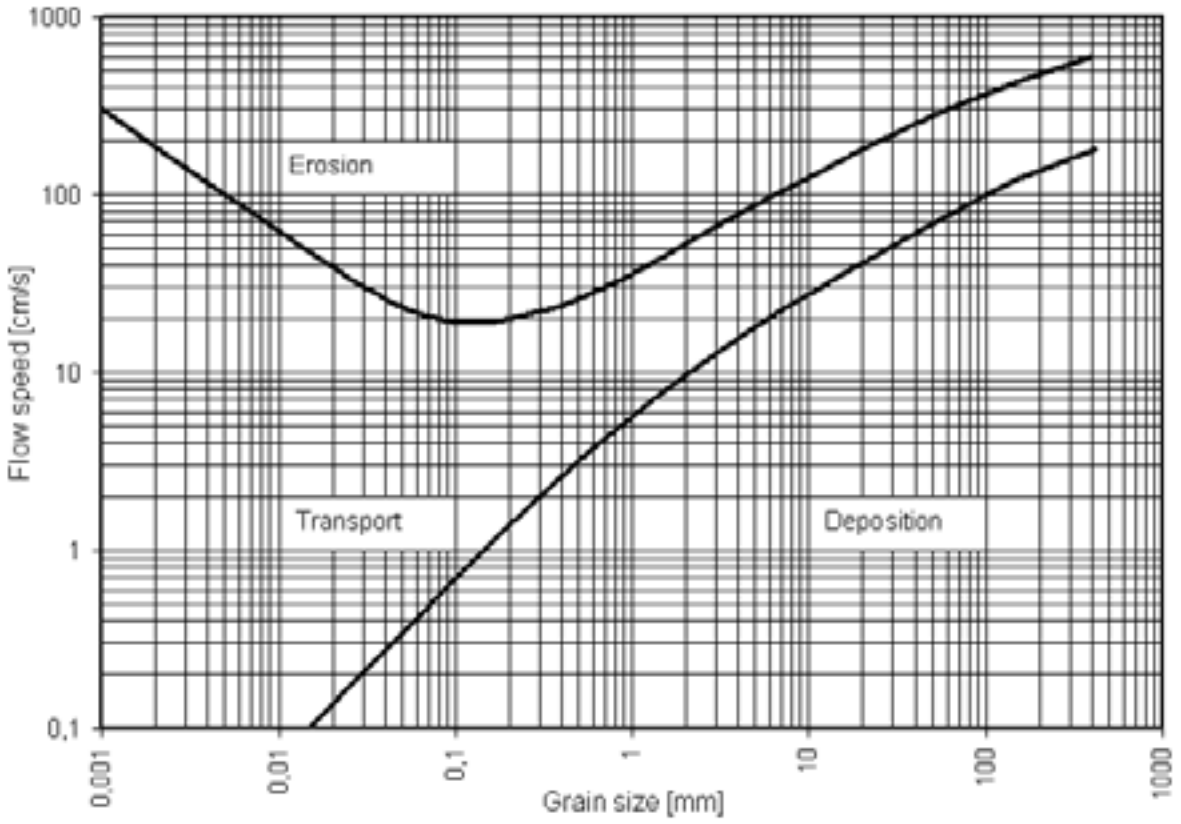

Figure 1.5 Hjulström curve (Hjulström, 1935)

1.3 Research works on flow and sediment transport in tank

1.3.1 A summary of sediment transport modeling

In the investigation of sediment transport, compared to the physical model, the computational modeling become more and more popular in solving sediment transport and fate problems. Technically speaking, the choice between computational models and physical models is dominated by several considerations, including the overall cost associated with the problem solution, the available resources and the nature of the problem that need to be solved. A better understanding of the processes under investigation can be obtained by a combination use of physical model and computational model (Vries DE, 1973).

The computational hydrodynamic/sediment transport model always involves the numerical solution of governing differential equation of continuity, momentum and energy of the fluid, sometimes the differential equation for sediment transport is also included. One advantage of computational model is that different physical domains can be modeled easier than in physical model, in which the site-specific condition is not able to represent. The physical models are subject to distortion effects when a solution can be obtained for the same flow condition (same length scale in three direction, identical Reynolds and Froude numbers), which is not a problem in computational models.

Over the past three decades, a large number of computational hydrodynamic/sediment transport models have been developed (Fan, 1988; Rodi, 2006). The currently representative models include one-dimensional model (1D model), two-dimensional model (2D model), three-dimensional model (3D model).

1D model have been successfully used in engineering practice and research since the early 1980s. The majority of the 1D model is formulated in a rectilinear coordinate system and solves the differential conservation of mass and momentum of the fluid along with the sediment mass continuity equation by using finite-difference scheme. Table 1.5 has demonstrated the most representative 1D model.

Table 1.5 Representative 1D model (Papanicolaou,2008)

Model and references	Last update	Flow	Bed sediment transport	Suspended sediment transport	Sediment mixtures	Cohesive sediment	Sediment exchange processes	Executable	Source code	Language
HEC-6: Hydraulic Engineering Center; Thomas and Prasham (1977)	V. 4.2 (2004)	Steady	Yes	Yes	Yes	No	Entrainment and deposition	PD	PD	F77
MOBED: MObile BED; Krishnappan (1981)	—	Unsteady	Yes	Yes	Yes	No	Entrainment and deposition	C	C	F90
IALLUVIAL: Iowa ALLUVIAL; Karim and Kennedy (1982)	—	Quasi-steady	Yes	Yes	Yes	No	Entrainment and deposition	C	C	FIV
FLUVIAL 11; Chang (1984)	—	Unsteady	Yes	Yes	Yes	No	Entrainment and deposition	C	P	FIV
GSTARS: Generalized sediment transport models for alluvial River simulation (Molinas and Yang, 1986)	V. 3 (2002)	Unsteady	Yes	Yes	Yes	No	Entrainment and deposition	PD	PD	F90/95
CHARIMA: Acronym of the word CHARiage which means bedload in French Holly et al. (1990)	—	Unsteady	Yes	Yes	Yes	Yes	Entrainment and deposition	C	C	F 77
SED8COUP: SEDiment COUPled; Holly and Rahuel (1990)	—	Unsteady	Yes	Yes	Yes	No	Entrainment and deposition	C	C	F77
OTIS: One-dimensional transport with inflow and storage; Runkel and Broshears (1991)	V. OTIS-P (1998)	Unsteady	No	Yes	No	No	Advection-diffusion	PD	PD	F 77
EFDC1D: Environmental fluid dynamics code; Hamrick (2001)	—	Unsteady	Yes	Yes	Yes	Yes	Entrainment and deposition	PD	PD	F77
3STD1, steep stream sediment Transport 1D model; Papanicolaou et al. (2004)	—	Unsteady	[a]Yes	[a]Yes	Yes	No	Entrainmentand deposition	C	P	F90

Note: V=Version; C=Copyrighted; LD=Limited distribution; P=Proprietary; PD=Public domain; F=Fortran;

[a] Treated as a total load without separation.

The computational research shifted to 2D models since the early 1990s. The advantages of the 2D models are good visualization results and easy data input due to the interface-based software has been introduced. In those 2D models, spatially varied information about bed elevation, water depth, transverse velocity components and magnitude of depth-averaged streamwise can be provided. The methods of finite difference, finite element or finite volume are used in most 2D models to solve Navier-Stokes and the depth-averaged continuity equations along with the sediment mass balance equation. Table 1.6 demonstrates the detailed information about some representative 2D models.

Table 1.6 Representative 2D model (Papanicolaou,2008)

Model and references	Last update	Flow	Bed sediment transport	Suspended sediment transport	Sediment mixtures	Cohesive sediment	Sediment exchange processes	Executable	Source code	Language
SERATRA: SEdiment and RAdionuclide TRAnsport; Onishi and Wise (1982)	—	Unsteady	[a]Yes	[a]Yes	No	Yes	Advection-diffusion	C	C/LD	F/V
SUTRENCH- 2D: SUspended sediment transport in TRENCHes; van Rijn and Tan (1985)	—	Quasi steady	[a]Yes	[a]Yes	No	No	Advection-diffusion	C	LD	F90
TABS-2; Thomas and McAnally (1985)	—	Unsteady	[a]Yes	[a]Yes	No	Yes	Entrainment and deposition	C	C	F77
MORED2: MObile BED; Spasojevic and Holly (1990a)	—	Unsteady	Yes	Yes	Yes	No	Entrainment and deposition	C	C	F77
ADCIRC: ADvanced CIRCulation; Luettich et al. (1992)	—	Unsteady	[a]Yes	[a]Yes	No	Yes	Advection-diffusion	C/LD	C/LD	F90
MIKE 21: Danish acronym of the word microcomputer; Danish Hydraulic Institute (1993)	—	Unsteady	[a]Yes	[a]Yes	No	Yes	Entrainment and deposition	C	P	F90
UNIBEST- TC: UNIform BEach Sediment Transport—Transport Cross-shore; Bosboom et al. (1997)	—	Quasi-steady	[a]Yes	[a]Yes	No	No	Entrainment and advection	C	LD	F90
USTARS: Unsteady Sediment Transport models for Alluvial Rivers Simulations; Lee et al. (1997)	—	Unsteady	Yes	Yes	Yes	No	Entrainment and deposition	P	P	F90
FAST2D: Flow Analysis Simulation Tool; Minh Duc et al. (1998)	—	Unsteady	Yes	Yes	No	No	Entrainment and deposition	LD	P	F90
FLUVIAL 12; Chang (1998)	—	Unsteady	Yes	Yes	Yes	No	Entrainment and deposition	C	P	F77
Delft 2D; Waldtra et al. (1998)	—	Unsteady	Yes	Yes	No	Yes	Advection-diffusion	C	LD	F90
CCHE2D: The National Center for Computational Hydroscience and Engineering; Jia and Wang (1999)	V. 2.1 (2001)	Unsteady	Yes	Yes	Yes	No	Advection-diffusion	PD/C	LD	F77/F90

Note: V=Version; C=Copyrighted; LD=Limited distribution; P=Proprietary; PD=Public domain; F=Fortran;

[a] Treated as a total load without separation.

In many hydraulic engineering applications, certain hydrodynamic/sediment transport processes are not suitable described by using 2D model, which impel researchers to use 3D model. For example, flow in the vicinity of piers and near hydraulic structures where 3D flow structures are ubiquitous, where the 2D models are not capable of representing the real physics. 3D model becomes the most popular application due to the development in computing technology. Table 1.7 shows the detailed information of some representative 3D models.

Table 1.7 Representative 3D model (Papanicolaou,2008)

Model and references	Last update	Flow	Bed sediment transport	Suspended sediment transport	Sediment mixtures	Cohesive sediment	Sediment exchange processes	Executable	Source code	Language
ECOMSED: Estuarine, Coastal, and Ocean Model—SEDiment transport; Blumberg and Mellor (1987)	V. 1.3 (2002)	Unsteady	[a]Yes	[a]Yes	No	Yes	Entrainment and deposition	PD	PD	F77
RMA-10: Resource Management Associates; King (1988)	—	Unsteady	[a]Yes	[a]Yes	No	Yes	Entrainment and deposition	C	P	F77
GBTOXe: Green Bay TOXic enhancement; Bierman et al. (1992)	—	Unsteady	No	Yes	No	Yes	Entrainment and deposition	NA	NA	F77
EFDC3D: Environmental Fluid Dynamics code; Hamrick (1992)	—	Unsteady	Yes	Yes	Yes	Yes	Entrainment and deposition	PD	P	F77
ROMS: Regional Ocean Modeling System; Song and Haidvogel (1994)	V. 1.7.2 (2002)	Unsteady	Yes	Yes	Yes	No	Entrainment and deposition	LD	LD	F77
CH3D-SED: Computational Hydraulics 3D-SEDiment; Spasojevic and Holly (1994)	—	Unsteady	Yes	Yes	Yes	Yes	Entrainment and deposition	C	C	F90
SSIIM: Sediment Simulation In Intakes with Multiblock options; Olsen (1994)	V. 2.0 (2006)	Steady	Yes	Yes	Yes	No	Advection-diffusion	PD	P	C-Langua.
MIKE 3: Danish acronym of the word Microcomputer; Jacobsen and Rasmussen (1997)	—	Unsteady	[a]Yes	[a]Yes	No	Yes	Entrainment and deposition	C	P	F90
FAST3D: Flow Analysis Simulation Tool; Landsberg et al. (1998)	V. Beta-1.1 (1998)	Unsteady	Yes	Yes	No	No	Entrainment and deposition	LD	P	F90
Delft 3D; Delft Hydraulics (1999)	V. 3.25.00 (2005)	Unsteady	Yes	Yes	No	Yes	Entrainment and deposition	C	LD	F77
TELEMAC; Hervouet and Bates (2000)	—	Unsteady	[a]Yes	[a]Yes	No	Yes	Entrainment and deposition	C	P	F90
Zeng et al. (2005)	—	Unsteady	Yes	Yes	No	No	Entrainment and deposition	P	P	F90

Note: V=Version; C=Copyrighted; LD=Limited distribution; P=Proprietary; PD=Public domain; F=Fortran;

[a] Treated as a total load without separation.

In the modeling the particulate phase, there are two main frameworks, the Lagrangian approach and the Eulerian approach. The Lagrangian method treat particles as points, one equation will be solved for each particle at one time, in consequence, the computational quantity will be tremendous enormous in a dense phase flow. In computational fluid dynamic, a huge computational quantity signifies increased computational time and more CPU power. However, the Lagrangian method will be very useful in a dilute phase flow, for example the simulation of a spray drier, to be more precisely, the particle concentration should not exceed 12%.

In Eulerian method, particles are regarded as continuum phase, which are in the same way of fluid. In comparison with the Lagrangian method, the Eulerian method is

better in saving computational resources and reducing calculating time. And also the Eulerian method can be used in modeling of transport and dispersion of a second fluid, where it's not possible for the Lagrangian method. However, due to neglect the interaction of particle on the flow, the Eulerian method shows its defects in describing the boundary condition properly.

1.3.2 Experiment works on flow and sediment transport in tank

Experimental investigation is the most direct way and the best way to understand the real physical process of the flow and sediment transport in tank. Most of the empirical models were established because of the common rule of the experiment data.

Horn (1988) carried out continuous settling experiments in a bench-scale vertical tank with same four material systems. Both continuous settling and batch experiments are processed to investigate four different suspensions ($CaCO_3$ and kaolin in the water, glass spheres in glycerol-water mixtures, activated sludge) with respect to their settling behavior. By taking the displacement flow, floc destruction and the effect of the channeling into account, the settling characteristics of kaolin was determined by several batch tests. It turned out the settling characteristic could be described by different correlation functions which include all the information about the settling behavior of ideal suspensions.

Ahmed (1993) found out the position of the baffle with different contractions had a significant influence on the solid removal efficiency, the flow patterns and the suspended solids concentration. The best location for the baffle should be at a distance within 5% of the tank length from the injection, the contraction at 67% of the tank depth.

For the sufficiently large Reynolds numbers, Maurel et al (1996) have observed the flow in a rectangular cavity (see Figure 1.6). In this work, the Reynolds numbers and cavity length are varying, it turns out in a fixed geometry system with sufficiently large Reynolds number, a well-defined wavelength and frequency of the jet can exhibit characterized self-oscillations.

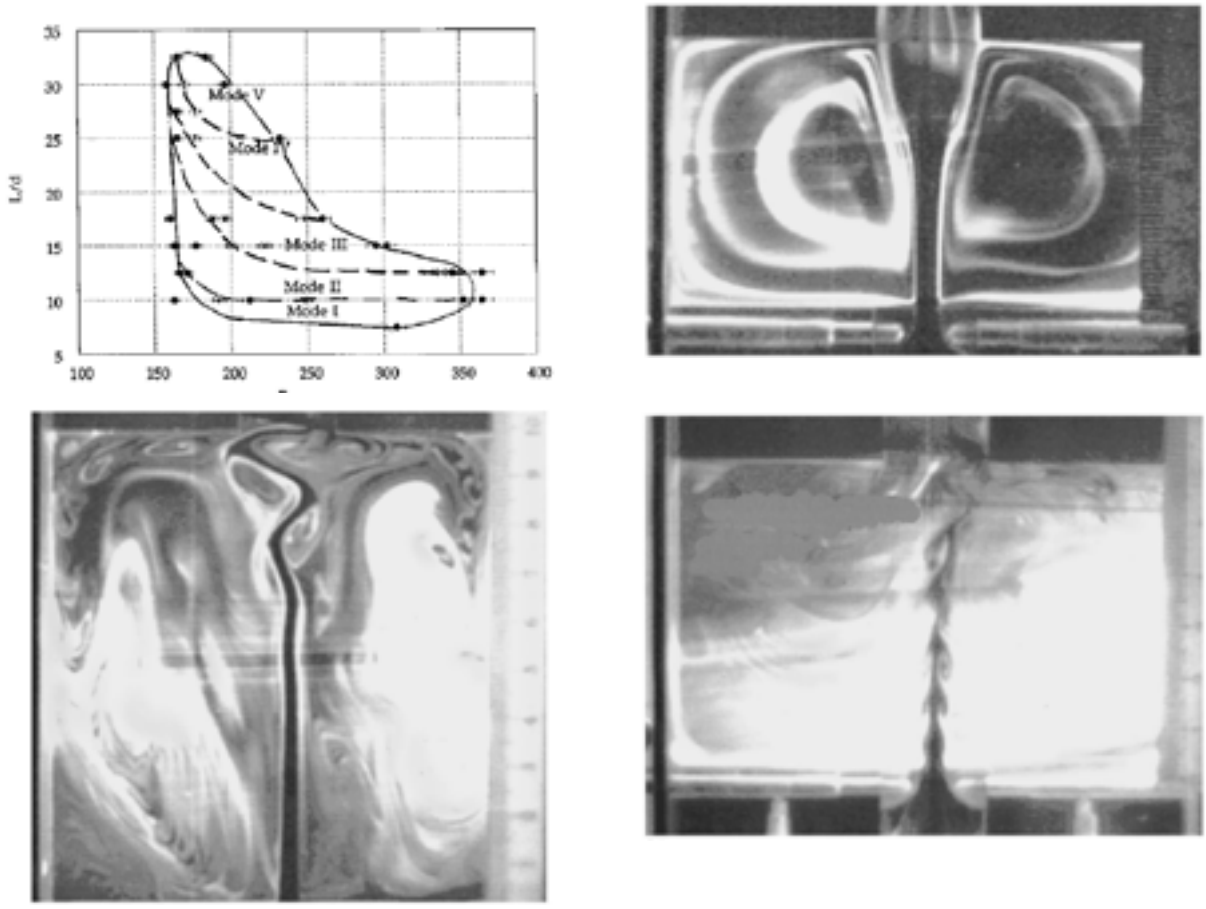

Figure 1.6 Flow observed by Maurel et al (1996) in a recrangular cavity

Dufresne (2008) investigated the flow and sediment transport in a rectangular basin, where two types of polystyrol particle were tested in the experiments and the velocity field was measured by Acoustic-Doppler Velocimeter (ADV) and Particle image Velocimetry (PIV) method. The experiment work could provide the visualization of the velocity field and the sediment deposition distribution was recorded by camara.

Jamshidnia (2010) used the ADV method to investigate the effect of the baffle on the velocity field in a primary rectangular sedimentation tank. The setting and position of the baffle influences the flow field and the development of the flow, where better conditions for sedimentation are provided.

Asgharzadeh (2011) processed an experimental study of particle-laden flow in a rectangular sedimentation tank, where the effects of the baffle configuration on the concentration profile along the tank and velocity field were examined. Different baffle arrangements with various heights were applied. The results showed the best baffle location was related to the inlet concentration, so does the proper baffle height. In the

end, suitable height baffle in the middle increases the performance of sedimentation tank.

Hongfei (2012) processed an experimental study on the research of close type separation device sedimentation tank (CTSDST), the change process of effluent turbidity along time includes two stages, including turbidity decreases slowly stage and turbidity decreases quickly stage. The experiment data show little effect on the sediment concentration and better effect of water purification. Moreover the CTSDST shows advantage in easy operation and maintenance, small footprint, stable discharging water and energy saving.

Peltier et al (2014) used large scale PIV method to investigate meandering jets in shallow reservoirs.

Isenmann (2016) processed experimental work on the sediment transport in a cylinder basin, where three different types of particle were tested, including Poraver 40 – 125 mm, Poraver 100 – 300 mm and Sable Mesh 350 mm.

Though experiment ways are more convincing, there still exist some limitations (Adamsson et al, 2005): it's too expensive to process an experiment, the experimental result is only available for the tested sedimentation tank, long-time period, the result can be only used in the existed tank.

1.3.3 Numerical simulations on flow and sediment transport in tank

With the development of computational science, most of the physical process can be modeled by numerical simulation. Due to the convenient and wide applied range, many researchers started to use numerical simulation to model the flow and sediment transport in tanks. However, the fatal weakness of numerical simulation is the accuracy, which has also been accused. Most of the researchers combined the numerical simulation with the experimental works, using the experimental data to verify the numerical results, then the accuracy of numerical simulation can be obtained.

As a traditional indicator in wastewater treatment plants, the residence time used to be applied to represent the removal efficiency (Nix et al, 1985; Persson, 2000; Marcoon and Guo, 2004; Akan, 2009). Nix (1985, 1988) indicated that it's wrong for using the residence time obtained from steady state, to most engineers, volume divided by flow rate is the definition of residence time, which is correct theoretically only if the flow is

under steady state. However due to the changing flow rate, temperature and sediment concentration, the flow condition is far more complicated than in steady state. Persson (2000) used 2-D vertically iterated numerical model to investigate the hydraulic performance of 13 ponds with different layouts, which confirmed that the pond hydraulic performance is significantly influenced by the location of in- and outlets, subsurface berm and length to width ratio. And he also recommended to replace the nominal detention time with another value in his work. In the end, Persson (2000) studied the influence of some design elements such as island, subsurface berm on the hydraulic performance of ponds, where the hydraulic performance was augmented.

Sumer (1991) derived a relationship for the efficiency of settling basins with a dimensional analysis by examining the results of plenty of settling tests in a rectangular flume. The relation was found in good agreement with the numerical simulations with the diffusion-advection equation.

Saul (1992) et al pointed out that the main concept for designing a storage tank is to provide storage and effective separation of suspended particles and gross solids in an economic way and without leading to weak self-cleansing. A laboratory computer controlled monitering system was developed to realize the flow visualization and estimate the removal performance and sediment deposition of different geometric configurations of storage tanks. Sophisticated control procedures were applied in those systems. It was turned out the flow patterns in the storage tanks were very complicated and the sediment transport process, sediment settlement and re-entrainment were governed by the flow patterns. And the velocity profile in each chamber was an expression of the tank volume, geometry, the shape and the through flow setting and the inflow hydrograph.

Kouyi et al (2003) investigated the free surface of a storm overflow in a sanitation system by using the 3D numerical simulation and experiment measurements. A model was prepared to develop the measurement instrument. The structured light method was used to measure the height of the free surface on an overflow.

Stovin et al (1996,1998,2000) applied CFD method in the efficiency prediction in a storage chambers, in which the flow patterns was shown in the figure 1.7, two methods were using to predict the efficiency, one is to using the bed shear stress distribution with a determined critical bed shear stress to evaluate the settling portion of sediment, the other is applying the particle tracking facility in fluent code and calculating the efficiency by the particle mass remaining in the chamber and the total injected particle mass. And that more simulations were taken to study the effect of the ratio of length to breadth on the chamber performance. The investigation had shown, the factors which are sensitive to the efficiency include the boundary condition, the

physical characteristic of the sediment, a number of relevant simulation parameters and the injection location.

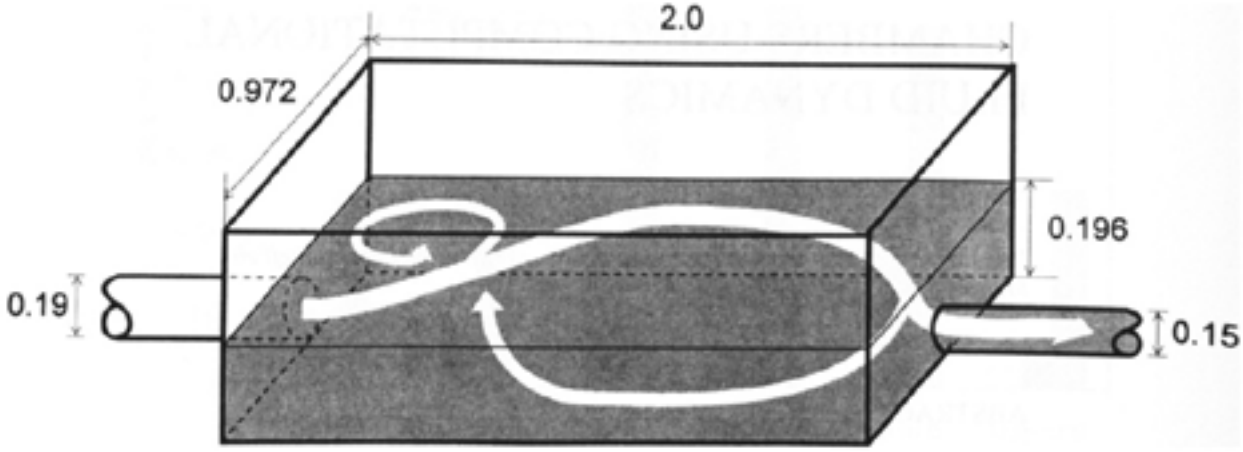

Figure 1.7 Flow field in the model storage chamber (Stovin et al. 1996)

Verstraeten (2000, 2001) developed a numerical model named as sediment trap efficiency for small ponds (STEP), in which the sediment trap efficiency the sediment deposition can be simulated. In order to simulate larger time periods, the algorithm in the model are kept simple. To test the model 8 runs with an experimental pond were executed. The prediction of sediment trap efficiency of this model is 0.38, and STEP model shows better ability in prediction of the sediment trap efficiency on the observed values, especially for pond conditions without permanent storage. For assessing sediment yield data, a weighed sediment trap efficiency is recommended rather than a simple arithmetic mean sediment trap efficiency. However, more detailed experimental data on deposition, runoff, outflow and sediment inflow are still necessary to make accurate predictions.

Tony (2004) applied a unified stormwater model on understanding the factors that influence stormwater treatment performance and describing the overall water quality process in treatment. The model included a first-order kinetic decay model ($k - C^*$ model, where k means the decay rate and C represents equilibrium concentration) for describing water quality, and a continuously stirred tank reactor (CSTR) concept used for hydrodynamics within a treatment device. It was recommended the device such as a sediment tank that has a short-circuiting or high degree of turbulence, a small number of CSTRs within a $k - C^*$model should be applied. By using this model, various treatment facilitied can be accommodated by changing the model parameters.

Adamsson et al (2005) processed both measurements and 3D simulation in a large physical model of a detention tank (19 m × 9 m × 1 m). In which the residence time

and flow patterns were selected to assess the hydraulic performance of the ponds. The numerical results showed good agreement with the measurements.

Takamatsu (2006) modeled sedimentation in stormwater detention basins, a conceptual model was established to assess the removal efficiency of the sediment in a rectangular detention basin for the treatment of stormwater runoff, where the water level is varied to extend ideal horizontal tank theory. A 1/5 scale physical model of the prototype was built to measure the removal efficiencies of the sediment and verify the conceptual model. Steady inflow condition was used in the measurements, but suspended solid concentrations, inflow rates and durations vary. The conceptual model calculated the outflow suspended solid concentrations accurately but underestimated the removal efficiencies.

Jing-xin (2007) proposed a vertical 2D numerical model on suspended sediment transport, where the vertical σ coordinate was used due to the purpose on fitting the free surface and bottom. The work outlined the contribution of Rouse parameter to the vertical profile of sediment concentration due to the aid of the established model, which fitted the theoretical analysis well. Except for some data, the agreement between the numerical simulation and experimental data was reached.

Zhang (2007) tested the performance of Lagrangian methods and Eulerian methods on the prediction of particle concentration distributions by using the CFD methods in enclosed space. The RANS equations with the $k-\varepsilon$ model were solved in the simulation. The numerical results showed good performance of Eulerian methods and Lagrangian methods by comparison with the experimental data. However there still existed differences of the two methods under steady state and unsteady state simulation. Lagrangian method was computationally more demanding in the steady state, however the Lagrangian method fitted better in the unsteady state.

Wei (2007) took the suction dredge into consideration in the investigation on the concentration distribution of sediment in the sedimentation tank. A suspended sediment transportation model was established to analyze the concentration distribution. Based on the assumptions that the horizontal rate was uniform and the vertical rate was zero, the results were in good accordance with theoretical analysis in the particle distribution and the concentration distribution were significantly influenced by the velocity field. However, the results of simulation and experiment showed large difference in vertical distribution curves of monitoring sections and iso-concentration distribution, which turned out it's necessary to increase the accuracy of the simulation on the velocity fields.

Kantoush (2008) carried out experiments in a shallow rectangular reservoir with different shapes due to the effect of geometry on recirculation flow. It is concluded

that the flow patterns will not be symmetric even though the geometry of reservoir is symmetric. The parameter which can determine the flow pattern is the length of the reservoir. Moreover, the ratio of length to width has great influence on the reattachment length. And the settle particles will form new bed form, which will alter the reattachment length in asymmetric flow patterns.

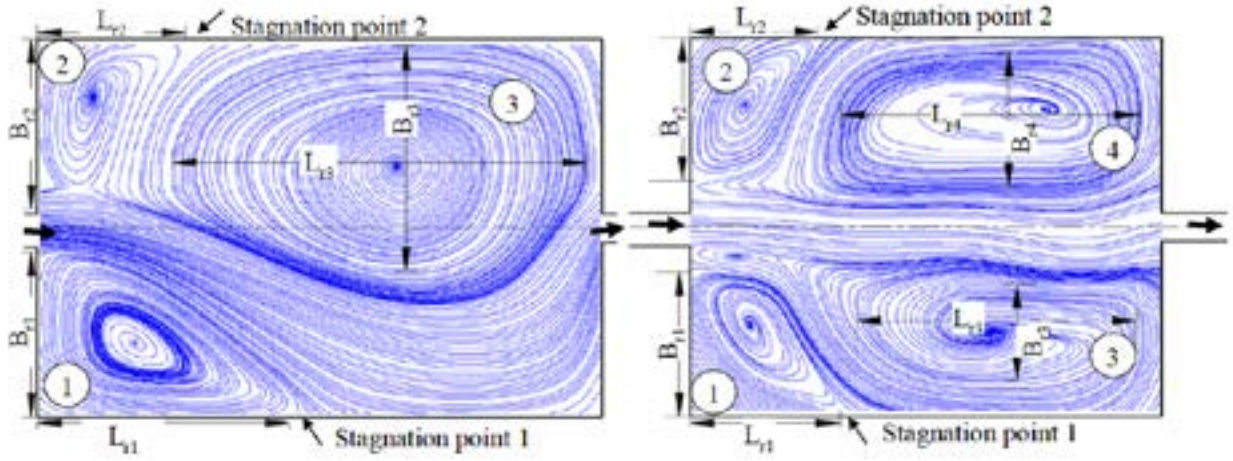

Figure 1.8 Time averaged streamlines by Kantoush (2007) using a LSPIV measurements

Dufresne (2008) modeled the flow and sediment transport in the experiment basin, which showed good agreement with measurements. Numerical simulation was applied in a full-scale structure, which was also validated by the experiment data, and the simulated efficiency showed good agreement with the experiment.

Dufresne (2008) carried out a series of experiment in a rectangular basin, in which the velocity was measured by using ADV and PIV method, a polystyrol particle was used for modeling the sediment transport, the spatial distribution of particles was recorded by camera (see Figure 1.9), and numerical simulation was also processed in comparison with the experiment works, different geometries of rectangular tank were used in numerical simulation to investigate the variation of flow pattern to the geometry, some baffles were placed on the tank to investigate the effect of the distribution of baffles on the sedimentation. In the end the numerical simulation was used to modeling the fluid flow in a real detention basin.

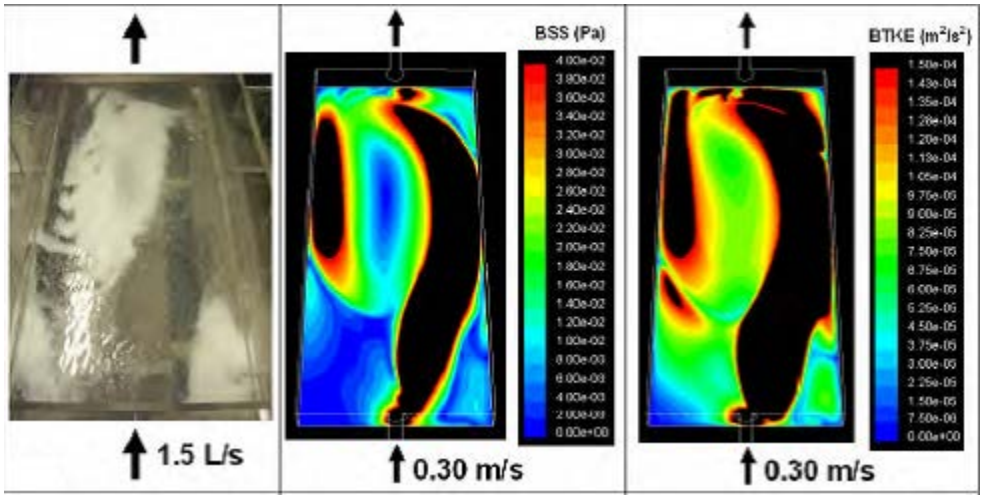

Figure 1.9 Comparison among the sedimentation zones, bed shear stress distribution and bed turbulent kinetic energy distribution(Dufresne, 2008)

Dufresne (2009) investigated flow, sedimentation and solids separation by applying 3D numerical simulation in a rectangular tank with one inlet and two outlets, where the bed shear stress and bed turbulent kinetic energy condition were implemented to the settling condition. In the meantime 23 experiments were carried out to validate the CFD modelling. A good agreement between experiment and numerical simulation has been obtained in the prediction of mass percentage and deposition zone despite some discrepancies in the case with low water depths.

Dufresne (2009) studied the solid separation in three small-scale models, where “trap”, “relect” and bed shear stress condition are used to simulate the sediment transport. Shields diagram was recommended to evaluate the critical bed shear stress and a methodology by CFD modelling for predicting the solid separation in combined sewer overflow chambers was proposed. Dufresne indicated that the bed boundary condition for settling should be given to great attention.

Stamou (2008) focused on improving the hydraulic efficiencies by simple modifications in the geometry of the tank. Various modified geometries were model by CFD method. In the original geometry, the flow field is dominated by high degrees of mixing, short-circuiting and large recirculation regions. By using guiding wall in the original geometry, significant volumes of plug flow is found with less mixing, reduced short-circuiting and smaller recirculation zones.

Rostami (2011) indicate that the design for the inlet in primary settling tanks should fulfill such requests like mitigating the effects of density currents, preventing short-circuiting, dissipating velocity or kinetic energy head of the mixed liquor and

minimizing blanket disturbances. In the numerical modeling, a two-dimensional computational and one phase fluid dynamic model were established, the flow separation, kinetic energy and the velocity profile were examined for understanding the flow properties in the sedimentation tank.

Shahrokhi et al (2012, 2013) studied the effect of number of baffles on the improvement efficiency of primary sedimentation tanks. The hydraulic performance of the primary sedimentation tanks was tested in two different ways: the Flow Through Curves (FTCs) method and the parameters of flow patterns. The comparison between the numerical simulation and experimental data from ADV indicates that in suitable positions the increasing number of the baffles can dissipate the kinetic energy, decrease the recirculation region and create a uniform flow field, in the end the hydraulic performance of the sedimentation tank should be improved. In 2012, Shahrokhi et al investigated the effect of the baffle location on the flow pattern of primary sedimentation tanks by numerical ways. The numerical simulation results were verified by the measured velocity field by ADV. In the computational modeling the GMRES algorithm was selected as pressure solver and it showed good agreement with experimental tests. Also, the function of the baffle is to dissipate the kinetic energy and provide small circulation regions in the tank.

Tarpagkou (2013) applied numerical simulation to investigate the 3D flow behaviour and hydrodynamics in a sedimentation tank, what makes this work different among previous numerical investigations is taking the momentum exchange between the primary and the secondary phase into consideration and using Discrete Phase Model(DPM) with two-way coupled calculation to track the particle. It turned out that by increasing the diameter and the volume fraction of the injected particles, the symmetry flow pattern is lost and new eddies are formed, and when the water depth in the sedimentation tank is increased the position of the recirculation eddies will alter.

Hexiang (2013) simulated sediment process by using the boundary based on turbulent kinetic energy and bed shear stress in steady and unsteady state, in the work a situ detention basin and a small scale rectangular basin were both under modeling. It turned out that the prediction of trap efficiency and spatial distribution of particles were better than the trap condition since the new boundary dealing with particle settling was introduced(see Figure 1.10). And the unsteady state simulation is more appropriate for the flow and sediment transport in a detention basin. Though the simulation results could not fit the experiment data completely, the work had shown the potential of bed shear stress and turbulence kinetic energy in dealing with the particle settling.

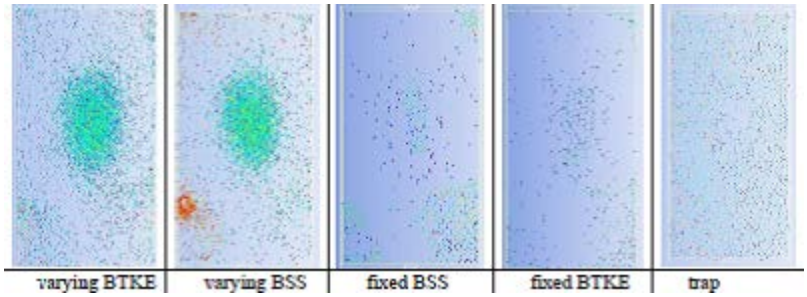

Figure 1.10 Sedimentation simulation in a small scale basin with different boundary condition (Hexiang, 2013)

Isenmann (2016) carried out a series of experiments and numerical simulations to investigate the sediment transport in tanks, Isenmann used the concept of bed shear stress and bed turbulent kinetic energy to implement the settling condition for calculation(see Figure 1.11). The simulation results showed better prediction in trap efficiency and deposition zones.

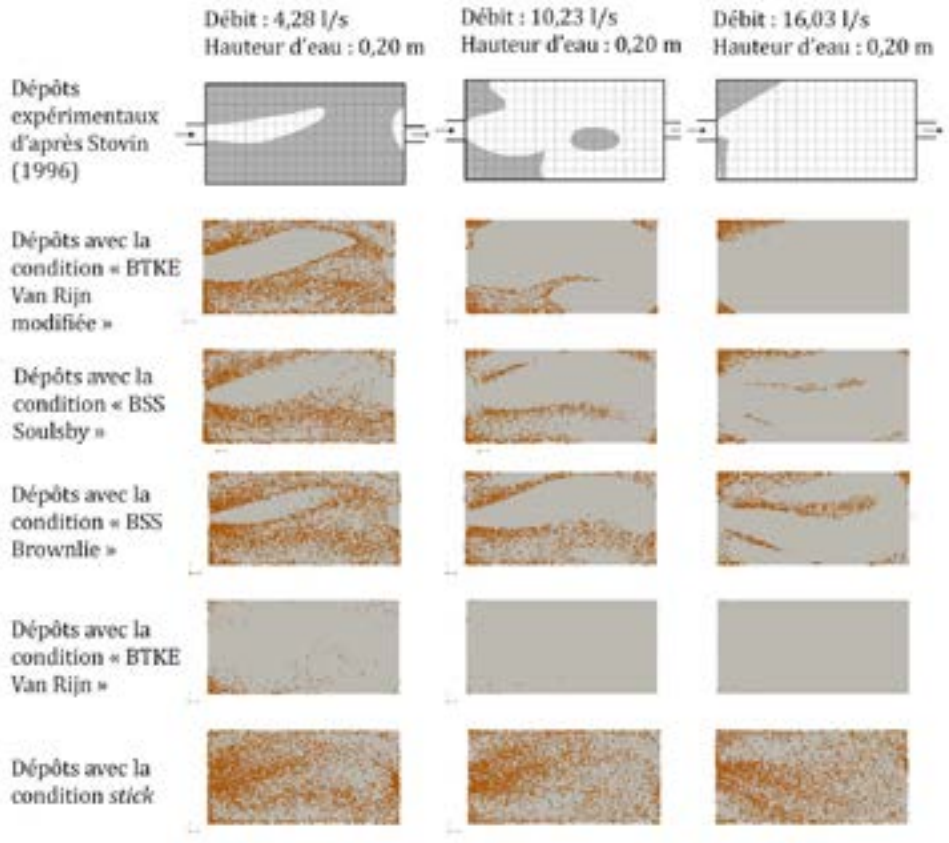

Figure 1.11 Comparison of particle deposition between numerical simulation and results from Stovin (Isenmann, 2016)

Numerical simulations provide a way to detailed investigation on flow and sediment characteristic, the only refinement is the computational resources if the accuracy can be guaranteed. In a model of different geometry, it will be very easy by numerical simulation, however many time is necessary for constructing the experiment device in experimental way. Numerical simulation can also simulate much more parameter than experiment, detailed information about flow field and particle characteristic will be obtained by numerical method.

1.4 Conclusions

In the investigation on sediment transport, the characteristic of the particle plays a very important role. The results differ due to the range of sediment size, shape, settling velocity and so on. The interaction of flow and particle should be considered due to the real physical process.

Both numerical simulation and experiments works on the investigation of flow and sediment transport in tank by others researchers have been demonstrated. The disadvantages and advantages of numerical simulation and experimental works are pointed out. With the addition of experiment works, numerical ways in investigating the flow and sediment transport in tank can be a very worthful and economic method.

All the investigations on the flow and sediment transport in the sedimentation tank aim at improving the hydraulic performance and trap efficiency of the sediment. The flow patterns in the sedimentation tank are the uppermost factor influencing the hydraulic performance and trap efficiency. The investigations on the modified geometry and using baffle in the tank are all working for changing the flow pattern in the tank in the end.

In the numerical simulation of sediment transport in the sedimentation tank, the simulation of resuspension is impossible with using the existed commercial CFD software. Therefore, the prediction of trap efficiency in the simulation will be much higher than in the practice. Many researchers begin to develop new boundary condition for the particle settling. Based on the incipient of sediment motion, the criterion provided by Shields curve based on the bed shear stress can be a useful method for modeling the particle settle and re-suspend process.

The discrete phase model (DPM) differs from species model and Euler-Euler approaches on particle tracking. DPM is a Lagrangian method in which the particle

trajectory is not the same in comparison with Euler-Euler approaches and species model.

2. Simulation of flow patterns in storm tank

2.1 Introduction

This chapter presents numerical investigations of free surface flows patterns in a storm tank. Indeed, the flow pattern is a crucial factor determining sediment deposition in a storm tank, hence its efficiency. As a matter of facts, the hydrodynamics is mainly influenced by boundary conditions namely the tank geometry and inlet/outlet flow conditions. In what follows, all simulations were performed with exact tank geometry from built for laboratory experiments.

The industrial Ansys Fluent code was used to perform all the 3D numerical simulations. This sophisticated commercial computational fluid dynamics (CFD) software, due to its stable accuracy and robustness, Fluent is widely used in the field of engineering. It is usable for many fluid dynamics problems. Though the core source is not accessible to the users, a user defined function (UDF) method is provided for all the users to exploit specific application: Euler-Lagrange sediment transport for instance in this PhD work. For example, the initial pressure distribution at the outlet due to the effect of the height and the boundary condition for estimate the sedimentation of the particle to substitute the default “trap” condition in Fluent.

2.2 Numerical method

2.2.1 Flow governing equations

Based on classical conservation laws invoked in mechanics flow equations can be derived. Versteeg and Malalasekera gave detail information of the flow governing equations in 1995. The mass conservation, here for incompressible flows, provides the so called continuity equation. The momentum conservation, second Newton law, gives three other momentum equations. The following equations are obtained in a

fixed referential, for a fixed control volume in the flow of a Newtonian fluid of volumetric mass ρ.

Continuity equation:

$$\frac{\partial \rho}{\partial t} + \nabla \cdot \left(\rho \vec{V}\right) = 0 \qquad (2.1)$$

Momentum equation:

$$\frac{\partial (\rho u)}{\partial t} + \nabla \cdot \left(\rho u \vec{V}\right) = -\frac{\partial p}{\partial x} + \frac{\partial \tau_{xx}}{\partial x} + \frac{\partial \tau_{yx}}{\partial y} + \frac{\partial \tau_{zx}}{\partial z} + \rho f_x \qquad (2.2a)$$

$$\frac{\partial (\rho v)}{\partial t} + \nabla \cdot \left(\rho v \vec{V}\right) = -\frac{\partial p}{\partial y} + \frac{\partial \tau_{xy}}{\partial x} + \frac{\partial \tau_{yy}}{\partial y} + \frac{\partial \tau_{zy}}{\partial z} + \rho f_y \qquad (2.2b)$$

$$\frac{\partial (\rho w)}{\partial t} + \nabla \cdot \left(\rho w \vec{V}\right) = -\frac{\partial p}{\partial z} + \frac{\partial \tau_{xz}}{\partial x} + \frac{\partial \tau_{yz}}{\partial y} + \frac{\partial \tau_{zz}}{\partial z} + \rho f_z \qquad (2.2c)$$

All the equations are in the Cartesian coordinates system, where ρ is the density of the fluid, $\vec{V} = (u, v, w)$ is the instant velocity vector, τ is the stress tensor where in a Newtonian fluid the density is a constant and the hypothesis that stress tensor linearly depends on deformation rates, f is the volume force, p is the pressure. Those equations are derived from a small element of fluid, and under the circumstance that the fluid is a incompressible Newtonian fluid.

All the equations are written in a Cartesian coordinates system, where ρ is the density of the fluid, $\vec{V} = (u, v, w)$ is the instant velocity vector, τ is the stress tensor, f is the sum of any body forces such as gravity, p is the pressure. In this work we deal with free surface flow of water which is an incompressible Newtonian fluid.

Despite the deterministic nature of Navier Stokes equations, it is impossible to predict the nature of a solution, at any time. This would require an infinite precision on the initial condition. An illustration of this unpredictability is meteorological forecast. Besides it is impossible to show the existence of solutions of Navier Stokes equations with initial conditions, for any time.

2.2.2 Discretization of the governing equations

Analytical solution of the Navier-Stokes equations, which are nonlinear partial differential equations, can only be found for few academic configurations. For most engineering and research problems a numerical method is required to approximate the solution. What distinguishes the finite volume method (FVM) from the finite difference method is the application of the control volume (Pletcher, 2012).

The governing equations are discretized thanks to a FVM approach. The main idea of finite volume discretization is to define a control volume and impose the conservation of the equations on this volume. From this volumetric conservation, generally considered at the center of the control volume, the issue is to evaluate the fluxes at the cell boundaries. The discrete equation derived with both methods describes the conservation of physical parameters in the control volume, which makes FVM a natural approach to express conservation laws in a discrete form.

FVM can be used for structured or unstructured meshes, which makes it possible to simulate fluid flows within complex geometries. The consecutiveness of the method can be guaranteed if the flux at the edge of close cells is balanced (Schiano, 1996). Every term of the approximation in FVM has an explicit physical meaning. At the meantime, the advantage of the concept of piecewise approximation in finite element method (FEM) and the concept of finite differential method can be used in FVM to develop high accuracy method. Due to the explicit physical concept and easy to program, FVM becomes the most popular numerical calculation method in the field of engineering.

The discretization of the computational domain is an important step of the numerical simulation. Indeed, as far as possible the sensitivity of the numerical results to the mesh has to be minimized. In other words the mesh must be sufficiently fine to ensure a good stability and accuracy of the numerical solutions. A trade-off between physical problems of interests, computational domain size and computational resources can sometimes be made.

The different terms of the equations can be discretized with several numerical schemes, each with its advantages and drawbacks in terms of robustness, accuracy and calculation cost. In Fluent several common methods are available for evaluating the fluxes: first order upwind scheme, exponential scheme, second order upwind scheme, QUICK scheme and central differencing scheme among others. The accuracy of the numerical solution can depend on this choice. The numerical schemes with higher order leads to high accuracy and long calculation time, In order to maintain high accuracy and acceptable calculation time, second order upwind scheme was chosen.

2.2.3 Turbulence model

Turbulent flows are highly unstationary and irregular. Navier-Stokes equations contain non-linear terms associated with motions at very different scales. Flow energy is transferred between those structures, limited by the geometry of the flow, stems from the mean flow itself. The smallest structures size is due to dissipative effects (Temam, 2006).

The dissipation of energy created at large scales is due to fluid viscosity. Turbulent flows are necessarily tridimensional, due to the chaotic nature of turbulence, and the mixing of momentum, heat and mass.

Flow regimes usually distinguished are Stokes flows, laminar flows, transitional or turbulent flows. The laminar flow regime occurs when the fluid flows in parallel layers with few disturbances and mixing, no eddies perpendicular to the direction of the flow. It can completely be described by the equation 2.1 and equation 2.2. As stated above, the continuity and momentum equations can be solved analytically for simple cases (Schilichiting, 1979). However, many cases in the natural world and in the field of engineering involve turbulent flows characterized by significant mixing, high three dimensionality of flow motion with a random property which makes them rather unpredictable. Therefore viable tools capable of representing the effects of turbulence are necessary to achieve reliable numerical solutions.

The Reynolds number provides a criterion to distinguish flow regimes. It is a dimensionless parameter comparing viscous forces to inertial forces (associated with advective effects). The Reynolds number writes:

$$\mathrm{Re} = \frac{Ud}{\nu} \tag{2.3}$$

Where U is the velocity of the fluid, d a characteristic length of the flow, ν is the cinematic viscosity of the fluid.

A complicated series of event occurs around the critical Reynolds number, the flow characteristics changes dramatically. The flow behavior is chaotic and random in the final state. Though with constant imposed boundary conditions, the flow becomes unsteady intrinsically, and all the flow parameter vary in a chaotic and random way. This regime is called turbulent flow. The measurement of velocity can explain this phenomenon explicitly .

As shown on figure 2.1 a measured time-series of turbulent velocity highlights its chaotic characteristics. In order to establish turbulent flow equations, a component of

the velocity is expressed as a sum of a steady mean value U and a fluctuating component $u'(t)$:

$$u(t) = U + u'(t) \tag{2.4}$$

Other flow variables are expressed as a sum of mean values (U, V, W, P) and a fluctuating component (u', v', w', p').

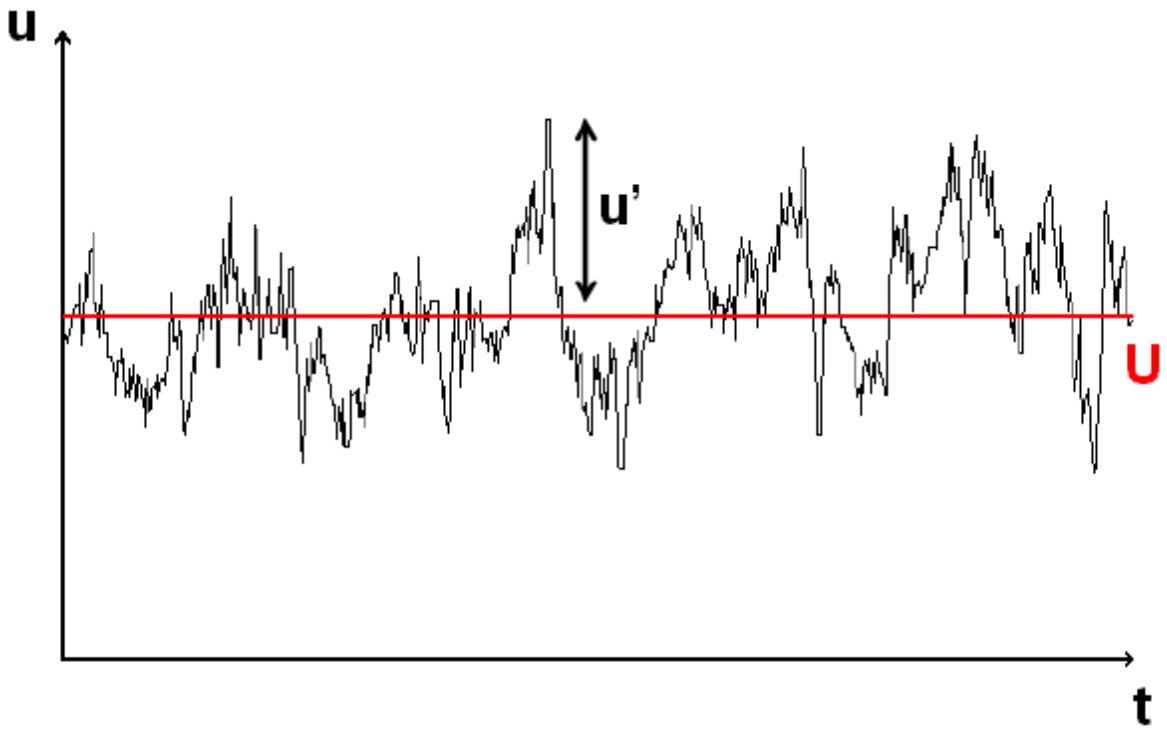

Figure 2.1 Velocity measurements in turbulent flow (Dufresne, 2008)

This section deals with the simulation of the complex turbulent flows involved in storm tanks. There are 3 methods for simulating turbulent flows, including direct numerical simulation (DNS), large eddy simulation (LES), Reynolds average Navier-Stokes (RANS). Direct numerical simulation of Navier-Stokes equations remain very expensive and limited to relatively low Reynolds flows and academic test cases. It is still and certainly for a certain time unaffordable for engineering applications. . The most accurate method is DNS, in which all flow scales are calculated directly, however DNS requires very fine meshes, which result in very high computational costs..

Generally turbulence is described through a closure model which leads to more affordable computations. RANS methods can simulate flows with high Reynolds numbers, however depending on the closure model and very detailed features of the

flow can't be represented. Based on the kinetic energy transport mechanism, LES method can calculate the movement of eddies of large scale and the effect of the eddy of small scale on the eddy of large scale is modelled.

In this work, we will use RANS where accuracy is satisfactory for studying average features of the flows. The turbulent flow statistical theory is used to average the transient Navier-Stokes equations and solve the averaged values of flow variables.

The Reynolds equation can be obtained by time averaging of transient Navier-Stokes equation and using Boussinesq eddy viscosity assumption postulated by Boussinesq in 1877 where the momentum transfer caused by turbulent eddy can be modelled with an eddy viscosity (Boussinesq,1877 & Schimitt, 2007). In Boussinesq assumption the Reynolds stress tensor, τ_{ij}, is stated proportional to the trace-less mean strain rate tensor, S_{ij}^{*} ,and can be written in the following ways:

$$\tau_{ij} = 2\mu_t S_{ij}^{*} - \frac{2}{3}\rho k \delta_{ij} \tag{2.5}$$

The Reynolds equation can be written as:

$$\frac{\partial \bar{u}_\iota}{\partial t} + \bar{u}_\jmath \frac{\partial \bar{u}_\iota}{\partial x_j} = \bar{f}_\iota - \frac{1}{\rho}\frac{\partial \bar{p}}{\partial x_i} + v\frac{\partial^2 \bar{u}_\iota}{\partial x_j \partial x_j} - \frac{\partial \overline{u_\iota' u_\jmath'}}{\partial x_j} \tag{2.6}$$

And for incompressible flow:

$$\frac{\partial \bar{u}_\iota}{\partial x_i} = 0 \tag{2.7}$$

Where the additional stress can be expressed as $\tau_{ij} = -p\overline{u_\iota' u_\jmath'}$, which is called Reynolds stress. Only large scale average flow can be calculated by this method, all the effect of turbulent fluctuations on the average flow is represented by the Reynolds stress. The Reynolds stress arises form fluctuating motion, i.e. from the flow itself. At this stage, the turbulence problem is not closed, i.e. it there are more unknowns than equations. Therefore a closure model has to be found. However the closure method usually used for viscous stress is not applicable to Reynolds stress.

There are six individual stress components $\overline{u_\iota' u_\jmath'}$, 3 for i = j and 3 for i ≠ j, which have to be related to the mean motion itself before any resolution can be attempted.

Two types of approaches are commonly distinguished for the closure of turbulent flow equations. The first approach is eddy (or turbulent) viscosity closure model based on the Boussinesq assumption for the eddy viscosity. Zero-equation model, one-equation model or two-equation models can be derived. The other approach introduces dynamical equations for the Reynolds Stress. Reynolds stress is really a functional of velocity (fluctuations) with such an approach.

Reynolds stress model

The Reynolds stress model (RSM), also called Reynolds Stress Transport (originated from Chou, 1945 & Rotta, 1951), are second order closure models. Each component of the Reynolds stress is directly computed from a partial differential transport equation accounting for several physical terms: convection, turbulent and molecular diffusion, stress production, buoyancy, rotation production and dissipation and pressure strain. The exact transport equations for the transport of the Reynolds stresses can be written as follows:

$$\frac{\partial \overline{u_\iota{}' u_j{}'}}{\partial t} + \overline{u_k}\frac{\partial \overline{u_\iota{}' u_j{}'}}{\partial x_k} = -\overline{u_\iota{}' u_k{}'}\frac{\partial \overline{u_j{}'}}{\partial x_k} - \overline{u_j{}' u_k{}'}\frac{\partial \overline{u_\iota{}'}}{\partial x_k} + \emptyset_{ij} + D_{ij} - \varepsilon_{ij} \tag{2.8}$$

Where $\emptyset_{ij}$ is the pressure strain, D_{ij} is the diffusion term and ε_{ij} is the dissipation term.

The RSM describes the evolution of Reynolds stress in space and time. This second order model may result in more accurate moment patterns than eddy patterns than eddy viscosity methods. The number of the equation is 15 in total with the retained Reynolds stress equation (Launder,1975). The computational cost for such methods is generally high which limits its application for engineering problem often involving large meshes.

Eddy viscosity model

Eddy viscosity model is widely used in the engineering field, according to the concept raised by Boussinesq following the thinking of molecular viscosity, the Reynolds stress can be expressed as:

$$\overline{u_\iota u_j} = -\vartheta_T\left(U_{i,j} + U_{j,i} + \frac{2}{3}U_{k,k}\delta_{ij}\right) + \frac{2}{3}k\delta_{ij} \tag{2.9}$$

Where $k = \frac{1}{2}\overline{u_\iota u_j}$ is the turbulent kinetic energy, ϑ_T is turbulent eddy viscosity coefficient. This is the earliest basic eddy viscosity model, a linear relation is

assumed between the Reynolds stress and the mean velocity strain rate $S_{ij} = \frac{1}{2}\left(\frac{\partial u_j}{\partial x_i} + \frac{\partial u_i}{\partial x_j}\right)$. If the mean velocity strain rate is already determined, the six Reynolds stress components can be obtained by determining a eddy viscosity coefficient ϑ_T. And due to the eddy viscosity coefficient is isotropy, which can be modeled by additional turbulent flux, for example kinetic energy k, specific dissipate rate ε, dissipate rate ω and others turbulent flow rate $\tau = {}^{k}/_{\varepsilon}$, $l = {}^{k^{3/2}}/_{\varepsilon}$, $q = \sqrt{k}$. Different eddy viscosity model can be obtained according to the introduced turbulent flux. The common eddy viscosity pattern include $S - A$, $k - \varepsilon$, $k - \omega$ and so on.

Among all the eddy viscosity patterns, the $k - \varepsilon$ model is the most widely used model in engineering field due to the sufficient accuracy for many practical cases. $k - \varepsilon$ model proposed by Launder and Spalding (1974), is a semi-empirical model where turbulent viscosity μ_t, is calculated by combining turbulent kinetic energy k and dissipation rate ε together as follows:

$$\mu_t = \rho C_\mu k^2/\varepsilon \tag{2.10}$$

$$\varepsilon = \vartheta \overline{\frac{\partial \mu_i'}{\partial x_k} \frac{\partial \mu_i'}{\partial x_k}} \tag{2.11}$$

There are still four others constants in the $k - \varepsilon$ model. Table 2.1 shows the suggested value of those constants by Launder and Spalding (1972).

Table 2.1 Suggested value of the constant in $k - \varepsilon$ model

C_μ	σ_k	σ_ε	$C_{1\varepsilon}$	$C_{2\varepsilon}$
0.09	1.00	1.30	1.44	1.92

In order to adapt different practical condition, the standard $k - \varepsilon$ model is been transformed to RNG and realizable $k - \varepsilon$ model by using different method of calculating turbulent viscosity, the turbulent Prandtl numbers governing the turbulent diffusion of k and ε ,the generation and destruction terms in the ε equation. Due to realizable $k - \varepsilon$ model predicts round jets spreading and recirculation correctly (Karthik, 2011), in this work the model for calculating turbulence is chosen as realizable $k - \varepsilon$ model.

2.2.4 Boundary condition

The simulation of fluid flows is very sensitive to boundary conditions (BCs) and can be very sensitive to the way they are handled depending on flow features. In this work we will distinguish 3 zones for applying BCs: inlet, outlet, walls. A volume of fluid method is applied to track the free surface.

2.2.4.1 Inlet

For the inlet, Fluent allows to set velocity-inlet, pressure-inlet and volume flow rate inlet conditions (inlet discharge). As the pressure at the entrance is an unknown variable, and since our experimental entrance pipe (the length is about 2.8 m) is long enough for the flow to develop completely, Therefore, both velocity-inlet and mass flow rate inlet from experimental data are used to define the inflow BC.

2.2.4.2 Outlet

For the outlet, Fluent allows to set pressure-outlet, mass flow outlet and outflow.

In those conditions for exit, there are some limitations. The pressure-outlet boundary condition can be only used under specific pressure configurations at exit and it turns out some specific value at the exit leads to the divergence of the calculation according to tested case in this research. The mass flow outlet boundary condition can be only used under specific volume flow rate at exit. All the geometry used in this work contain two outlet (one for air, the other for water), and due to the pressure-outlet boundary condition and outflow boundary condition can’t be used in combination, the boundary condition for the outlet can only be both pressure-outlet or outflow.

As taking all the limitations and the request of this thesis into considerations and according to the results of tested case by using different boundary condition, the pressure-outlet boundary condition is selected as the boundary condition for the exit.

2.2.4.3 Free surface

In order to track the interface, the choice is made to use a volume of fluid model (VOF). VOF method is designed to track the position of the interface between two or more immiscible fluids. Tracking is accomplished by solution of phase continuity equation.

This method assumes that the interface corresponds to abrupt volume fraction change locations. A momentum equation of the diphasic mixture of fluids is solved using mixture material properties. . It is possible with such a of diphasic and incompressible flow of two non miscible phases like air and water to track the interface. Turbulence equations are also solved for this mixture of fluid. Surface tension and wall adhesion effects can be taken into account. Phases can be incompressible and be mixtures of species.

$$\frac{\partial F_w}{\partial t} + U\frac{\partial F_w}{\partial x} + V\frac{\partial F_w}{\partial y} + W\frac{\partial F_w}{\partial z} = 0 \qquad (2.12)$$

Where F_w is the water volume fraction, U, V, W are the component velocity in X, Y,Z direction.

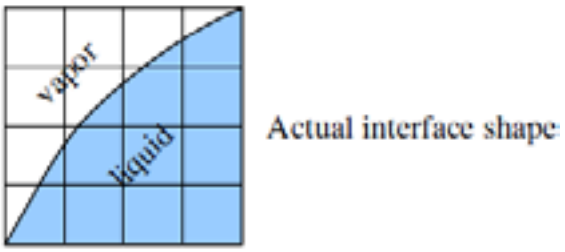

Figure 2.2 Actual interface shape

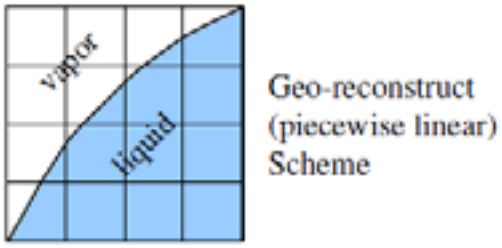

Figure 2.3 Geo-reconstruct scheme

The standard interpolation schemes used in VOF are obtaining the face fluxes whenever a cell is completely filled with one phase. Those schemes are: geometric reconstruction, Euler explicit and Euler implicit.

2.2.4.4 Wall

The physics of fluid flows is not simple and boundary layer phenomena often present strong gradients and nonlinearities of velocity profiles due to viscous effects. It is however an important phenomena that can influence general flow patterns. Shallow free surface flows are generally highly influenced by basal friction. That is why particular attention has to be paid to model and simulate the flow in the near wall region where viscous effects are important and can influence global flow patterns. A special treatment of the mesh distribution in the near wall region is usually necessary for performing realistic flow simulations. This mesh refinement is also of importance regarding turbulence modeling. In the boundary layer, the tangential velocity fluctuation is decreased due to the viscous damping and the normal velocity fluctuation is stopped.

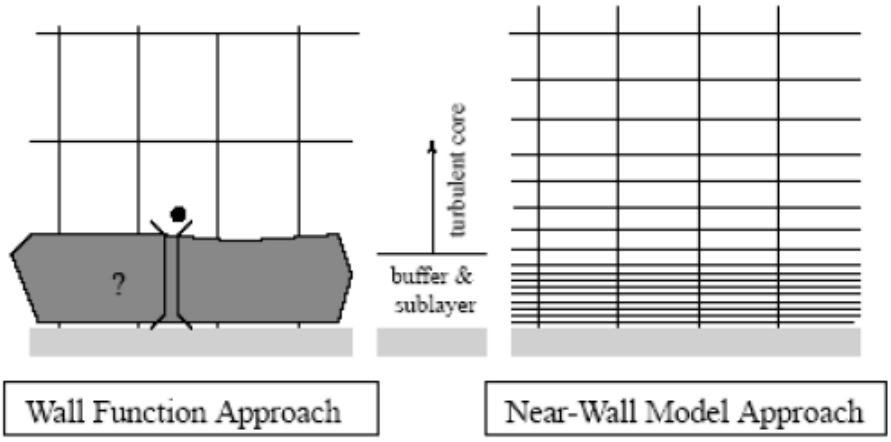

Figure 2.4 Two approaches treating the near wall region (Fluent, 2002)

In CFD two approaches are usually used to account for boundary layer effects and involve different mesh treatments in the near wall region (shown in Figure 2.4). The first approach is called Wall Function Approach and a semi-empirical parameterization of the viscous sublayer and blending region is introduced. Indeed a simple turbulent model such as $S-A$ model used here would not be able to predict a logarithmic velocity profile near a wall. A wall function is used to provide a near wall boundary condition for the momentum and turbulence transport equations. The second approach is called Near-Wall Model Approach, where the mesh near the wall should be refined very carefully and an appropriate turbulence model should be chosen to adapt the boundary turbulence, the mesh number is really important in this method.

Normally, the near wall region can be divided into viscous layer, blending region or buffer layer and fully turbulent region or log-law region, which is shown by Figure 2.5. A crucial criterion for the mesh treatment in the near wall region is the dimensionless wall distance y^+,

$$y^+ = \frac{u_* y}{\nu} \tag{2.13}$$

Where u_* is the friction velocity at the nearest wall, y is the distance to the nearest wall and ν is the local kinematic viscosity of the fluid.

In order to achieve a relatively reliable result, the first grid point to the nearest wall should be placed in the log-law region, which require $11.5\sim30 < y^+ < 200\sim400$.

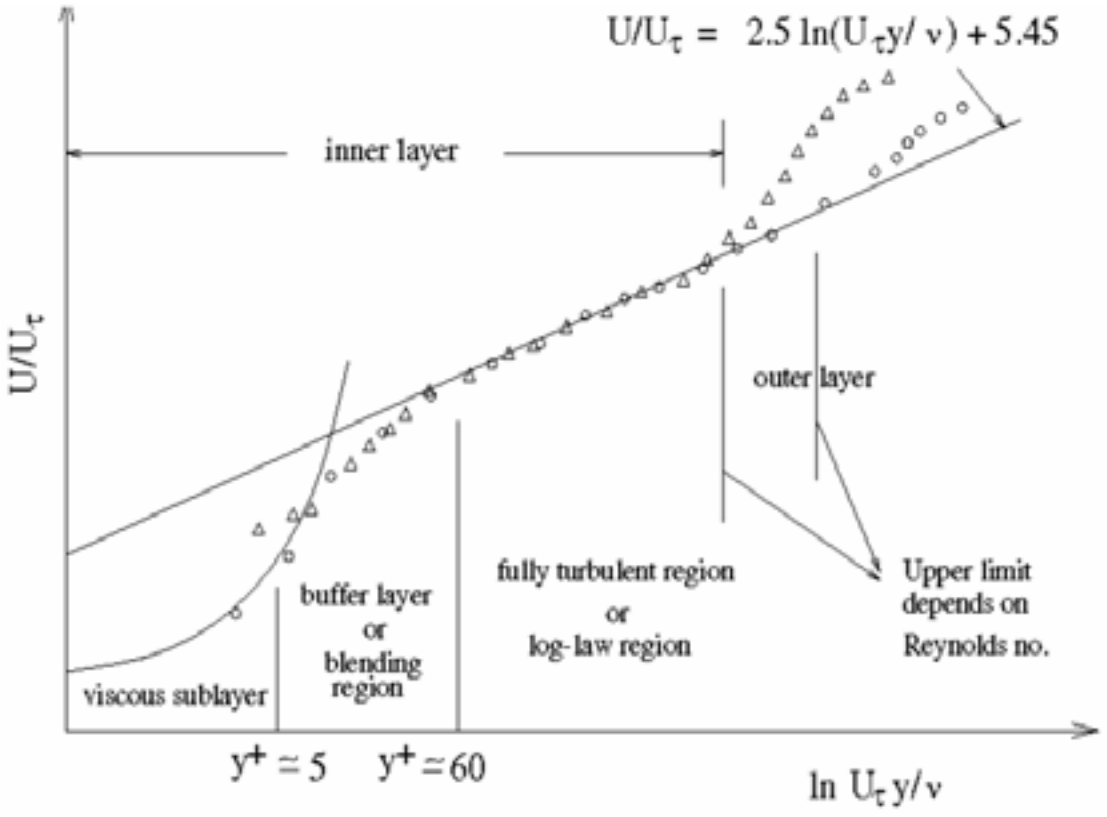

Figure 2.5 Velocity distribution in the near wall region (Fluent, 2002)

For flow modeling on engineering cases, relatively reliable simulations can be obtained by using a wall function, including standard wall function and non-equilibrium wall function. Table 2.2 shows the advantages and disadvantages of standard wall function and non-equilibrium wall function. There still exists more wall function with the development of CFD, for example scalable wall function and enhanced wall treatment. In this thesis, a test for enhanced wall treatment has been done, for refined mesh the turbulent viscosity near the wall increase sharply, which leads to the divergence of the calculation, therefore all the simulation results in this thesis used the standard wall function to treat the near wall region.

Table 2.2 Advantages and disadvantages of wall function

Type of wall function	Advantages	Disadvantages
Standard wall function	Wide application range, small computational quantities and good accuracy.	Appropriate for the high Reynolds number flow, inappropriate for the low Reynolds number flow with pressure gradient, strong volume force and strong 3D flow.
Non-equilibrium wall function	Taking pressure gradient into consideration, capable of solving separation, reattachment and collision problem.	Inappropriate for the low Reynolds number flow with pressure gradient, strong volume force and strong 3D flow.

2.3 Simulation setup

2.3.1 Geometry and mesh

The tank used in this thesis consists in a rectangular reservoir where free surface flows occur, a pipe inlet and a pipe outlet. The dimensions of the model geometry are all derived from the experimental device. The first model in this thesis is derived from the experimental work of Dufresne (2008). The dimensions of the rectangular reservoir are 1800 mm × 760 mm × 400 mm, the two circular pipes diameters are equal to 80 mm. The second model presented in this thesis is also derived from the experimental work. The dimensions of the second rectangular reservoir are 4240 mm × 760 mm × 405 mm, two circular pipes of diameters equal to 80 mm. The third model is of the same dimension than the second model, but with the addition of a cavity at the bottom, the dimension of the cavity is 760 mm × 325 mm × 80 mm. The details of the model are showed in the figure as follow. Detailed views of the geometry are presented in Figure 2.6-2.9.

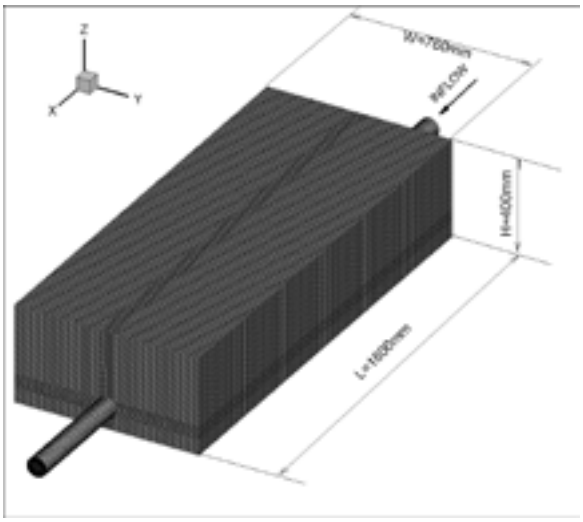

Figure 2.6 Detailed geometry and mesh of short tank (ST)

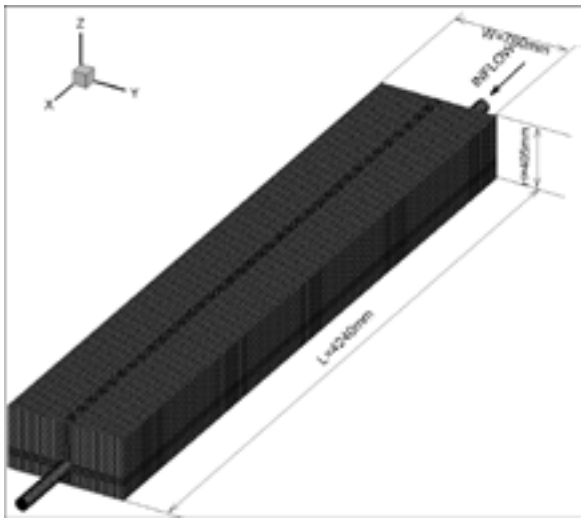

Figure 2.7 Detailed geometry and mesh of long tank (LT)

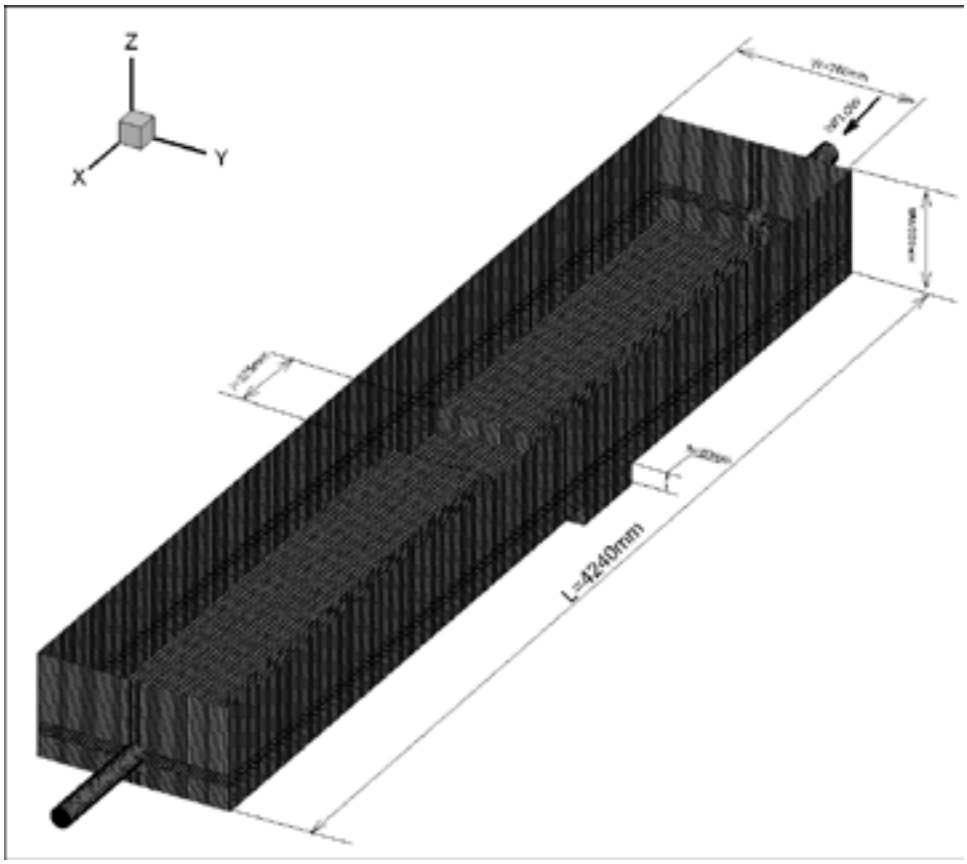

Figure 2.8 Detailed geometry and mesh of long tank with cavity (LTWC)

For creating a mesh, it is possible to choose between tetrahedral and tetrahedral mesh elements, depending on the complexity of the domain geometry. The mesh design can have important impacts on the numerical solutions performed and numerical diffusion has to be minimized as it is not a real physical phenomenon. Indeed partial differential discretization, approximations and mesh properties can lead to a purely numerical effect similar to increasing real diffusion coefficient. Numerical diffusion can be really significant when the physical diffusion of the flow is relatively low. This diffusion also depends on the resolution of the mesh, indeed refining the mesh is one useful way to deal with numerical diffusion. Hexahedral mesh provides less numerical diffusion than tetrahedral along with lower calculation, due to numerical diffusion is minimized when the flow is aligned with the mesh which is not possible if a tetrahedral mesh is selected (Fluent, 2002).

The mesh used for simulation is built with Ansys ICEM, an industrial mesh creation software. As it is mentioned above, a hexahedral mesh is chosen for all the simulation in the work.

2.3.2 Mesh sensitivity

In a simulation process, the first step is to test the mesh refinement in order to ensure a sufficient accuracy and independency of numerical results. Numerical method produced by essence numerical errors, because of truncation error that can result in significant numerical error through temporal iterative processes. If the numerical error is too high, the simulation results can be inappropriate to study a physical phenomenon. One solution to control the numerical errors is to refine the mesh, however boundlessly refining the mesh means huge increasing of computational resources. In practice, users will find a trade-off between numerical accuracy and computational resources, and this is so called grid independence verification or mesh sensitivity verification. Normally, the accuracy of a numerical simulation will depend on the quality and the number of the mesh. Errors will exist if the mesh size refinement and the quality of the mesh are not appropriate, and errors will accumulate with the continuous numerical calculation process.

The mesh sensitivity test is finished by using the geometry in Figure 2.7. Realizable $k-\varepsilon$ model is used for the turbulence, second order upwind is selected for momentum and turbulent kinetic energy, “Modified HRIC” is selected for volume fraction calculation.

The parameters chosen to examine the mesh sensitivity are mass flow rate at the outlet and the range of interface. The mesh sizes chosen for the tests are as follows: 0.468

$\times 10^6$, 0.616×10^6, 0.808×10^6, 1.145×10^6, 1.305×10^6, 2.259×10^6. The increase of mesh size is not just based on number, it's by increasing the global variable factor, which is a factor that can control the minimum and maximum element of the mesh, and refining the part mesh by changing the point distribution in the edge.

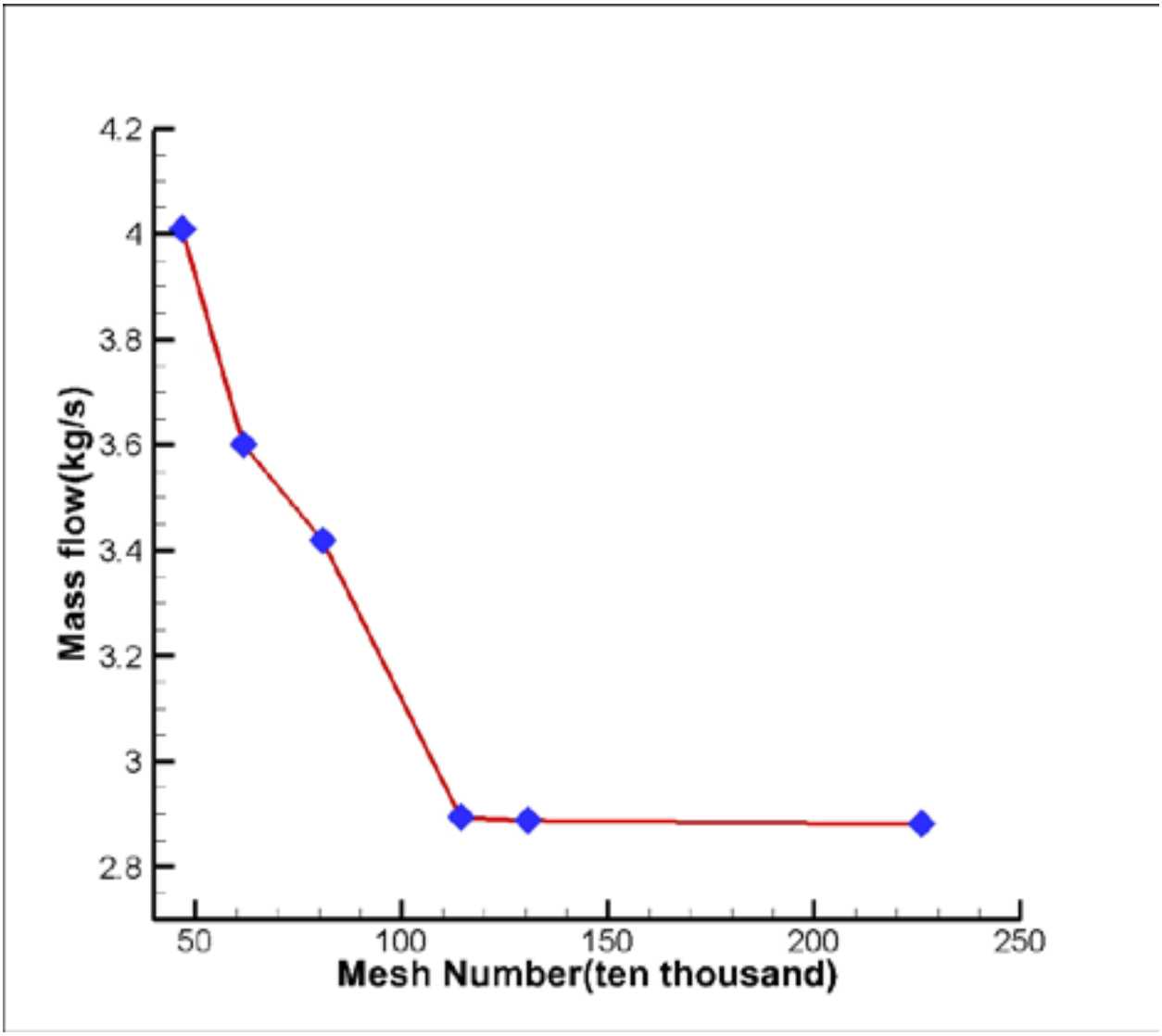

Figure 2.9 Variation of mass flow at outlet along the mesh number

From the curve in Figure 2.9, it turns out the numerical results will be stable if the mesh number is larger than 1.3×10^6. This mesh refinement also ensures good convergence of the VOF method and interface tracking sensitivity. However different tank geometries will be used in this thesis, so different mesh sizes may be required to ensure convergence. Following the mesh sensitivity test, the choice is made to use the

same element size factor ranging from 2.8 to 3.3 (defined through the “global variable factor”) for meshing the different geometries. This assumes similar flow features and spatial-temporal variabilities.

2.4 Simulation results of the short tank

In this part, all the simulations were based on the geometry of ST (see Figure 2.6). Steady calculation is processed. Two water levels configurations were simulated, a low or a medium water level due to the changing height of the outlet. And the inlet discharges tested range from 1 L/s to 5 L/s, with increments 0.5 L/s. The mesh used for those simulations contains 900,000 cells respecting the element size factor determined in section 2.3.2. The detailed geometry and mesh are shown in the Figure 2.8.

2.4.1 Water level

The water levels simulated range from 11.5 cm to 30 cm for water inflows ranging from 1 L/s to 5 L/s. The average water level is determined as a spatial average of interface elevations, corresponding to the cells where the water volume fraction equals to 0.5 (see Figure 2.10). From the isosurface where the water volume fraction equals to 0.5, the free surface does not fluctuate too much due to the comparison of the contour of water volume fraction. When the entrance volume flow rate is fixed, the free surface seems to be horizontal. And the free surface becomes more flat with the increase of the water level.

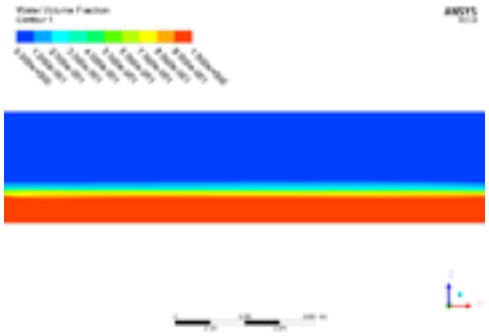

Figure 2.10 Water volume fraction at volume flow rate 1 L/s

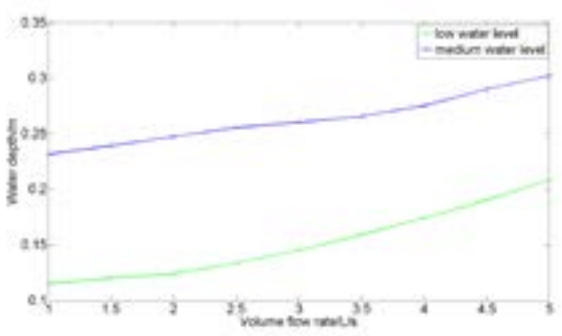

Figure 2.11 Averaged water level along increasing entrance volume flow rate

With the increasing of the entrance volume flow rate, the water level in the tank increases respectively.

2.4.2 Flow pattern

The flow pattern in the tank is analyzed here. Figures 2.12 to 2.27 present 3D streamlines and 2D streamlines in the horizontal plane of Z = 0.04 m which is the height of the center of the inlet, namely the center of the flow injection .All the figures showed correspond to simulations with increasing inflow discharge from 1 L/s to 5 L/s corresponding to water depth in the tank from 11 cm to 21 cm. The 3D streamlines with the “random aspect” for the higher Z values correspond to the air volume fraction. Basically the flow in the short tank is mainly dominated by two eddies (see Figures 2.13, 2.15, 2.17, 2.19, 2.21, 2.23, 2.25 and 2.27), the eddy size decreases along the height direction as the flow injection is near to the bottom (see Figures 2.12, 2.14, 2.16, 2.18, 2.20, 2.22, 2.24 and 2.26). The eddy size and center position change when the entrance mass flow rate increases.

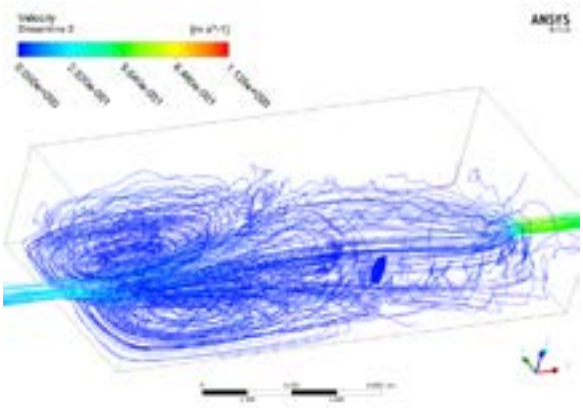

Figure 2.12 3D streamlines at volume flow rate 1 L/s

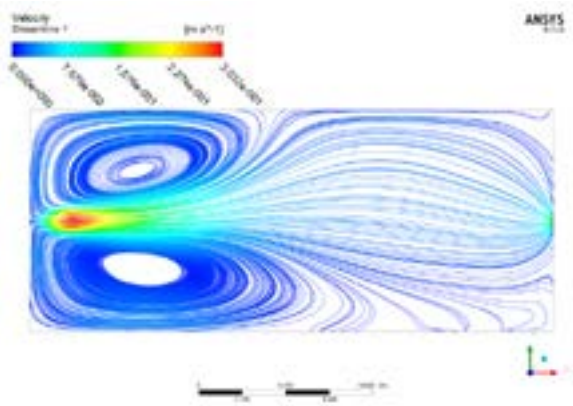

Figure 2.13 2D streamlines at Z = 0.04 m at volume flow rate 1 L/s

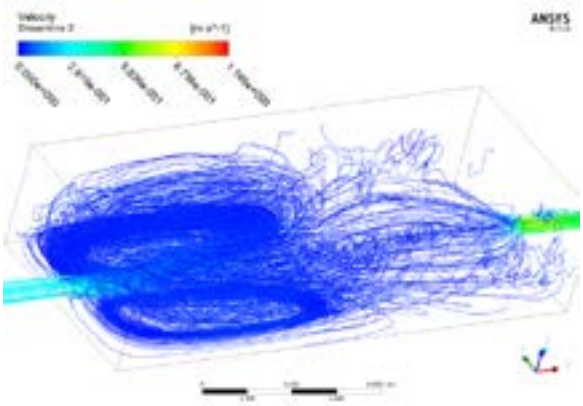

Figure 2.14 3D streamlines at volume flow rate 1.5 L/s

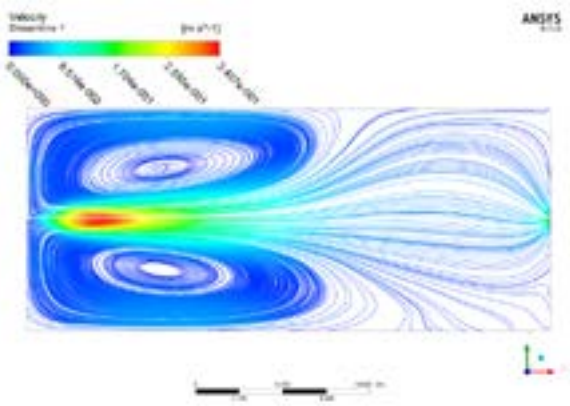

Figure 2.15 2D streamlines at Z = 0.04 m at volume flow rate 1.5 L/s

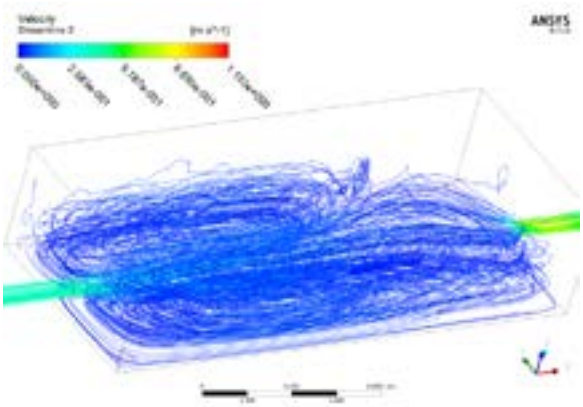

Figure 2.16 3D streamlines at volume flow rate 2 L/s

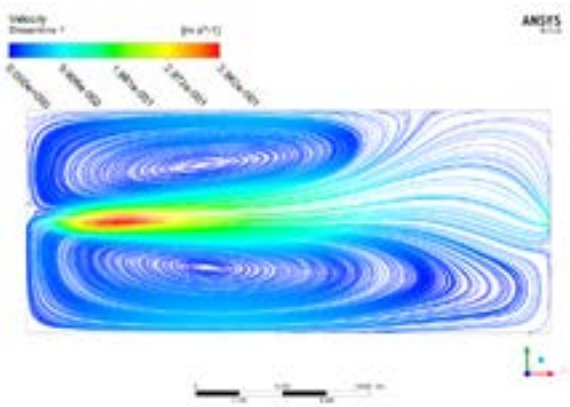

Figure 2.17 2D streamlines at Z = 0.04 m at volume flow rate 2 L/s

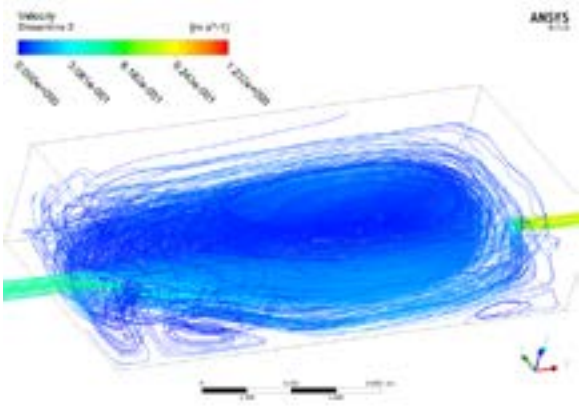

Figure 2.18 3D streamlines at volume flow rate 2.5 L/s

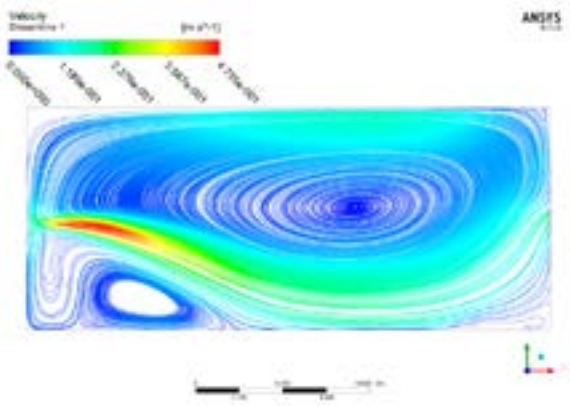

Figure 2.19 2D streamlines at Z = 0.04 m at volume flow rate 2.5 L/s

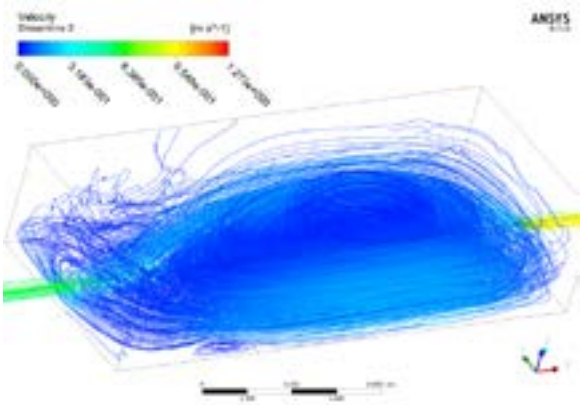

Figure 2.20 3D streamlines at volume flow rate 3 L/s

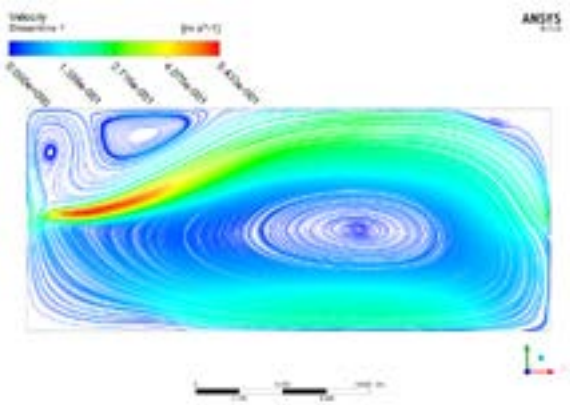

Figure 2.21 2D streamlines at Z = 0.04m at volume flow rate 3 L/s

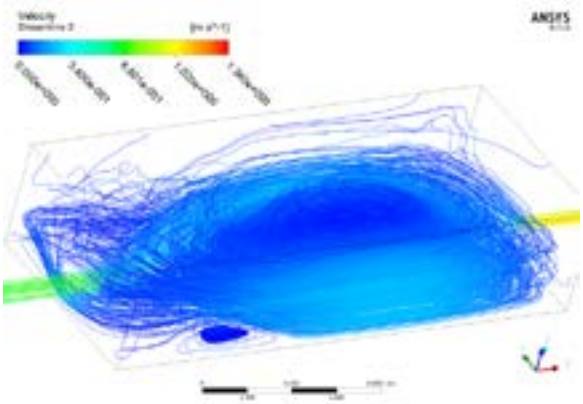

Figure 2.22 3D streamlines at volume flow rate 3.5 L/s

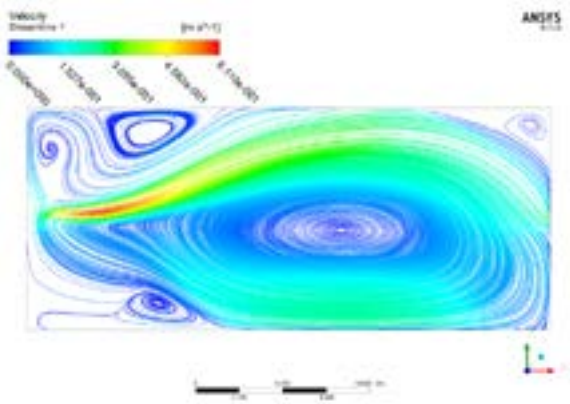

Figure 2.23 2D streamlines at Z = 0.04 m at volume flow rate 3.5 L/s

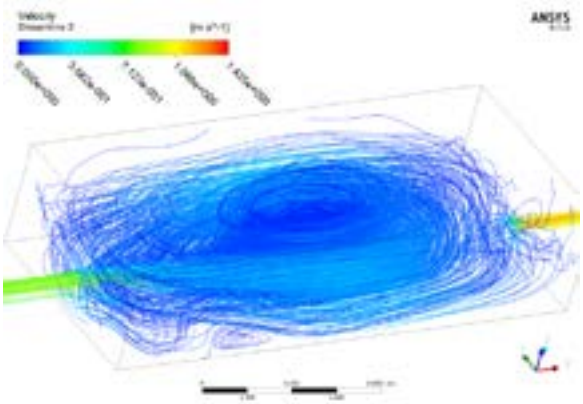

Figure 2.24 3D streamlines at volume flow rate 4 L/s

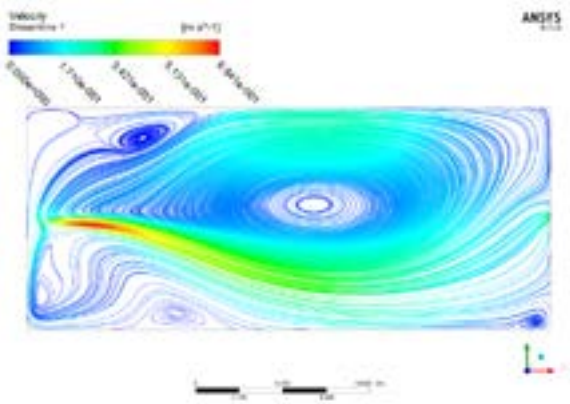

Figure 2.25 2D streamlines at Z = 0.04 m at volume flow rate 4 L/s

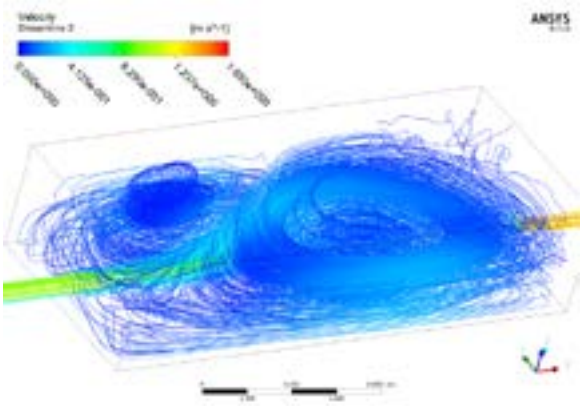

Figure 2.26 3D streamlines at volume flow rate 5 L/s

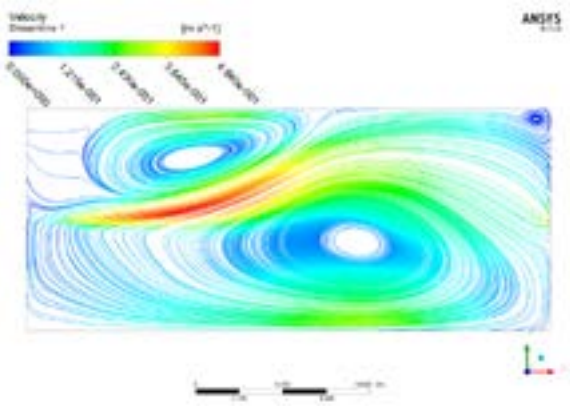

Figure 2.27 2D streamlines at Z = 0.04m at volume flow rate 5 L/s

For volume flow rate lower than 2.5 L/s, the whole flow field is mainly constituted by two eddies of nearly the same size. As evidenced by Figure 2.13, 2.15 and 2.17 eddies are bigger on each side of the jet for increasing inflow discharges.

When the volume flow rate is greater than 2.5 L/s, one eddy is extruded to one corner, the jet corresponding to the flow injection is deviated from the x axis to one side and the other eddy nearly occupies all the rest of the tank's surface. With increasing the entrance volume flow rate continuously, other small size eddies appear near the corners and walls. Note that symmetric or quasi-symmetric patterns only occur for mass flow rates equal to 1 L/s and 1.5 L/s hence low water levels. Other cases with increasing inflow discharge result in asymmetries and complex flow patterns.

The flow pattern will be different when the water level in the tank changes under same entrance volume flow rate. Table 2.2 and Table 2.3 describe the flow patterns when the water depth is at low level and medium level respectively.

Table 2.3 Flow patterns under low water level

Inlet discharges (L/s)	Averaged water depth (cm)	Flow patterns
1	11.48	Quasi-symmetry
1.5	11.98	Symmetry
2	12.37	Quasi-symmetry
2.5	13.35	Asymmetry
3	14.49	Asymmetry
3.5	15.91	Asymmetry
4	17.39	Asymmetry

4.5	19.01	Asymmetry
5	20.82	Asymmetry

Table 2.4 Flow patterns under medium water level

Inlet discharges (L/s)	Averaged water depth (cm)	Flow patterns
1	23.13	Symmetry
1.5	23.90	Symmetry
2	24.71	Symmetry
2.5	25.52	Symmetry
3	26.00	Asymmetry
3.5	26.53	Asymmetry
4	27.51	Asymmetry
4.5	28.99	Asymmetry
5	30.20	Asymmetry

The flow patterns are influenced by the water level for similar inflow discharge. In the symmetry pattern, the eddy for medium water level has bigger size than that under low water level. In the asymmetry pattern, both eddies have almost the same size for medium water level, unlike the situation for low water level where one eddy is extruded to the corner.

2.4.3 Wall shear stress and turbulent kinetic energy

Wall shear stress and turbulent kinetic energy are flow parameters that can play an important role for sediment transport. Indeed, in the following those two parameters are treated as criterion for the sedimentation of particles.

The calculation of wall shear stress can be written as:

$$\tau_w = \mu \left(\frac{\partial u}{\partial y}\right)_{y=0}$$

Where μ is the dynamic viscosity, u is the flow velocity parallel to the wall and y is the distance to the wall. According to the definition of the wall shear stress, the value of wall shear stress mainly is mainly determined by the gradient near the wall, namely the flow area with less turbulence is the region where the shear stress is quite low.

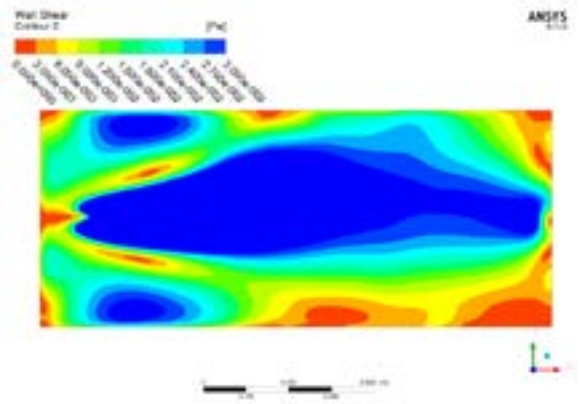

Figure 2.28 Wall shear stress at volume flow rate 1 L/s

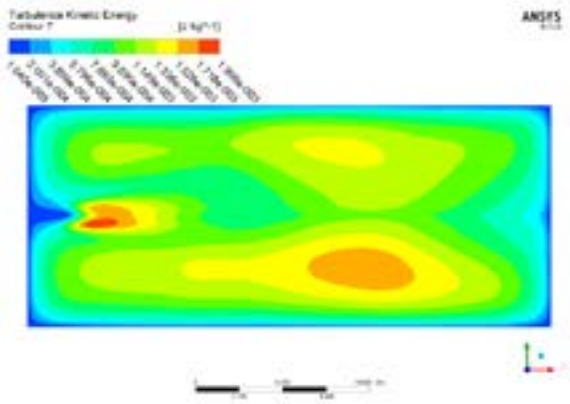

Figure 2.29 Turbulent kinetic energy at volume flow rate 1 L/s

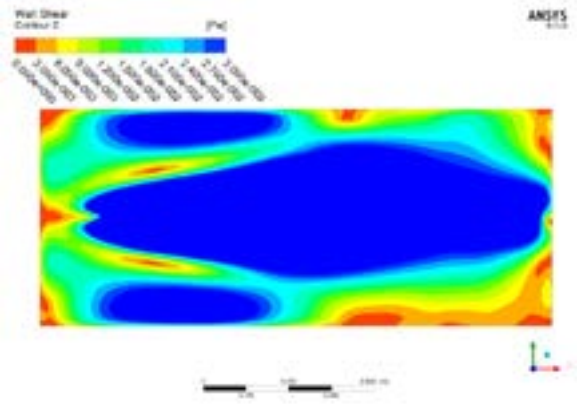

Figure 2.30 Wall shear stress at volume flow rate 1.5 L/s

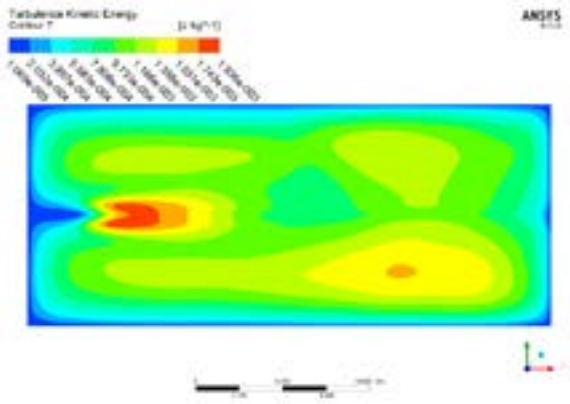

Figure 2.31 Turbulent kinetic energy at volume flow rate 1.5 L/s

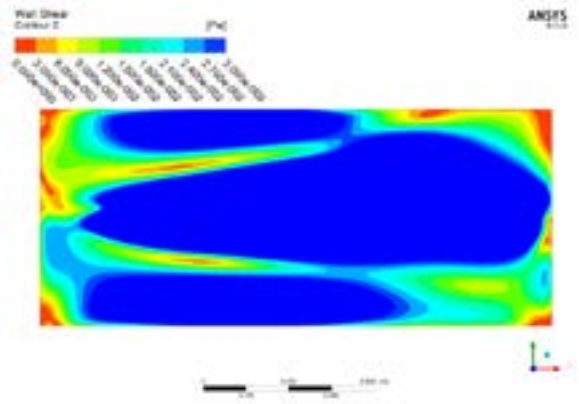

Figure 2.32 Wall shear stress at volume flow rate 2 L/s

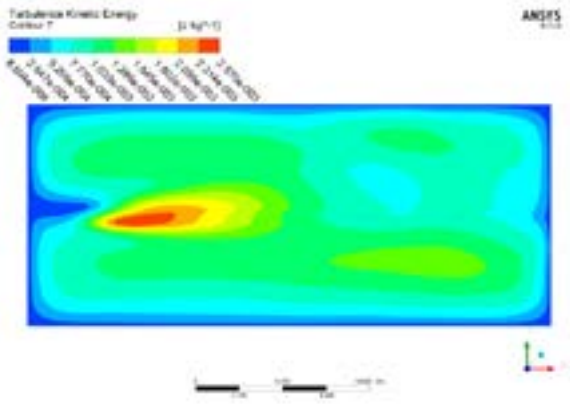

Figure 2.33 Turbulent kinetic energy at volume flow rate 2 L/s

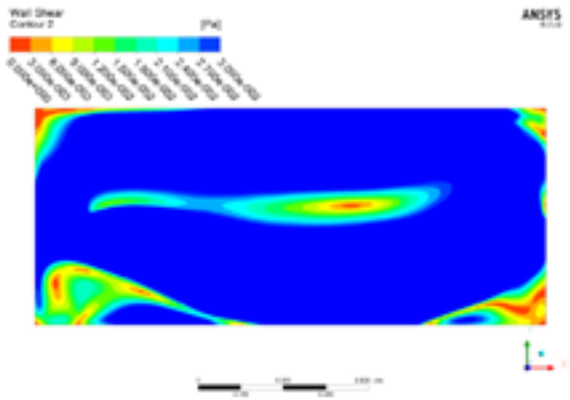

Figure 2.34 Wall shear stress at volume flow rate 2.5 L/s

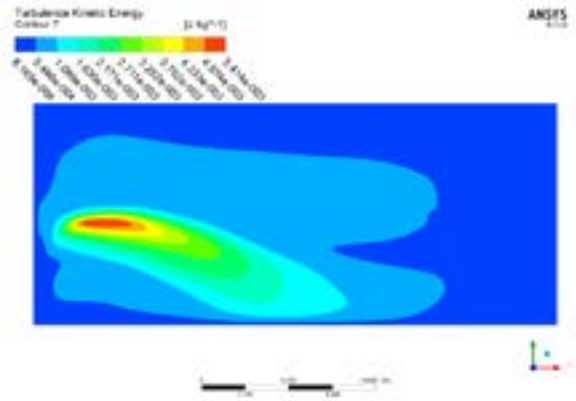

Figure 2.35 Turbulent kinetic energy at volume flow rate 2.5 L/s

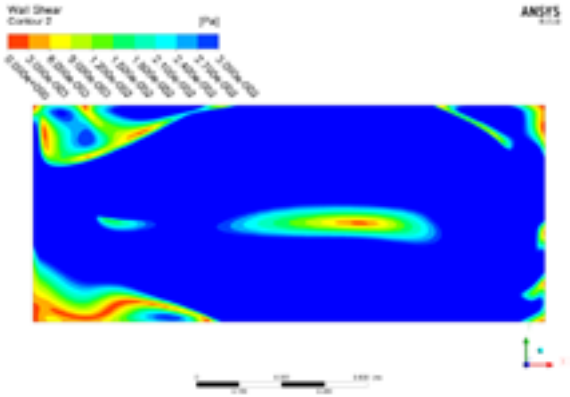

Figure 2.36 Wall shear stress at volume flow rate 3 L/s

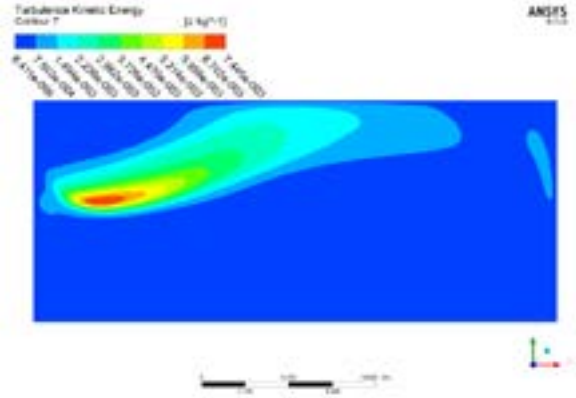

Figure 2.37 Turbulent kinetic energy at volume flow rate 3 L/s

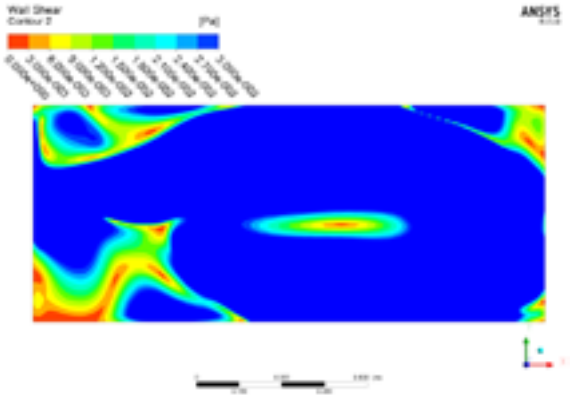

Figure 2.38 Wall shear stress at volume flow rate 3.5 L/s

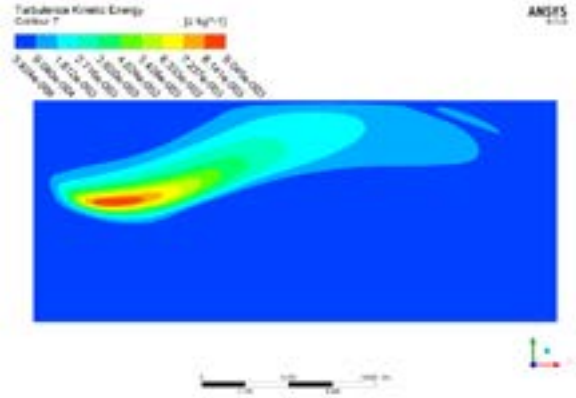

Figure 2.39 Turbulent kinetic energy at volume flow rate 3.5 L/s

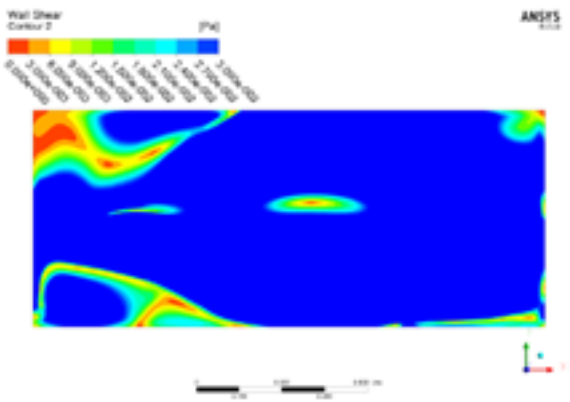

Figure 2.40 Wall shear stress at volume flow rate 4 L/s

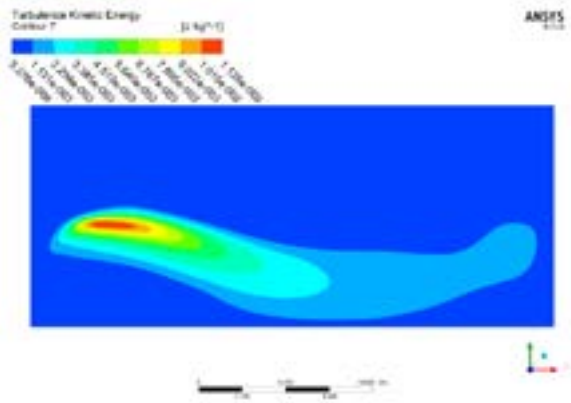

Figure 2.41 Turbulent kinetic energy at volume flow rate 4 L/s

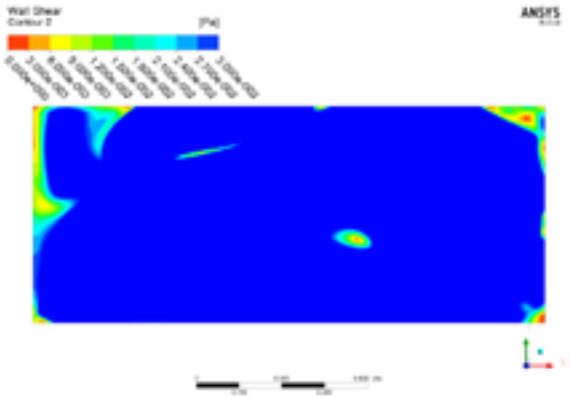

Figure 2.42 Wall shear stress at volume flow rate 5 L/s

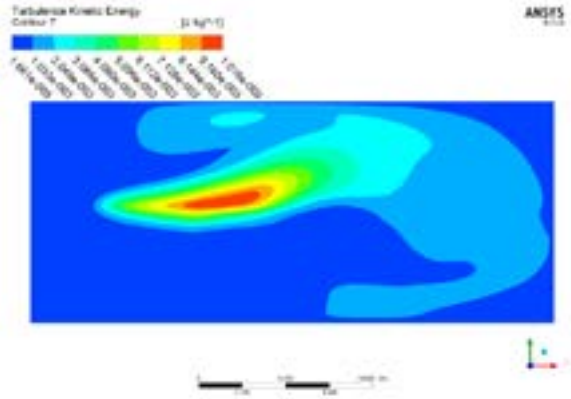

Figure 2.43 Turbulent kinetic energy at volume flow rate 5 L/s

The region where the value of wall shear stress is quite low occurs at the center of the eddy, near the corners and walls. With the increase of entrance volume flow rate wall shear stress and turbulent kinetic energy generally increase. The high value region of turbulent kinetic energy appears at the flow injection region.

2.4.4 Velocity

Velocity field is another important parameter to analyze the flow. To demonstrate the velocity field in the tank, the detailed information of velocity of entrance volume flow rate equals to 1L/s is shown. Five vertical lines are selected where the velocity at X

direction along Z position are presented, the position of these five vertical lines are: X=0.3, 0.6, 0.9, 1.2, 1.5 m. The center line of the pipe is selected to show the velocity distribution along X direction. Three Y-Z planes are chosen for display the X-velocity contour, those planes are placed at X = 0.3, 0.6, 0.9 m.

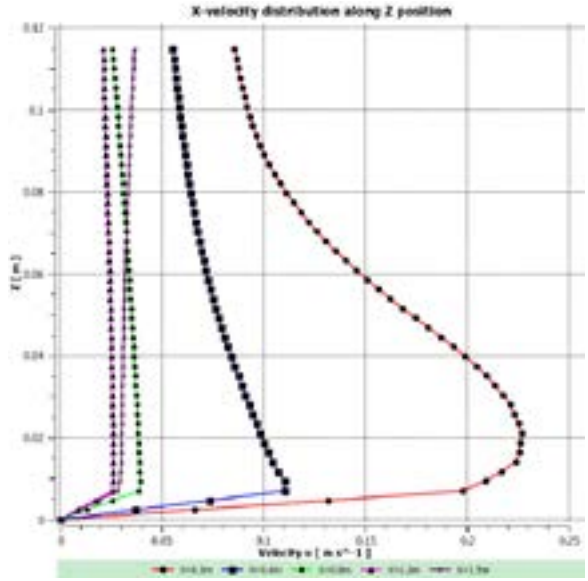

Figure 2.44 X-velocity distribution along Z position at volume flow rate 1 L/s

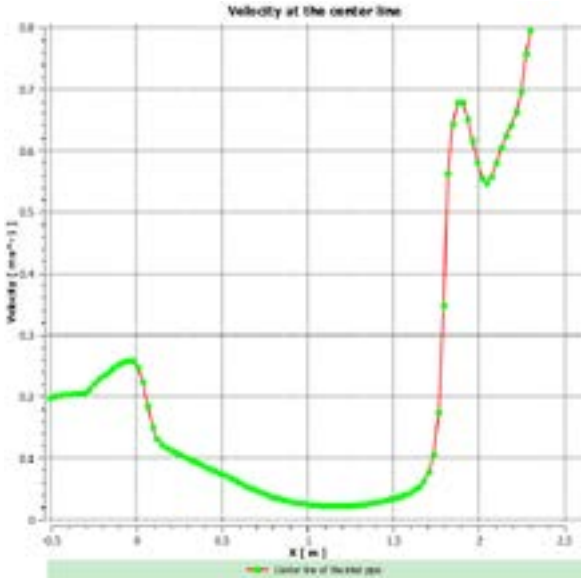

Figure 2.45 Velocity distribution at the center line at volume flow rate 1 L/s

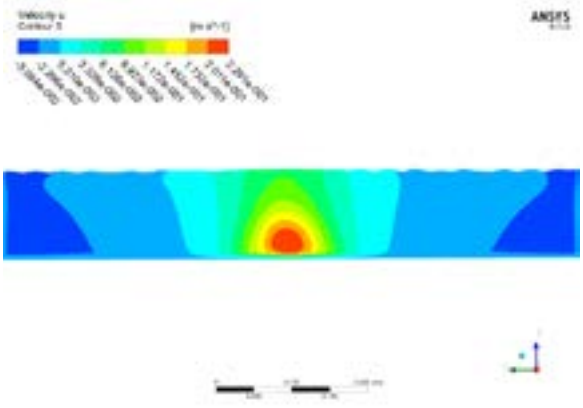

Figure 2.46 X-velocity contour at X = 0.3 m at volume flow rate 1 L/s

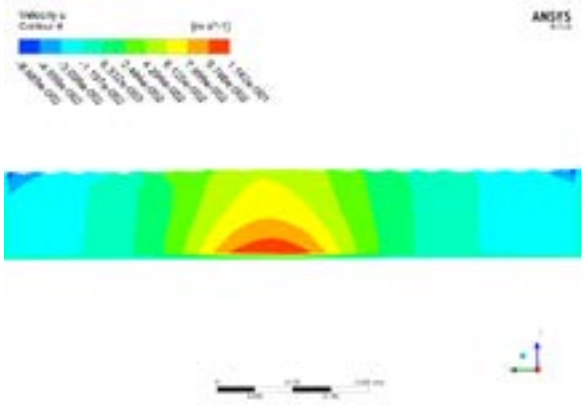

Figure 2.47 X-velocity contour at X = 0.6 m at volume flow rate 1 L/s

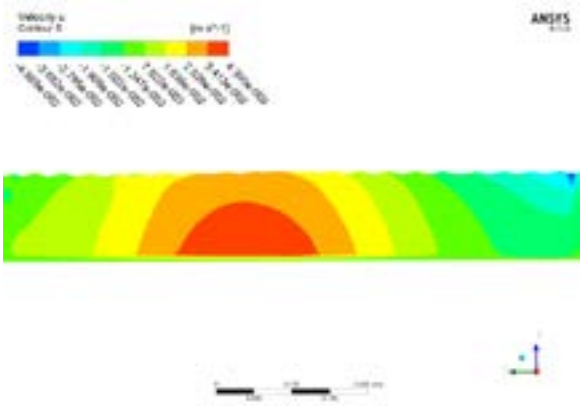

Figure 2.48 X-velocity contour at X = 0.3 m at volume flow rate 1 L/s

From Figure 2.44, the variation of velocity along the Z position can be divided into two parts, the first part is from the bottom to the center of flow injection where the velocity increases along Z position. The second part is from the center of flow injection to the free-surface where the velocity decreases along Z position. The maximum value of each curve in the figure corresponds to the center of the flow injection. Note that unsurprisingly, this maximum flow injection velocity increases with inflow discharge. For longitudinal positions X > 50% of the tank length, velocity decreases by 90%.

The velocity distribution along the center line can be divided into three parts (see Figure 2.45). The first part is the influence zone of the inlet pipe with the significant variability and maximal velocity described above. The second part is in the tank, where the velocity decreases continuously along the flow direction. The third part is in the outlet pipe, where the flow cross section diminishes sharply and the velocity augments rapidly.

The velocity contour (see Figure 2.46, 2.47 and 2.48) along X direction shows the deviation of maximal velocity zone along Y direction. Along flow direction, the height of the center of injection is decreasing and the center of injection deviate to one side of the tank with the variation of the entrance volume flow rate.

2.5 Simulation results of the long tank

In this part, all the simulations are based on the geometry of LT (see Figure 2.7). Due to the modified outlet height, two water level configurations were simulated: a low or a medium water level. The volume flow rate simulated range from 1 L/s to 5 L/s, with

increments of 0.5 L/s. The mesh used in the simulation contains about 1,600,000 cells. The detailed geometry and mesh are shown in the Figure 2.7.

2.5.1 Water level

The VOF method is able to track the interface between water and air depending on air and water volume fraction as explained in section 2.4.1. The water levels simulated range from 14 cm to about 30 cm for water inflows ranging from 1 L/s to 5 L/s with increments 0.5 L/s for low water level.

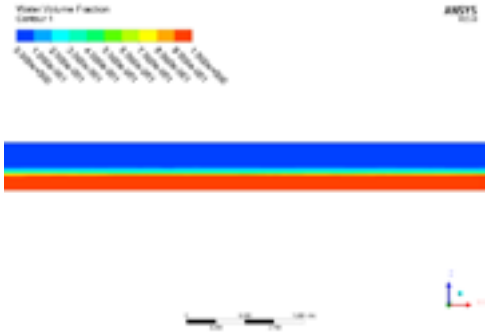

Figure 2.49 Water volume fraction at volume flow rate 1 L/s

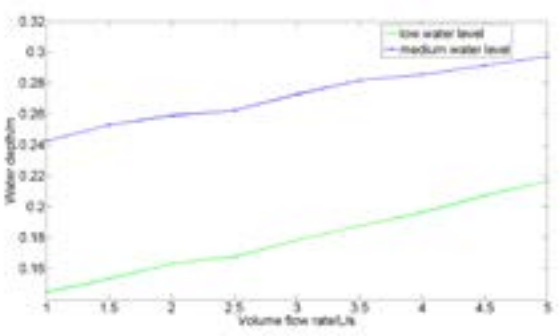

Figure 2.50 Averaged water level along increasing entrance volume flow rate

The variation of the water level in the tank with the increase of the entrance mass flow rate is similar to the situation of simulation in ST.

2.5.2 Flow pattern

As previously, the flow patterns in LT is investigated through the analysis of simulated eddy distributions, streamlines in an horizontal plane corresponding to the center of the inlet pipe. Indeed streamlines in this plane are supposed to be the most representative of inlet jet influence.

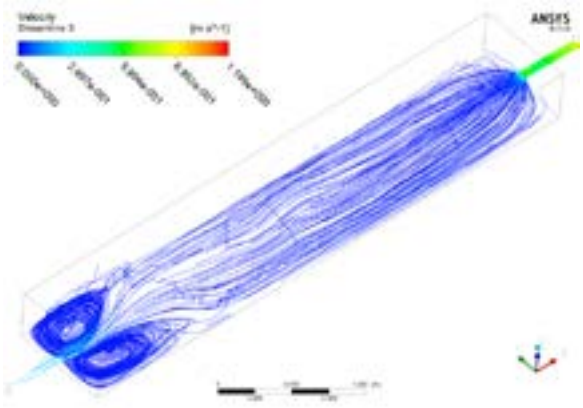

Figure 2.51 3D streamlines at volume flow rate 1 L/s

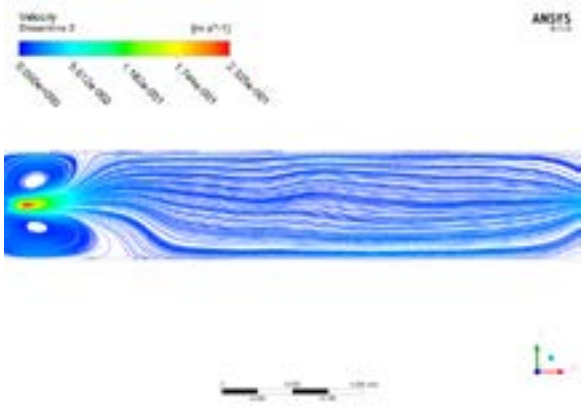

Figure 2.52 2D streamlines at Z = 0.04 m at volume flow rate 1 L/s

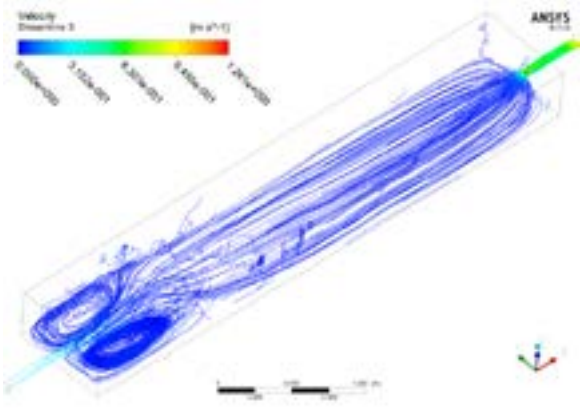

Figure 2.53 3D streamlines at volume flow rate 1.5 L/s

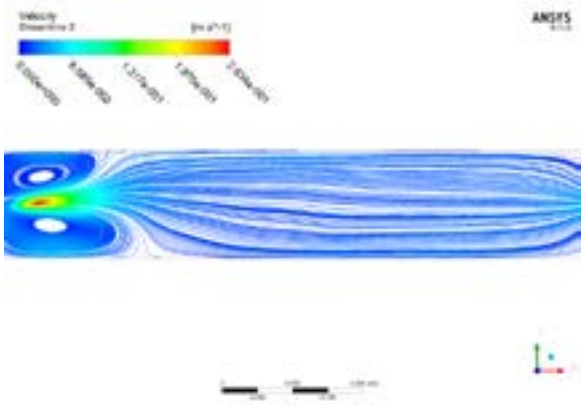

Figure 2.54 2D streamlines at Z = 0.04 m at volume flow rate 1.5 L/s

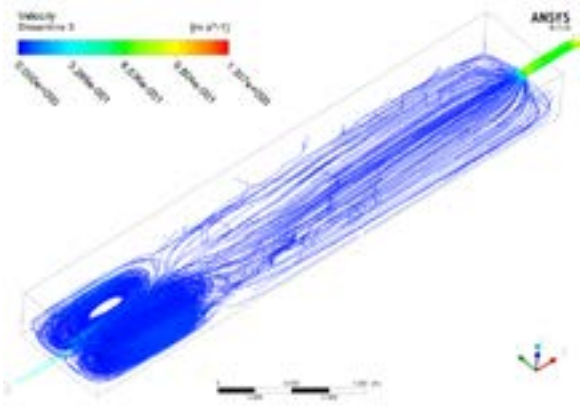

Figure 2.55 3D streamlines at volume flow rate 2 L/s

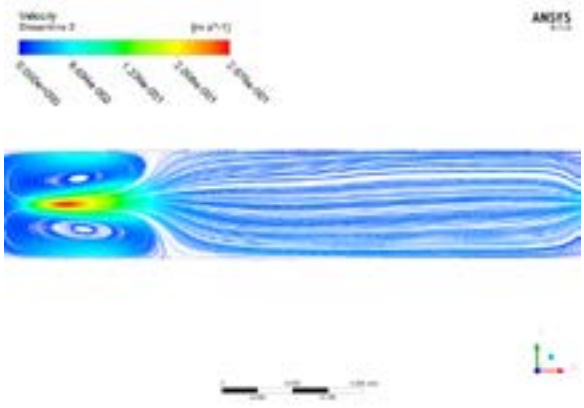

Figure 2.56 2D streamlines at Z = 0.04 m at volume flow rate 2 L/s

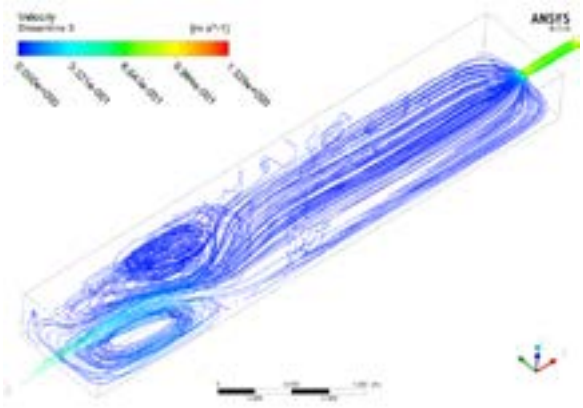

Figure 2.57 3D streamlines at volume flow rate 2.5 L/s

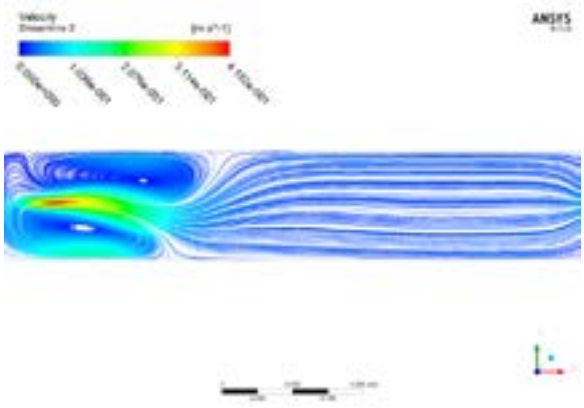

Figure 2.58 2D streamlines at Z = 0.04 m at volume flow rate 2.5 L/s

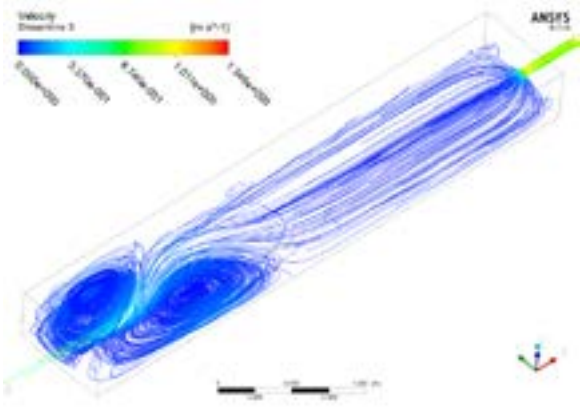

Figure 2.59 3D streamlines at volume flow rate 3 L/s

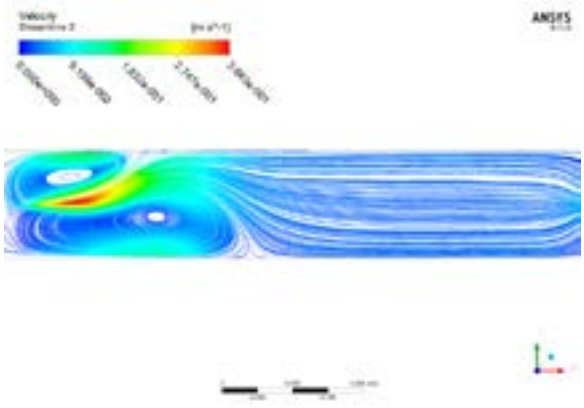

Figure 2.60 2D streamlines at Z = 0.04 m at volume flow rate 3 L/s

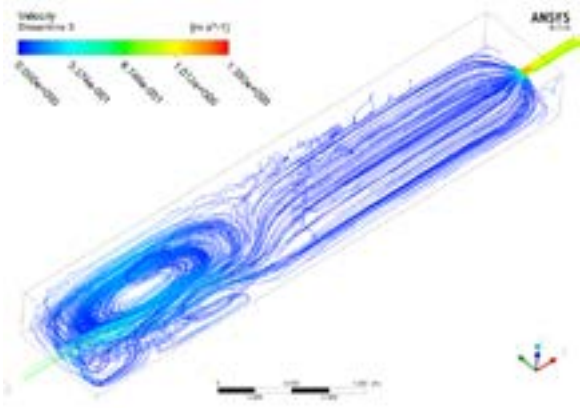

Figure 2.61 3D streamlines at volume flow rate 3.5 L/s

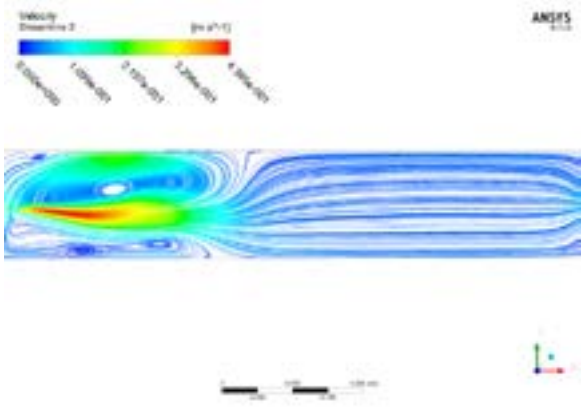

Figure 2.62 2D streamlines at Z = 0.04 m at volume flow rate 3.5 L/s

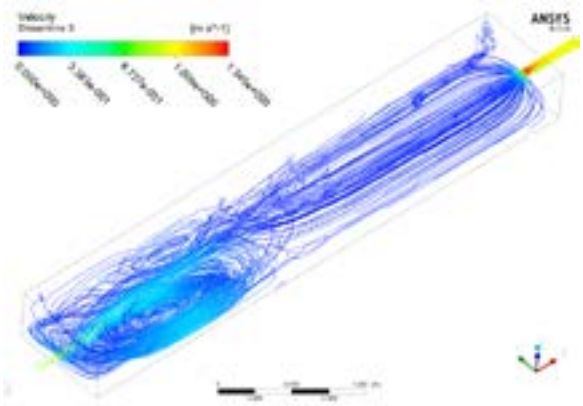

Figure 2.63 3D streamlines at volume flow rate 4 L/s

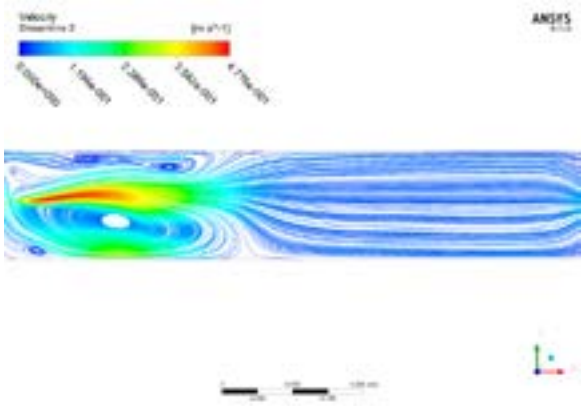

Figure 2.64 2D streamlines at Z = 0.04 m at volume flow rate 4 L/s

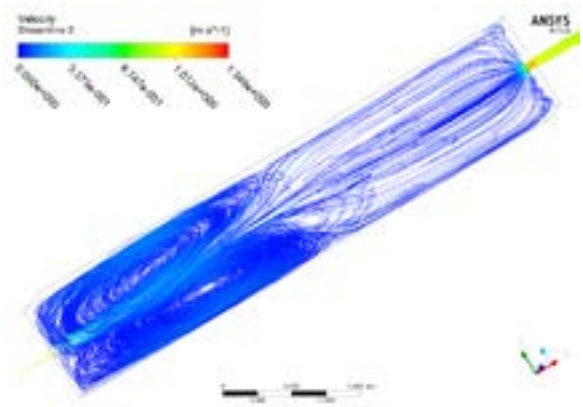

Figure 2.65 3D streamlines at volume flow rate 4.5 L/s

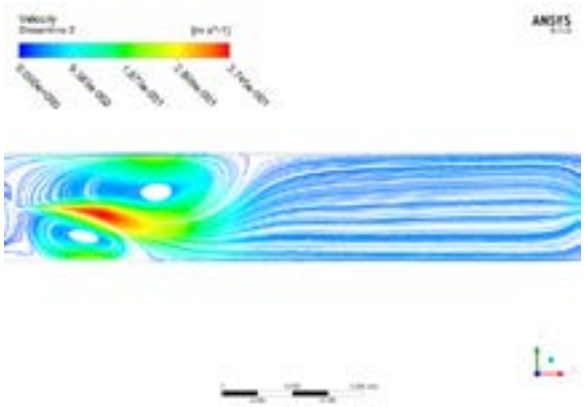

Figure 2.66 2D streamlines at Z = 0.04 m at volume flow rate 4.5 L/s

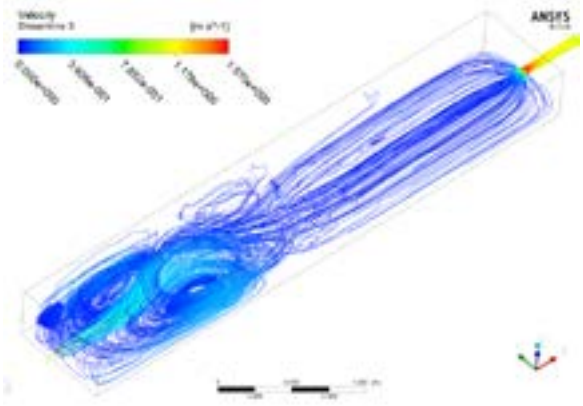

Figure 2.67 3D streamlines at volume flow rate 5 L/s

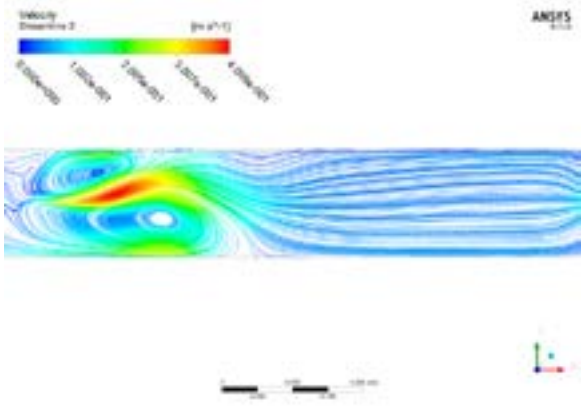

Figure 2.68 2D streamlines at Z = 0.04 m at volume flow rate 5 L/s

The flow structures are mainly composed of two eddies in the front of the tank and a rather uniform flow part in the back of the tank. Again the size and location of eddies changes with increasing mass flow rates as the dissymmetry of the flow pattern. In the back of the tank the flow is smoother and the velocity remains quite low compared to the entrance velocity. Symmetric flow patterns do not exist when the water level is low, the reason might be that the injection is close to the free surface, hence less water pressure acts on the jet which develops with less limitations.

Table 2.5 Flow patterns under low water level

Inlet discharges (L/s)	Averaged water depth (cm)	Flow patterns
1	14.46	Quasi-symmetry
1.5	15.32	Quasi-symmetry
2	16.29	Quasi-symmetry
2.5	16.74	Quasi-symmetry
3	17.83	Asymmetry
3.5	18.75	Asymmetry
4	19.61	Asymmetry
4.5	20.72	Asymmetry
5	21.65	Asymmetry

Table 2.6 Flow patterns under low water level

Inlet discharges (L/s)	Averaged water depth (cm)	Flow patterns
1	24.25	Symmetry
1.5	25.28	Symmetry
2	25.89	Symmetry
2.5	26.22	Asymmetry
3	27.27	Quasi-symmetry
3.5	28.18	Symmetry
4	28.54	Symmetry
4.5	29.14	Quasi-symmetry
5	29.72	Asymmetry

The eddies in the long tank only exist in a region corresponding to the first 40% of the tank along flow direction, the rest of the tank is filled by uniform flow. With higher water level in the tank, the flow pattern is more likely to be symmetry. With higher inlet discharges, the flow pattern in low water level is asymmetry and the flow pattern change from symmetry to asymmetry in high water level.

2.5.3 Wall shear stress and turbulent kinetic energy

As previously, shear stress is calculated. From Figures 2.69 to 2.86, it is clear that the distribution of wall shear stress on the bottom varies significantly when the mass flow rate changes from 1 L/s to 5 L/s. The more inflow discharge and the more uniform shear stress distribution tending to the value 0.017 Pa.

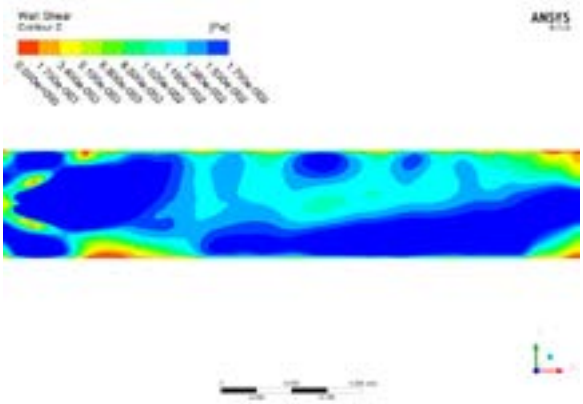

Figure 2.69 Wall shear stress at volume flow rate 1 L/s

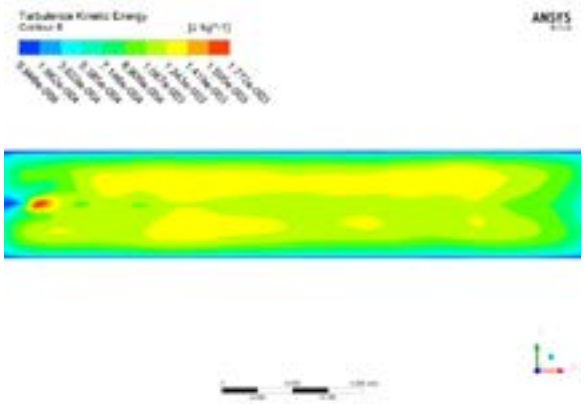

Figure 2.70 Turbulent kinetic energy at volume flow rate 1 L/s

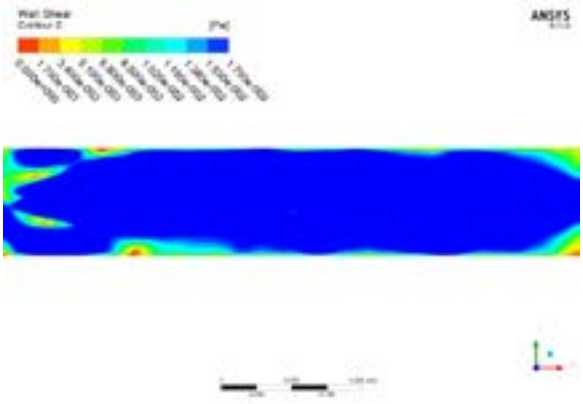

Figure 2.71 Wall shear stress at volume flow rate 1.5 L/s

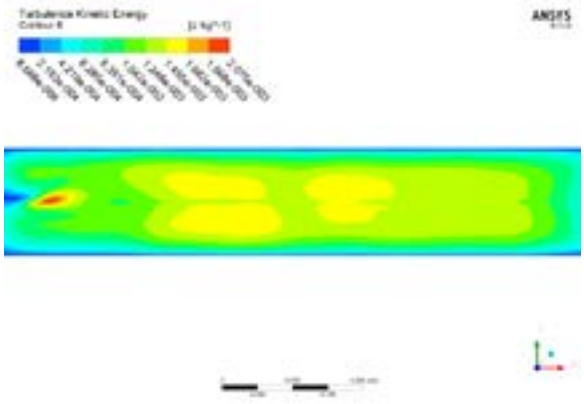

Figure 2.72 Turbulent kinetic energy at volume flow rate 1.5 L/s

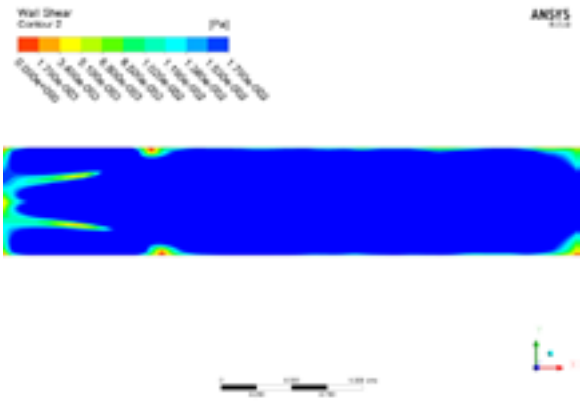

Figure 2.73 Wall shear stress at volume flow rate 2 L/s

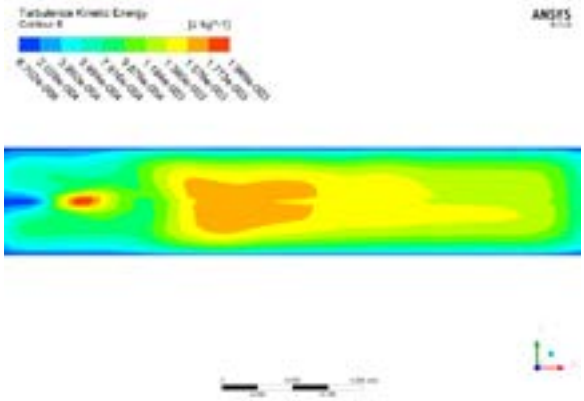

Figure 2.74 Turbulent kinetic energy at volume flow rate 2 L/s

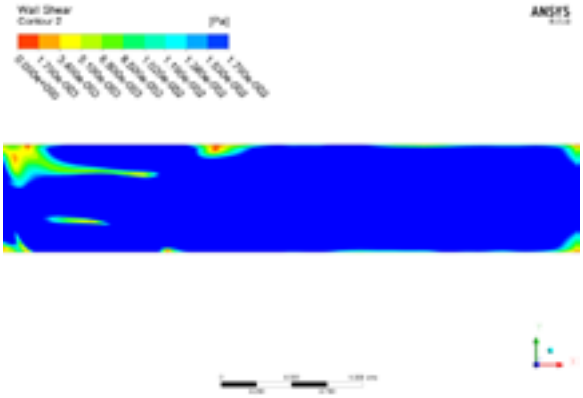

Figure 2.75 Wall shear stress at volume flow rate 2.5 L/s

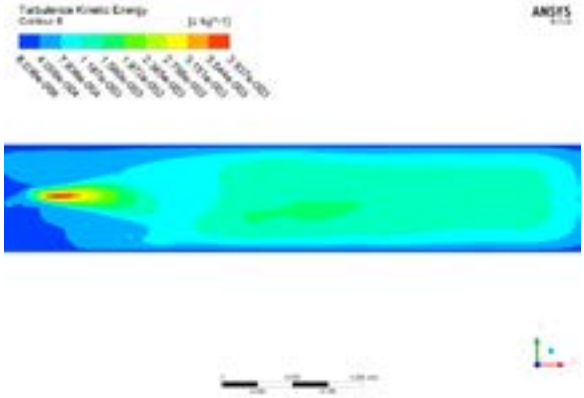

Figure 2.76 Turbulent kinetic energy at volume flow rate 2.5 L/s

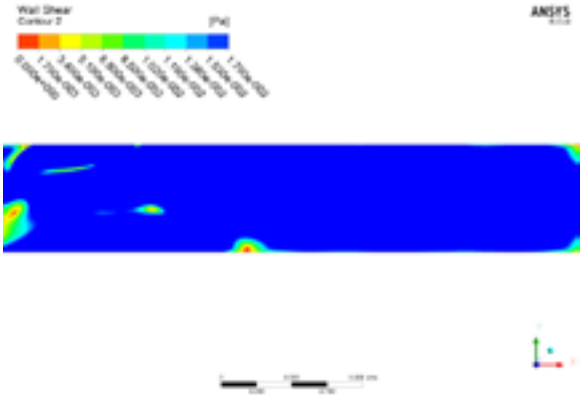

Figure 2.77 Wall shear stress at volume flow rate 3 L/s

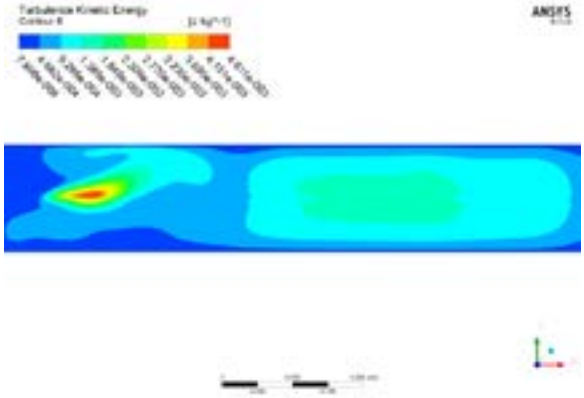

Figure 2.78 Turbulent kinetic energy at volume flow rate 3 L/s

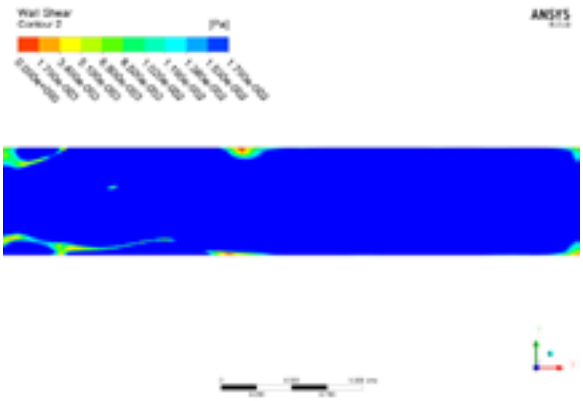

Figure 2.79 Wall shear stress at volume flow rate 3.5 L/s

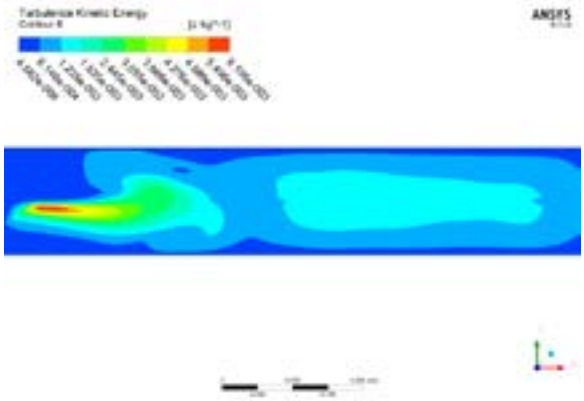

Figure 2.80 Turbulent kinetic energy at volume flow rate 3.5 L/s

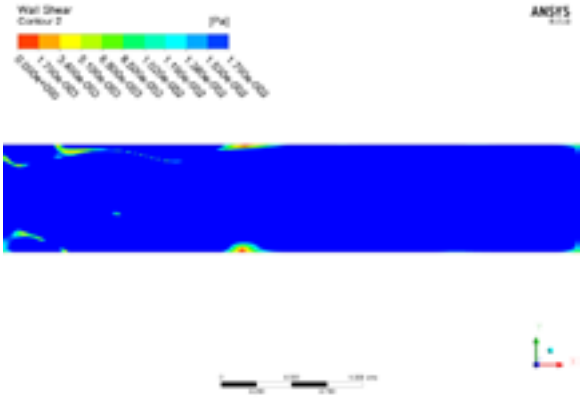

Figure 2.81 Wall shear stress at volume flow rate 4 L/s

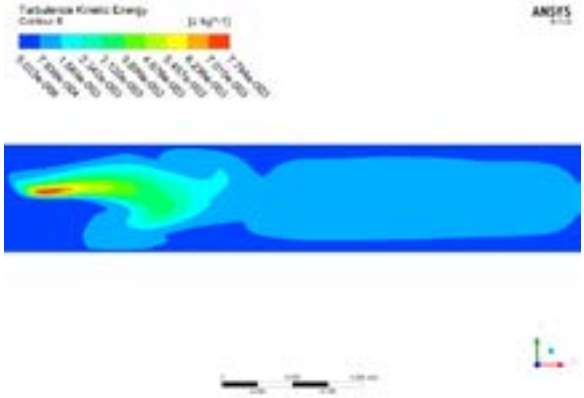

Figure 2.82 Turbulent kinetic energy at volume flow rate 4 L/s

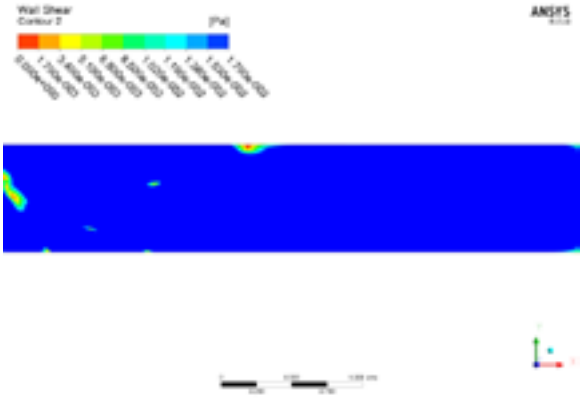

Figure 2.83 Wall shear stress at volume flow rate 4.5 L/s

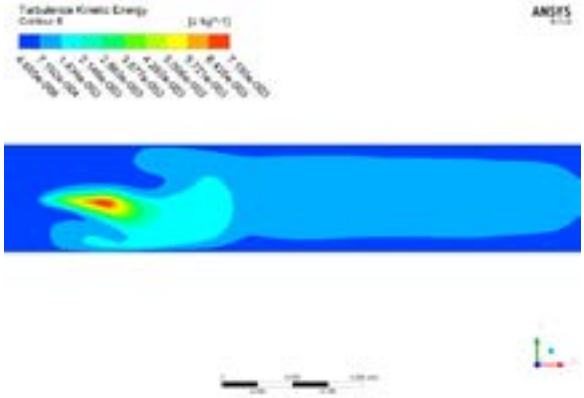

Figure 2.84 Turbulent kinetic energy at volume flow rate 4.5 L/s

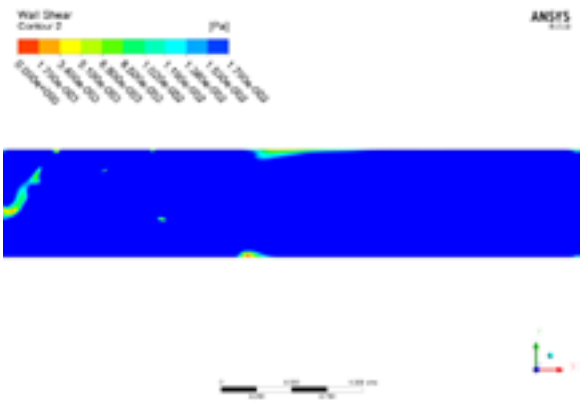

Figure 2.85 Wall shear stress at volume flow rate 5 L/s

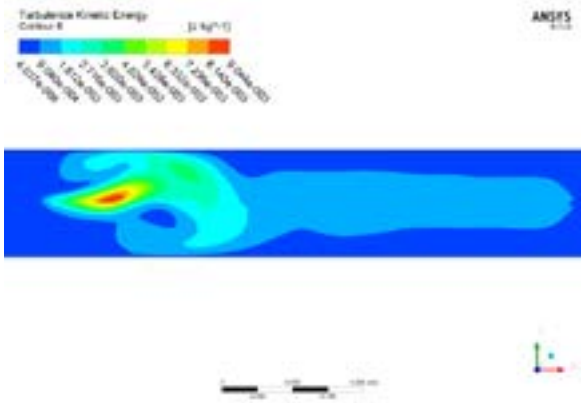

Figure 2.86 Turbulent kinetic energy at volume flow rate 5 L/s

Normally, low shear stress corresponds to the particle deposition zone. With the increase of entrance inlet discharge, the region where the value of wall shear stress is below the estimated critical bed shear stress diminish sharply. In the meantime, turbulent kinetic energy increases rapidly with inlet discharge.

2.5.4 Velocity

Again, velocity field in the tank is analyzed here for inflow discharge corresponding to 1 L/s. 12 vertical lines are selected along the X axis (for y=0) for plotting the vertical variation (along Z) of the longitudinal component of velocity. The position of these vertical lines are: X = 0.3, 0.6, 0.9, 1.2, 1.5, 1.6, 1.7, 1.8, 2.1, 2.4, 2.7, 3 m. The center line of the pipe is selected to show the velocity distribution along X direction. Three Y-Z planes are chosen for displaying the X-velocity contour, those planes are placed at X = 0.3, 0.6, 0.9 m.

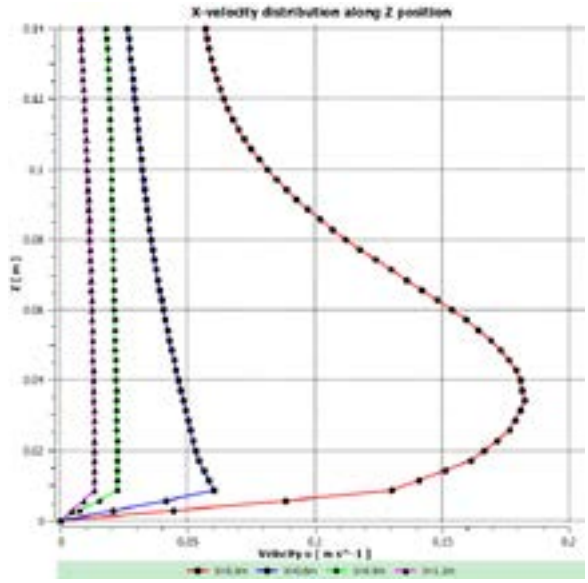

Figure 2.87 X-velocity distribution along Z position at volume flow rate 1 L/s

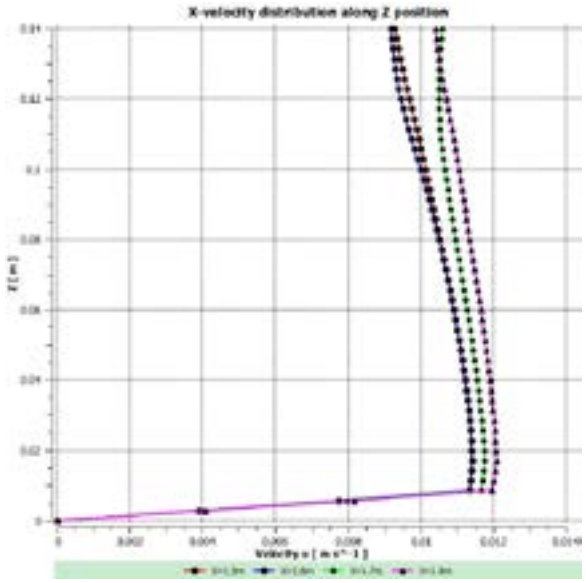

Figure 2.88 X-velocity distribution along Z position at volume flow rate 1 L/s

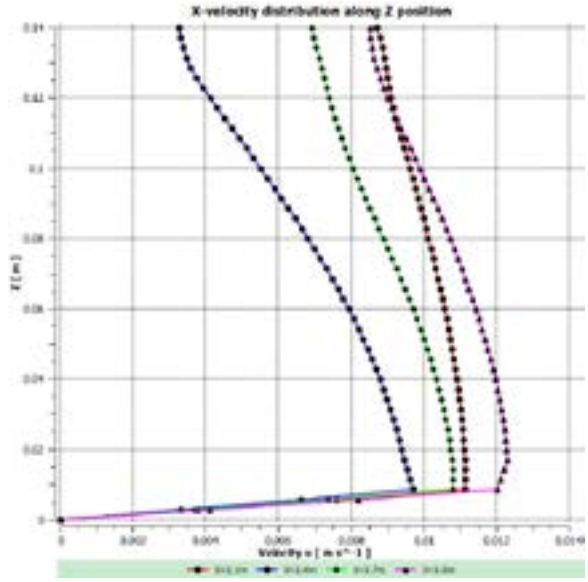

Figure 2.89 X-velocity distribution along Z position at volume flow rate 1 L/s

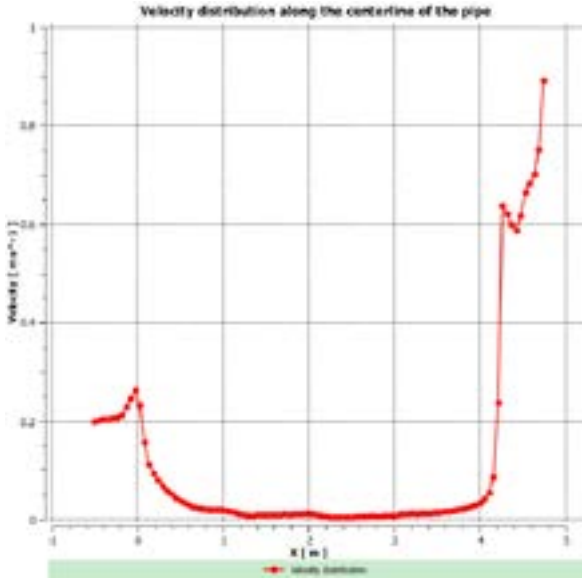

Figure 2.90 Velocity distribution at the center line at volume flow rate 1 L/s

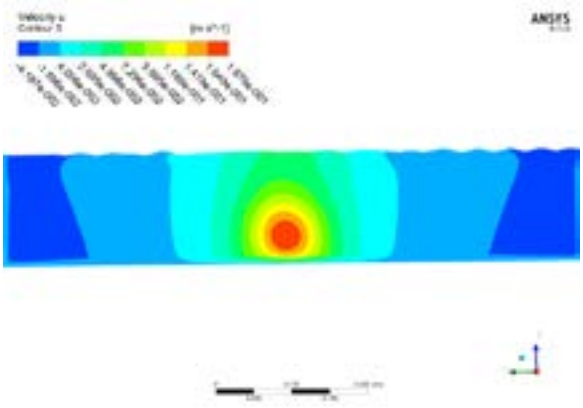

Figure 2.91 X-velocity contour at X = 0.3 m at volume flow rate 1 L/s

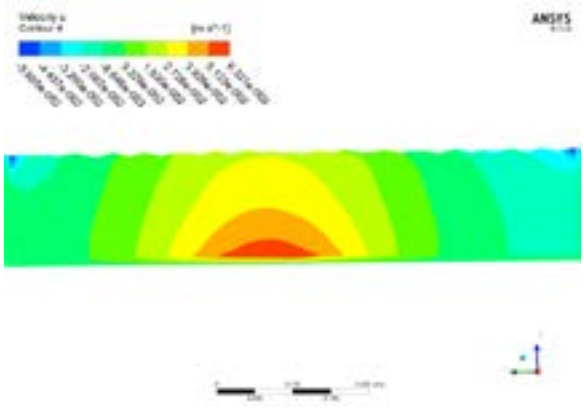

Figure 2.92 X-velocity contour at X = 0.6 m at volume flow rate 1 L/s

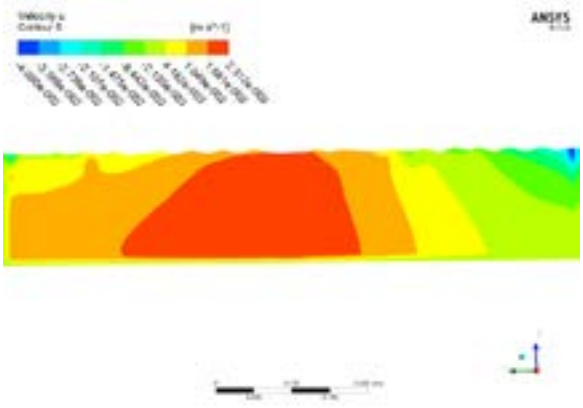

Figure 2.93 X-velocity contour at X = 0.9 m at volume flow rate 1 L/s

For the low water level simulation, the injection does not deviate much from the center, which makes the flow patterns under all the value of mass flow rate quasi-symmetric.

From the distribution of the velocity in Figure 2.90, X = 0.9 m, velocity decreases to 20% of the entrance velocity. Moreover the flow field after X = 0.9 m tends to be more uniform, and no big recirculation exist in this part. The variation trend of the velocity along the Z position becomes the same and more simple. With the increasing of the volume flow rate, the center of the injection moves up (not shown in the Figures, from the comparison of all the velocity distribution with all the volume flow rate).

2.6 Simulation results of the long tank with cavity

In this section, all the simulations are based on the geometry of the long tank plus a cavity positioned at X =2.1 m (where the center of the cavity locates). Five ratio of length (Y direction in Figure 2.8) to width (X direction in Figure 2.8) of the cavity are simulated, including 2, 3, 4, 5, 6. The ratio 4 is approximately the same as the experimental device presented in chapter 4. Two different water levels, low and medium are simulated thanks to different boundary condition. Again the mass flow rate ranges from 1 L/s to 5 L/s, with increments of 0.5 L/s. The mesh used in the simulation is about 1,800,000 cells. The detailed geometry and mesh are shown in the Figure 2.8.

2.6.1 Water level

Water volume fraction is also used for tracking the interface. The water height in the tank with cavity is similar to the water height in the tank without cavity.

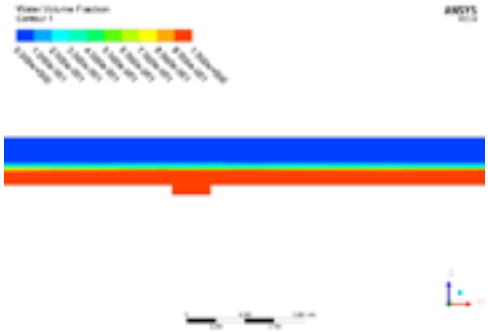

Figure 2.94 Water volume fraction at volume flow rate 1 L/s

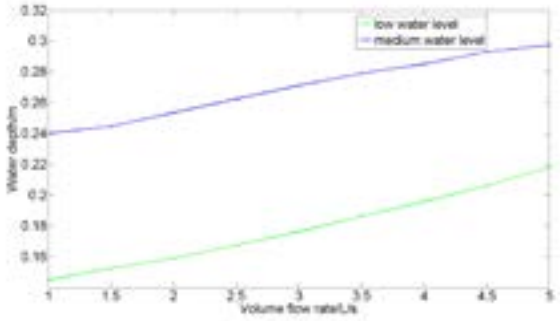

Figure 2.95 Averaged water level along increasing inlet discharge

2.6.2 Flow pattern

Surface streamlines and 3D streamlines are also used for characterizing the flow pattern in the long tank with cavity.

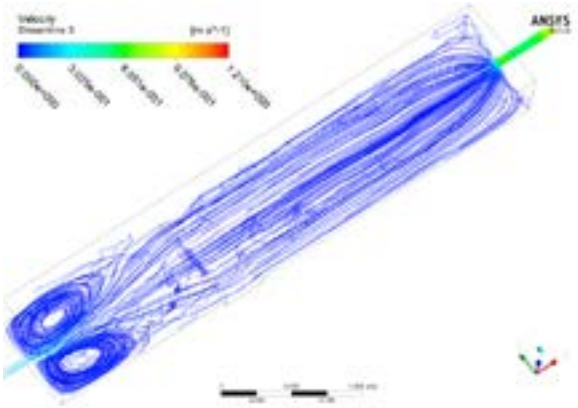

Figure 2.96 3D streamlines at volume flow rate 1 L/s

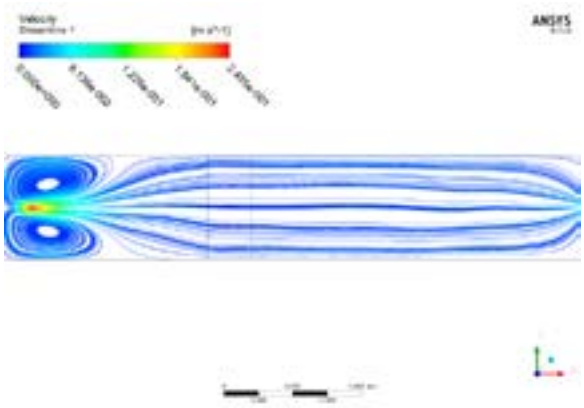

Figure 2.97 2D streamlines at Z = 0.04 m at volume flow rate 1 L/s

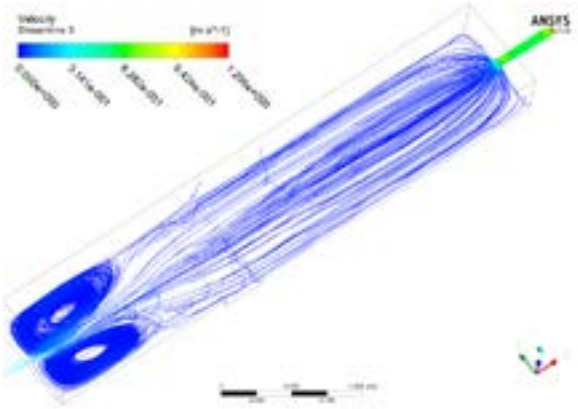

Figure 2.98 3D streamlines at volume flow rate 2.5 L/s

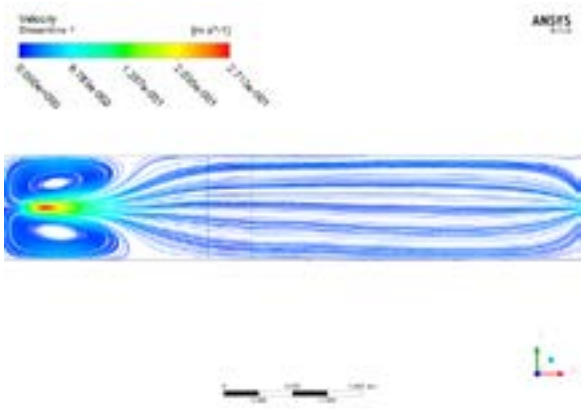

Figure 2.99 2D streamlines at Z = 0.04 m at volume flow rate 1.5 L/s

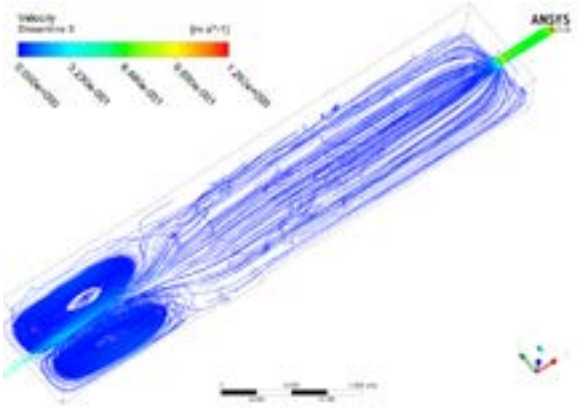

Figure 2.100 3D streamlines at volume flow rate 2 L/s

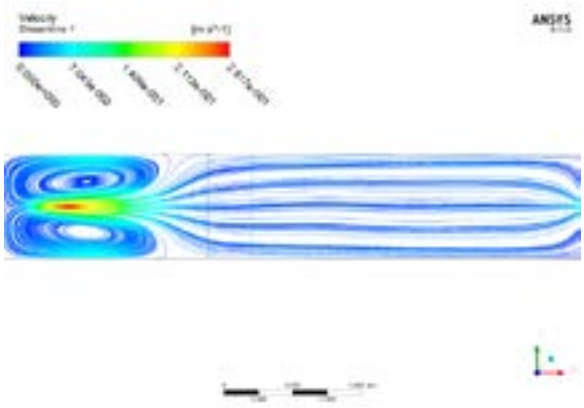

Figure 2.101 2D streamlines at Z = 0.04 m at volume flow rate 2 L/s

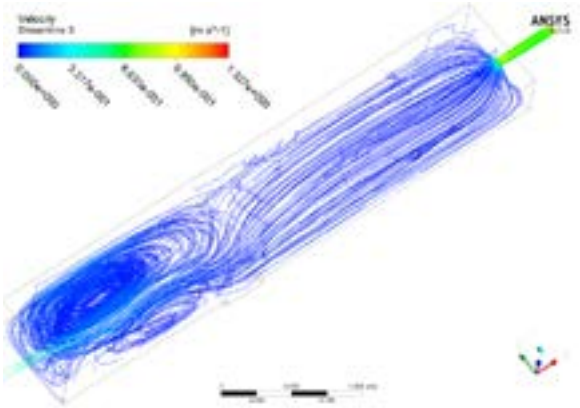

Figure2.102 3D streamlines at volume flow rate 2.5 L/s

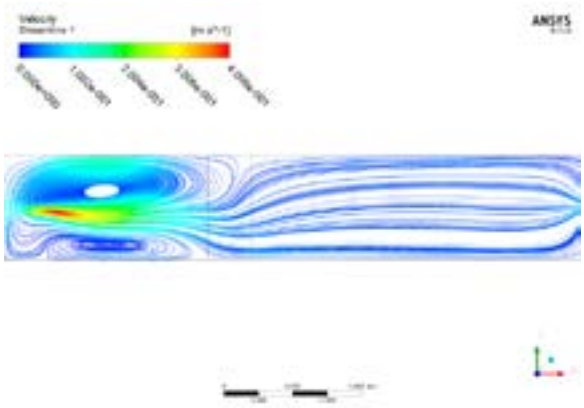

Figure 2.103 2D streamlines at Z = 0.04 m at volume flow rate 2.5 L/s

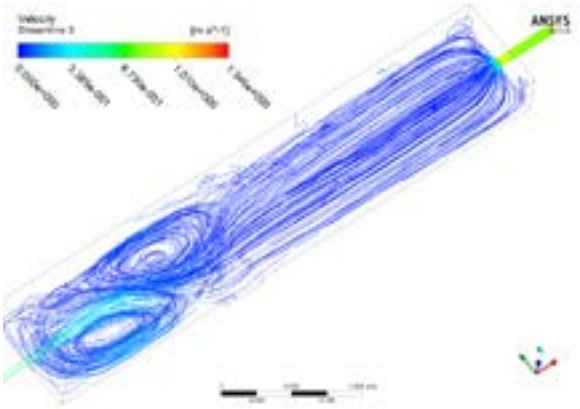

Figure 2.104 3D streamlines at volume flow rate 3 L/s

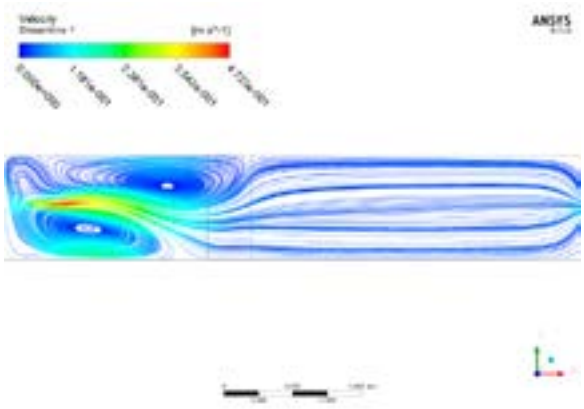

Figure 2.105 2D streamlines at Z = 0.04 m at volume flow rate 3 L/s

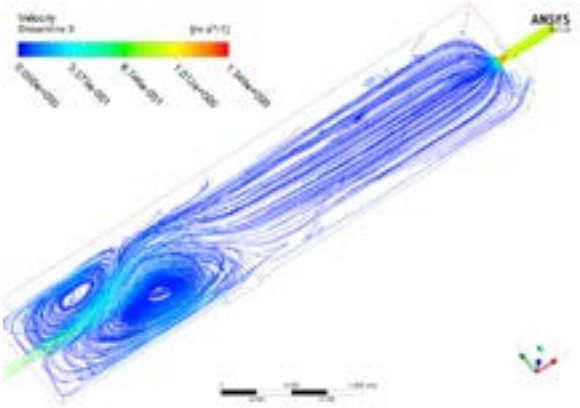

Figure 2.106 3D streamlines at volume flow rate 3.5 L/s

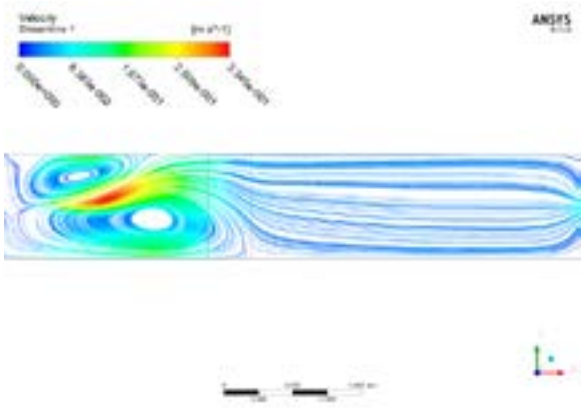

Figure 2.107 2D streamlines at Z = 0.04 m at volume flow rate 3.5 L/s

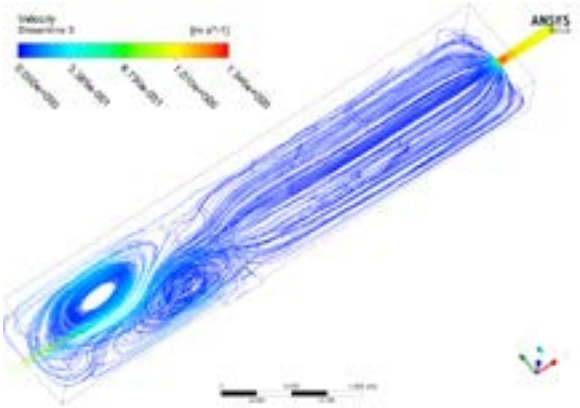

Figure 2.108 3D streamlines at volume flow rate 4 L/s

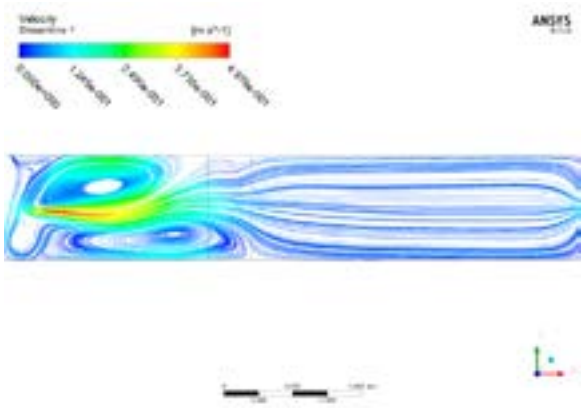

Figure 2.109 2D streamlines at Z = 0.04 m at volume flow rate 4 L/s

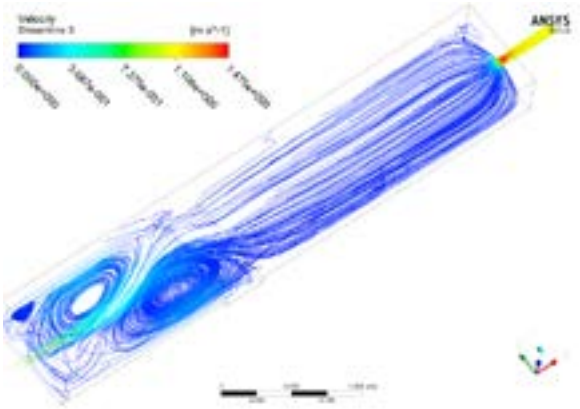

Figure 2.110 3D streamlines at volume flow rate 4.5 L/s

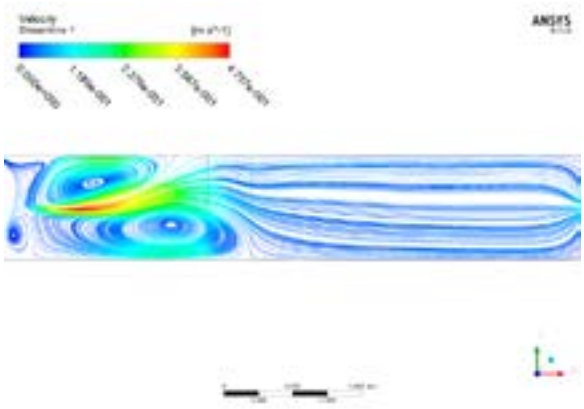

Figure 2.111 2D streamlines at Z = 0.04 m at volume flow rate 4.5 L/s

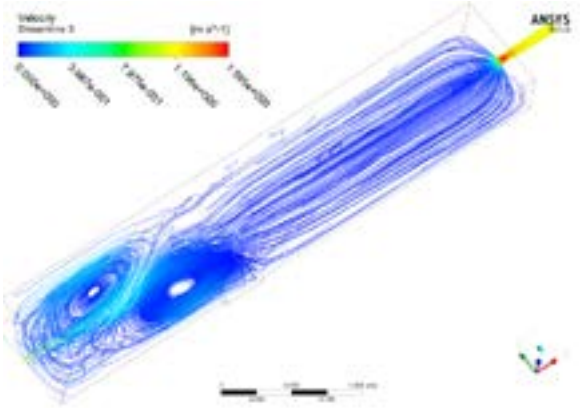

Figure2.112 3D streamlines at volume flow rate 5 L/s

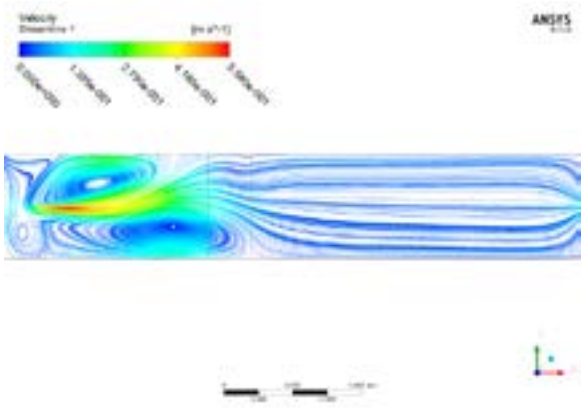

Figure 2.113 2D streamlines at Z = 0.04 m at volume flow rate 5 L/s

Table 2.7 Flow patterns under low water level

Inlet discharges (L/s)	Averaged water depth (cm)	Flow patterns
1	14.48	Symmetry
1.5	15.23	Symmetry
2	15.88	Symmetry
2.5	16.73	Asymmetry
3	17.62	Asymmetry
3.5	18.62	Asymmetry
4	19.57	Asymmetry
4.5	20.61	Asymmetry
5	21.82	Asymmetry

Table 2.8 Flow patterns under low water level

Inlet discharges (L/s)	Averaged water depth (cm)	Flow patterns
1	24.00	Asymmetry
1.5	24.46	Quasi-symmetry
2	25.34	Quasi-symmetry
2.5	26.24	Symmetry
3	27.11	Symmetry
3.5	27.90	Asymmetry
4	28.51	Asymmetry
4.5	29.31	Asymmetry
5	29.73	Asymmetry

Basically, the flow field in the tank with cavity is mainly dominated by two eddies in the front and a uniform flow part in the back, which is similar to the flow field in the tank without cavity.

The existence of the cavity can't change the number of the eddy in the front part, however it changes their distribution, location and size. The presence of the cavity can even change the flow pattern to symmetry in some extent. The variation differs depending on the ratio of length to width of the cavity.

If the ratio of the cavity is equal to 2, only one big eddy is generated and it occupies almost the whole cavity region. When the ratio of the cavity is equal to 3,4,5,6, two small eddies are generated, they are located at the front corner and back corner respectively. The number of eddies in the cavity is also affected by the entrance mass flow rate. For example in the simulation with cavity aspect ratio equal to 3 and entrance mass flow rate of 5 L/s, there is only one big vertical eddy in the cavity.

2.6.3 Wall shear stress and turbulent kinetic energy

Wall shear stress and turbulent kinetic energy at the bottom are also presented in this section.

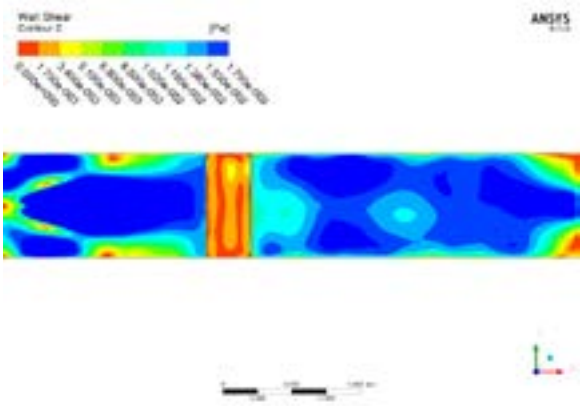

Figure 2.114 Wall shear stress at volume flow rate 1 L/s

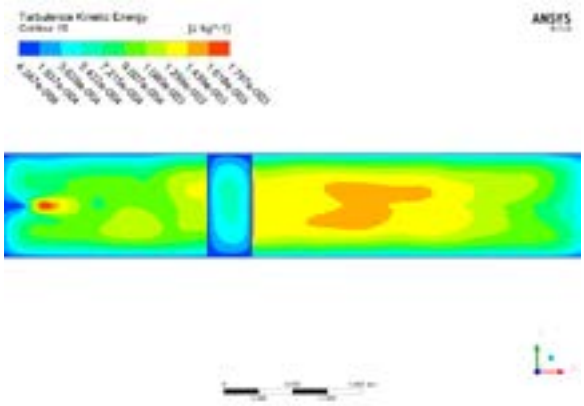

Figure 2.115 Turbulent kinetic energy at volume flow rate 1 L/s

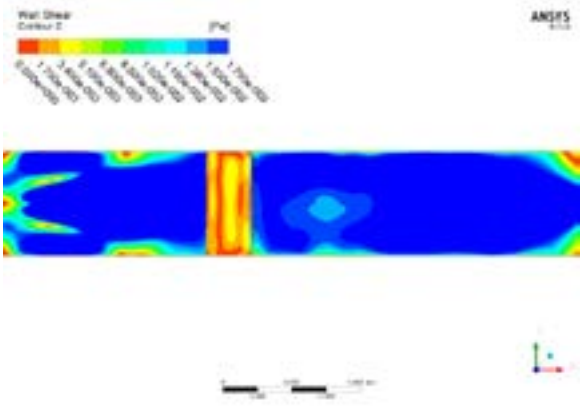

Figure 2.116 Wall shear stress at volume flow rate 1.5 L/s

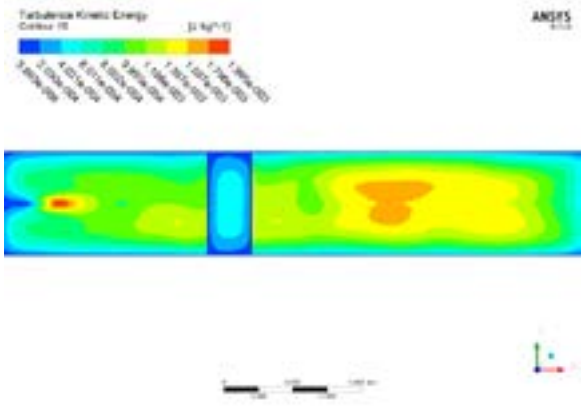

Figure 2.117 Turbulent kinetic energy at volume flow rate 1.5 L/s

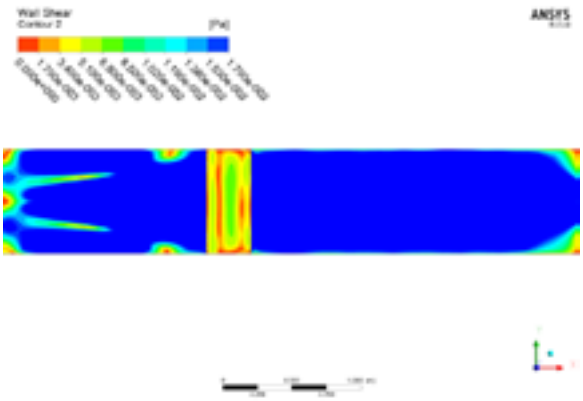

Figure 2.118 Wall shear stress at volume flow rate 2 L/s

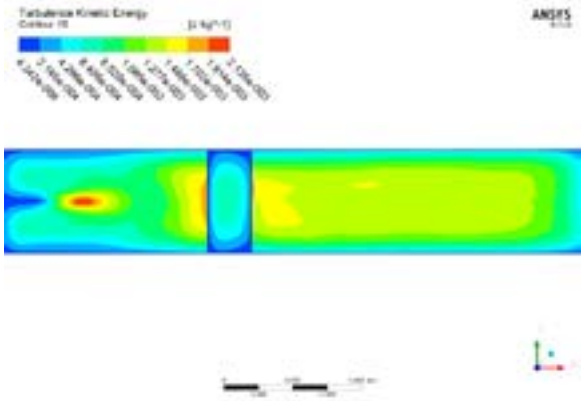

Figure 2.119 Turbulent kinetic energy at volume flow rate 2 L/s

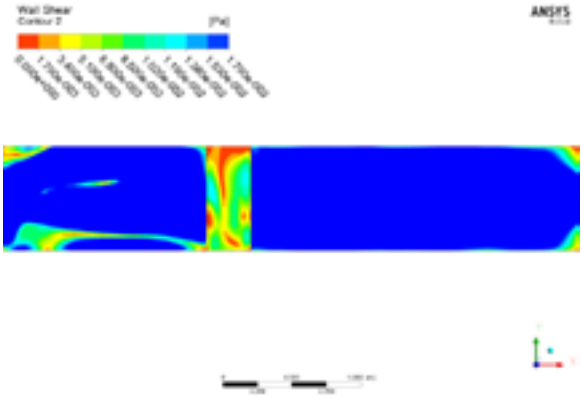

Figure 2.120 Wall shear stress at volume flow rate 2.5 L/s

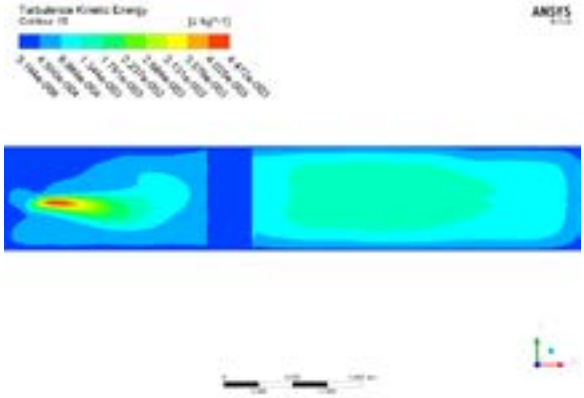

Figure 2.121 Turbulent kinetic energy at volume flow rate 2.5 L/s

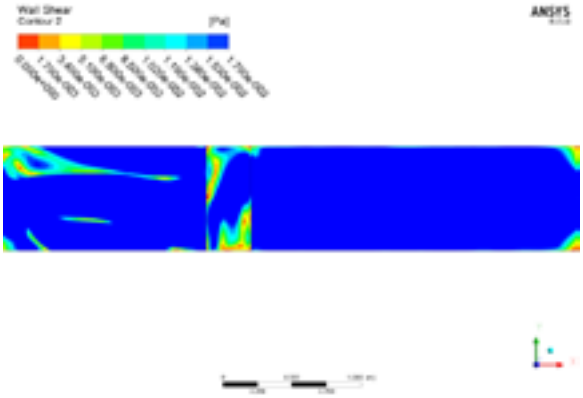

Figure 2.122 Wall shear stress at volume flow rate 3 L/s

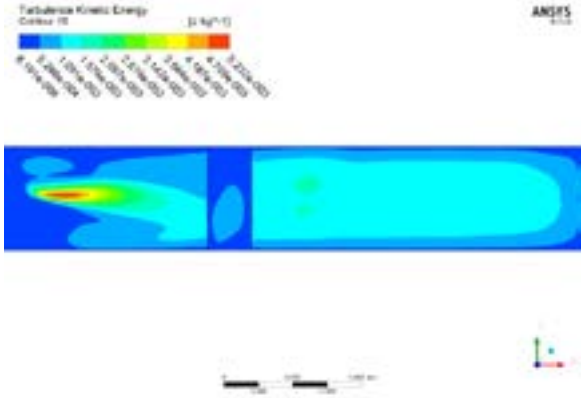

Figure 2.123 Turbulent kinetic energy at volume flow rate 3 L/s

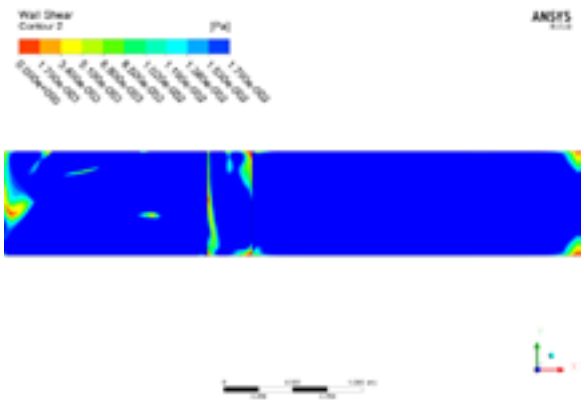

Figure 2.124 Wall shear stress at volume flow rate 3.5 L/s

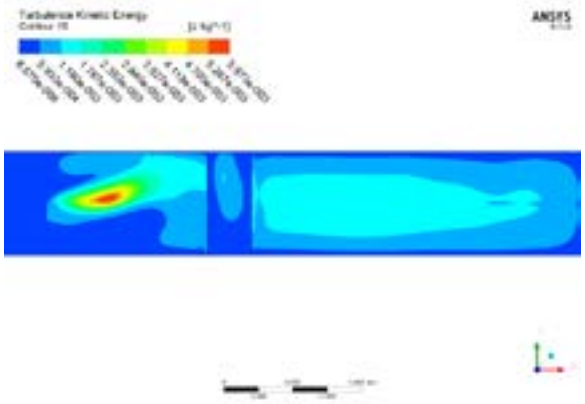

Figure 2.125 Turbulent kinetic energy at volume flow rate 3.5 L/s

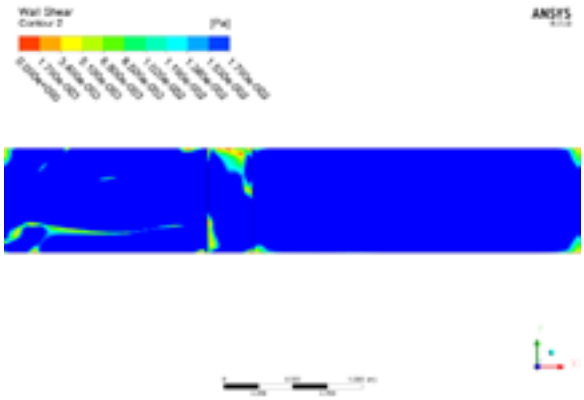

Figure 2.126 Wall shear stress at volume flow rate 3 L/s

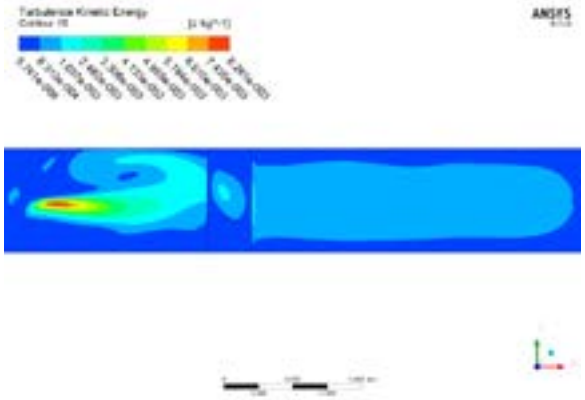

Figure 2.127 Turbulent kinetic energy at volume flow rate 3 L/s

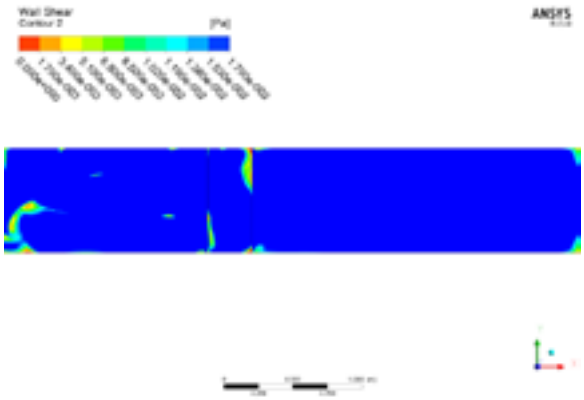

Figure 2.128 Wall shear stress at volume flow rate 4.5 L/s

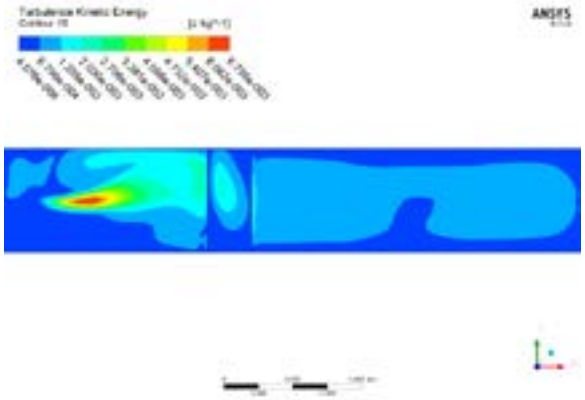

Figure 2.129 Turbulent kinetic energy at volume flow rate 4.5 L/s

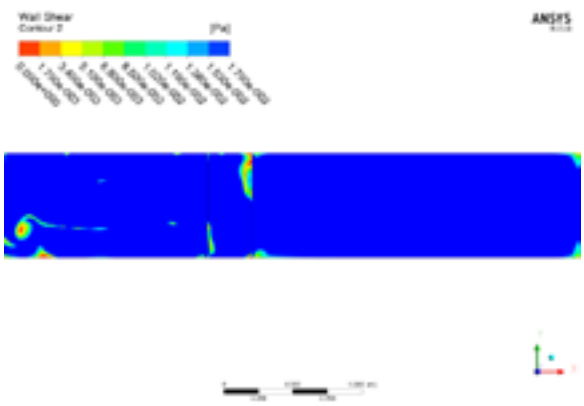

Figure 2.130 Wall shear stress at volume flow rate 5 L/s

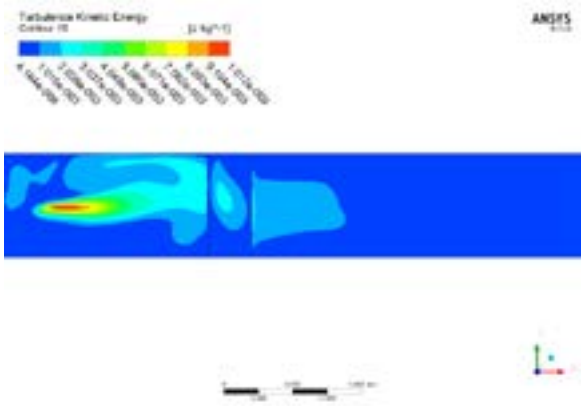

Figure 2.131 Turbulent kinetic energy at volume flow rate 5 L/s

The most different point of the flow field in the tank with cavity is that the existence of the cavity creates a part where the wall shear stress and turbulent kinetic energy are quite low even for high inlet discharges. The distributions of wall shear stress and turbulent kinetic energy are more uniform at the bottom.

2.6.4 Velocity

The velocity along the flow direction is always decreasing, the existence of the cavity decreases the damping rate of the velocity and creates a more uniform flow in the tank. The change tendency of the velocity along Z coordinate is in the same type as the case without cavity, increasing from bottom to the center of the injection and decreasing from the center of the flow injection to the free-surface, the difference is the peak value at the center of the injection, where the peak value is about 10% higher in the same location. The deviated extent of the injection is also decreased because of the cavity, that's why in the case with cavity the flow pattern is more likely to develop to a symmetry pattern. It turns out that the existence of the cavity can't change the flow field essentially, but it can create a more uniform flow field and with different ratio of the length to width, the variation will be different.

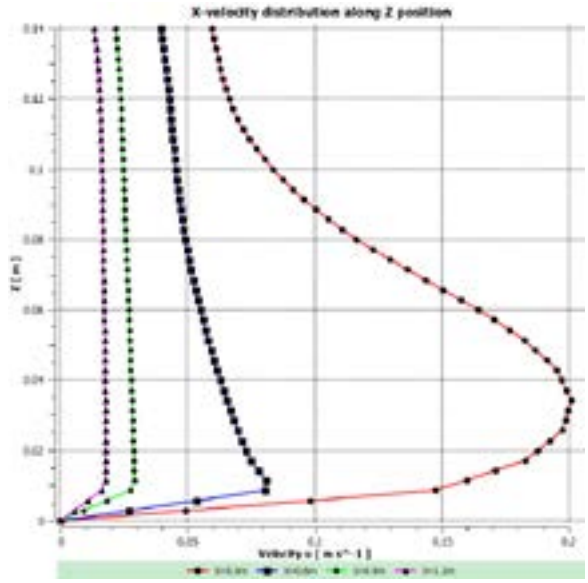

Figure 2.132 X-velocity distribution along Z position at volume flow rate 1 L/s

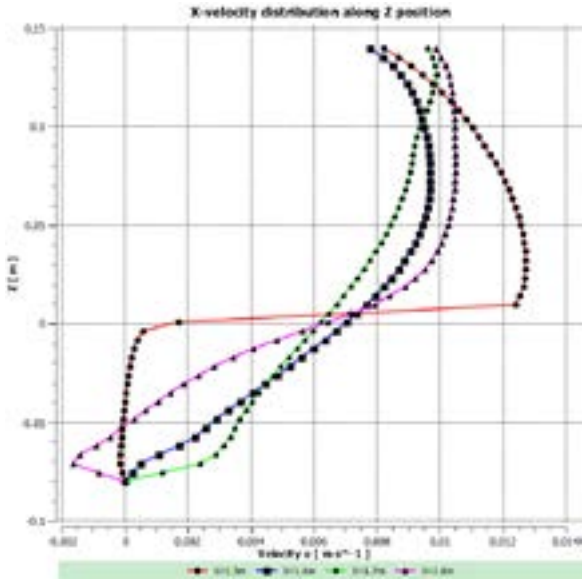

Figure 2.133 X-velocity distribution along Z position at volume flow rate 1 L/s

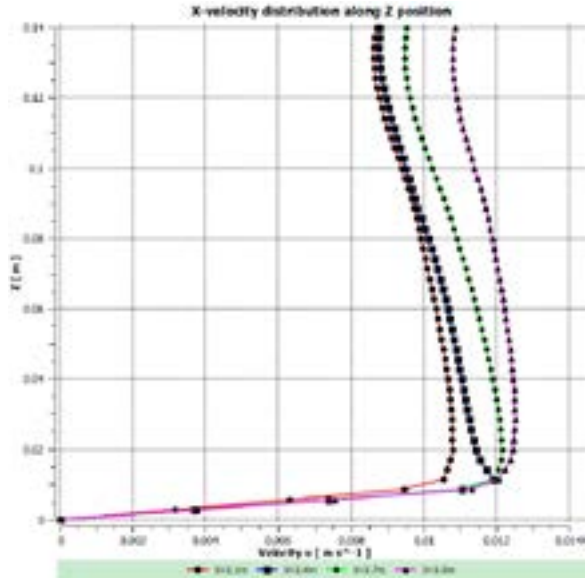

Figure 2.134 X-velocity distribution along Z position at volume flow rate 1 L/s

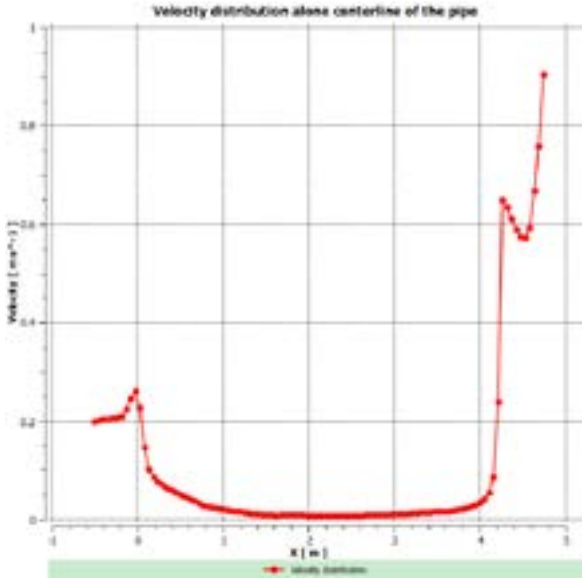

Figure 2.135 Velocity distribution at the center line at volume flow rate 1 L/s

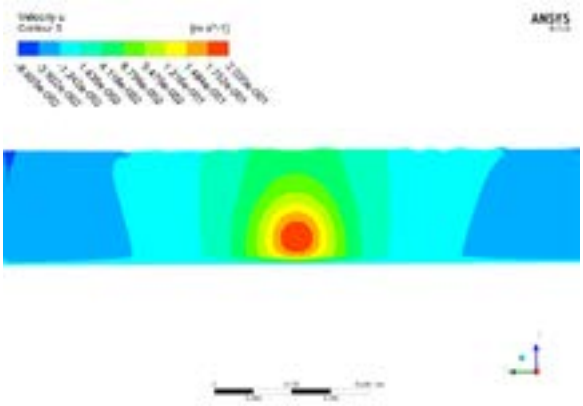

Figure 2.136 X-velocity contour at X = 0.3 m at volume flow rate 1 L/s

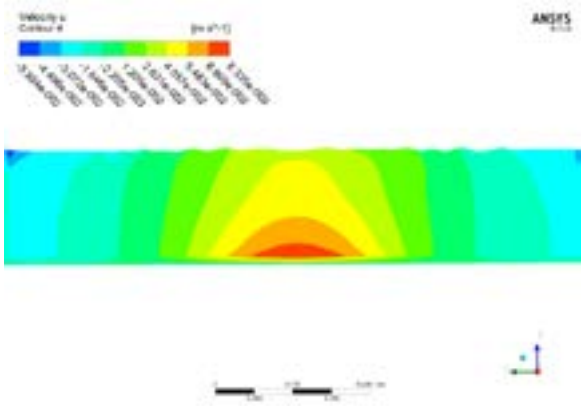

Figure 2.137 X-velocity contour at X = 0.6 m at volume flow rate 1 L/s

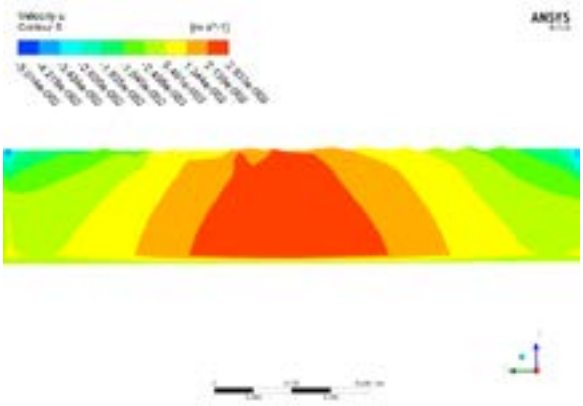

Figure 2.138 X-velocity contour at X = 0.9 m at volume flow rate 1 L/s

2.7 Conclusions

This chapter tried to analyze the flow pattern for various tank geometries with and without cavity – sediment trap. Several general flow features have been identified. For a given geometry, the flow pattern is sensitive to the entrance mass flow rate and water depth in the tank. With an increasing entrance mass flow rate, the flow pattern loses its symmetry. An increase of water depth can ensure a symmetric pattern for higher inlet discharges to some extent.

For different geometry and the same inflow discharge range than previously, the flow patterns highlight a sensitivity to the ratio of length to width. For the short tank with

low ratio of length to width, with the increase of entrance mass flow rate, the eddy will fill all the tank. But for the long tank with high ratio of length to width, the eddy only occupies the first 40% of the tank, uniform flow occurring elsewhere for tested range of discharges and depth.

The existence of the cavity can't change the flow field essentially, the function of the cavity is to change the flow parameters locally and create a zone with low value of wall shear stress and turbulent kinetic energy for fostering sediment deposition.

The ratio of length to width of the cavity don't have an obvious effect on changing the entire flow field in the tank, it can only affect the flow in the cavity. In the case with low ratio or high entrance volume flow rate, only one vertical eddy exists in the cavity and the eddy almost occupy all the cavity. In the case with high ratio or low entrance volume flow rate, two vertical eddies exist in the front corner and the back corner of the cavity respectively, and in some case with high volume flow rate the eddy in the back corner disappears and the cavity become a passage for smooth uniform flow.

All in all, the flow pattern in a rectangular tank is really complex and highly sensitive to entrance mass flow rate, water level and tank geometry. Small variation of those parameters can trigger significant and non-linear influences on flow patterns.

3. Simulation of sediment transport in rectangular reservoir

3.1 Introduction

This chapter aims to present the investigation of sediment deposition in the reservoir by numerical simulation. As it was mentioned in chapter 1, discrete phase model (DPM) is used to track the movement of the particles. The coupling between flow and particle is a weak coupling, which means the solver solves the flow equation and sediment transport equations separately, instead of simultaneously.

DPM model is a Lagrangian method for calculating the discrete phase state. The possible conditions at a boundary for particles can be trap, reflect, escape, wall-jet and wall-film. Concerning this work consideration, only trap, reflect and escape are suitable for the boundary. Adamsson et al (2003) highlight that the boundary condition at the bottom of a tank should be given careful consideration, as the prediction of trap efficiency and deposition depend on it. Their prediction of trap efficiency by using stick condition is too high and the deposition zone is vast. A useful criterion to overcome these defects is critical bed shear stress. The method based on bed shear stress shows better agreement with measured sedimentation efficiency data, and the spatial distribution of sediment is more similar measured deposition patterns (see Figure 3.1 and 3.2).

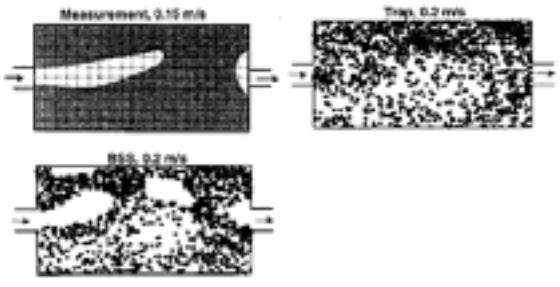

Figure 3.1 Spatial distribution of sediment in measurements and in simulations (Stovin,1996)

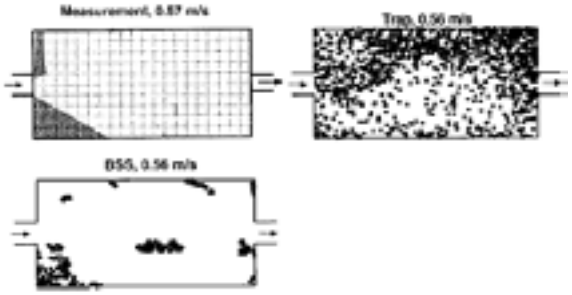

Figure 3.2 Spatial distribution of sediment in measurements and in simulations (Stovin,1996)

3.2 Method for modelling sediment transport

3.2.1 Approaches for particle trajectory

The modelling of sediment transport is a multi-phase flow problem, in a free-surface system. The fluid phases include the water phase (primary phase), the air phase (secondary phase) and solid phase composed of the particles (tertiary phase). In this thesis, the water phase has direct contact with both air phase and particle phase, but the air phase has no contact with the particle phase. The contact between water phase and air phase is realized by the application of the VOF method (presented in the chapter 2) to track the interface, and the contact between water phase and particle phase is accomplished by the application of DPM to track the particle trajectory.

In CFD, the trajectories of particles are usually described by two different approaches, namely the Euler-Eulerian method or the Lagrange-Eulerian method.

The Euler-Eulerian method treats all the involved phases as continuum medium. Each of the involved phases is defined as a volume fraction. Flow equations are then solved for each phase volumetric fraction, for each cell, with the constrain of the sum of all volumetric fractions equal to one. In Fluent codes, several model based on the Euler-Euler method are provided, including VOF, mixture model, Euler model (Fluent, 2002) .

Normally, VOF can be used for the simulation of stratified flows, where the different phases are not miscible and the equation for a single phase with averaged properties are solved. If the ratio of mixed phase in the flow is high a more complex has to be used. For such mixture models, the velocity difference and the interaction between continuous phase and discrete phase is taken into consideration.

The Lagrange-Eulerian method treats the fluid as a continuous medium, and for the movement of the particle, the calculation is achieved with a Lagrange method.

DPM is a typical Lagrange-Eulerian method, where each particle trajectory can be tracked separately, however the effect of particle on the fluid is ignored. Consequently DPM can only be used for flows containing less than 10% volumetric fraction of particles.

In DPM, trajectories of particles/droplets/bubbles are computed in a Lagrange framework, where the mechanic method is used to depict the framework with generalized coordinate which is the parameter representing the physical framework. Particles can exchange heat, mass, and momentum with the continuous fluid phase.

As the trajectory of a particle is computed, the heat, mass, momentum gained along the particle stream is tracked. The effect of the discrete phase trajectories on the continuous fluid phase can be accounted. This two-way coupling is accomplished by alternately solving the discrete and the continuous phase equations until the solutions in both phases have stopped changing. This interphase exchange of heat, mass and momentum from the particle to the continuous phase is depicted qualitatively in Figure 3.3. Each trajectory represents a group of particles with the same initial properties. Particle-particle interactions are neglected.

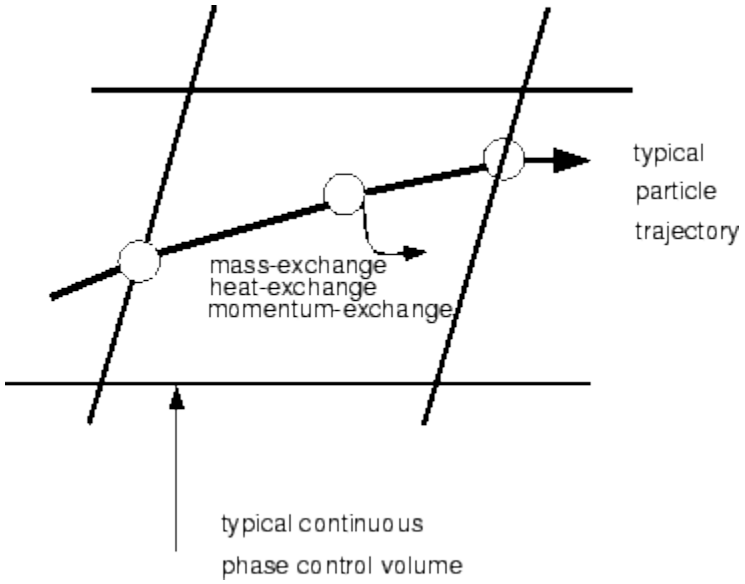

Figure 3.3 Heat, Mass, and Momentum Transfer Between the Discrete and Continuous Phases (Fluent, 2002)

There are two ways to calculate the movement of the discrete phase in the Fluent code, namely uncoupled calculations and weakly coupled calculations.

- One-way coupling, where the impact of the discrete phase on the continuous phase is not taken into account and the particle trajectory is predicted in a fixed continuous phase flow field, the procedures of the uncoupled approach is displayed in Figure 3.4.

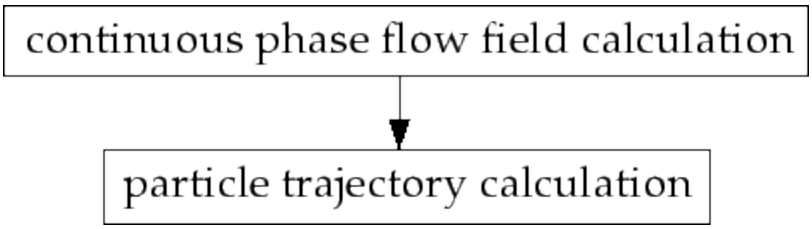

Figure 3.4 Uncoupled discrete phase calculation (Fluent,2002)

- Two-way coupling, where the interaction between the discrete phase and the continuous phase is taken into consideration, the procedures of the coupled approach is displayed in Figure 3.5

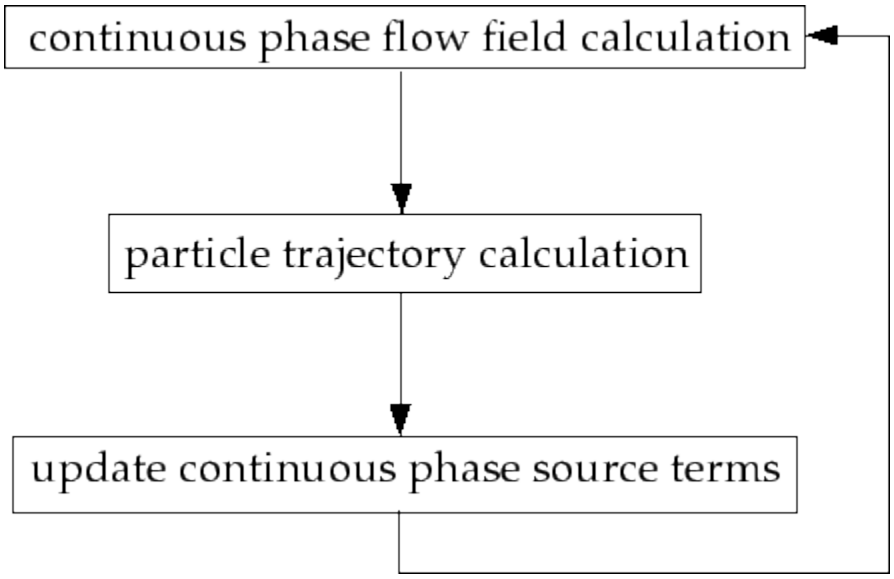

Figure 3.5 Coupled discrete phase calculation (Fluent,2002)

A moving particle in a fluid flow is affected by several volumetric and superficial forces, including gravity force, lift force, drag force, pressure gradient force, additional body force, and others forces (see Figure 3.6).

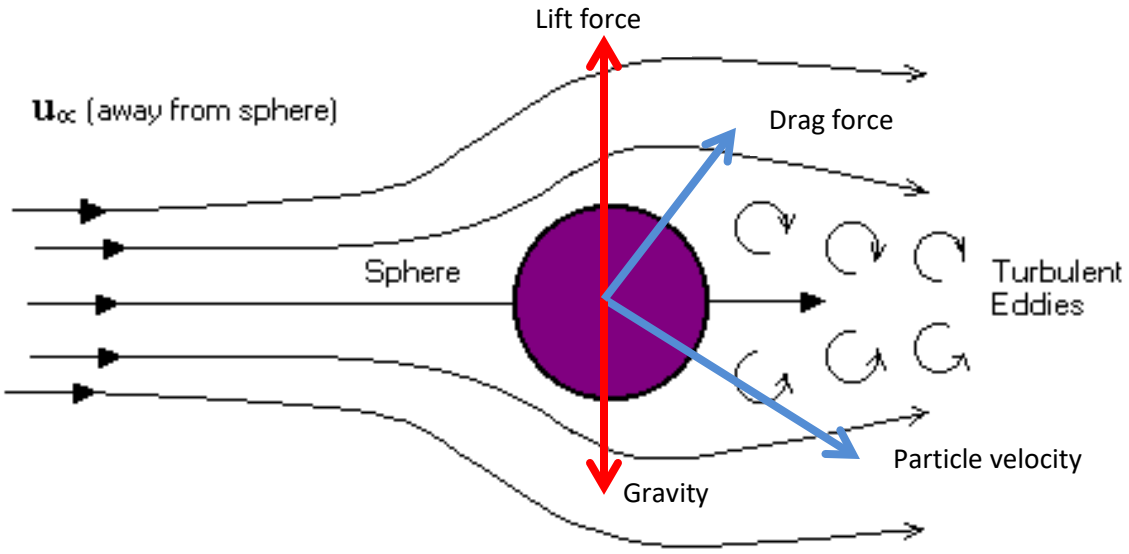

Figure 3.6 Mechanical analysis of particle in the fluid

Fundamental principle of mechanics applied to a particle in a fluid flow is accounted in Fluent as follows:

$$\frac{du_p}{dt} = F_D(u - u_p) + \frac{g_i(\rho_P - \rho)}{\rho_P} + F_i/\rho_P \tag{3.1}$$

Where u is the fluid phase velocity, u_p is the particle velocity, ρ is the density of fluid, ρ_P is the density of particle, g_i is the gravity acceleration and F_i are the additional forces. F_D and F_i are described below.

The term on the left hand of the equation represents the acceleration of the particle.

The first term in the right side of the equation is the drag force, the coefficient F_D can be expressed mathematically as:

$$F_D = \frac{18\mu}{\rho_P d^2}\frac{C_D Re}{24} \tag{3.2}$$

Where μ is the dynamic viscosity of the fluid, d is the particle diameter, C_D is the drag coefficient, and Re is the Reynolds number of the particle. Unlike the equation of

Reynolds number of a single fluid, due to the relative velocity between the fluid and the particle, Re is defined as:

$$Re = \frac{\rho d|u_p - u|}{\mu} \tag{3.3}$$

For the drag coefficient, there exist many different expressions, with the assumption that the particle is spherical, the expression given by Morsi and Alexander (1972) is adopted

$$C_D = a_1 + \frac{a_2}{Re} + \frac{a_3}{Re^2} \tag{3.4}$$

Where $a_1, a_2\ and\ a_3$ are constants applied to smooth spherical particles over several ranges of Reynolds number, or

$$C_D = \frac{24}{Re_{sph}}\left(1 + b_1 {Re_{sph}}^{b_2}\right) + \frac{b_3 Re_{sph}}{b_4 + Re_{sph}} \tag{3.5a}$$

Where

$$b_1 = \exp(2.3288 - 6.4581\phi + 2.4486\phi^2) \tag{3.5b}$$

$$b_2 = 0.0964 + 0.5565\ \phi \tag{3.5b}$$

$$b_3 = exp(4.905 - 13.8944\phi + 18.4222\phi^2 - 10.2599\phi^3) \tag{3.5c}$$

$$b_4 = exp(1.4681 + 12.258\phi - 20.7322\phi^2 + 15.8855\phi^3) \tag{3.5d}$$

Where ϕ is the shape factor taken from Haider and Levenspiel (1989), ϕ is defined as

$$\phi = \frac{s}{S} \tag{3.6}$$

Where s is the surface area of a sphere having the same volume as the particle of interest and S is the actual surface area of the particle. The Reynolds number Re_{sph} is calculated with the diameter of a sphere particle having the same volume.

The second term on the right hand of the equation is the gravity force.

The third term on the right side of the equation contains all the additional forces. The pressure gradient force and additional body force are the largest forces in those additional forces.

The additional body force, which is also called virtual mass force, tends to accelerate the fluid surrounding the particle. It can be expressed as:

$$F_i = \frac{1}{2}\rho \frac{d}{dt}\left(u_i - u_i^p\right) \tag{3.7}$$

In a flow with pressure gradient, the resulting force from the fluid pressure exerted on the particle, can be expressed as

$$F_i = \left(\frac{\rho}{\rho_p}\right) u_i^p \frac{\partial u}{\partial x_i} \tag{3.8}$$

Except for these two forces, the other ones evocated above and exerted on a moving particle in a fluid flow are smaller. Consequently, Basset force is even no longer implemented in the latest Fluent code version (Fluent,2002).

Mass or heat transfer from/to the particle are described by the trajectory equations and others auxiliary equations, which are solved by stepwise integration over discrete time steps. Along the trajectory the velocity of the particle at each point is yield by the integration in time of equation (3.1), the trajectory can be predicted by

$$\frac{dx}{dt} = u_p \tag{3.9}$$

Equations (3.1) and (3.9) are a set of ordinary differential equation, equation (3.1) can be cast into the following general form

$$\frac{du_p}{dt} = \frac{1}{\tau_p}\left(u_p^n - u^n\right) + a \tag{3.10}$$

Where the term a represent all the other accelerations resulting from all other forces except drag force.

Analytical integration of equation (3.10) can be obtained for constants $u, a\ and\ \tau_p$. At the new location for the particle velocity u_p^{n+1} we get

$$u_p^{n+1} = u^n + e^{-\frac{\Delta t}{\tau_p}}\left(u_p^n - u^n\right) - a\tau_p\left(e^{-\frac{\Delta t}{\tau_p}} - 1\right) \tag{3.11}$$

The new location x_p^{n+1} can be computed from a similar relationship.

$$x_p^{n+1} = x_p^n + \Delta t\left(u^n + a\tau_p\right) + \tau_p\left(1 - e^{-\frac{\Delta t}{\tau_p}}\right)\left(u_p^n - u^n - a\tau_p\right) \tag{3.12}$$

Where u^n and u_p^n are fluid velocities and particle velocities at the old location respectively. Equation 3.11 and 3.12 are applied in analytical discretization scheme.

And by using numerical discretization schemes the set of equations 3.1 and 3.9 can also be solved. By applying the Euler implicit discretization scheme to equation 3.10, following equation is obtained,

$$u_p^{n+1} = \frac{u_p^n + \Delta t\left(a + \frac{u^n}{\tau_p}\right)}{1 + \frac{\Delta\, t}{\tau_p}} \tag{3.13}$$

When applying a trapezoidal discretization to equation 3.10, the variables u^n and u_p^n on the right hand side are taken as averages, while accelerations, a, due to other forces are held constant, following equation is obtained,

$$\frac{u_p^{n+1} - u_p^n}{\Delta t} = \frac{1}{\tau_p}\left(u^* - u_p^*\right) + a^n \tag{3.14}$$

The averages u_p^* and u^* are computed from

$$u_p^* = \frac{1}{2}\left(u_p^{n+1} + u_p^n\right) \tag{3.15}$$

$$u^* = \frac{1}{2}\left(u^{n+1} + u^n\right) \tag{3.16}$$

$$u^{n+1} = u^n + \Delta t u_p^n \cdot \nabla u^n \tag{3.17}$$

The particle velocity at the new location $n+1$ is computed by

$$u_p^{n+1} = \frac{u_p^n\left(1 - \frac{1}{2}\frac{\Delta t}{\tau_p}\right) + \frac{\Delta t}{\tau_p}\left(u^n + \frac{1}{2}\Delta t u_p^n \cdot \nabla u^n\right) + \Delta t a}{1 + \frac{1}{2}\frac{\Delta t}{\tau_p}} \tag{3.18}$$

The particle location at the new location $n+1$ is computed by a trapezoidal discretization of equation 3.9 in the implicit and the trapezoidal schemes.

$$x_p^{n+1} = x_p^n + \frac{1}{2}\Delta t\left(u_p^{n+1} + u_p^n\right) \tag{3.19}$$

3.2.2 Turbulence dispersion of particles

Dispersion of particles due to turbulence in the fluid phase can be modeled by using stochastic tracking or a “particle cloud” model. By the use of stochastic methods the effect of instantaneous turbulent velocity fluctuation on the particle trajectories is included in the stochastic tracking (random walk) model. The statistical evolution of a cloud of particle around a mean trajectory is tracked with a particle cloud model. It consists in a Gaussian probability density applied to the mean trajectory in order to represent the concentration of particles within the cloud.

In a turbulent flow, the trajectories of particles will be predicted by using the mean fluid phase velocity and the instantaneous value of the fluctuating fluid flow velocity which is in the same form with equation (2.5) in chapter 2. The random effect of turbulence on the particle can be taken into account by computing the trajectory of a sufficient number of representative particles.

The instantaneous velocity in Fluent is determined by a stochastic method (random walk model). The fluctuating velocity components are discrete piecewise constant

functions of time in the discrete random walk model(DRWM), where a constant random value is kept over an interval of time given by the characteristic lifetime of the eddies.

The concept of the integral time scale, T , is used to predict particle dispersion, where the time spent in turbulent motion along the particle path is described as:

$$T = \int_0^\infty \frac{u_p'(t)u_p'(t+s)}{\overline{u_p'^2}}\,ds \tag{3.20}$$

The integral time is proportional to the particle dispersion rate, larger values indicate more turbulent motion in the flow. The particle diffusivity can be obtained by $\overline{u_i'u_j'}T$.

For small "tracer" particles that moves with the fluid (zero drift velocity), the integral time becomes the fluid Lagrange integral time, T_L , which can be described as:

$$T_L = C_L\frac{k}{\varepsilon} \tag{3.21a}$$

Where C_L is unknown and needs to be determined. By matching the diffusivity of tracer particle, $\overline{u_i'u_j'}T$, to the scalar diffusion rate predicted by the turbulent model, $\frac{\upsilon_t}{\sigma}$, one can obtain,

$$T_L \approx 0.15\frac{k}{\varepsilon} \tag{3.21b}$$

For the $k-\varepsilon$ model and its variants, and

$$T_L \approx 0.30\frac{k}{\varepsilon} \tag{3.21c}$$

C_L differs with different turbulent model.

3.2.3 Discrete random walk model

In DRWM, or eddy lifetime model, the interaction of a particle with a succession of discrete stylized fluid phase turbulent eddies is simulated, where the eddy is characterized by

- A time scale, τ_e.
- A Gaussian distributed random velocity fluctuation, u', v', and w'.

Their values prevail during the lifetime of the turbulent and are sampled by assuming that they obey a Gaussian probability distribution, so that,

$$u' = \zeta\sqrt{\overline{u'^2}} \tag{3.22}$$

Where ζ represents a normally distributed random number, and the rest part in the right-hand side of the equation represents the local RMS value of the velocity fluctuations. Due to the turbulent kinetic energy in the flow at each point is already known, the RMS fluctuating components of these values can be defined (assuming turbulence isotropy) as,

$$\sqrt{\overline{u'^2}} = \sqrt{\overline{v'^2}} = \sqrt{\overline{w'^2}} = \sqrt{\frac{2k}{3}} \tag{3.23}$$

For the $k-\omega$ model, the $k-\varepsilon$ model and their variants. When the RSM is used, nonisotropy of the stresses is included in the derivation of the velocity fluctuation,

$$\begin{aligned} u' &= \zeta\sqrt{\overline{u'^2}} \\ v' &= \zeta\sqrt{\overline{v'^2}} \\ w' &= \zeta\sqrt{\overline{w'^2}} \end{aligned} \tag{3.24}$$

The second moment of the turbulence is diagonal when the equation is viewed in a reference frame.

The characteristic lifetime of the eddy is defined either as a constant,

$$\tau_e = 2T_L \tag{3.25}$$

Or as a random variation about T_L ,

$$\tau_e = -T_L \log(r) \tag{3.26}$$

The particle eddy crossing time is defined as,

$$t_{cross} = -\tau \ln\left(1 - \frac{L_e}{\tau|u - u_p|}\right) \tag{3.27}$$

The trap efficiencies of the tank rely on the time scale factor in discrete random walk model (DRWM) (see Figure 3.7). Dufresne (2008) and Yan (2013) tested the effect of the time scale factor on the trap efficiencies, and it turned out that the predicted efficiency is more accurate when the values of C_L locates in the range of 0.15 to 2.Therefore in this work, the time scale factor is selected as 0.15 regarding to the tested cases.

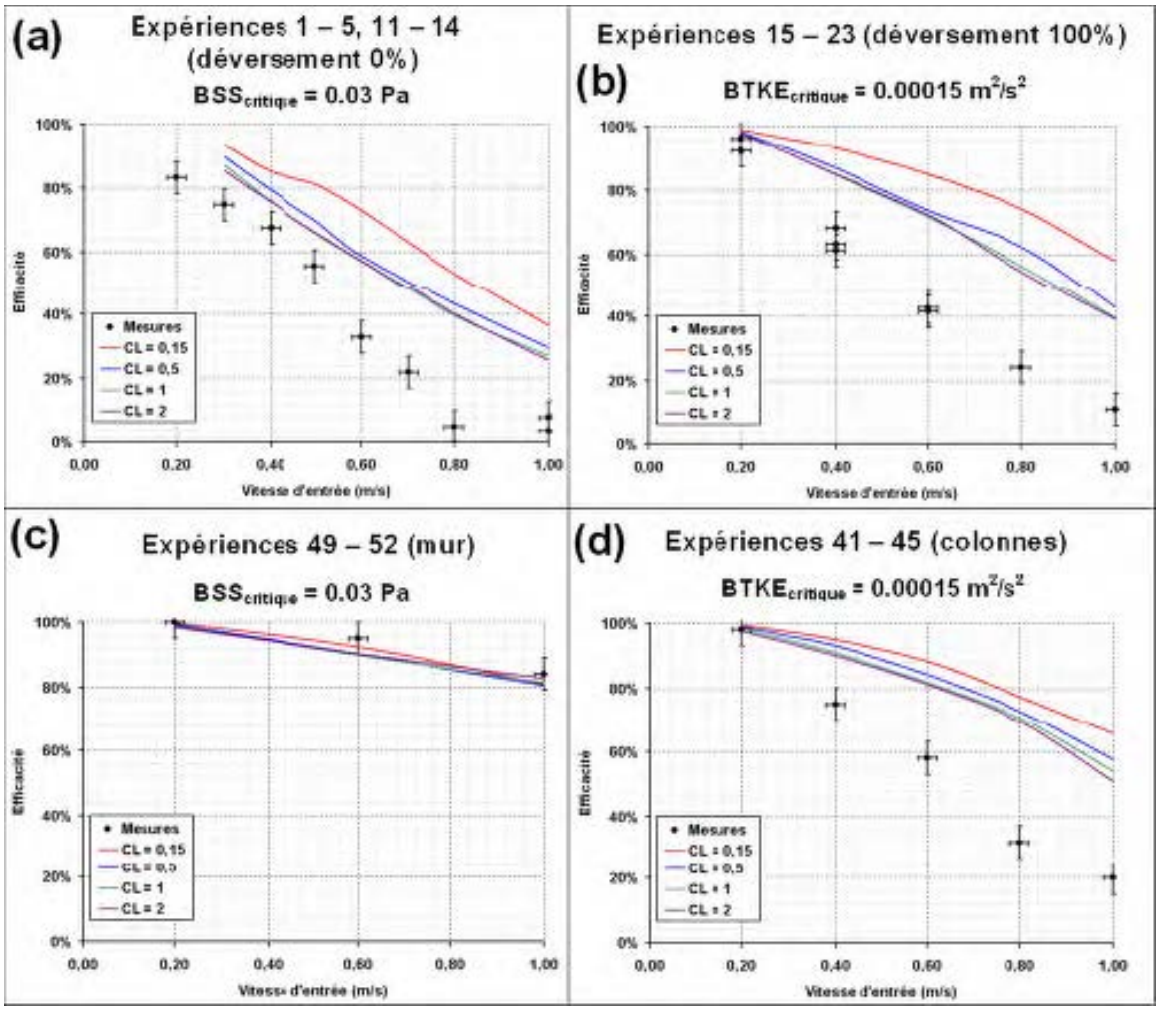

Figure 3.7 Comparison between experiment results and numerical simulation with different time scale factor(Dufresne,2008)

3.2.4 Boundary condition

As previously for the fluid flow, it is necessary to setup several parameters and boundary condition before the calculation. In order to compute the particle trajectories, some specific boundary conditions are necessary.

A particle “injection”, with specific properties, is created in the flow at the inlet boundary condition in Fluent. There are 11 types in Fluent to define the injection, including single, group, cone (only in 3D), solid-cone (only in 3D), surface, plain-orifice atomizer, pressure-swirl atomizer, flat-fan-atomizer, air-blast-atomizer, effervescent-atomizer and file. In this thesis, the injection is assumed fully developed and homogenous across the whole surface, therefore a surface injection is selected.

For each injection type, the initial condition should be specified, including the velocities, starting positions and other parameters for each particle stream. The starting values are provided by these initial conditions for all of the dependent discrete phase variables that describe the instantaneous conditions of an individual particle, these initial conditions can be specified the following:

- Position of the particle
- Velocity of the particle
- Diameter of the particle
- Temperature of the particle
- Mass flow rate of the particle stream that will follow the particle trajectory
- Additional parameters if one of the atomizer models is used for the injection

In this thesis, the injected particles are set to be inertia. For the size distribution of the particles, firstly the complete range of sizes is divided into an adequate number of discrete intervals, where each interval is represented by a mean diameter for which trajectory calculations are performed, secondly using the Rosin-Rammler type to obtain the mass fraction of the particle. The mass fraction distribution of particles in this thesis is taken from the experimental measurements. Two particle distributions are used in the simulation of sediment transport in a rectangular tank.

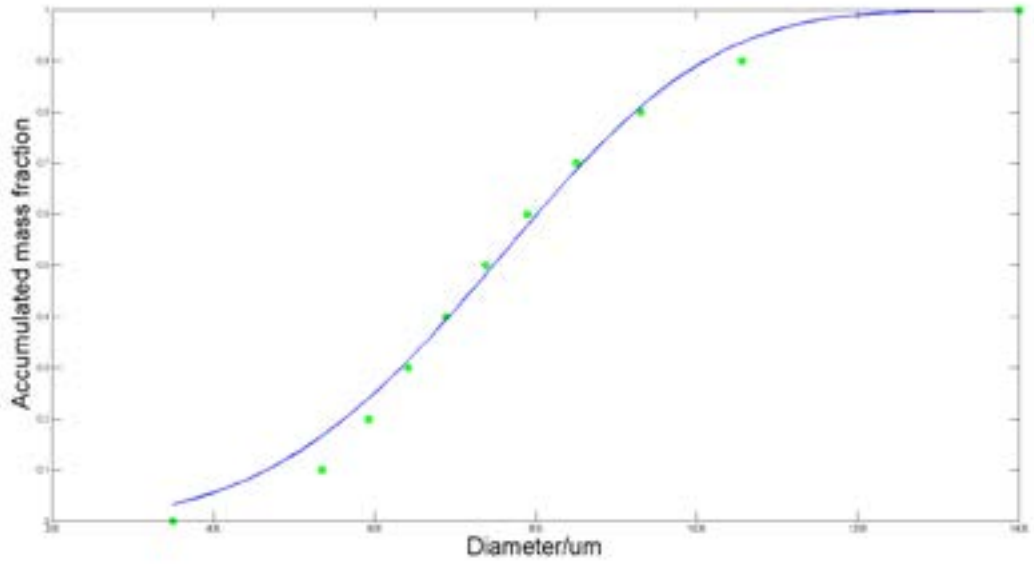

Figure 3.8 Accumulated mass fraction along diameter

According to the fitting to experimental data the resulting Rosin-Rammler distribution can be obtained (shown in Figure 3.8). The spread number is $n = 3.785 - 4.714$; in

the initial condition choosing $n = 4$ as the final value and the diameter constant $\bar{d} = 820$ μm. For the other particle distribution, $n = 9$ and $\bar{d} = 837$ μm.

In DPM, the particle trajectory is processed in the flow domain, when a particle arrives at a physical boundary (e.g., bottom of the rectangular tank), in order to determine the state of the trajectory and to present particle motion the interaction between the particle and physical boundary must be processed. Normally there are six types of boundary condition in DPM (four types of the boundary condition are showed in Figure 3.9).

- Escape, where the particle is reported as having "escaped" when it encounters the boundary in question and the trajectory calculations are terminated.
- Reflect, where the particle rebounds on the boundary of interest with a change in its momentum as defined by the coefficient of restitution.
- Trap, where the trajectory calculations are terminated and the fate of the particle is recorded as "trapped".
- Wall-jet, where the direction and velocity of the droplet particles are given by the resulting momentum flux, which is a function of the impingement angle and Weber number.
- Wall-film, where four regimes exist, including stick, rebound, spread and splash, which are based on the wall temperature and impact energy
- Interior, where the particles will pass through.

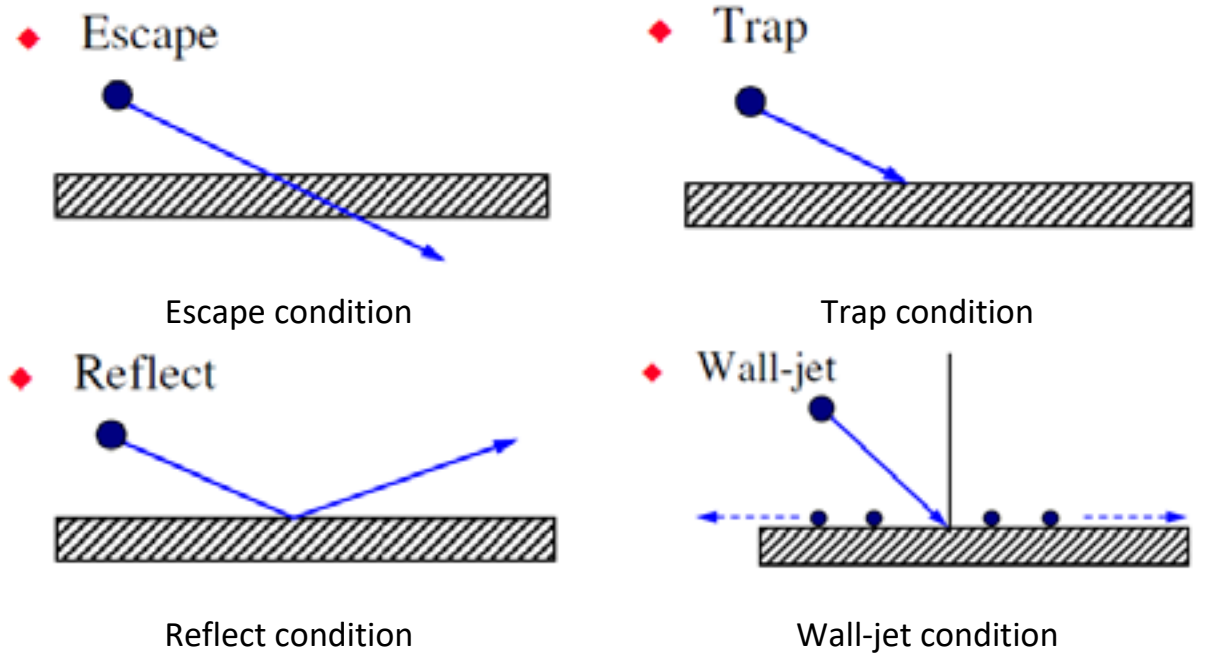

Figure 3.9 Different conditions for particle

The calculation of particle trajectory starts when the particle enters the flow domain at the inlet part, the calculation of particle trajectory terminates when the particle leaves the flow domain at the exit part. The escape type boundary condition is used at the inlet, outlet part and the free-surface, indeed the particle remains in the fluid and will not go into the air phase, so any particle will escape the flow domain from the free-surface.

The treatment when particle hits the bottom is crucial to predict realistic sediment transport and deposits as suggested in the literature (Stovin et Saul (1994, 1996, 1998), Adamsson et al (2001, 2003), Dufresne (2008), Vosswinkel (2012) and Yan (2013)). Normally, a trap condition can be selected for the bottom a reflect condition for the walls. Many studies confirm that trap condition overestimates the trap efficiencies and improvements of the boundary condition for modelling the sedimentation process is necessary for predicting the trap efficiency and deposition zone more accurately. The rest of this chapter presents some tests on the effect of different boundary condition types and parameterizations for modelling the sedimentation process.

3.2.5 Approaches for implementation of settling condition

The “trap” condition for settling used in Fluent code is a stick condition, which has been proved to overestimate the trap efficiency and predict the deposition zone mistakenly by many researchers such as Adamsson (2003), Dufresne (2008), Yan (2013) and Isenmann (2016). Though the core code of Fluent is not opened, Fluent provides a method for user defined function (UDF). In order to substitute the “trap” condition, several attempts were made to implement other settling boundary conditions using UDF.

The core idea for improving settling boundary conditions is to find an accurate criterion resulting from flow variables. Several modeling options used in the literature for deriving settling conditions are listed as follows:

- Critical velocity: illustrated in chapter 1, Table 1.4 listed some classical formulas for calculating the critical velocity.
- Critical shear stress: mentioned in chapter 1, Shields curve and its modification is the most widely used to determine critical shear stress, where Shields parameter is used to fit the curve. Several well-known fitting equations have been derived to estimate the critical shear stress.

- Critical turbulent kinetic energy: some researchers tried to calculate critical turbulent kinetic energy for the criterion (Dufresne, 2008; Yan, 2013; Isenmann).
- The ratio of shear velocity and settling velocity: the suspension of a particle mainly relies on the balance between the component of the turbulent velocity fluctuation and the particle settling velocity in the normal direction to the bed (Chanson, 2004).
- The probabilistic approach: many models that illustrate the entrainment of sediment have been developed (Wu and Chou, 2003).
- The turbulent burst: this phenomenon revealed by experiments many authors of the close relation between particle motion near the bottom and turbulent bursting (Sumer and Oguz, 1978; Sumer and Deigaard, 1981; Grass, 1982).

Among all these approaches, critical shear stress is the most widely used approach.

3.3 Sediment transport with using the trap condition in steady state

In Fluent code, the boundary condition for modelling the sedimentation of particles is trap condition, where the particle trajectory are terminated when the particle make contact with the boundary optioned as “trap”. Physically, this boundary condition ignores the effect of resuspension and sliding.

The calculations of the flow and the particle trajectory are processed under a two-way coupling, the injection of the particle starts when the flow condition is stable. Realizable $k-\varepsilon$ model is applied to model the turbulence, which has been proved to be able to give satisfactory results. All the boundary selection in the simulation are showed as follows:

- Inlet, velocity-inlet with an inflow rate 3 L/s and the velocity is 0.5968 m/s.
- Side wall and the bottom, no-slip wall and standard wall function.
- Free-surface, pressure-outlet.
- Outlet, pressure-outlet.

The boundary conditions for the discrete phase are as follows:

- DPM sources update per flow iteration, particle tracking is in unsteady state and the particle time step size is 0.001 s, the maximum number of tracking steps is 50000 and the step length factor is 5.

- Particles are injected from the inlet surface from 0s to 10s with the flow rate 0.5kg/s, the diameter distribution of particles is the fitted rosin-rammler one presented above, the minimum diameter is 0.35 mm, the maximum diameter is 1.4 mm, the mean diameter is 0.81 mm and the spread parameter is 4. Turbulent dispersion of particle is simulated by DRWM with constant time scale $C_L = 0.15$, the injection of the particle uses constant-number parcel release method where a parcel of particle contains 50 particles. Normally, about 800 thousands particles are injected into the tank, the number of the injected particles can decrease the numerical error and ensure there will be enough particle spreading at the outlet.
- The density of the particle is 1034 kg/m^3 and the particle is inert.
- The inlet, outlet and free-surface are "escape" type, the side wall are "reflect" type, the bottom is "trap" type.

Table 3.1 shows the particles trap efficiency of the numerical simulation by using "trap" condition as the settling boundary for particle, comparing to the 33% from the experimental results by Dufresne (2008), which proves that the trap condition in Fluent code may overestimate the trap efficiency.

Table 3.1 Particle portion of different final state

Particle type	Trapped	Escape	Suspension
Percentage	81.66%	17.424%	0.916%

Figure 3.10 shows the particle trajectory for a 3 L/s inflow and using the "trap" condition at the bottom. The particle deviates to the top when entering the tank, part of the particle moves in the anticlockwise sense to the corner at the top left side. The rest of the particle moves in the clockwise sense spreading in the whole tank. Plenty of particles escape the tank when they reach the outlet pipe. The center of the big eddy in the flow is an area with less particles.

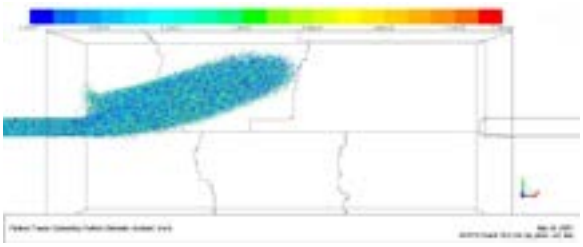

Particle trajectory at 3000 iterations

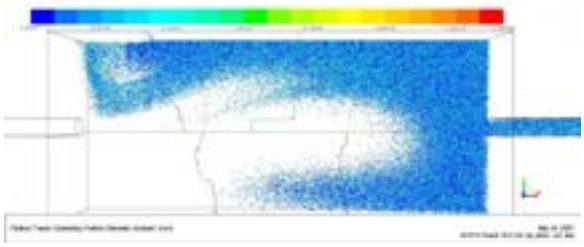

Particle trajectory at 15000 iterations

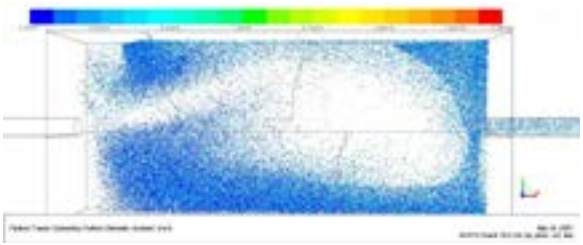

Particle trajectory at 25000 iterations

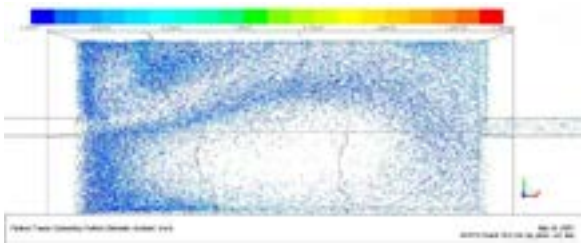

Particle trajectory at 35000 iterations

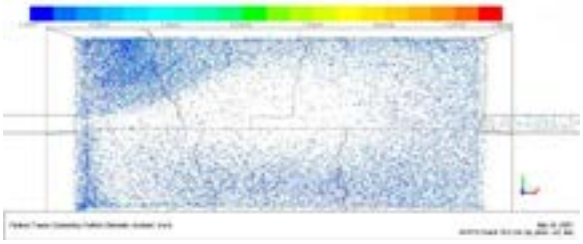

Particle trajectory at 45000 iterations

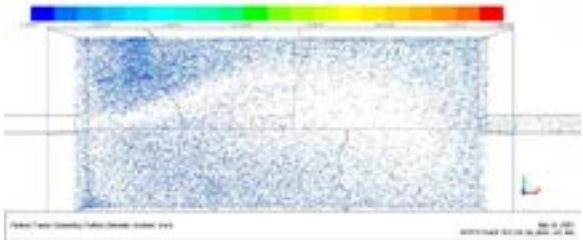

Particle trajectory at 50000 iterations

Figure 3.10 Particle trajectory at 3 L/s

3.4 Implementation of settling condition with bed shear stress

The “trap” condition in Fluent code treats all the particles reaching the “trap” boundary as trapped permanently. The rebounding, resuspension and sliding effect are ignored directly, which can lead to an overestimation of the trap efficiency and inaccurate prediction of the deposition zone. The defect of Fluent in predicting the settling of the particle requires improvement of the settling boundary for discrete phase. Bed shear stress and turbulent kinetic energy are two parameters chosen for the improvement.

The shields curve (see Figure 3.11) provides a criterion to estimate the critical bed shear stress for particle sedimentation, where this criterion can be used for improving the estimation of particle sedimentation.

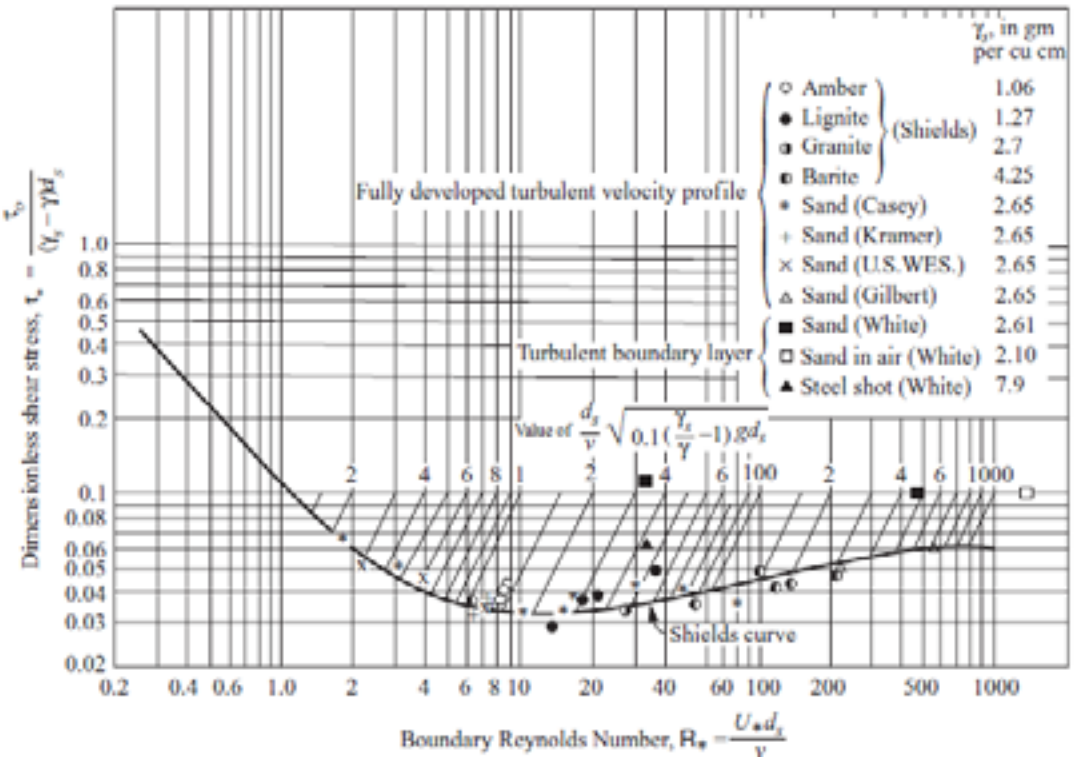

Figure 3.11 Shields curve

Fit equations have been proposed to calculate the Shields parameter. Based on the Bonneville (1963) parameter, Brownlis (1981) presented the following equation:

$$\theta = \frac{0.22}{D_*^{0.9}} + 0.06e^{-17.77D_*^{-0.9}} \tag{3.28}$$

Where $D_* = \left(\frac{(\rho_p-\rho)gd^3}{\rho\nu^2}\right)^{\frac{1}{3}}$ is the dimensionless grain diameter, θ is the dimensionless shear stress.

Another famous fit equation proposed by Soulsby & Whitehous (1997), it is also based on the Bonneville parameter. In these two equations the asymptotic values are different. Brownlie uses 0.06 for very large Reynolds numbers, while Soulsby & Whitehouse use 0.055. For very small Reynolds number the asymptote for the Brownlie equation is proportional to $Re^{-0.9}$, while Shields (1936) proposed $0.1Re^{-1}$. But Soulsby & Whitehouse (1997) found a value of 0.3, at the end the fit equation can be written as:

$$\theta = \frac{0.30}{1 + 1.2D_*} + 0.055(1 - e^{-0.02D_*}) \tag{3.29}$$

Yan (2013) choosed 0.06 as asymptotic value to fit the shield curve and implemented the settling condition with the fit equation of Shields curve by Brownlie, Yan also implemented the settling condition based on bed turbulent kinetic energy (BTKE) threshold, the simulation result indicated that all the simulations overestimate the trap efficiency, but the prediction of the simulation with using new settling condition was much better than stick condition.

Dufresne (2008) used a fixed bed turbulent kinetic energy (BTKE) as threshold to estimate the settling of particles. Yan et al (2011) presented a formula for calculating BTKE to implement the settling conditions for particles, which can be written:

$$k_c = \xi w_s^2 \tag{3.30}$$

Where k_c is the BTKE threshold, ξ is an adjustment coefficient which is in relation with particle shape, collision effects, energy transferring rate and concentration, etc., w_s is the particle settling velocity.

Isenmann (2016) implemented the boundary condition based on these two fit equations by Brownlie and Soulsby & Whitehouse, Isenmann also applied BTKE threshold proposed by Van Rjin (1984) to implement the settling condition, the simulation results showed improvements in predicting of the trap efficiency but the overestimation problem is not solved.

Isenmann (2016) tested BTKE by using equation 3.30 when $\xi = 1$ and $\xi = 1$, and modified the equation based on Van Rjin(1984), the modified equation can be written as:

$$k_c = \frac{320}{324}\left[\left(\frac{\rho_p}{\rho} - 1\right) g\nu\right]^{\frac{2}{3}} \tag{3.31}$$

The modified Van Rjin showed better prediction in sediment transport in the comparison between simulation and Stovin's experimental works.

It was suggested by turbulence studies that shear velocity U_* is of the same order of magnitude than turbulent velocity fluctuation u'（Yan, 2013）. BSS is a function of shear velocity, $\tau = \rho U_*^2$. BTKE is a function of turbulent velocity fluctuation, $k = \frac{3}{2}\overline{(u')^2}$. The two above equations mean that a relation between BSS and BTKE can be determined. Harsha (1970) investigated the correlation between turbulent shear stress and turbulent kinetic energy, and he proved a linear relationship between turbulent shear stress and turbulent kinetic energy by a study of a substantial amount of turbulent kinetic energy and turbulent shear stress data, which is well supported over a wide range of experimental conditions in incompressible flow.

Therefore, settling conditions based on BTKE or BSS may lead to comparable results (see Figure 3.11). Therefore, in this work the implementation for settling condition were focused on the widely used BSS method.

Based on the experiment data of Paintal (1971), Miller (1977) pointed out that the asymptotic value should be 0.045 not 0.06 for very large Reynolds number. In this work 0.045 was chosen for the fit equation (shown in equation 3.32b). Therefore the Shields curve in the figure 3.11 can be fitted thanks to the following expressions:

$$d_* = \left(v\sqrt{(\rho_P - \rho)gd^3/\rho}\right)^{-0.6} \tag{3.32a}$$

$$\theta = 0.22d_* + 0.045 \times 10^{-7.7d_*} \tag{3.32b}$$

Where d_* is a transformed dimensionless grain diameter and ρ is the fluid density, ρ_P is the particle density, d is the particle diameter, g is the gravity acceleration and v is the dynamic viscosity. Those two equations are used in defining the critical bed shear stress, where these two equations are coded in the user defined function to calculate the coefficient of critical bed shear stress.

Mathematically, the critical bed shear stress is defined as,

$$\theta = \frac{\tau_0}{(\gamma_s - \gamma)d} \tag{3.33}$$

Where τ_0 is the bed shear stress, γ_s is the particle specific weight, γ is the fluid specific weight and d is the particle diameter.

And the boundary Reynolds number can be presented as,

$$R_* = \frac{U_* d}{\upsilon} \tag{3.34}$$

Where R_* is the boundary Reynolds number, U_* is the shear velocity, υ is the dynamic viscosity and d is the particle diameter.

From equation 3.29, the critical bed shear stress can be obtained by knowing the coefficient of critical bed shear stress and the particle parameters, equations 3.28a and 3.28b give the calculation of the coefficient of critical bed shear stress.

$$\tau_c = \theta(\gamma_s - \gamma)d = \theta(\rho_s - \rho)gd \tag{3.35}$$

Where τ_c is the critical bed shear stress.

The process of particle tracking is showed in Figure 3.12. In the calculation of each case the user defined function is applied at the bottom to substitute the “trap” condition , where the critical bed shear stress can be calculated by the above equations and the local bed shear stress is obtained from the instantaneous calculation result, if the local bed shear stress is lower than the critical bed shear stress the particle will be defined as settled and the particle tracking terminates, otherwise the particle will be defined as “reflect” and the particle tracking continues.

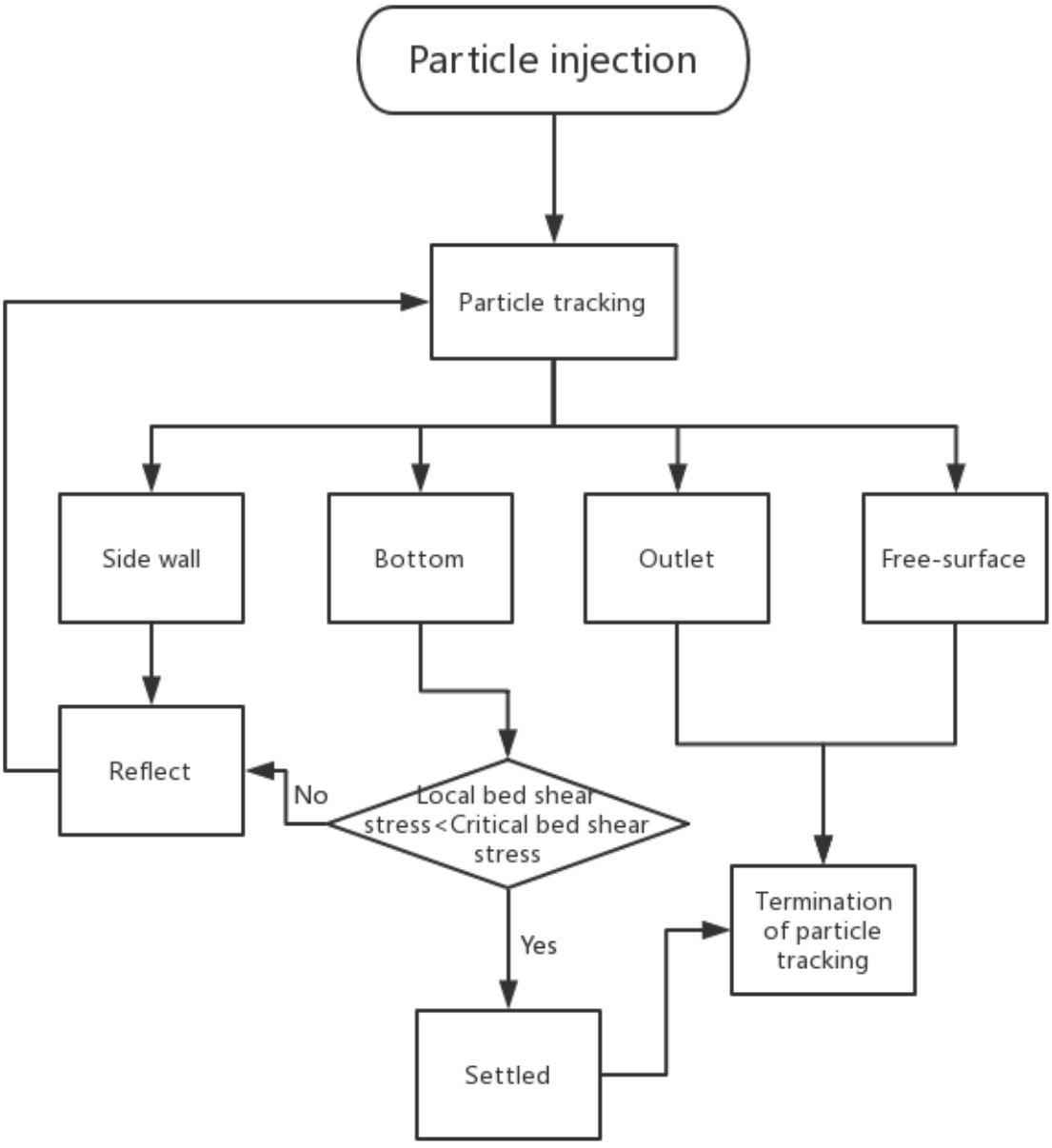

Figure 3.12 Particle tracking process

3.4.1 Suspension particle tracking

For all the cases with different entrance mass flow rate and variable water depth in the tank, the path line of the particles is also different. The eddy structure of the flow is

the main factor that will affect the path line of the particle. Figure 3.13-19 show all the path lines of the particles in some cases.

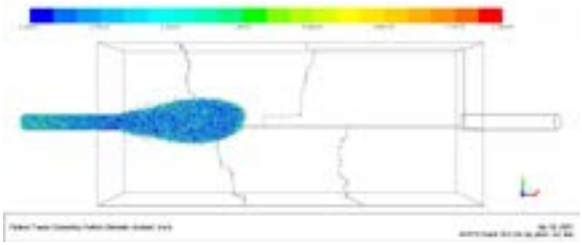

Particle trajectory at 3000 iterations

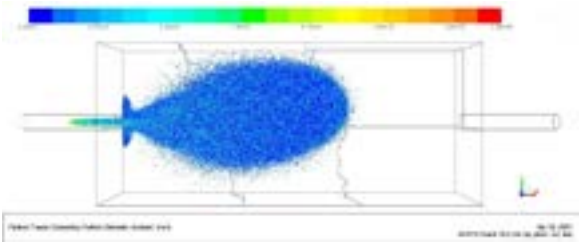

Particle trajectory at 15000 iterations

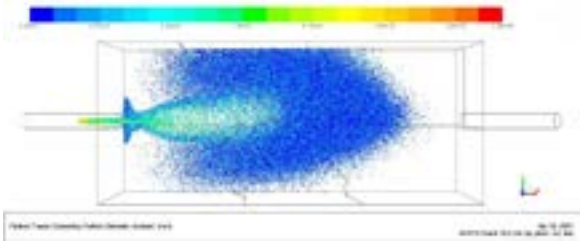

Particle trajectory at 25000 iterations

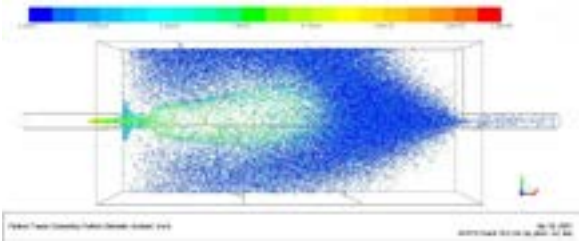

Particle trajectory at 35000 iterations

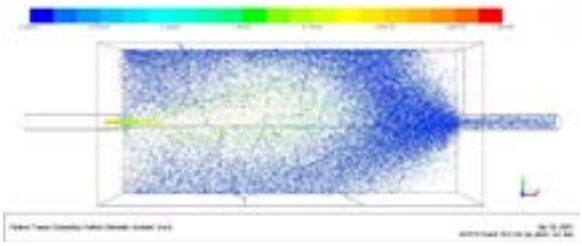

Particle trajectory at 45000 iterations

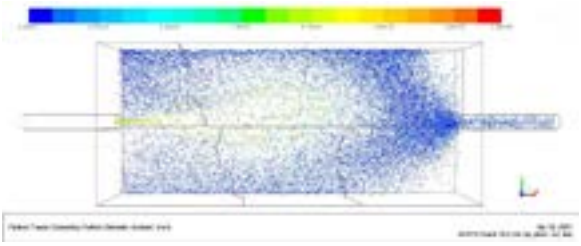

Particle trajectory at 50000 iterations

Figure 3.13 Particle trajectory at 1 L/s

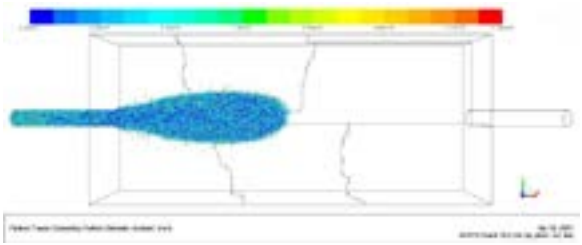

Particle trajectory at 3000 iterations

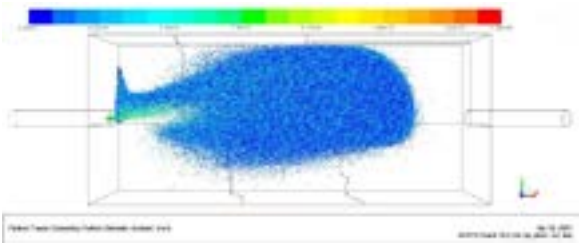

Particle trajectory at 15000 iterations

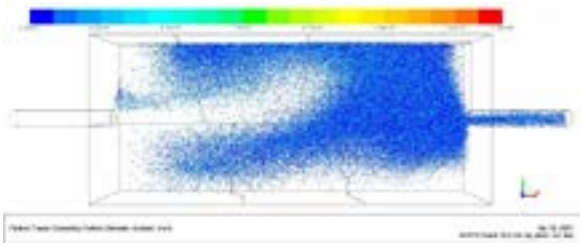

Particle trajectory at 25000 iterations

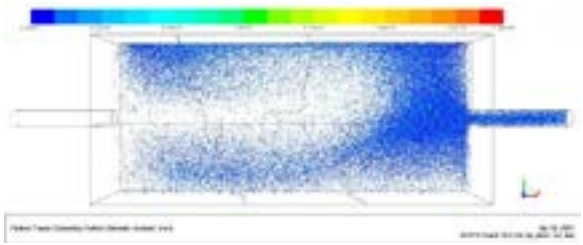

Particle trajectory at 35000 iterations

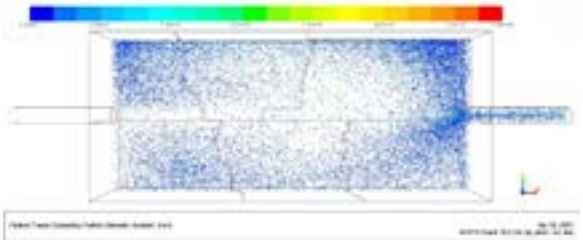

Particle trajectory at 45000 iterations

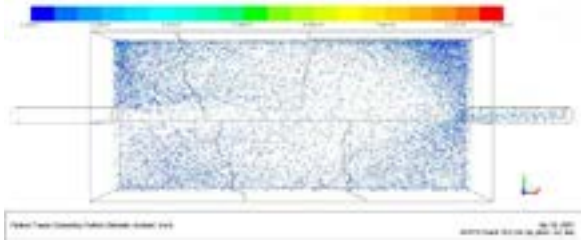

Particle trajectory at 50000 iterations

Figure 3.14 Particle trajectory at 1.5 L/s

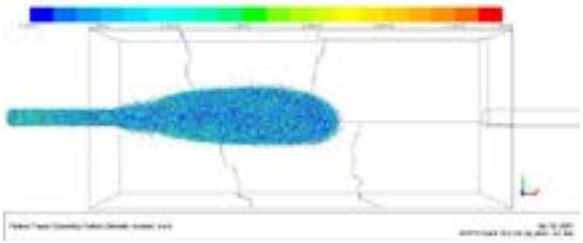

Particle trajectory at 3000 iterations

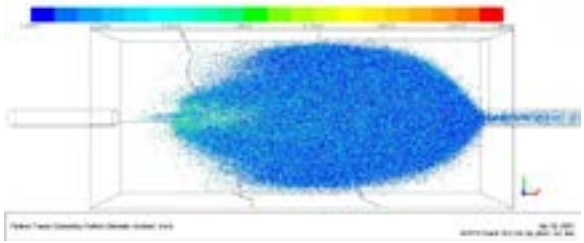

Particle trajectory at 15000 iterations

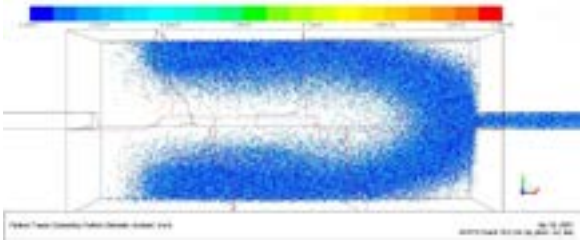

Particle trajectory at 25000 iterations

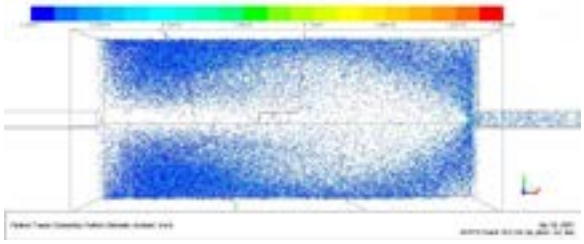

Particle trajectory at 35000 iterations

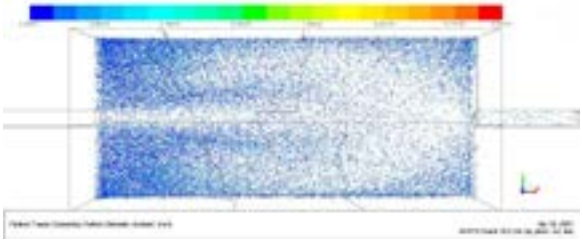

Particle trajectory at 45000 iterations

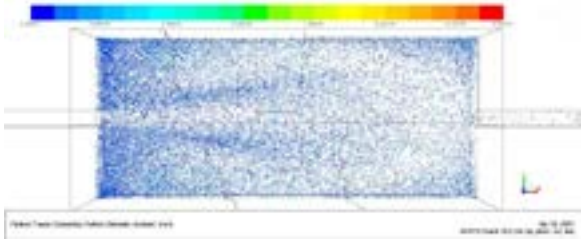

Particle trajectory at 50000 iterations

Figure 3.15 Particle trajectory at 2 L/s

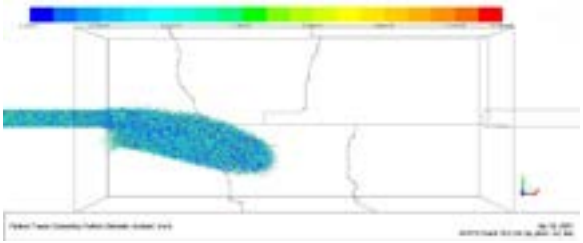

Particle trajectory at 3000 iterations

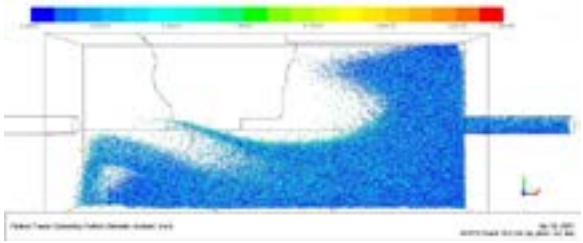

Particle trajectory at 15000 iterations

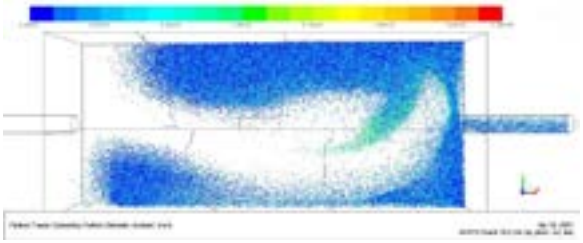

Particle trajectory at 25000 iterations

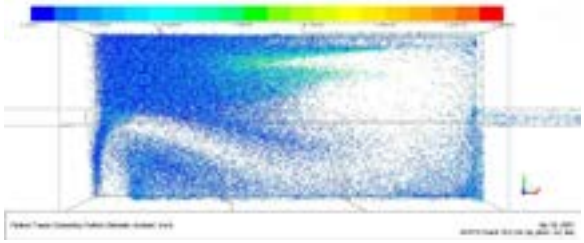

Particle trajectory at 35000 iterations

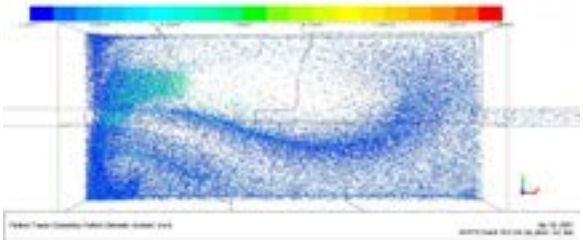

Particle trajectory at 45000 iterations

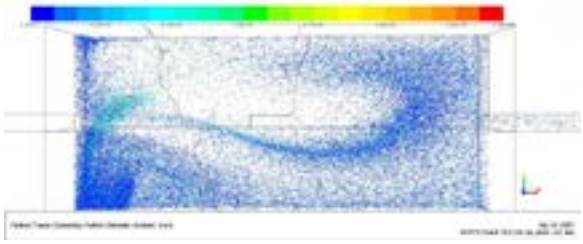

Particle trajectory at 50000 iterations

Figure 3.16 Particle trajectory at 2.5 L/s

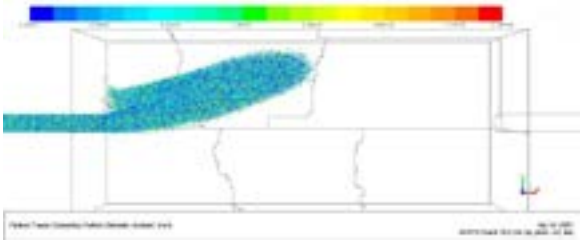

Particle trajectory at 3000 iterations

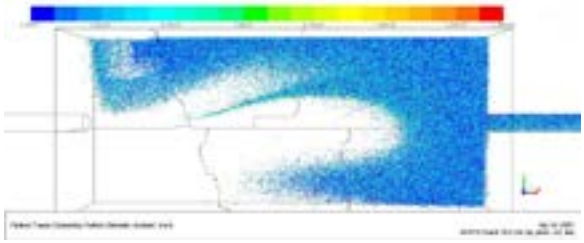

Particle trajectory at 15000 iterations

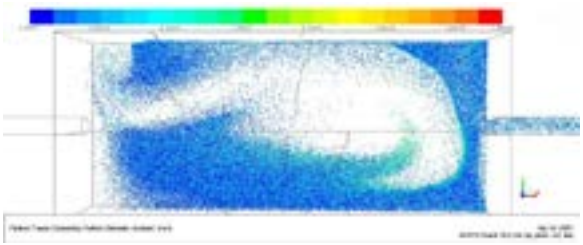

Particle trajectory at 25000 iterations

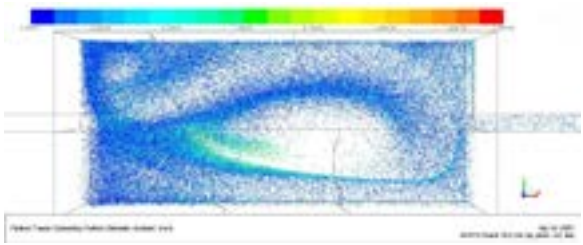

Particle trajectory at 35000 iterations

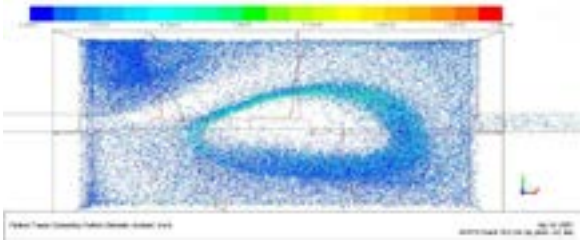

Particle trajectory at 45000 iterations

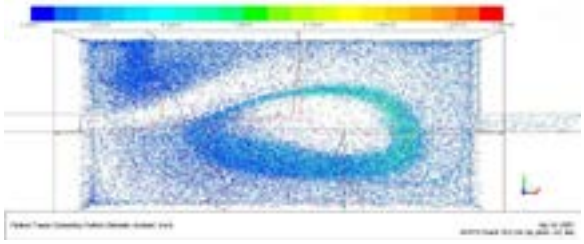

Particle trajectory at 50000 iterations

Figure 3.17 Particle trajectory at 3 L/s

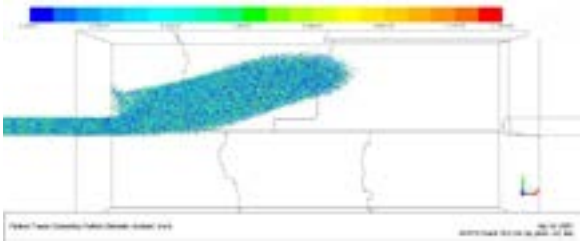

Particle trajectory at 3000 iterations

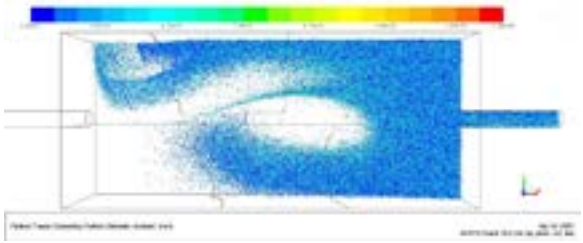

Particle trajectory at 15000 iterations

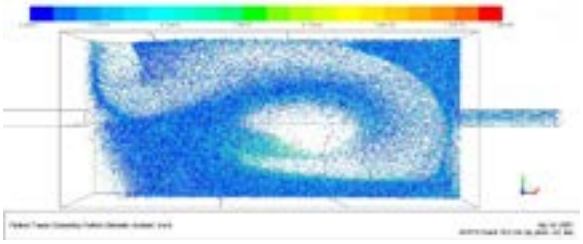

Particle trajectory at 25000 iterations

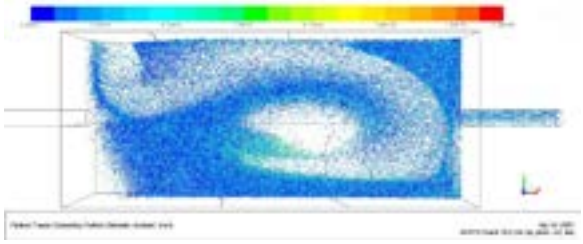

Particle trajectory at 35000 iterations

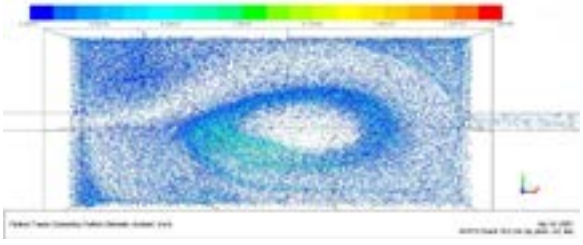

Particle trajectory at 45000 iterations

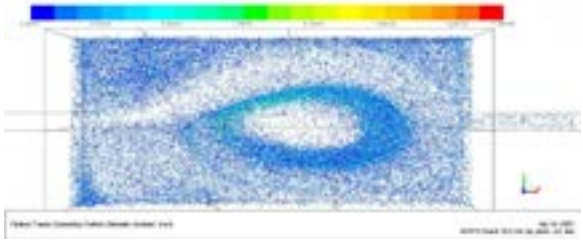

Particle trajectory at 50000 iterations

Figure 3.18 Particle trajectory at 3.5 L/s

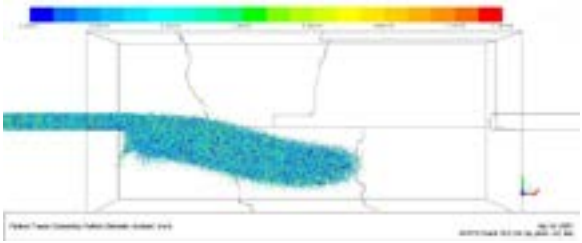

Particle trajectory at 3000 iterations

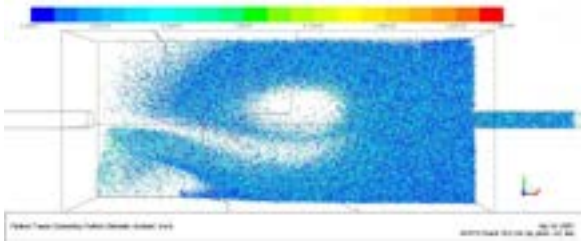

Particle trajectory at 15000 iterations

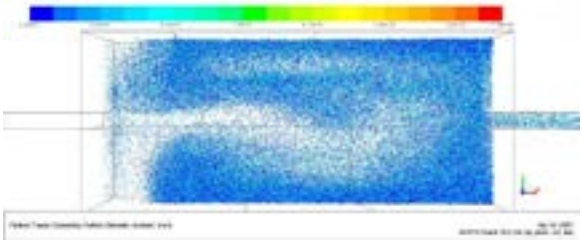

Particle trajectory at 25000 iterations

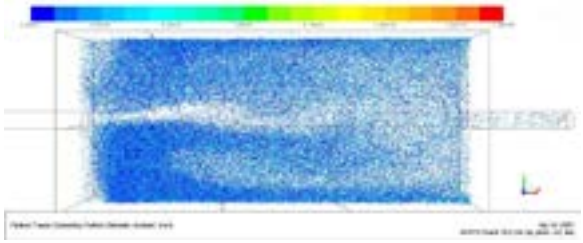

Particle trajectory at 35000 iterations

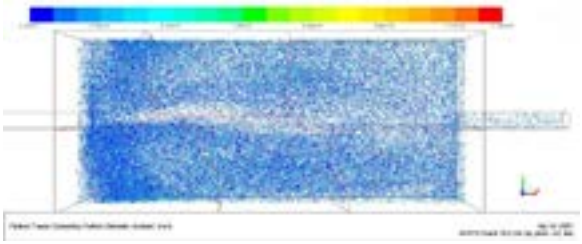

Particle trajectory at 45000 iterations

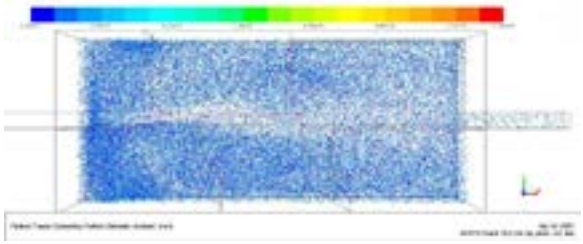

Particle trajectory at 50000 iterations

Figure 3.19 Particle trajectory at 4 L/s

All the particles enter the tank with the flow injection spread to all the tank according to the eddy distribution of the flow, and the area contains less suspended particle located at the center of the eddy, four corner of the tank are the region that much more suspended particle exist.

From the those figures, one significant conclusion can be obtained which is that all the particle with large diameter are more easily to settle, the critical bed shear stress for particle with large diameter is higher than those particle with small diameter, which proved by equation 3.31 theoretically.

Table 3.2 Comparison of trap efficiency between simulation and experiment

Inlet discharges (L/s)	Water depth (cm)		Trap efficiency	
	Simulation	Experiment	Simulation	Experiment

1	11.48	8.3~8.6	77%	83%
1.5	11.98	12.0~12.2	74%	75%
2	12.37	13.2~13.4	70%	68%
2.5	13.35	14.5~14.9	62%	56%
3	14.49	14.7	54%	33%
3.5	15.91	14.9~15.2	43%	22%
4	17.39	15.8~16	46%	5%

Table 3.3 shows the comparison of trap efficiency between simulation and experiment, in the cases with low entrance mass flow rate the prediction of trap efficiency is close to the experiment results, however the difference increasing due to the increasing entrance mass flow rate.

3.4.2 Particle deposition zone

When the particle reaches the bottom and the local bed shear stress is lower than the calculated critical bed shear stress, particle will be defined as settled and the particle trajectory terminate. The information of the settled particle including the location, the mass and the diameter will be recorded by the user defined function. And the following figures show the visualization of the spatial distribution of settled particle and the real spatial distribution of settled particle in the experiments made by Dufresne(2008). In Dufresne's experiment works, the deposition zones of particle can be only estimated by the camera visualization and the trap efficiency can be obtained by the measurement at the final step of the experiment.

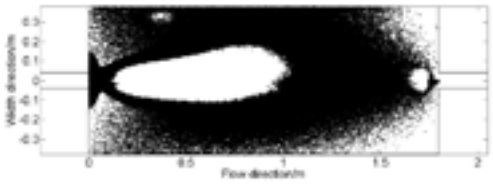

Figure 3.20 The comparison of deposition zones between numerical simulation and experiment results at 1 L/s

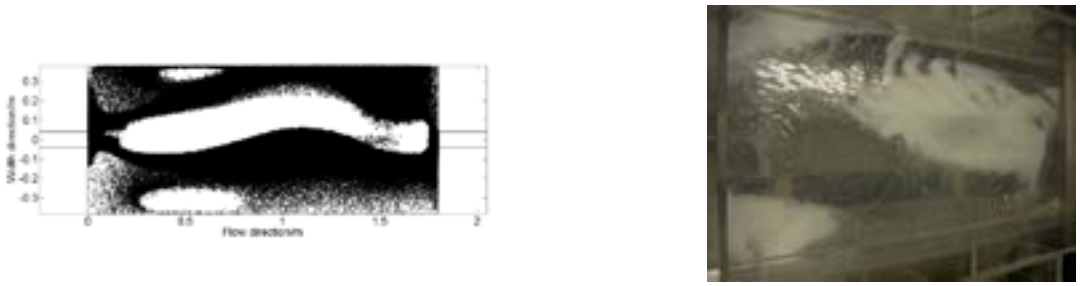

Figure 3.21 The comparison of deposition zones between numerical simulation and experiment results at 1.5 L/s

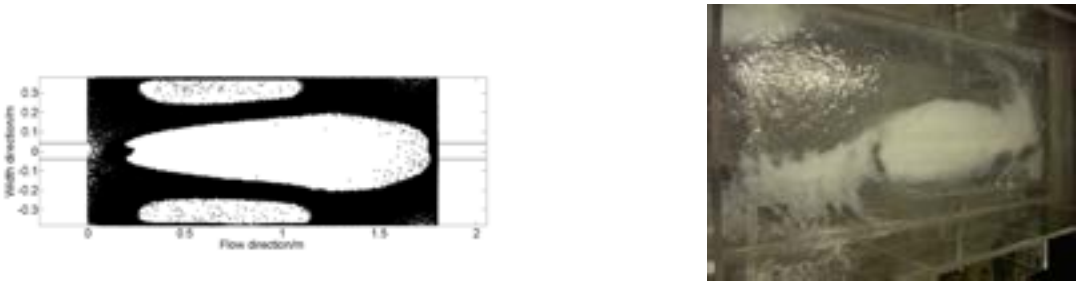

Figure 3.22 The comparison of deposition zones between numerical simulation and experiment results at 2 L/s

Figure 3.23 The comparison of deposition zones between numerical simulation and experiment results at 2.5 L/s

Figure 3.24 The comparison of deposition zones between numerical simulation and experiment results at 3 L/s

Figure 3.25 The comparison of deposition zones between numerical simulation and experiment results at 3.5 L/s

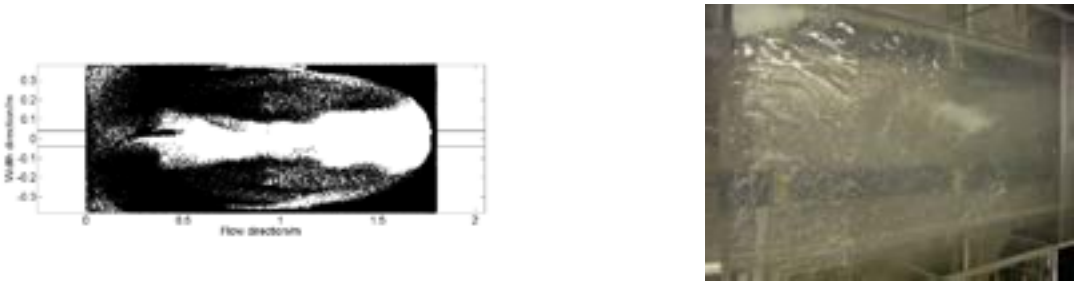

Figure 3.26 The comparison of deposition zones between numerical simulation and experiment results at 4 L/s

Figure 3.20-3.26 show the deposition zone at the bottom in the numerical simulation of particle sedimentation, which show a large settle possibility in the four corner of the rectangular tank, which is not correct at the two corners in the backward of the

tank. In case where the entrance mass flow rate is 1 L/s, the simulation results of particle sedimentation is almost the same with the experiment results, in cases with higher entrance mass flow rate, the result show large settle possibility at the center of the big eddy and two corners at the front of the tank.

The result showed very bad prediction in the deposition zone and trap efficiency in the case with higher mass flow rate such as 4 L/s and 5 L/s. The reason for this phenomenon is the re-suspension, at the beginning of the injection many areas are in agreement with the settling criterion, however the flow with higher mass flow rate is more turbulent than the flow with lower mass flow rate, the changing BSS distribution at the bottom makes the area which used to be accord with settling condition don't conform to the condition anymore, however in calculation the settled particle can't re-suspension again, which leads to the bad prediction.

Bed shear stress at the bottom changes even the eddy structure of the flow is stable. The eddy structure is a dynamic equilibrium when the flow is stable, the others parameter of the flow is still changing with the continuous water injecting in the tank, especially the bed shear stress, which makes the deposition zone predicted by the critical bed shear stress varies with the continuous injecting water. The continuous variation of bed shear stress makes the sedimentation of particles become a dynamic process, the onefold criterion for settling can't evaluate the real process of particle sedimentation precisely.

3.4.3 Statistic analysis for the sedimentation

Sediment transport is a random process, where the statistics theory is widely used in the analysis. In this part, some concepts of statistic theory are used to analyze the sedimentation information, including mathematical expectation and variance.

Figure 3.27 shows portion distribution of settled particle diameter with different flow rate, where a same diameter distribution type of settled particle is found though the flow rate varies.

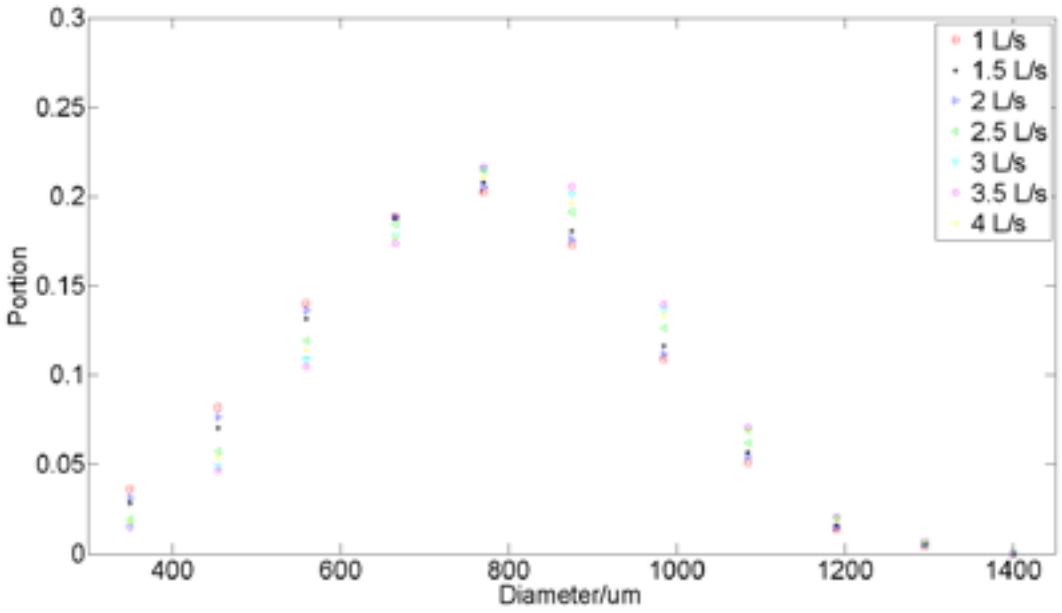

Figure 3.27 The portion of settled particle with variable diameter in all cases

Due to not all the tank is the area for sedimentation, the tank is divided into five parts to analyze the sedimentation (shown in Figure 3.28). Figure 3.28 shows the averaged settling location in each part. In part 1 and 2, the center of settling location move to the side wall in the left and right from the flow direction with increasing flow rate. In part 3, 4 and 5, the center of settling location is more dispersive, the entire tendency of the center is moving to the downstream.

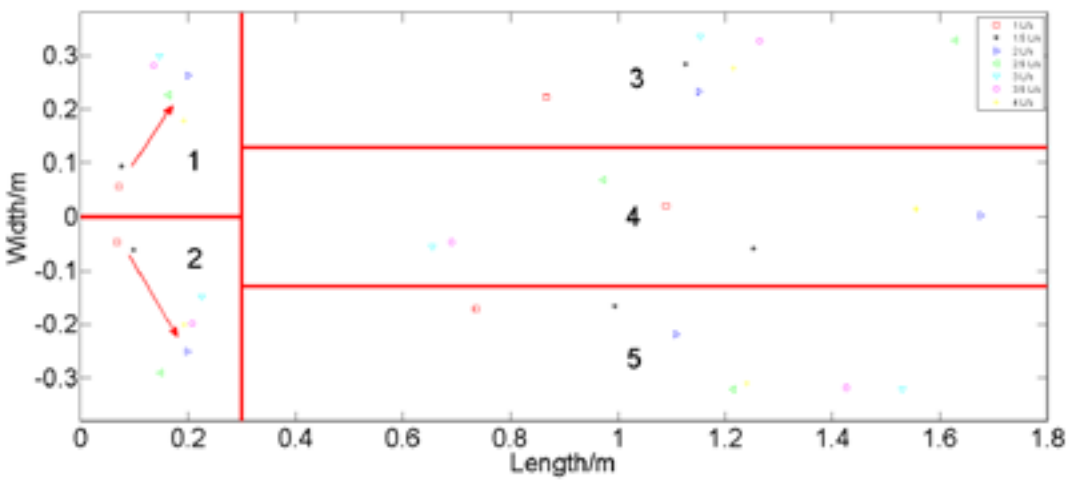

Figure 3.28 Averaged deposition location in 5 parts

Figure 3.29 and 3.30 show the variance of X and Y coordinates in 5 different parts respectively. Firstly, the variance in X coordinates is more significant than that in Y coordinates, the order of magnitudes of variance in X coordinates is 200 times to that in Y coordinate, which can also prove that the fluctuation in flow direction in the flow of tank is the most significant. Secondly, the variance is increasing with increasing flow rate, the increasing flow rate means the increasing intensity of the flow injection and much more impact of the flow injection on the whole flow field.

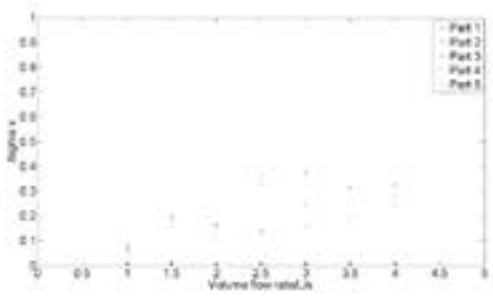

Figure 3.29 Variance of X coordinates in 5 parts

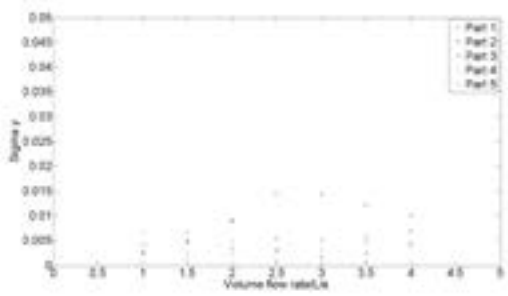

Figure 3.30 Variance of Y coordinates in 5 parts

Figure 3.31 shows trap efficiency of 5 parts with increasing flow rate. The difference of trap efficiency in different part is small when the flow rate is low, which increases

with the augmentation of flow rate. The portion of settled particle in part 1 and 2 is decreasing and correspondingly the portion of settled particle in part 3, 4 and 5 is increasing with the enlarging inlet discharge.

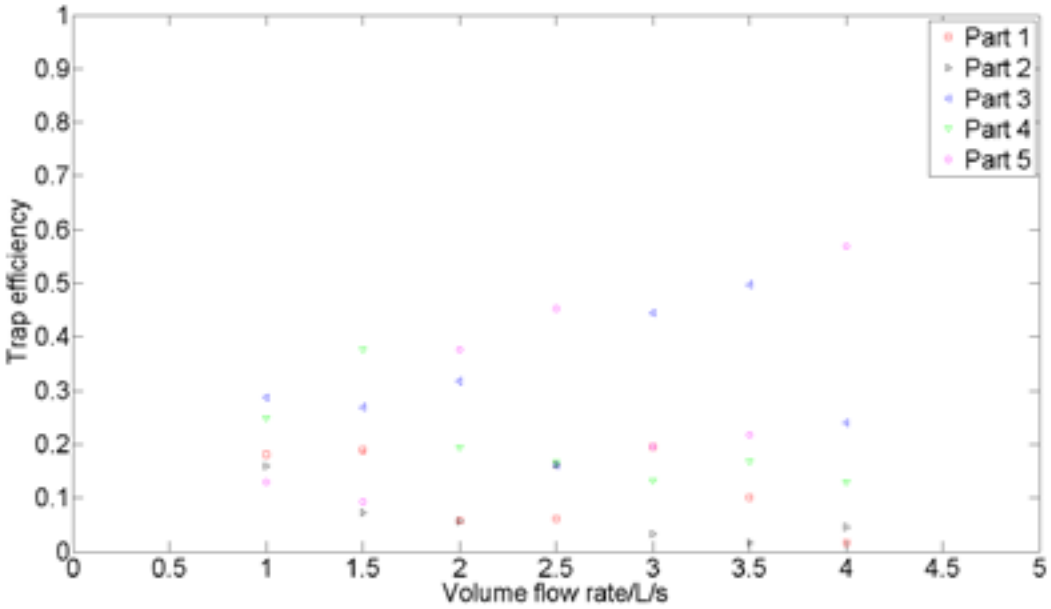

Figure 3.31 Trap efficiency of 5 parts with increasing flow rate

3.5 Conclusions

Particle tracking is available in the numerical simulation, the path line of suspension particle is mainly determined by the eddy structure of the flow in the tank. However the sedimentation of particle is more complicated. The “trap” condition in the fluent codes can’t restore the real physical process of sedimentation, due to the high overestimation in trap efficiency and inaccurate deposition zones. In order to solve the problem, a user defined function based on the shields curve was added to the bottom boundary to improving the prediction of particle sedimentation.

The improved boundary condition for simulating particle sedimentation can promote the prediction of trap efficiency and deposition zones in some extent. However it still can’t restore the real condition completely. The improved boundary condition is more accurate in conditions with low entrance mass flow rate rather than high entrance mass flow rate. The reason is that the particle movement becomes more complicated due to the increasing entrance mass flow rate lead to a more turbulent flow, the

particle will settle, roll, slide at the bottom and even re-suspend from the bottom rather than only settle at the bottom when entrance mass flow rate is relatively low.

The simulation on sediment transport in ST shows, the center of the deposition zone is retrusive and the uncertainty in X coordinates is much higher than that in Y coordinates. And the diameter distribution of settled particles belongs to a similar type though the inlet discharge is changing.

The process of sediment transport is a random process, the criterion for settling and initiation theoretically is not the only norm that will determine the state of the particle. Introducing the stochastic method to the criterion might be a useful idea in improving the prediction of trap efficiency and deposition zone of sediment transport.

The accumulated particle at the bottom form the new boundary, the difference between the particle material and bed material means the changing of settling condition, which might lead to the wrong prediction in the numerical simulation.

4. Experiment of flow patterns and sediment transport in storm tank with variable cavity

4.1 Introduction

This chapter introduces the experiment works on a rectangular pilot basin with a cavity at the bottom. The reason for the selection is to investigate the effect of the cavity on the flow patterns and sediment transport in storm tank.

The investigation on a rectangular tank has been processed by many researchers, for example Stovin et Saul (1994), Stovin (1996), Kantoush (2007) and Dufresne (2008). However the application of a simple rectangular tank is not necessary to fulfill the request of the stormwater management system. New design for the rectangular tank is needed to catch up with the quickly change of urban water system due to high development of the urbanization.

In the end, a rectangular tank with high ratio of length to width and cavity was chosen for experiment on flow and sediment transport. This work will not just provide velocity measurement of the flow in the tank with cavity, but also provide the sediment deposition measurement in the tank with cavity. And the results obtained from experiment can be used for verification of the numerical simulation of flow and sediment transport in the tank.

4.2 Experiment devices

4.2.1 Geometry

The experiment system is showed in Figures 4.1, 4.2 and 4.3 as follow. As it can be seen, the experiment device is a circulation system, the water is under cyclic utilization. The experiment system is mainly constituted by two rectangular basins, one is for experiment and the other is for collecting the sediment and store water for the circulation. The length of the experiment basin is 4240 mm, the width is 760 mm, the height is 405 mm, and the dimension of the cavity is 325 mm × 760 mm × 80 mm. The entrance part is a circular pipe with the diameter equals to 80 mm, there are two exits in the experiment basin, the upper exit is a circular pipe with the diameter equals to 160 mm and the nether exit is a circular pipe with the diameter equals to 80 mm.

Figure 4.1 Experimental tank

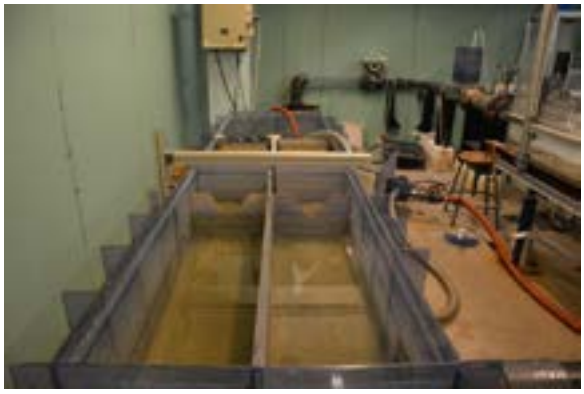

Figure 4.2 Collecting tank

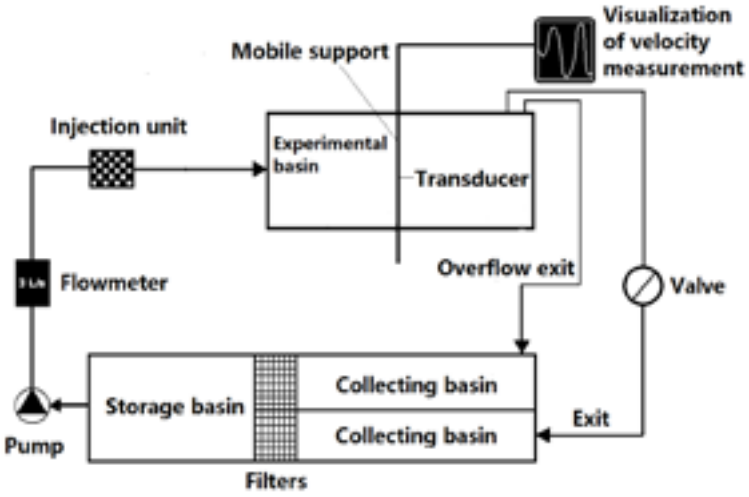

Figure 4.3 Scheme of experiment devices

The whole experiment measurement system is showed in the Figure 4.3. The measuring device (transducer) is based on the analysis of ultrasonic signals backscattered by a particle cloud. The measurement transducer is fixed in a mobile support on the experimental tank, which is able to move in the length direction and width direction of the tank. By the pumping action, water enters the pipe from the storage basin, the particle is injected in the injection unit, after mixture in the pipe, water and particle enters the experimental basin. Water and particle will be discharged to collecting basin through the two exits, at the end of the collecting basin particle will be intercept by the filters and the water pass through the filters entering into the storage basin. The valve in the exit part is to control the water level in the experimental basin.

In front of the injection unit, it's a flowmeter for controlling the volume flow rate. Normally, for the accuracy of the entrance volume flow rate, the value in the machine will be checked about every two minutes. And the volume flow rate can’t be fixed at a stable value all the time, the value will fluctuate around the expected value, the fluctuation range of the machine is +/- 0.1 L/s.

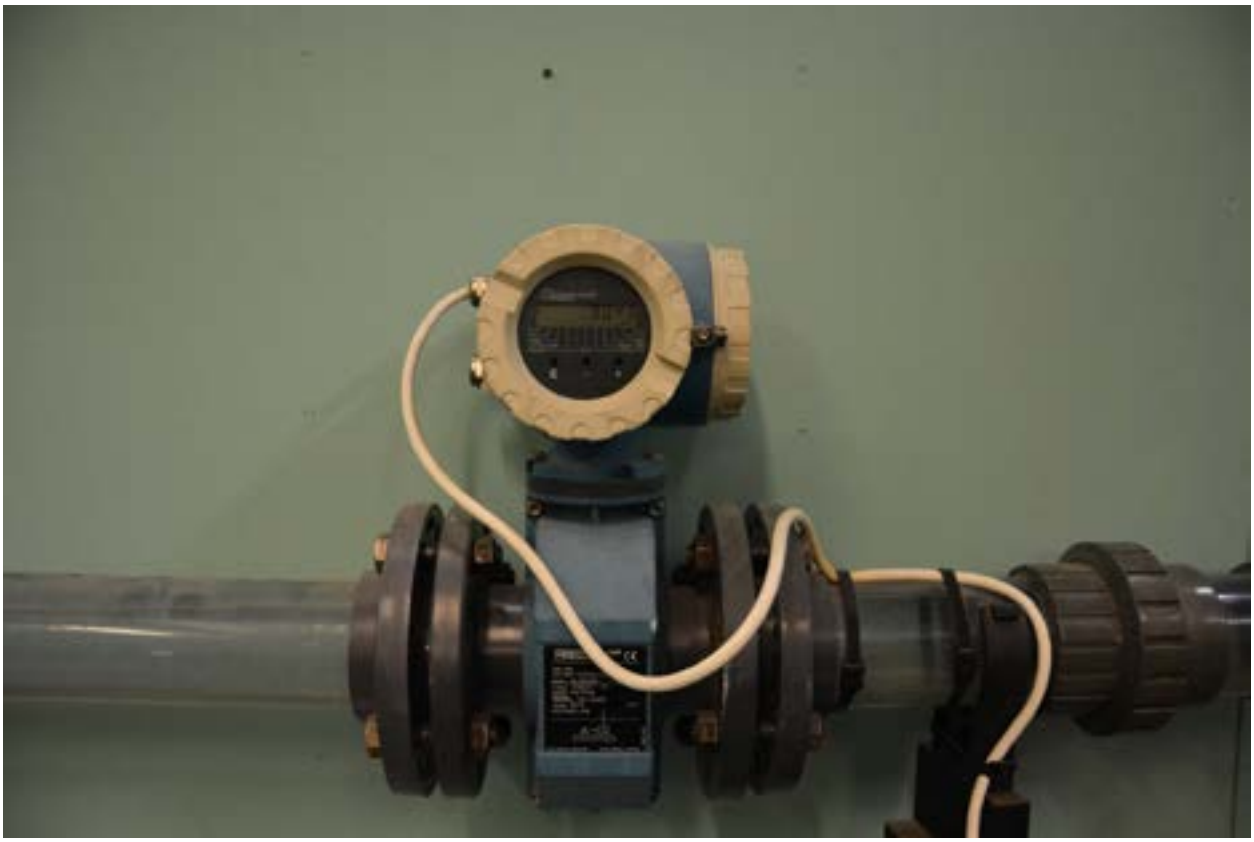

Figure 4.4 Flowmeter

To obtain a uniform injection of the particle, a particle mixture is generated by an agitator first and the particle is transported from the column through a plastic pipe into the injection part of particles. The mixture of particles is shown in Figure 4.5.

Figure 4.5 Mixture system

The rotation of the agitator leads to vibration of the whole mixture system, the support around the column is to keep the stabilization of the mixture system. And some weights are placed on the base of the support to obtain stabilization.

In front of the experiment basin, there is an assembly unit for injecting the particles. The particle is transported into the inlet pipe of the experimental basin by a plastic pipe from the mixture column via a machine for controlling the injection velocity, the injection velocity is controlled by Masterflex L/S ECONOMY DRIVE.

Figure 4.6 Masterflex L/S ECONOMY DRIVE

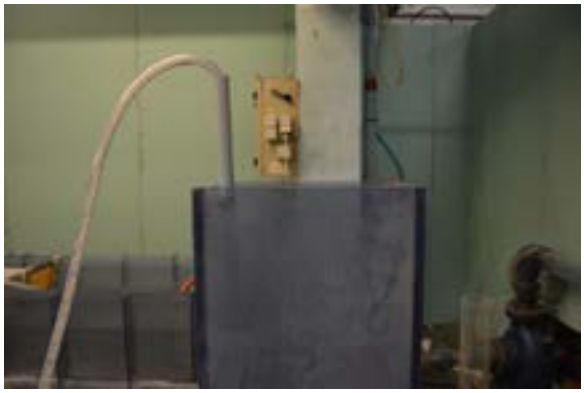

Figure 4.7 Injection unit

Two transducers accomplish the velocity measurement, the beam and the plastic container are for the fixation to the support. The support is designed to move along length direction and width direction for the transducer to measure the velocity at different locations.

Figure 4.8 Transducer

Figure 4.9 Support for fixing the transducer

The signal received by the transducer is transferred to the signal receive machine and the signal is transformed to velocity value which will be displayed on the computer screen. The fluctuation of the velocity at one location can be displayed on the screen. From the display of the velocity fluctuation and amplitude of the particle energy, the

appropriateness of the measurements can be determined. The interface for the measurements is based on Labview.

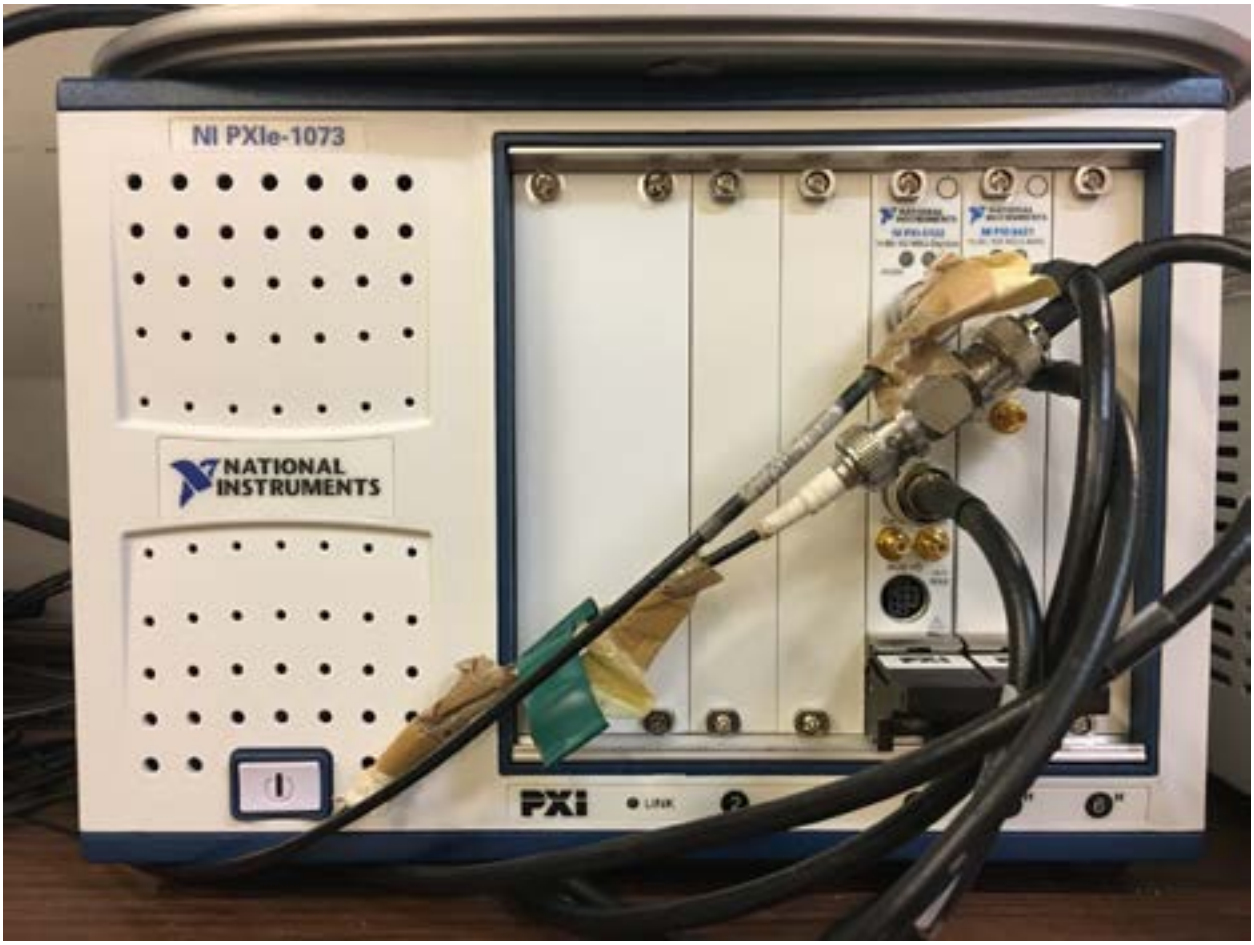

Figure 4.10 Signal receive machine

4.2.2 Particle characteristic

4.2.2.1 Introduction

In the same way as for hydraulics, in order to transfer the results of solid transport obtained on a physical model to a life-size structure, the laws of similarity adapted to solid transport must be respect.

Normally, three dimensionless numbers are used to characterize solid transport: i) the particle Reynolds number, ii) the constraint of Shields, iii) Froude number.

The similarity laws can be expressed by the equations as follows:

$$\frac{\Delta\rho_M}{\Delta\rho_R}\frac{d_M}{d_R}=\frac{h_M}{h_R} \tag{4-1}$$

$$\frac{d_M}{d_R}=\left(\frac{h_M}{h_R}\right)^{-\frac{1}{2}} \tag{4-2}$$

Where $\Delta\rho$ is the difference between the density of particles and the fluid. d is the diameter of the particles. M represents the physical model and R represents the real work.

4.2.2.2 Description of the particles

In order to fulfill the request of this thesis, the deposition zone of the particles in the reservoir should be acquired. The chosen particle was already investigated in the laboratory (Schmidt,2003), the particle was proved to be sphere and the granulometric distribution is non-uniform, the specific information for the diameter of the particle is shown in Table 4.1. The material of the particle is polystryrol.

Table 4.1 Granulometric characteristics of the polystyrol particles (Schmidt, 2003)

d_{min}	350 μm
d_{10}	535 μm
d_{20}	593 μm
d_{30}	642 μm
d_{40}	689 μm
d_{50}	738 μm
d_{60}	790 μm
d_{70}	851 μm
d_{80}	931 μm
d_{90}	1056 μm
d_{max}	1400 μm

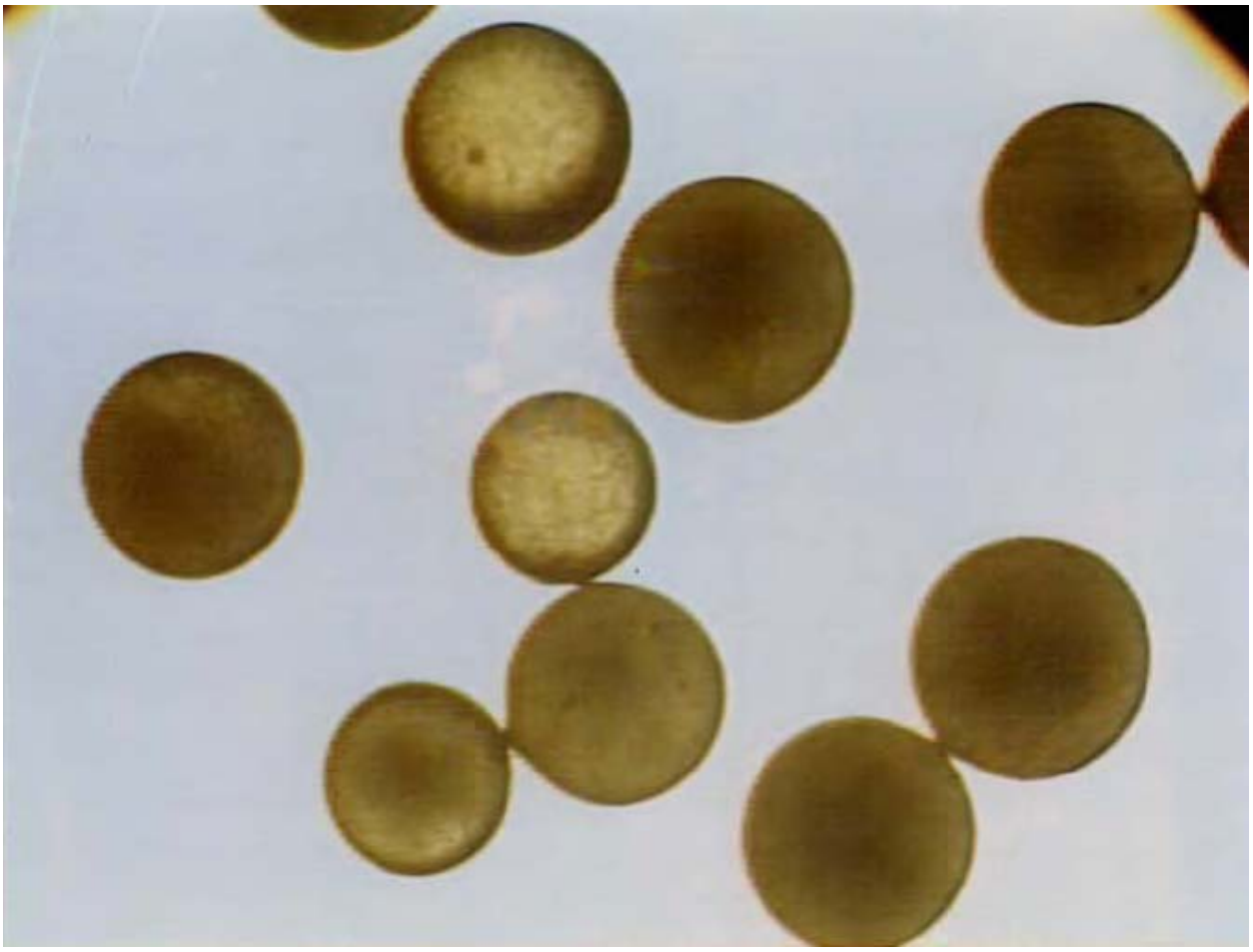

Figure 4.11 Polystyrol particles observed under microscope (Schmidt, 2003)

Schmidt obtained the density of the particle by pycnometry through 21 measurements, also the settling velocity was obtained, the results are shown in Table 4.2.

Table 4.2 Density and settling velocity of the polystyrol particles (Schmidt, 2003)

Density (kg/m^3)	1034 +/- 19
Settling velocity (m/s)	0.0104 +/- 0.0008

4.2.2.3 Granulometric analysis for the particles

Due to the necessity to know the diameter distribution of the particles, a granulometric analysis has been finished in the laboratory. The device used for the granulometric

analysis are series of sieves, including 0.063 mm,0.08 mm,0.125 mm, 0.16 mm, 0.25 mm, 0.5 mm, 1 mm, 2 mm.

The lack of sieves between 0.5 mm to 1 mm makes it hard to determine the specific diameter distribution of the particles. The results of the granulometric analysis can only prove that most of the diameter of the polystyrol particle is situated between 0.5 mm to 1 mm, which is different from the results of Schmidt.

And the measurement for determining the settling velocity of the particle can also obtain the diameter distribution of the particle.

Figure 4.12 Sieves for granulometric analysis

4.2.2.4 Measurements of the settling velocities of particles

The measuring device is based on the analysis of backsacttered ultrasonic signal by a particle cloud. The temporal displacement of the signal of the signal with respect to the emission makes it possible to determine the spatial positions of the particles, the phase slip (Doppler effect) the speed of the particles and the backscattered amplitude the local concentration. A punctual release of a set of particles is carried out on the surface of a measuring tank in the immediate vicinity of an ultrasonic transducer oriented vertically downwards. During their sedimentation, vertical segregation of the particles appears as a function of their velocity. At a sufficient depth (of the order of at least 50 cm) and at a given instant, all the particles have the same rate of sedimentation, the temporal evolution of the velocities and the backscattered amplitudes is recorded throughout the passage of the cloud of particles.

At the end of a particle release, the data presented in Figure 4.13 and 4.14 are obtained. On one hand, the evolution of the backscattered amplitudes is in Figure 4.13, on the other hand, the velocity evolution is in Figure 4.14. As it can be seen at a given instant, the backscattered amplitudes exhibit very significant spatial-temporal variations. This is inherent in the method and is not related to fluctuations in concentration. Indeed, at a given concentration, the amplitude backscattered by a cloud of particle follows an exponential probability law due to the summation of the intensities at random phase. It follows that the method implies a certain level of slippery average. Here the average is performed on 5 consecutive profiles.

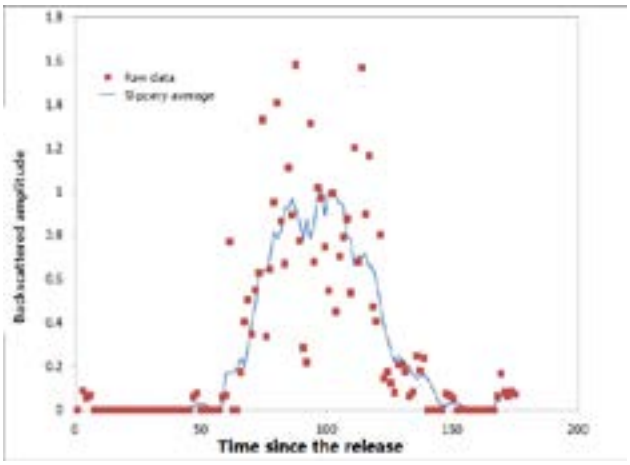

Figure 4.13 Temporal evolution of the backscattered intensities at 75 cm depth

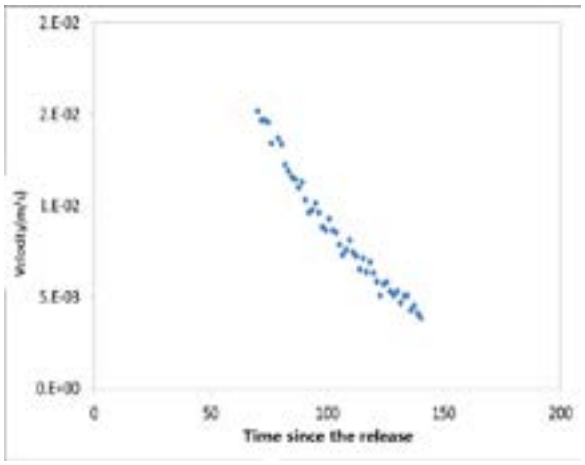

Figure 4.14 Temporal evolution of speeds at 75 cm depth

The velocity shown in Figure 4.14 is calculated from the Doppler frequency f_D of the sound velocity c and the ultrasonic frequency f_P :

$$V = \frac{cf_D}{2f_P} \tag{4-3}$$

The average effective voltage U_s from the intensity backscattered by a homogeneous cloud of particle of radius a and volume concentration C_v situated at the distance r of the emitter in the far field is expressed by:

$$\langle U_s^2 \rangle = \langle U_e^2 G \rangle C_v \frac{f(x)}{a} \frac{3c\Delta t}{32} e^{-(\alpha_w + \alpha_p)2r} \tag{4-4}$$

Where U_e is the emission voltage, G is the gain of the transducer, Δt is the emission time, α_w and α_p represent the attenuation coefficients relative to the fluid and the particles respectively.

The function $f(x)$ is the form function of the particles, it is expressed by:

$$f(x) = \frac{1.21x^2}{1 + 1.1x^2} \tag{4-5}$$

For spheroidal particles with $= \frac{2\pi a}{\lambda}$, where λ is the ultrasonic wavelength. Thus with a given distance from the emitter and considering a attenuation by the negligible particles in the case of very low concentration it comes as:

$$\langle U_s^2 \rangle = KC_v \frac{f(x)}{a} \tag{4-6}$$

Where K is constant. Thus the backscattered intensity not only depends on the concentration of the particles but also on their size. Therefore it is necessary to estimate the particle sizes in order to eliminate the backscattered size-intensity dependency effect.

The sedimentation velocity, V of the particles is related to the diameter by the relation:

$$V = \sqrt{\frac{4}{3C_d} g 2a \left(\frac{\rho_p}{\rho_w} - 1\right)} \tag{4-7}$$

The drag coefficient C_d is related to the Reynolds number of the particles by the semi-empirical relation:

$$C_x = \frac{24}{Re} \quad if\ R_e < 1 \tag{4-8a}$$

$$C_x = 3.69 + \frac{24}{Re} + \frac{0.09}{Re^2} \quad if\ 1 < R_e < 10 \tag{4-8b}$$

$$C_x = 1.12 + \frac{29.17}{Re} - \frac{3.889}{Re^2} \quad if\ \ R_e > 10 \tag{4-8c}$$

Knowning the density and settling velocity of the particles, then the diameter can be found by iterations, which make it possible to compute at each instant, therefore for each speed class the correction coefficient of diameter is $\frac{f(x)^2}{a}$.

The volume fraction of the particles $\gamma(V_i)$ having a velocity V_i for a radius a_i thus can be given as:

$$\gamma(V_i) = \frac{\frac{\langle U_s(V_i)^2 \rangle}{\frac{f(x_i)^2}{a_i}}}{\sum_{j=1}^{n} \frac{\langle U_s(V_j)^2 \rangle}{\frac{f(x_j)^2}{a_j}}} \tag{4-9}$$

Conversely, if the granulometric distribution is known, the density of the particles can be found. This is adjusted so that the granulometric distributions calculated by ultrasonic method coincide with the true particle size distribution.

The result of this measurement showed, the density of the particle should be 1050 kg/m^3, which is similar to the test of Schmidt. And the settling velocity distribution

and diameter distribution are shown in Figures 4.15 and 4.16. Apparently, the settling velocity varies with the changing of the particle diameter.

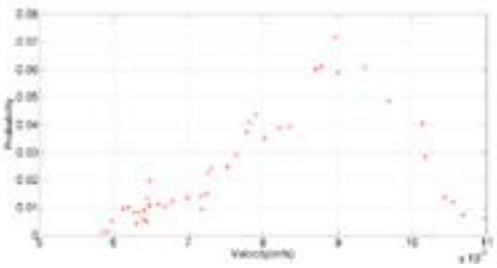

Figure 4.15 Settling velocity distribution

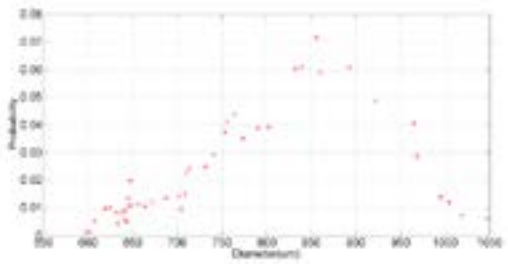

Figure 4.16 Diameter distribution

Normally, the distribution of the size of the particles can be defined with different method. In the Fluent code, a method named Rosin-Rammler distribution(R-R distribution) is used in the description of particle size. The mathematical expression of this method is:

$$Y_d = 1 - \exp\left(-\left(\frac{d}{\bar{d}}\right)^n\right) \tag{4-10}$$

Where Y_d is the accumulated mass fraction, d is the particle diameter and $\bar{d}$ is the particle diameter when $Y_d = 63.2\ \%$, n is the spread parameter.

The measured data of the particle diameter distribution is showed as green circle in the figure 4.17. By using the R-R distribution to fit the measured data, where $\bar{d} = 837\ \mu m$ and the spread parameter n is in the range of 8.5 to 9.5, the blue curve in the figure is under $n = 9$.The particle diameter distribution fit the R-R distribution quite well.

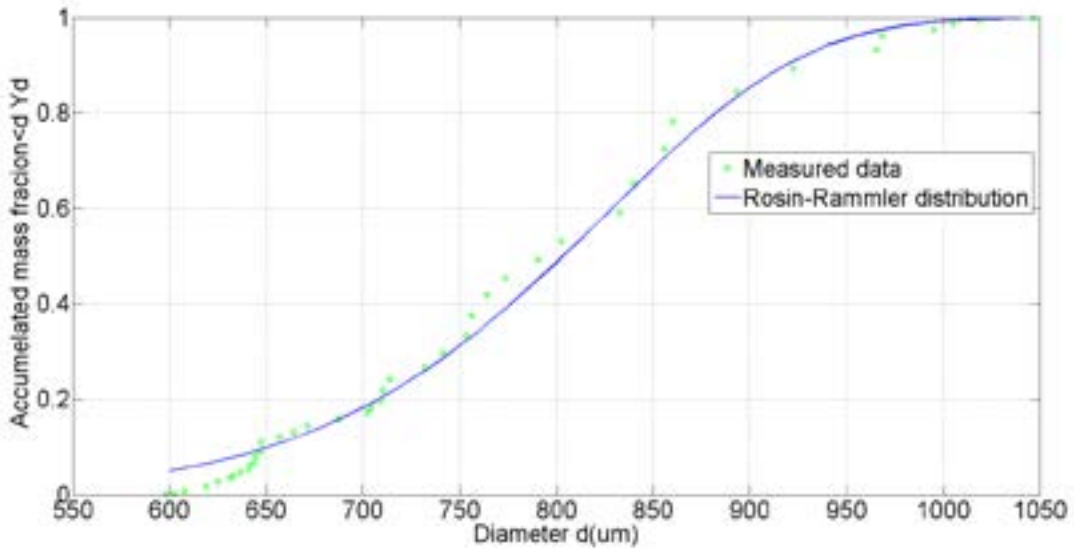

Figure 4.17 Accumulated size distribution of particles

And from the measurements, the granulometric distribution of the polystyrol particles is also obtained, which is showed in Table 4.2. The result proves that the granulometric test with using sieve is correct about the range of particle diameter. Though the polystryrol particle is the same as in the investigation of Schmidt, the distribution of particle diameter is not the same.

Table 4.3 Granulometric distribution of the polystyrol particles

d_{min}	600 µm
d_{10}	650 µm
d_{20}	708 µm
d_{30}	746 µm
d_{40}	776 µm
d_{50}	803 µm
d_{60}	829 µm
d_{70}	854 µm
d_{80}	882 µm
d_{90}	918 µm
d_{max}	1047 µm

4.3 Measurements of the velocity field

As the transducers can only test one location at one time, to obtain the detail information of the flow in the whole tank, the best method is to measure enough data at different location of the tank, and then average the velocity at each location by time to obtain the time-averaged velocity. By taking the processing time of the experiment into consideration, 60 points are measured for each entrance volume flow rate, and each test of one point sustains for two minutes. The distribution of measured points is showed in Figure 4.18.

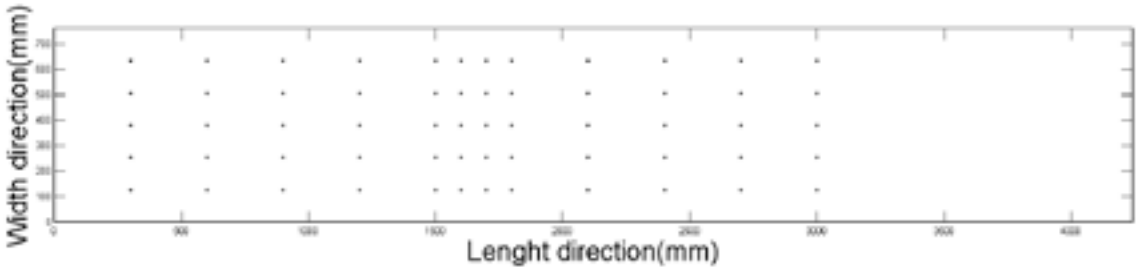

Figure 4.18 Test points distribution

In the process of measuring the velocity, the velocity is transient, the changing rate of the velocity displayed on the screen depends on the optional frequency, which can also affect the accuracy of the velocity measurement.

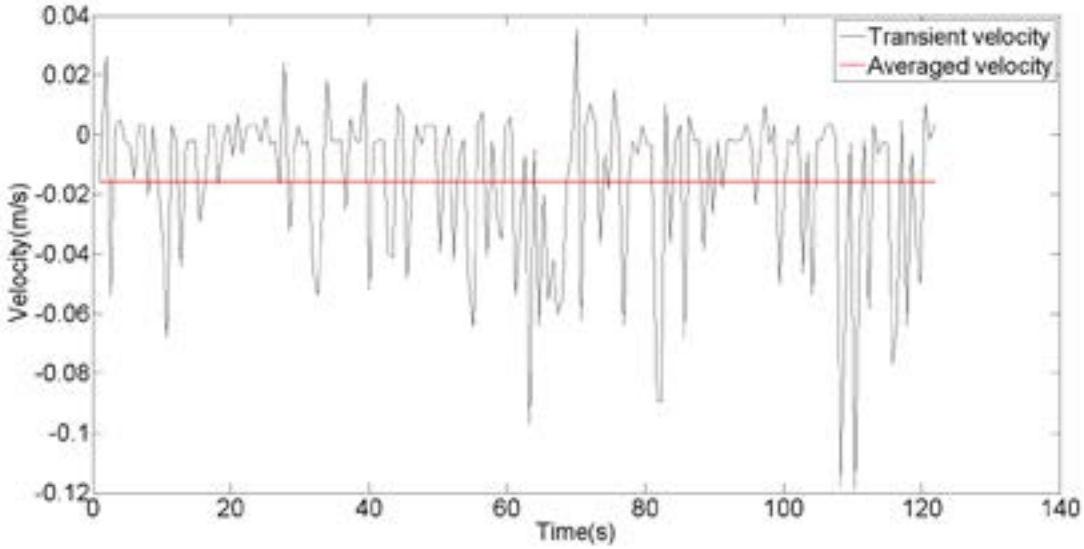

Figure 4.19 Transient velocity in the measurement

As the transient velocity changes in the measurement of 2 minutes, the velocity profile on the screen changes respectively, the velocity profile at one fixed time is shown in Figure 4.19. The transducer tests all the velocity from the bottom of the transducer to an optional distance. The water level of Figure 4.20 showed below is about 13 cm except for the cavity, so the distance was set as 0.25 m, the part where the velocity almost equal to 0 in the figure represent the bottom, and after the bottom it's air. The part before the bottom is the velocity of fluid, and at a fixed time the velocity should be continuous, if the distribution of the velocity is chaotic, it means the measurement is wrong. And the velocity profile showed in figure is normal.

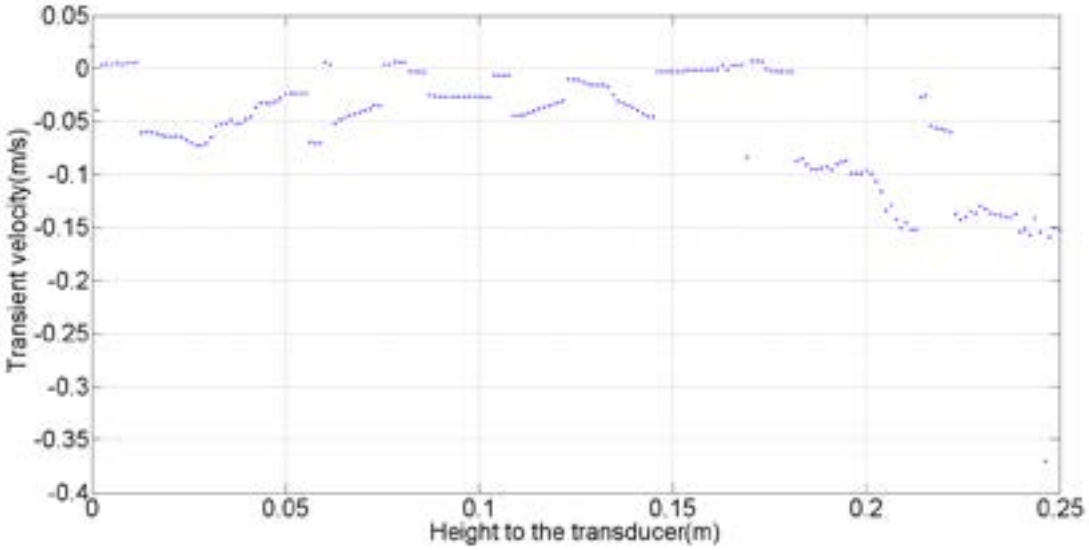

Figure 4.20 Transient velocity in the measurement

The accuracy of the velocity measurement depends on the calibration of the transducer, the optional frequency and the number of particles in suspension. With the processing of the experiment, some bubbles or particle attach to the bottom of the transducer which makes the measurement incorrect, and the large noise can affect the same influence. Appropriate optional frequency should be determined before the experiment, otherwise the measurement is incorrect. The number of particles in suspension determines the amplitude of particles energy, which would also affect the accuracy of the measurement.

4.3.1 Vertical velocity profile

For each entrance volume flow rate, 60 locations in the tank are measured. The combinations of locations with the same X coordinate can form the vertical profile of the flow.

All the experiments contain two groups, the low water level and the high water level. The results of the vertical velocity profile are one case for each group. There are two kinds of are showed for vertical velocity profile. The first one is the distribution of velocity component in X-direction (flow direction) in the vertical plane, the plane is positioned at 0.3m from the entrance in the flow direction. The second is the distribution of velocity component in X-direction along Z position in the vertical lines, all the lines are positioned at 0.3 m, 0.6 m, 0.9 m, 1.2 m, 1.5 m, 1.6 m, 1.7 m, 1.8 m, 2.1 m, 2.4 m, 2.7 m and 3 m from the entrance in the flow condition in the symmetry plane of horizontal direction.

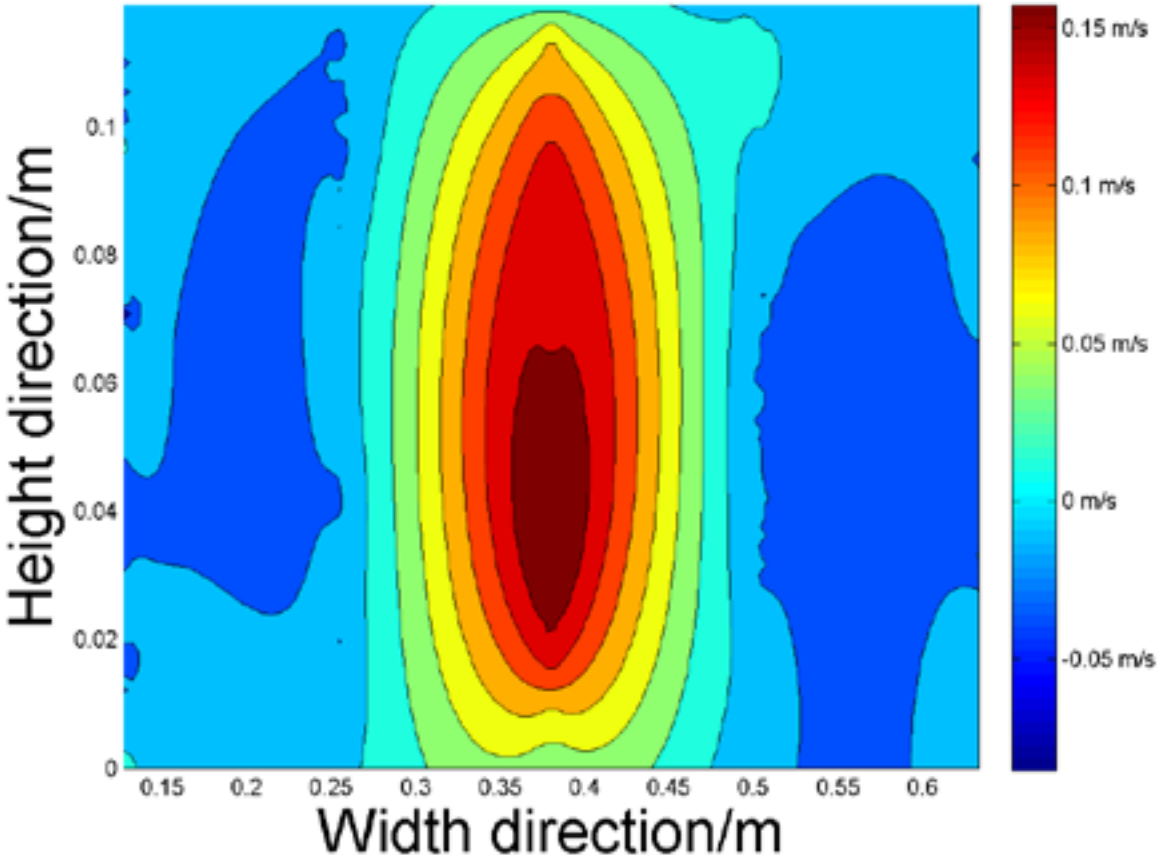

Figure 4.21 Vertical profile of velocity component in the X direction at X = 0.3 m where the volume flow rate is 1 L/s at low water level

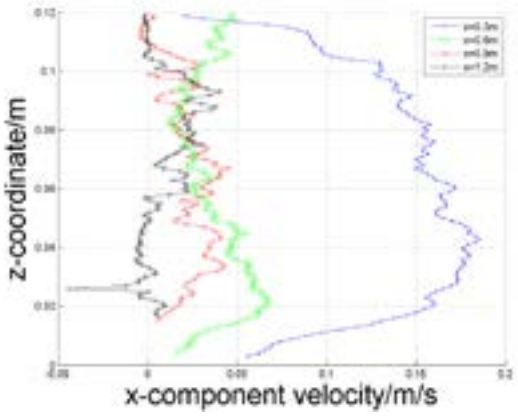

Figure 4.22 X-velocity distribution along Z position at volume flow rate 1 L/s

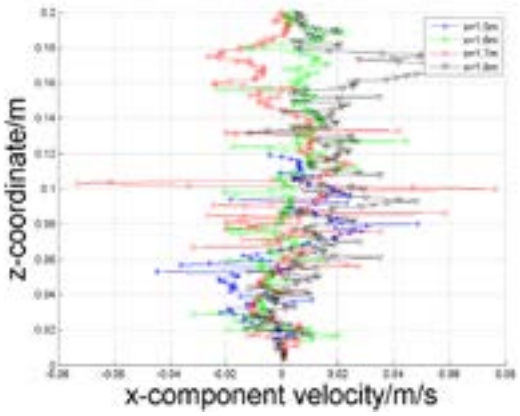

Figure 4.23 X-velocity distribution along Z position at volume flow rate 1 L/s

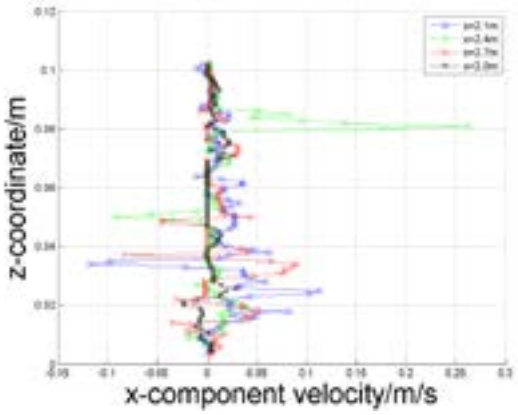

Figure 4.24 X-velocity distribution along Z position at volume flow rate 1 L/s

Figure 4.21 shows that the flow injection is in the center, both sides of the flow injection has the negative velocity, which means the recirculation, the two eddies are located in two sides of the flow injection, one of with is close to the free-surface and the other is close to the bottom, which can prove that the flow is asymmetry.

Figure 4.22, 4.23 and 4.24 show the distribution of velocity component in X-direction along the Z coordinate. In chapter 2, the same figure is also been presented, the difference between the experiment and the simulation is that the experiment data is fluctuating, though the data is time-averaged. Apparently the fluctuation is more obvious in the cavity. In front of the cavity, the velocity distribution is in Figure 4.43, the velocity is increasing from the bottom to the center of flow injection and descending from the center of flow injection to the free-surface, which is identical with the numerical simulation results. The velocity from X=0.6 m has decreased by 80%

comparing to the entrance velocity. The flow in the cavity is quite unstable, the fluctuating intensity of velocity in the cavity is larger than other part of the tank. The velocity in the back part is quite low and more uniform except for a few echoes.

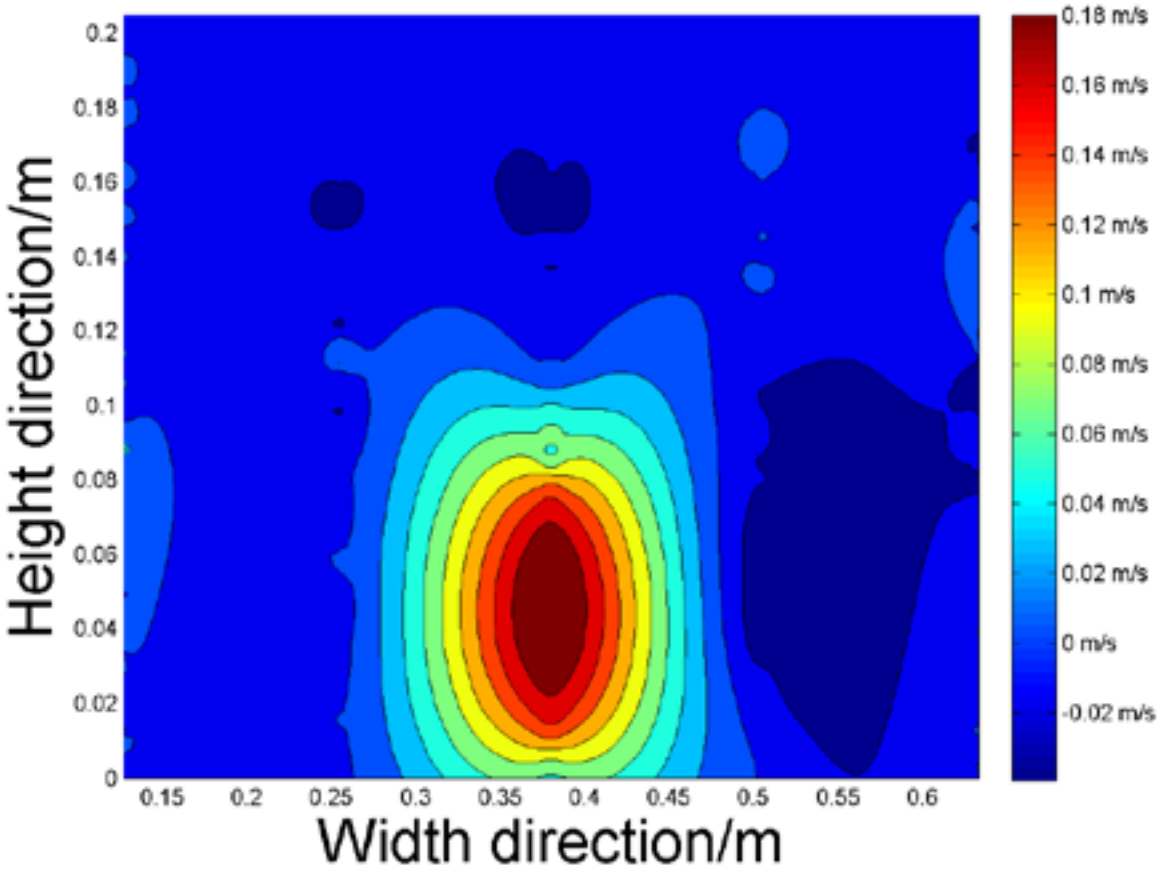

Figure 4.25 Vertical profile of velocity component in the X direction at X = 0.3 m where the volume flow rate is 1 L/s at high water level

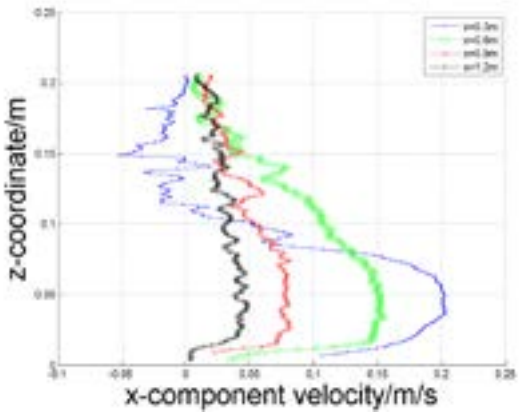

Figure 4.26 X-velocity distribution along Z position at volume flow rate 1 L/s

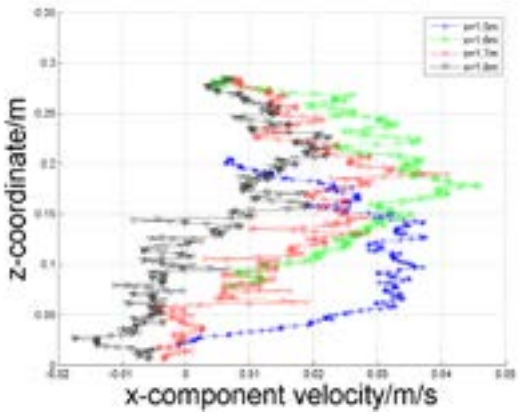

Figure 4.27 X-velocity distribution along Z position at volume flow rate 1 L/s

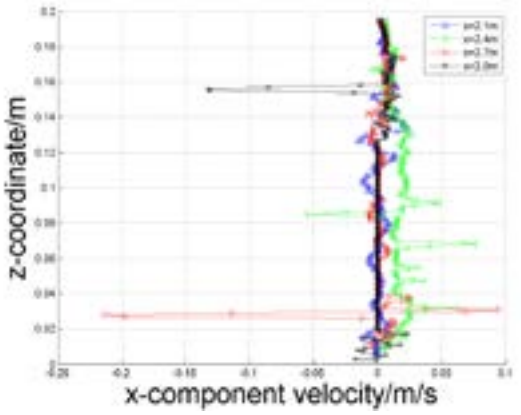

Figure 4.28 X-velocity distribution along Z position at volume flow rate 1 L/s

The flow injection showed in the Figure 4.25 is positioned from 0 to about 0.1 m in the height direction. And in the right side, the velocity is negative. The damping of the velocity along the flow direction is decreased comparing to the condition at low water level, which is showed in the Figure 4.22. The velocity in the cavity is still very fluctuating, increasing to a peak and then descending. The velocity in the back part is still low and uniform except for several echoes.

4.3.2 Horizontal velocity profile

To visualize the horizontal velocity profile, the velocity components in X-direction and Y-direction are both necessary. However from the experiment, only the velocity components in X-direction and Z-direction can be obtained. In order to obtain the

velocity component in Y-direction, the continuity equation is solved by central difference method. The mathematic expression of the continuity equation is mentioned in the chapter 2 in equation (2.1). In the experiment, water is non compressible, then the density of the water should be a constant, the term $\frac{\partial \rho}{\partial t}$ in the continuity equation should equal to zero, therefore the continuity equation can be simplified as

$$\frac{du}{dx} + \frac{dv}{dy} + \frac{dw}{dz} = 0 \tag{4-11}$$

Where u, v, w are the velocity components in x, y and z direction respectively.

From the experiment the data for $u\ and\ w$ are already obtained. The only problem is to use the equation (4-11) to solve the velocity component in Y direction. The point on the wall is used for those test location near the wall. As the test location can't be placed very close, an error should exist, however in a jet flow the velocity component in X direction is the main velocity component, which also means the velocity component in Y and Z direction is quite small comparing to the velocity component in X direction, so the error is under a control range, which is confirmed by previous experiment investigation in the lab with using the same measurement system.

The basic concept of central difference method is using grid points to discrete the controlling volume. The parameter of point P is calculated by the parameter of point N, W, S and E.

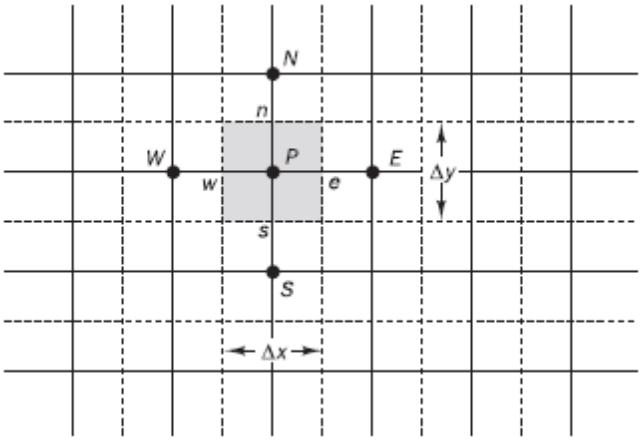

Figure 4.29 Grid points

$$\frac{u_E - u_W}{2\Delta x} + \frac{v_N - v_S}{2\Delta y} + \frac{w_U - w_D}{2\Delta z} = 0 \tag{4-12}$$

Where U and D represent the points in the up and down direction of the point P, which are not displayed in the figure.

After the calculation, the velocity component in Y-direction is obtained. With using the MATLAB for the code to deal with the velocity component in X and Y direction, several horizontal velocity profile are showed in the Figure 4.30, 4.31 and 4.32.

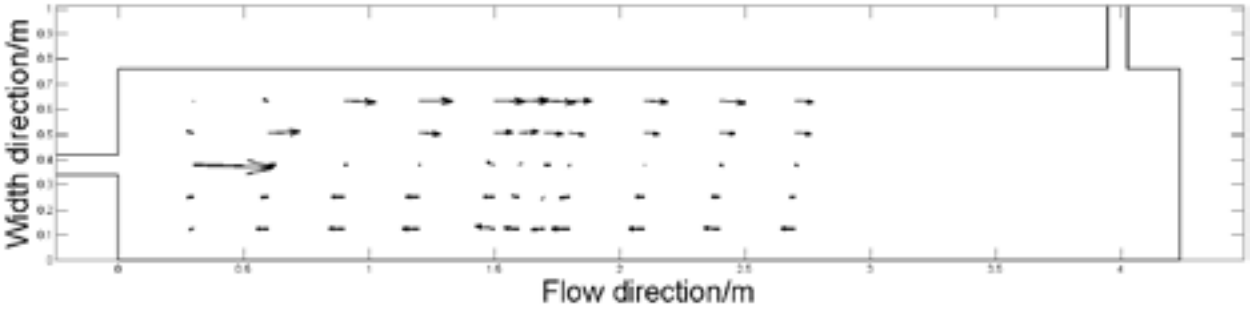

Figure 4.30 Velocity vector at the h = 0.04 m of volume flow rate equaling to 3 L/s at low water level

Figure 4.30 shows the velocity vector of the volume flow rate equaling to 3 L/s at low water level and the horizontal plane is placed at Z = 0.04 m. Two eddies exist in the flow, one small eddy in the left side watching from the flow direction and one big eddies in the right side spreading to the downstream. From 1 L/s to 3.5 L/s, the velocity vector is almost in same kind, the difference is just the size of the eddy.

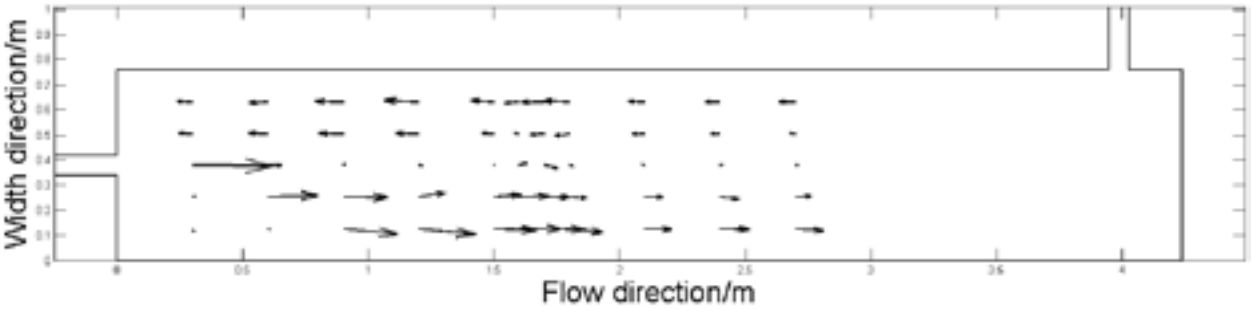

Figure 4.31 Velocity vector at the h = 0.04 m of volume flow rate equaling to 4 L/s at low water level

Figure 4.31 shows the velocity vector of the volume flow rate equaling to 4 L/s at low water level and the horizontal plane is placed at Z = 0.04 m. The difference in this case is that the injection flow deviates to the opposite direction comparing to the condition under volume flow rate equaling to 1 L/s to 3.5 L/s. And the deviating direction is the same in the case where the volume flow rate equals to 4.5 L/s.

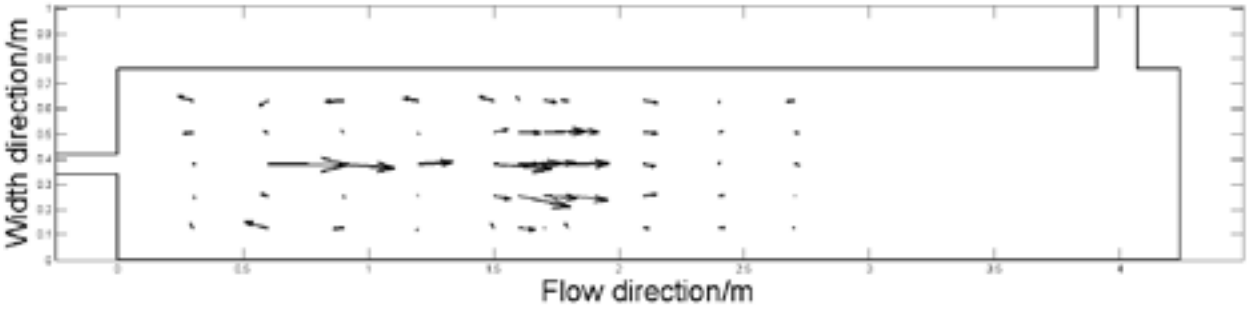

Figure 4.32 Velocity vector at the h = 0.04 m of volume flow rate equaling to 3 L/s at high water level

Figure 4.32 shows the velocity vector of the volume flow rate equaling to 3 L/s at low water level and the horizontal plane is placed at Z = 0.04 m. The flow shows two eddies in both side of the injection flow and the injection flow maintain the center position. Two eddies are mainly confined in the area before the cavity.

4.4 Measurements of sediment transport

The measurements of sediment transport in the experiment work are mainly divided in to two parts. The first part is taking photos in each direction of the devices. When the

experiment system is running, the particle release starts when the water depth in the experimental basin is stable, then every one hour the sediment distribution is recorded by photos. The second part is measuring the particle weight remaining in the experimental basin when the velocity measurement is finished.

4.4.1 Cases of low water level

4.4.1.1 Photograph of the sediment distribution

In the experiment process of low water level, it takes more time for particle to settle down, the percentage of particles in suspension is also higher than in the high water level. Figures 4.33-4.40 showed below are constituted by three part for each volume flow rate, including front, cavity and back, the inlet part is in front of the front part and the outlet part is in back of the back part, both the inlet part and outlet part are not showed in the figures. The flow direction is from the left to right.

Front Cavity Back

Figure 4.33 Sediment distribution at 1 L/s

Front Cavity Back

Figure 4.34 Sediment distribution at 1.5 L/s

Front Cavity Back

Figure 4.35 Sediment distribution at 2 L/s

Front Cavity Back

Figure 4.36 Sediment distribution at 2.5 L/s

Front Cavity Back

Figure 4.37 Sediment distribution at 3 L/s

Front Cavity Back

Figure 4.38 Sediment distribution at 3.5 L/s

Front Cavity Back

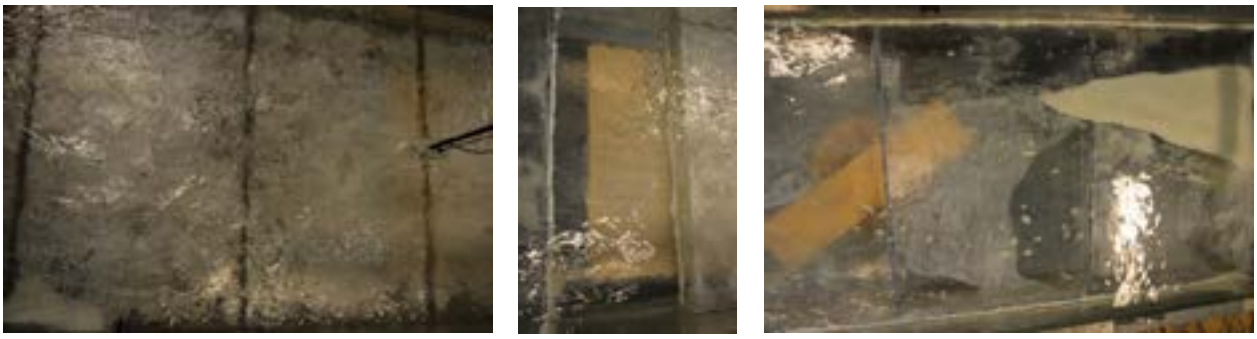

Figure 4.39 Sediment distribution at 4 L/s

Front Cavity Back

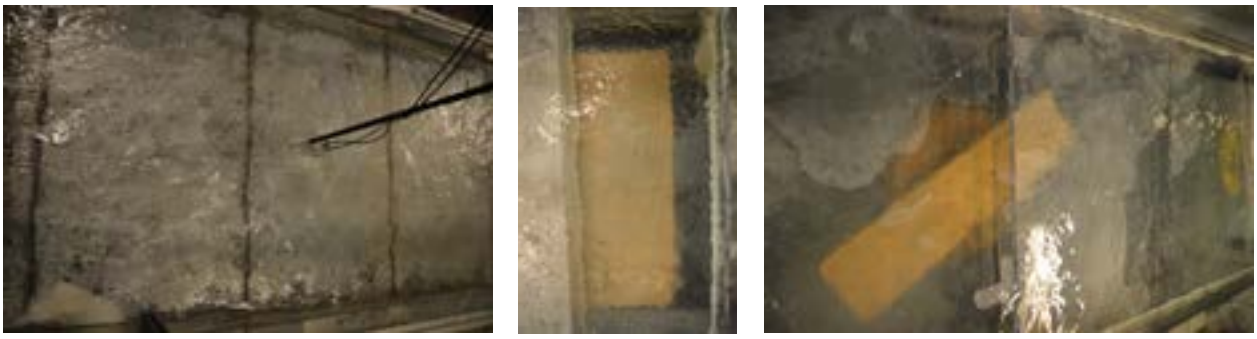

Figure 4.40 Sediment distribution at 4.5 L/s

The process of sediment transport in the sediment tank is really complicated. Sliding, saltating, suspension, resuspension and settling, all these movement can be found in the experiment. With the accumulation of the particle at the bottom, a new bed constituted by particles is formed, in this condition the sliding of the particle can be presented as the movement of the new bed, from the figure some effect similar to the scouring occurs in the new bed.

The flow in the tank is quite fluctuating, especially in the front part of the tank, where the free-surface fluctuates very often, apparently the fluctuation is caused by the flow injection. As a consequence of the fluctuation of the flow, the movement of the particles in suspension is quite chaotic, which makes it take much more time for the settling of the majority of particles.

At the beginning, the sediment would form a distribution zone, which is not the final zone, as time goes on, the distribution zones are decreased by the scour effect of the flow, where some distribution zones disappear.

As the signal emitted by the transducer can determine the existence of the bed, which means from the experiment data, the height of the bed at each test points can be obtained. By the application of code to transform the data into appropriate coordinate, the sediment height can be visualized as follows.

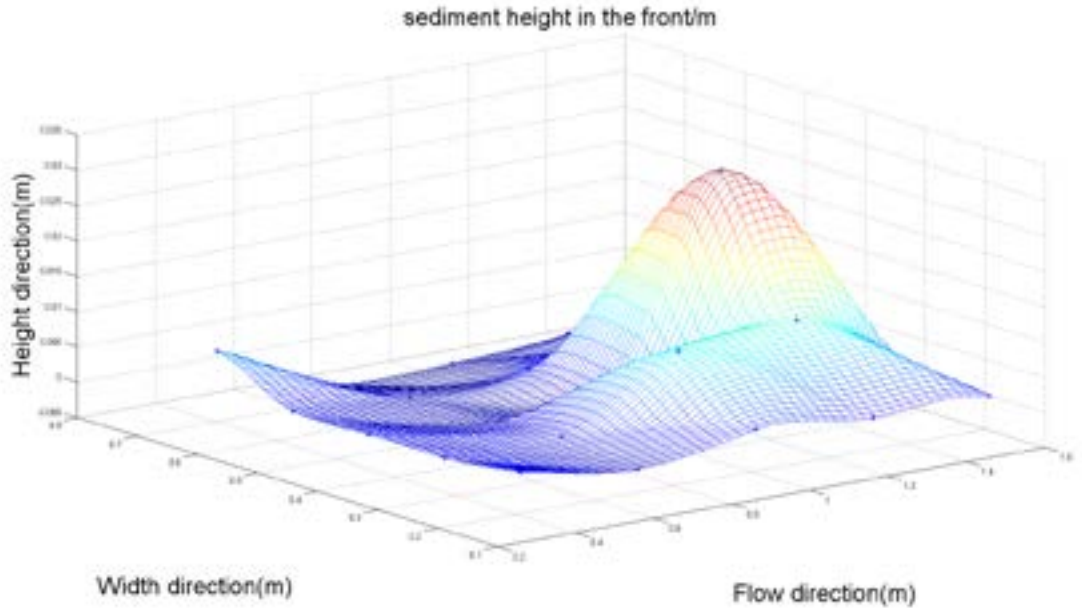

Figure 4.41 Sediment height in the front at 1.5 L/s

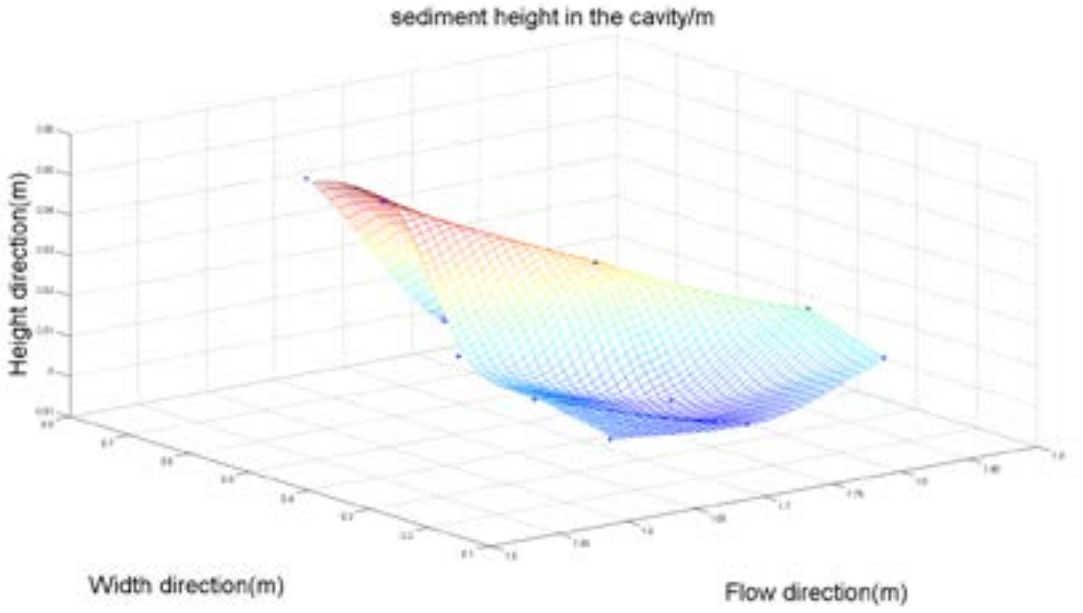

Figure 4.42 Sediment height in the cavity at 1.5 L/s

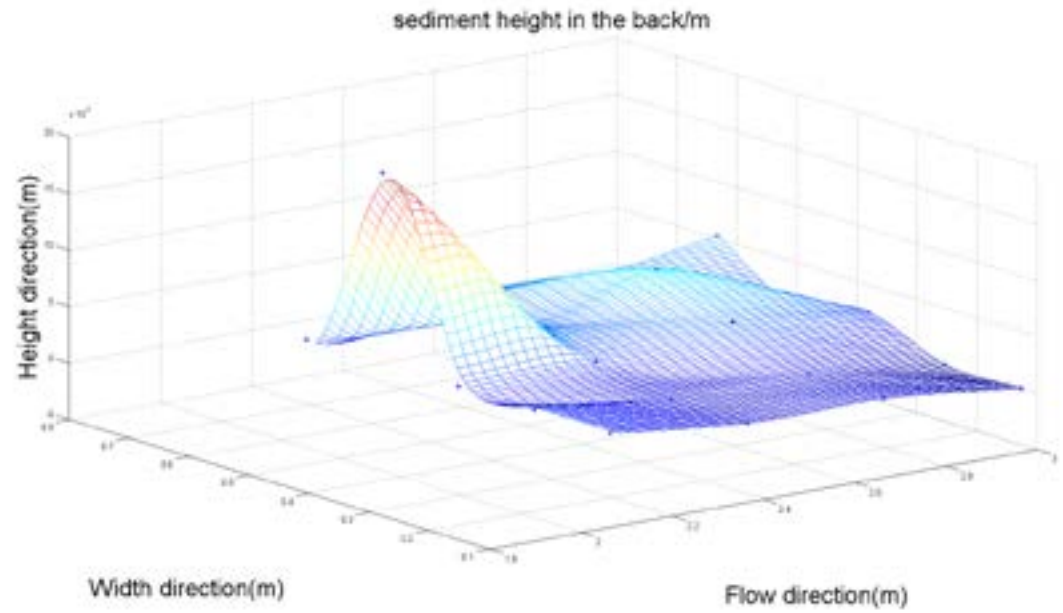

Figure 4.43 Sediment height in the back at 1.5 L/s

Those figures show a good agreement with the photograph of the sediment deposition, however in some case the results are not satisfactory, due to the transducer stop measure at a place where is not the boundary, for example a cloud of particle can be misdeem as bottom by the signal and the measurements end at the location of a cloud of particle which is not the real bottom.

4.4.1.2 Trap efficiency

The calculation of the trap efficiency of the particles can be determined by two parameters, the mass of total injected particles and the mass of settled particles.

$$\eta_{trap} = \frac{m_{settled}}{m_{total}} \tag{4-13}$$

In the experimental basin, the bottom is divided into three parts by the cavity, three trap efficiencies are defined due to different part of the bottom.

$$\eta_{front} = \frac{m_{settled\ in\ front}}{m_{total}} \tag{4-14}$$

$$\eta_{cavity} = \frac{m_{settled\ in\ cavity}}{m_{total}} \tag{4-15}$$

$$\eta_{back} = \frac{m_{settled\ in\ back}}{m_{total}} \tag{4-16}$$

Table 4.4 has shown the trap efficiency in different part of the tank, with the flow condition respectively.

Table 4.4 Trap efficiency in different part of the tank

Inlet discharges (L/s)	Water height (cm)	Trap efficiency			
		Front	Cavity	Back	Total
1	11.8	60.16 %	30 %	9.85 %	100 %
1.5	12.5	25.84 %	44.1 %	29.56 %	99.5 %

2	12.5	16.97 %	38.48 %	42.22 %	97.67 %
2.5	12.5	8.58 %	17.58 %	56.14 %	82.3 %
3	12.5	2.63 %	11.48 %	41.92 %	56.03 %
3.5	12.6	7.91 %	2.76 %	31.78 %	42.45 %
4	13	1.75 %	1.06 %	18.83 %	21.64 %
4.5	13.5	1.2 %	0.3 %	0.5 %	1.8 %

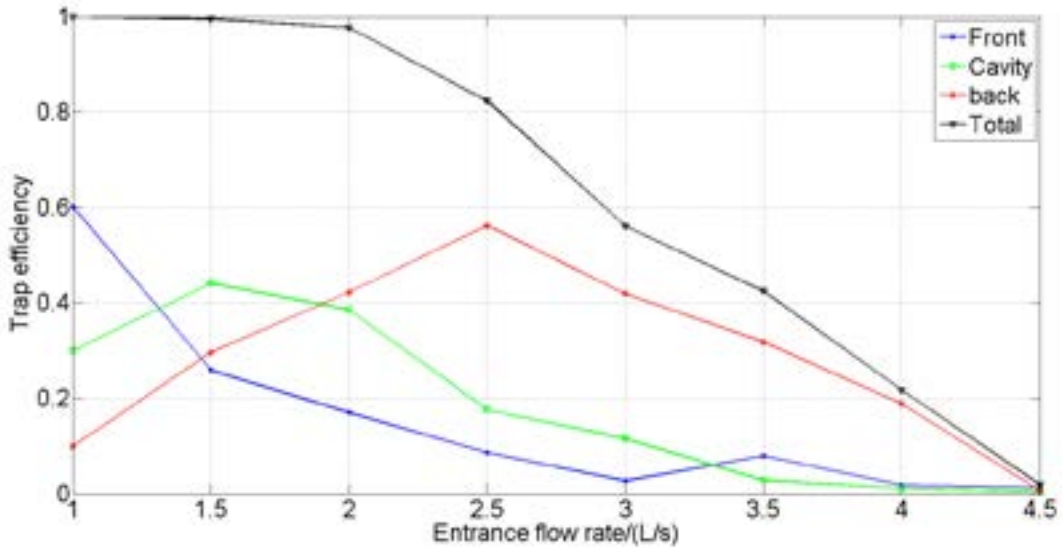

Figure 4.44 Trap efficiency in different part of the tank

The total trap efficiency is decreasing with the increasing entrance volume flow rate, when the volume flow rate is higher than 4.5 L/s, the trap efficiency is close to 0. A demonstrative experiment under the flow rate equaling to 5 L/s was processed, the injected particle escaped the tank in a short time.

The overall tendency of the front trap efficiency is also descending, only with a small rise at the volume flow rate equaling to 3.5 L/s. In the case where the volume flow rate is larger than 2 L/s, the trap efficiency in the front part all decrease to 10%.

The cavity trap efficiency has a large rise when the volume flow rate swifts from 1 L/s to 1.5 L/s. Then the trap efficiency is descending continuously with the increasing of volume flow rate, until 3L/s the trap efficiency is below 10%.

The back trap efficiency is increasing from 1 L/s to 2.5 L/s and then descending.

4.4.2 Cases of high water level

4.4.2.1 Photograph of the sediment distribution

In the experiment process of high water level, it takes less time for particle to settle down, the flow seems to be more peaceful and fewer particles will remain in suspension, which increase the difficulty of velocity measurement sometimes. The illustration of all the below figures from 4.45-4.52 are the same in 4.4.1.1.

Front Cavity Back

Figure 4.45 Sediment distribution at 1 L/s

Front Cavity Back

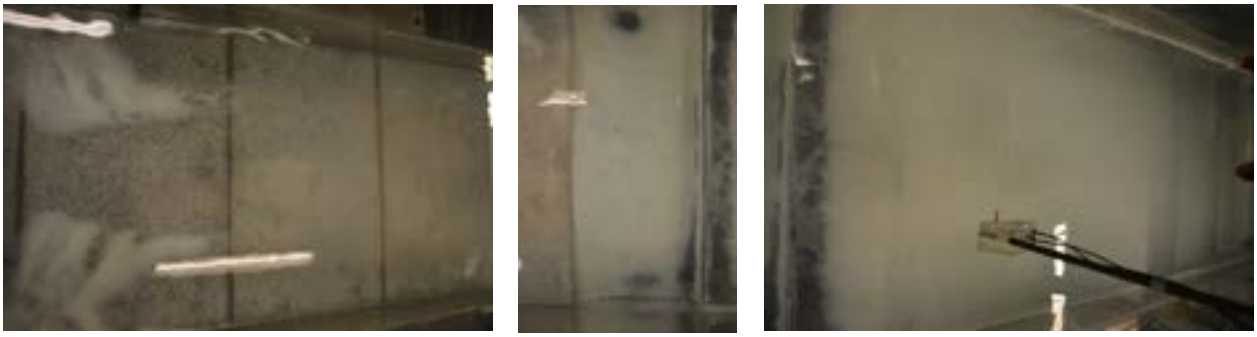

Figure 4.46 Sediment distribution at 1.5 L/s

Front Cavity Back

Figure 4.47 Sediment distribution at 2 L/s

Front Cavity Back

Figure 4.48 Sediment distribution at 2.5 L/s

Front Cavity Back

Figure 4.49 Sediment distribution at 3 L/s

Front Cavity Back

Figure 4.50 Sediment distribution at 3.5 L/s

Front Cavity Back

Figure 4.51 Sediment distribution at 4 L/s

Front Cavity Back

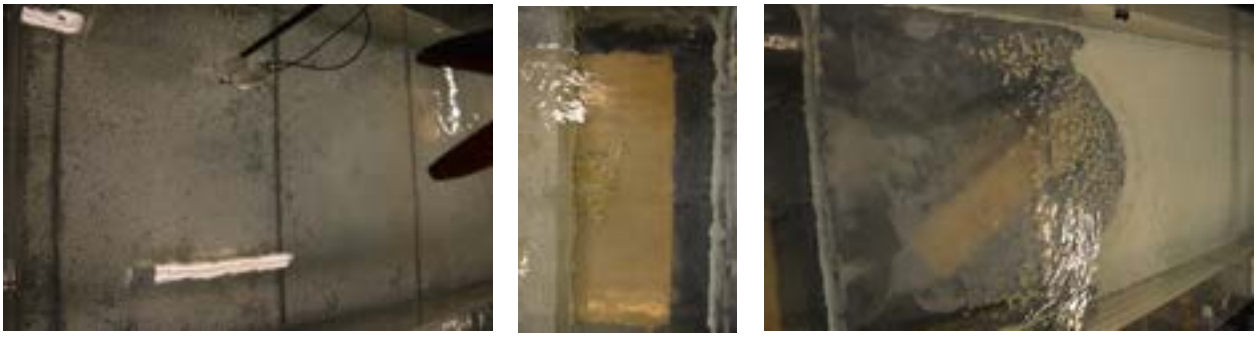

Figure 4.52 Sediment distribution at 4.5 L/s

The flow in the tank seems more quiet than the flow in the low water level, which can be presented in the stabilization of the free-surface and the number of particle in

suspension at the same time after releasing the particle. And the phenomenon of sliding, saltating and resuspension is less than the case of low water level.

Unlike the scouring effect of flow to the new bed formed by particles, the push of the flow to the new bed is more significant. And with the increasing of volume flow rate, the push intensity is increasing. The push can be represented from the comparison of sediment distribution in the back part under different volume flow rate. At the beginning the boundary of the new bed is all close to the back edge of the cavity and parallel to the width direction, as time goes on, the boundary of the new bed is pushed to the back, and the shape of the boundary appears to be concave, the higher the volume flow rate is, the larger distance the boundary would move to the back.

4.4.2.2 Trap efficiency

The definition of the trap efficiency is the same as low water level in 4.4.1.2 from equation 4-13~4-16. And the trap efficiency in different part of the tank is showed in Table 4.5 with the entrance volume flow rate ant water depth in the tank

Table 4.5 Trap efficiency in different part of the tank

Inlet discharges (L/s)	Water height (cm)	Trap efficiency			
		Front	Cavity	Back	Total
1	21.2	67.97 %	25.23 %	6.8 %	100 %
1.5	22.1	3.32 %	59.35 %	37.33 %	100 %
2	22.8	3.6 %	37.44 %	58.96 %	100 %
2.5	23.5	9.31 %	31.74 %	58.96 %	100 %
3	24.3	5.41 %	5.17 %	82.72 %	93.3 %
3.5	24.7	2.82 %	1.99 %	73.79 %	78.6 %

4	**25.3**	**0.82 %**	**0.41 %**	**75.47 %**	**76.7 %**
4.5	**26.1**	**0**	**0**	**74.67 %**	**74.67 %**

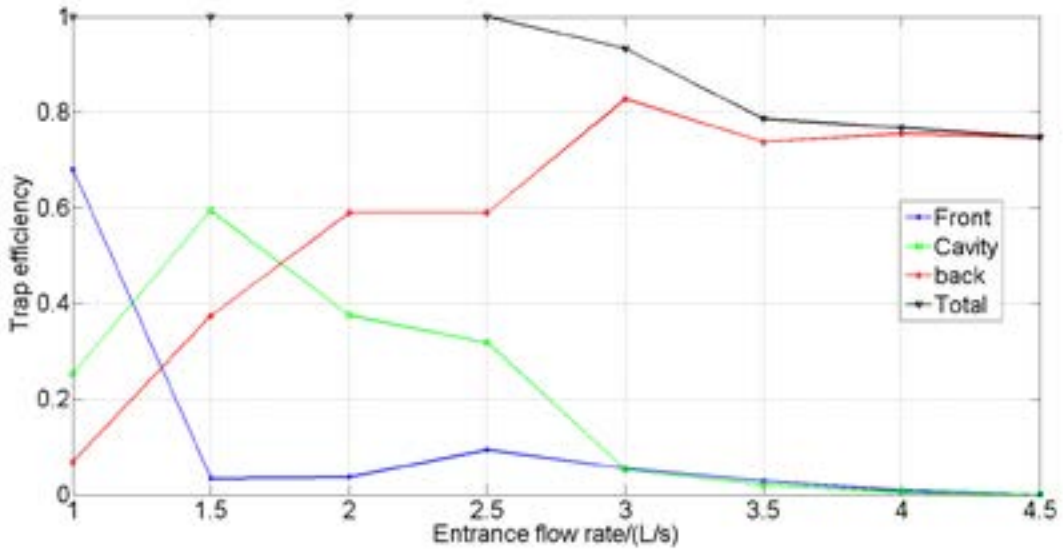

Figure 4.53 Trap efficiency in different part of the tank

On the whole, the total trap efficiency of high water level is higher than that of low water level, especially in the case where the volume flow rate is higher than 2.5 L/s. Though the overall tendency of the total trap efficiency is descending, the decreasing extent is much lower than the decreasing of the total trap efficiency in the low water level.

The front trap efficiency decrease rapidly with the increasing entrance volume flow rate, from the volume flow rate larger than 1 L/s, the front trap efficiency has decreased to below 10 % and at the volume flow rate equaling to 2.5 the trap efficiency occur a small rise.

From the volume flow rate 1 L/s to 1.5 L/s, the cavity trap efficiency shows a large amplification, which is about 35%, the cavity trap efficiency arrives at a peak and then the trap efficiency goes down with the increasing volume flow rate.

The increase of the back trap efficiency is huge with the increasing volume flow rate, and the trap efficiency in the back stay stable when the volume flow rate reach to 3 L/s.

4.5 Comparison of numerical simulation and experimental results in sediment transport

The boundary condition mentioned in Chapter 3 to model the particle sedimentation was also used in the geometry with cavity. The simulation setup is listed as follows:

- DPM sources update every flow iteration, particle tracking is in unsteady state and the particle time step size is 0.001 s, the maximum number of tracking steps is 50000 and the step length factor is 5.
- Particles are injected from the inlet surface from 0 s to 10 s with the flow rate 0.5 kg/s, the diameter distribution of particle is rosin-rammler, the minimum diameter is 0.6 mm, the maximum diameter is 1.047 mm, the mean diameter is 0.837 mm and the spread parameter is 9. Turbulent dispersion of particle is simulated by DRWM with constant time scale $C_L = 0.15$, the injection of the particle uses constant-number parcel release method where a parcel of particle contains 50 particles. Normally, about 800 thousands particles are injected into the tank, the number of the injected particles can decrease the numeric error furthest and ensure there will be enough particle spreading to the outlet.
- The density of the particle is 1034 kg/m^3 and the particle is inert type.
- The inlet, outlet and free-surface are “escape” type, the side wall are “reflect” type, the bottom is “trap” type.
- Realizable $k-\varepsilon$ model is chosen for calculating the turbulence, standard wall function is used for boundary layer.

Figure 4.54 shows the particle trajectory in the numerical calculation. And Figure 4.55 shows the simulated particle deposition zones.

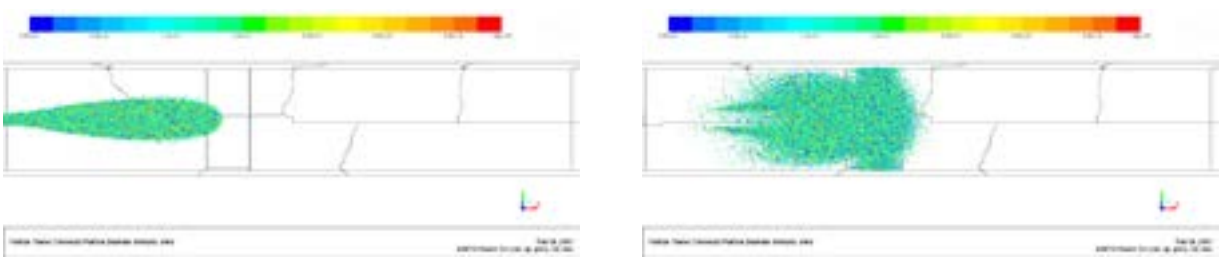

Particle trajectory at 5000 iterations

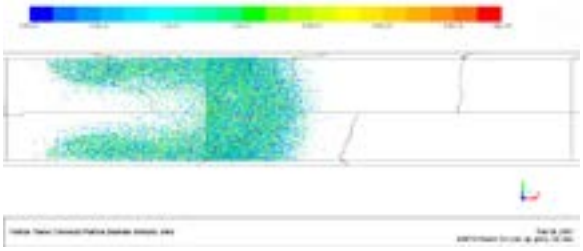

Particle trajectory at 15000 iterations

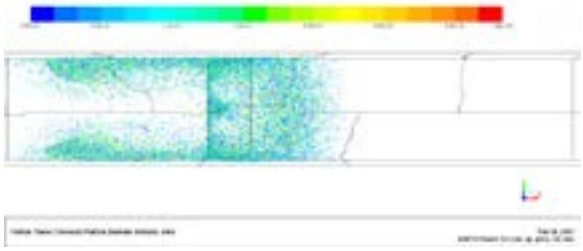

Particle trajectory at 25000 iterations

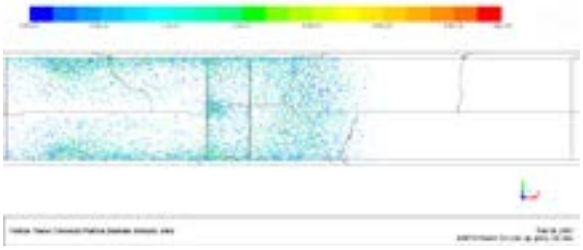

Particle trajectory at 35000 iterations

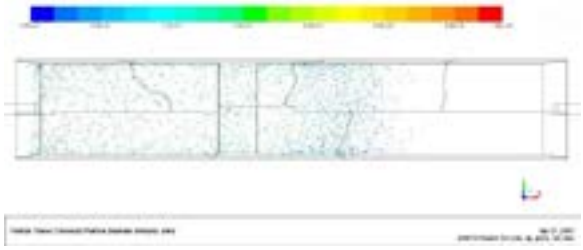

Particle trajectory at 45000 iterations

Particle trajectory at 65000 iterations

Figure 4.54 Particle trajectory at 3 L/s

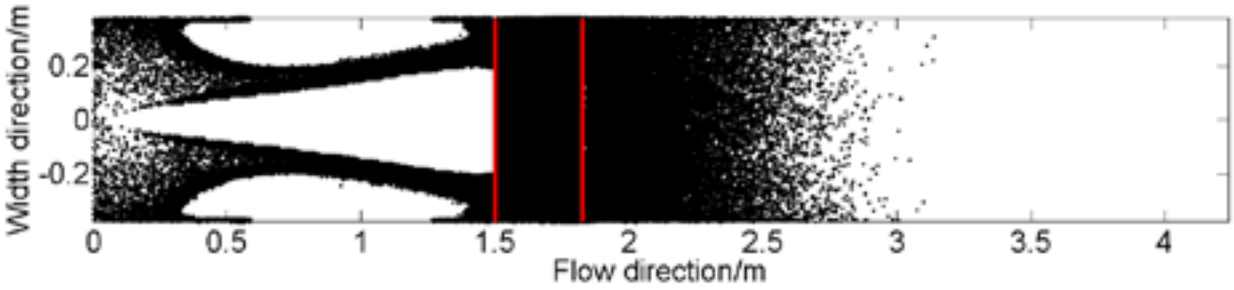

Figure 4.55 Simulated particle distribution zones

From the experiment result, at the beginning of particle release (in 1 hour after the release), the particle deposition zone is showed in Figure 4.56. Zones named 1, 2, 3 and 4 are the main deposition zones after the particle release and all the four parts are covered by particles at the beginning, which is in good agreement with the simulated particle distribution zones in Figure 4.55.

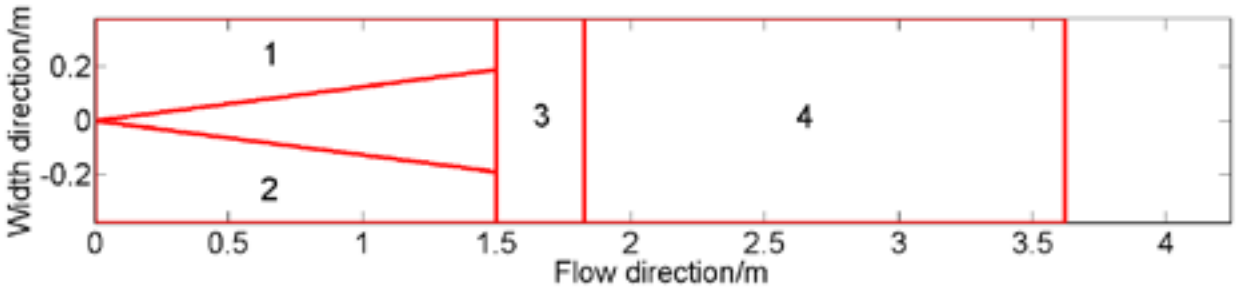

Figure 4.56 Particle deposition zone at the beginning of the particle release

In part 1, 2 and 3, parts of particle leave the region by the effect of re-suspension, in part 4, due to the effect of scouring of the flow, the front part of particles are scoured to back and a concave curve is formed. Figures 4.56 to 4.59 shows the sediment distribution from 1 hour to 4 hour after the particle release and Figure 4.49 shows the final sediment distribution of the experiment at 3 L/s.

Front Cavity Back

Figure 4.57 Sediment distribution at 3 L/s 1 hour after particle release

Figure 4.58 Sediment distribution at 3 L/s 2 hours after particle release

Figure 4.59 Sediment distribution at 3 L/s 3 hours after particle release

Figure 4.60 Sediment distribution at 3 L/s 4 hours after particle release

From the comparison between numerical simulation and experiment data, we can get the conclusion that the defect of the implemented settling boundary is not able to simulate the effect of re-suspension and scouring.

4.6 Conclusions

In this chapter, the experiment aims at demonstrating the flow patterns in a rectangular with large ratio of length to width and a rectangular cavity at the bottom, presenting the sediment deposition zones.

The first objective is completed by the velocity measurement and mathematic implement. Comparing to the numerical simulation, the experiment can show much more information than numerical simulation, due to the experiment deal with the transient velocity and the velocity in the simulation is time-averaged. The vertical velocity distribution can be divided into two kinds, the first is the area near the injection flow where the vertical velocity increase from the bottom to the center of injection flow to a peak and then decrease from the center injection to the free-surface. The second is the area far away from the flow injection, the vertical velocity is more uniform. The flow pattern in the case where the water depth is lower than 13cm is

mainly dominated by two eddies, where one eddy is in the corner near the entrance and the other is large and spread to the downstream, entrance flow rate can alter the deviation of the flow injection. The flow pattern in the case were the water depth is higher than 13cm is also constituted by two eddies, but those two eddies are mainly constrained in the part before the cavity and the downstream is a uniform flow.

The second objective is to visualize the deposition zone in the rectangular tank with cavity. The cavity shows better performance in trapping the sediment when the entrance flow rate is lower than 3.0 L/s, with higher entrance flow rate, the trap efficiency is quite low. The water depth in the rectangular tank is an important factor to the trap efficiency, in general, the trap efficiency is much higher with higher water depth in the tank.

The comparison of the numerical simulation result using implemented settling condition and experiment shows good agreement in the prediction of the deposition zone, the whole trap efficiency is the same with the experiment, the defect is the prediction of trap efficiency in each part of the tank is not accurate.

General conclusions

The main purpose of this investigation is to understand the flow and sediment transport in tank better, due to the investigation on a rectangular tank has been widely studied, a new geometry (cavity at the bottom of the tank) to the tank is put forward to see the influence of the cavity on the flow and sediment transport.

In this thesis, both numerical simulation and experiment method are used. The flow is modeled with three geometries, namely short tank (ST) , long tank (LT) and long tank with cavity (LTWC) , the experiment of ST has been finished by Dufresne (2008), and the experiment of LTWC is processed in this research. The sediment transport is mainly simulated using the geometry of ST and LTWC.

Numerical simulation

The simulation of flow is processed under steady state, and the particle tracking is under unsteady state, a weak coupled way is selected for calculation of flow and particle tracking. A volume of fluid (VOF) method is optioned to track the interface between water and air for free surface flow, discrete phase model (DPM) method is selected to calculate particle trajectory. The realizable $\boldsymbol{k-\varepsilon}$ model is chosen for simulating the turbulent effect, where a standard wall function is chosen for the wall treatment. In the simulation, different inlet discharges ranging from 1 L/s to 5 L/s with increment 0.5 L/s are tested, two water levels are simulated.

The simulation results show the structure of flow pattern in tank with different geometry. In ST, the main characteristic of the flow is that two eddies dominate the whole flow field. The variant flow rate is the main factor which can affect the size and position of two eddies, and water depth is another factor. In LT, the two eddies structure are mainly constrained in the front 35% of the tank, the flow in the rest of the tank is basically uniform flow, the recirculation in the front part is also controlled by inlet discharge and water depth which is the same type as the condition in ST, but not exactly the same where the size and center of eddy are different under the same inlet discharge. In LTWC, the existence of the cavity don’t change the eddy structure essentially, the meaning of the cavity is creating a more uniform flow field in the tank, which means reduced fluctuation, gently transition from recirculation zone to uniform flow zone. The cavity also leads to several vertical eddy structures, which are

constrained in the space of the cavity and lead to hardly any changes to the eddy structure in the mainstream.

The application of VOF model shows the ability in tracking the interface between water and air in the tank, in two types of water level the height of the interface is increasing along the increase of inlet discharge, which also occurs in the measurements, however, the difference of the height in maximum and minimum inlet discharge in simulation is higher than the experimental results.

The simulation on sediment transport contains 8 cases in ST and 1 case in LTWC, where steady calculation for the flow and unsteady calculation for the particle are coupled. The prediction in trap efficiency is in good agreement with the experiment when the inlet discharge is lower than 2.5 L/s, in cases with higher inlet discharge the higher the inlet discharge is the more overestimation is made. The case in LTWC shows good agreement in prediction in deposition zone and trap efficiency with experiment, the defect is the bad prediction of trap efficiency in different part of settling zone of the tank.

The simulation on sediment transport shows the possibility of using numerical ways to predict the complex particle movement. The most important thing in predicting sediment transport is how to treat the settling boundary. In this work, an implementation based on Shields diagram has been finished, where the settling condition is been improved. However, the improvement in estimation of settling can’t reproduce the real particle movement entirely, which leads to overestimation in trap efficiency and bad prediction in deposition zones.

The existence of the cavity at the bottom for the sedimentation is creating a part which is appropriate for settling particle, and a more uniform flow due to the cavity is formed, especially the gentle transition from recirculation zone to uniform zone. The uniform zone means lower fluctuation in flow parameter.

Experiment investigation

As the most intuitionistic way, experiment investigation provides the most convincing results to this research. In this work, velocity field has been measured with a series of inlet discharges by backscattered ultrasonic signal measurement method. The sediment deposition is recorded by the photograph and the trap efficiency is calculated by weighting the mass of settled particle in each part of the tank and the total mass of particle injected into the system. 16 experiments have been finished, which can be divided into two types (classified by the water level in the tank) due to different

effective outlet pipe, and the variate in each type is the inlet discharge ranging from 1 L/s to 4.5 L/s with increment of 0.5 L/s.

The velocity measurements restore the flow field by time averaging method after the treatment to the raw experimental data. The restored velocity field in medium water level shows good agreement with the numerical simulation, including the velocity distribution along Z coordinates and the velocity vector field in horizontal plane.

The most outstanding point of this experiment work is perhaps the measurement of bottom height. The mechanism of the velocity measurements enable the measurements of the height between the transducer to the bottom, and due to the accumulation of particle at the bottom, the measured height in all tested location varies which leads to the possibility to reproduce the accumulated state of the particle at the bottom, the only problem is to make sure that the measurement work normally all the time (the measurements terminate even the signal don't reach the bottom sometimes, the reason for this phenomenon is probably the emitted signal reach a particle cloud which is treated as bottom mistakenly).

In low water level measurements, the flow field is more fluctuate and it takes much more time for settling particle comparing to the condition of high water level. In measurements with low inlet discharge, the settled particle rarely re-suspend or move on the bottom, the particle motion become more complex when the inlet discharge increases.

The measurements on the trap efficiency show that the water depth in the tank is an important factor, the trap efficiency in low water level cases decreases from 100% to 1.8% with continuous increasing inlet discharge, however the trap efficiency in high water level cases decreases from 100% to 74.67% with continuous increasing inlet discharge. This result indicates the settling condition for particle is highly impacted by the water depth in the tank. In high water level measurements, the sedimentation of particle is basically symmetry except for one inlet discharge, and the center of the sedimentation is in retrocession when the inlet discharge is increasing. In low water level measurements, the particle deposition is more uncertain.

Perspectives

From the experience in the experiment, in the front part and the cavity, the movement of particle contains deposition, sliding, saltation and re-suspension, and in the back part of the tank, the movement of particle contains deposition and scouring. All these phenomena indicate that the particle movement is not just settling, the others motions

should also be taken into consideration to predict particle movement in a more credible way, and that's why the implementation on settling condition can improve the prediction of sediment transport but can't reproduce the real particle motion perfectly. The Fluent codes contain an erosion model which can be coupled into the calculation, though the coupling might be difficult. The others motion of particle might be implemented to the boundary condition by user defined function (UDF), the criterion can refer to the theory of bed load transport.

As the sediment transport is a random process, the probability method should be implemented in the estimation of criterion of deposition. Namely, when the particle reach the bottom and conform to the settling condition, the particle will not settle in 100% percent.

Normally, the numerical ways terminate the particle trajectory once the particle is defined as settled, and the settling condition is still the same for the particle reach the bottom afterwards. However in real condition, the accumulation of the particle create a new boundary in the deposition zone, due to the material difference between particle and the bottom, the settling condition for particle is changed. Therefore, in numerical simulation if the accumulation effect of particle is taken into consideration, the prediction of sediment transport may be more accurate. The idea to simulate the accumulation process is to couple the accumulation model in Fluent codes and change the settling condition by UDF after the primary bottom is covered by the particle.

References

Ackers, P., and White, W.R. 1973. Sediment Transport: New Approach and Analysis, Journal of the Hydraulics Division, ASCE, No. HY11.

Adamsson Å, Stovin V.R, and Bergdahl L. (2003). Bed shear stress boundary condition for storage tank sedimentation. Journal of Environmental Engineering, 129(7), 651-657.

Adamsson Å, Bergdahl L., and Lyngfelt S. (2005). Measurement and three dimensional simulation of flow in a rectangular detention tank. Urban Water Journal, 2(4), 277-287.

Ahmed, F. H., Kamel, A., & Abdel Jawad, S. (1996). Experimental determination of the optimal location and contraction of sedimentation tank baffles. Water, Air, & Soil Pollution, 92(3), 251-271.

Akan, A. O. (2009). Design aid for water quality detention basins. Journal of Hydrologic Engineering, 15(1), 39-48.

Asgharzadeh, H., Firoozabadi, B., & Afshin, H. (2011). Experimental investigation of effects of baffle configurations on the performance of a secondary sedimentation tank. Scientia Iranica, 18(4), 938-949.

Bertrand-Krajewski, J.-L. (1993) Pollution des rejets urbains par temps de pluie. Synthèse général. Rapport CIRSEE Lyonnaise des Eaux, Le Pecq, Novermber, 136 pp.

Bogardi J.L. (1968). Incipient sediment motion in terms of the critical mean velocity. Acta Tech. Acad. Sci. Hung, 62(1-2), 1-24.

Bonneville, R. (1963). Essais de synthese des lois de debut d'entrainment des sediment sous l'action d'un courant en regime uniform. Bull. Du CREC, 5.

Boussinesq, J. (1877), Essai sur la théorie des eaux courantes, Mémoires présentés par divers savants à l'Académie des Sciences 23 (1): 1-680

Brahms A.(1753). Anfangsgründe der deich-und[J]. Wasserbaukunst, Aurich (Source: Raju, KMAH, 2011).

Brownlie WR (1981). Prediction of flow depth and sediment discharge in open channels. Report No. KH-R-43A, W. M. Keck Laboratory of Hydraulics and Water Resources, California Institute of Technology, Pasadena, California, USA.

Cailleux A. (1946). Application de la pétrographie sédimentaire aux recherches préhistoriques[J]. Bulletin de la Société préhistorique de France, 43(5/6): 182-191.

Chanson, H. (2004). Hydraulics of open channel flow. Butterworth-Heinemann, 2nd Edition.

Chou, P. (1945), On velocity correlations and the solutions of the equations of turbulent fluctuation. , Quarterly of Applied Mathematics, Vol. 3(1), pp. 38-54.

Crabtree, R. W., Ashley, R. M., & Saul, A. J. (1991). Review of research into sediments in sewers and ancillary structures. FWR Report no. FR205, Foundation for Water Research, UK.

Delft Hydraulics Laboratory (1982), Initiation of Motion and Suspension, Development of Concentration Profiles in a Steady, Uniform Flow without Initial Sediment Load, Report M1531-III, Delft, The Netherlands.

Dufresne, M., Terfous, A., Ghenaim, A., Poulet, J. B., & Vazquez, J. (2008). Prévoir l'efficacité des bassins d'orage par modélisation 3D: du bassin expérimental à l'ouvrage réel. La Houille Blanche, (5), 92-98.

Dufresne M. (2008). La modélisation 3D du transport solide dans les bassins en assainissement: du pilote expérimental à l'ouvrage réel. Thèse de doctorat, Université Louis Pasteur, Strasbourg, France.

Dufresne M., Vazquez J., and Terfous A. (2009). Experimental investigation and CFD modeling of flow, sedimentation, and solids separation in a combined sewer detention tank. Computers and Fluids, 38, 1042-1049.

Dufresne M., Vazquez J., Terfous A., Ghenaim A., and Poulet J.-B. (2009). CFD modelling of solid separation in three combined sewer overflow chamber. Journal of Environmental Engineering, 135(9), 776-787

Fluent (2002). Fluent user's guide. Fluent Inc.

Goldstein S. (1929) The steady flow of viscous fluid past a fixed spherical obstacle at small Reynolds numbers[C]//Proceedings of the Royal Society of London A:

Mathematical, Physical and Engineering Sciences. The Royal Society, 123(791): 225-235.

Grass A.J. (1982). The influence of boundary layer turbulence on the mechanics of sediment transport. Proc. Euromech 156: Mech. of Sediment Transport, Tech. Univ. of Istanbul, Istanbul.

Einstein, H.A., and Chien, N. (1955). Effects of Heavy Sediment Concentration near the Bed on Velocity and Sediment Distribution, M.R.D. sediment series No. 8, University of California, Institute of Engineering Research and United States Army Engineering Division, Missouri River, Corps of Engineers, Omaha, Neb.

Engelund, F., & Hansen, E. (1967). A monograph on sediment transport in alluvial streams. TEKNISKFORLAG Skelbrekgade 4 Copenhagen V, Denmark..

Haider, A., & Levenspiel, O. (1989). Drag coefficient and terminal velocity of spherical and nonspherical particles. Powder technology, 58(1), 63-70.

Harsha, P. T., & Lee, S. C. (1970). Correlation between turbulent shear stress and turbulent kinetic energy. AIAA Journal, 8(8), 1508-1510.

Henze, M., Harremoes, P., la Cour Jansen, J., & Arvin, E. (1995). Wastewater treatment: biological and chemical processes. Springer Science & Business Media, Berlin, Germany (ISBN 3-540-58816-7).

Hirsch, C. (2007). Numerical computation of internal and external flows: The fundamentals of computational fluid dynamics. Butterworth-Heinemann.

Hjulström F. (1935). Studies of the morphological activity of rivers as illustrated by the River Fyris: Inaugural Dissertation[M]. Almqvist & Wiksells.

Horan N J. (1990).Biological wastewater treatment systems: theory and operation[M]. John Wiley & Sons Ltd, New York, USA.

Horn, E. M., & Wiesmann, U. (1988). Theoretical and experimental study of sedimentation in vertical flow tanks. Chemical engineering & technology, 11(1), 95-104.

Isenmann, G. (2016). Approche Euler–Lagrange Pour la Modelisation du Transport Solide dans les Ouvrages de Decantation (Doctoral dissertation, PhD Thesis , Université de Strasbourg).

Jamshidnia, H., & Firoozabadi, B. (2010). Experimental Investigation of Baffle Effect on the Flow in a Rectangular Primary Sedimentation Tank. Scientia Iranica. Transaction B, Mechanical Engineering, 17(4), 241.

Julien P.Y. (2010). Erosion and sedimentation. 2nd, Cambridge University Press, the Edinburgh Building, Cambridge CB2 8RU, UK.

Kantoush, S. A., De Cesare, G., Boillat, J. L., & Schleiss, A. J. (2008). Flow field investigation in a rectangular shallow reservoir using UVP, LSPIV and numerical modelling. Flow measurement and Instrumentation, 19(3), 139-144.

Karthik, T. S. D., & Durst, F. (2011). Turbulence models and their applications. Indian Institute of Technology. MADRAS.

Kouyi, G. L., Vazquez, J., & Poulet, J. B. (2003). 3D free surface measurement and numerical modelling of flows in storm overflows. Flow measurement and instrumentation, 14(3), 79-87.

Krumbein W.C., Pettijohn F J. (1938).Manual of sedimentary petrography[J]. Appleton-Century-Croffs, Inc., N.Y., pp. 228-268.

Launder, B. E., & Spalding, D. B. (1972). Lectures in mathematical models of turbulence .Academic Press, London, England.

Launder, B. E., & Spalding, D. B. (1974). The numerical computation of turbulent flows. Computer methods in applied mechanics and engineering, 3(2), 269-289.

Launder, B. E., Reece, G. J. and Rodi, W. (1975), "Progress in the Development of a Reynolds-Stress Turbulent Closure.", Journal of Fluid Mechanics, Vol. 68(3), pp. 537-566.

Leliavsky S.(1955). Introduction to fluvial hydraulics[J].

Ma Department of Environmental Protection (MDEP) and MCZM (1997). Stormwater Management: stormwater policy handbook. Volume I, Massachusetts, U.S.

Marcoon, K. B., & Guo, Q. (2004). Detention basin retrofit: optimization of water quality improvement and flood control. In Critical Transitions in Water and Environmental Resources Management (pp. 1-10).

Maurel, A., Ern, P., Zielinska, B. J. A., & Wesfreid, J. E. (1996). Experimental study of self-sustained oscillations in a confined jet. Physical Review E, 54(4), 3643-3651

McNown J S, Malaika J, Pramanik R. (1951).Particle shape and settling velocity[C]//Proc Int Hydr Res, 4th Meeting, Bombay. 511-522.

Metcalf E, Eddy H P. (1991). Wastewater Engineering: Treatment, Disposal, and Reuse. 3rd edition, McGraw-Hill, New York, USA.

Miller, M. C., McCave, I. N., & Komar, P. (1977). Threshold of sediment motion under unidirectional currents. Sedimentology, 24(4), 507-527.

Morsi, S., & Alexander, A. J. (1972). An investigation of particle trajectories in two-phase flow systems. Journal of Fluid mechanics, 55(02), 193-208.

Nascimento N.O., Ellis J.B., Baptista M.B. and Deutsch J.-C. (1999). Using detention basins: operational experience and lessons. Urban water, 1, 113-124.

Nix, S. J. (1985). Residence time in stormwater detention basins. Journal of Environmental Engineering, 111(1), 95-100.

Nix, S. J., & Heaney, J. P. (1988). Optimization of storm water storage - release strategies. Water Resources Research, 24(11), 1831-1838.

Novak P, Nalluri C, Sirin S. (1972). A study into the correlation of sediment motion. in pipe and open channel flow[C]//Proc. 2nd. Intern. Conf. on the Hydraulic Transport of Solids in Pipes, Hydrotransport. 1972, 2: D4.

Novak P, Nalluri C. (1975). Sediment transport in smooth fixed bed channels[J]. Journal of the Hydraulics Division, 101(9), 1139-1154 (ASCE# 11556 Proceeding).

Novak P, Nalluri C. (1984). Incipient motion of sediment particles over fixed beds[J]. Journal of Hydraulic Research, 1984, 22(3): 181-197.

Olson, R., (1961). Essential of Engeneering fluid Mechanics, chap. 11, International Textbook, Scranton.Pa.

Oseen C. W. (1927) Neuere Methoden und Ergebnisse in der Hydrodynamik[J]. Leipzig: Akademie Ver-lagsgesellschaft.

Paintal, A. S. (1971). A stochastic model of bed load transport. Journal of Hydraulic Research, 9(4), 527-554.

Papanicolaou A.T.N., Elhakeem M, Krallis G, et al. (2008). Sediment transport modeling review—current and future developments[J]. Journal of Hydraulic Engineering, 134(1): 1-14.

Peltier, Y., Erpicum, S., Archambeau, P., Pirotton, M., & Dewals, B. (2014). Experimental investigation of meandering jets in shallow reservoirs. Environmental Fluid Mechanics, 14(3), 699-710.

Persson, J. (2000). The hydraulic performance of ponds of various layouts. Urban Water, 2(3), 243-250.

Pitt, R. (2004). Sediment transport in storm Drainage Systems.

Pletcher, R. H., Tannehill, J. C., & Anderson, D. (2012). Computational fluid mechanics and heat transfer. CRC Press.

Pope, N. D., Widdows, J., & Brinsley, M. D. (2006). Estimation of bed shear stress using the turbulent kinetic energy approach—a comparison of annular flume and field data. Continental Shelf Research, 26(8), 959-970.

Rostami, F., Shahrokhi, M., Said, M. A. M., & Abdullah, R. (2011). Numerical modeling on inlet aperture effects on flow pattern in primary settling tanks. Applied Mathematical Modelling, 35(6), 3012-3020.

Rotta, J. (1951), Statistische theorie nichthomogener turbulenz, Zeitschrift für Physik A, Vol. 129(6), pp. 547-572.

Saul, A. J., & Ellis, D. R. (1992). Sediment deposition in storage tanks. Water Science and Technology, 25(8), 189-198.

Schiano, P., Satofuka, N., Ecer, A., & Periaux, J. (Eds.). (1996). Parallel Computational Fluid Dynamics' 96: Algorithms and Results Using Advanced Computers. Elsevier.

Schlichting, H. (1979). Boundary-layer Theory, 7th edn, McGraw-Hill, New York.

Schiller L, Naumann A. (1933). Fundamental calculations in gravitational processing[J]. Zeitschrift Des Vereines Deutscher Ingenieure, 77: 318-320.

Schmitt, F.G. (2007), About Boussinesq’s turbulent viscosity hypothesis: historical remarks and a direct evaluation of its validity, Comptes Rendus Mécanique 335 ((9-10)): 617-627

Shahrokhi, M., Rostami, F., Said, M. A. M., & Yazdi, S. R. S. (2012). The effect of number of baffles on the improvement efficiency of primary sedimentation tanks. Applied Mathematical Modelling, 36(8), 3725-3735.

Shahrokhi, M., Rostami, F., & Said, M. A. M. (2013). Numerical modeling of baffle location effects on the flow pattern of primary sedimentation tanks. Applied Mathematical Modelling, 37(6), 4486-4496.

Shen, H.W. and Hung, C.S., 1971. ”An Engineering Approach to Total Bed Material Load by Regression Analysis”, Proc. Sedimentation Symposium, Berkeley.

Shields A. (1936). Application of similarity principles and turbulence research to bed-load movement[R]. Soil Conservation Service.

Simões, F. J. (2014). Shear velocity criterion for incipient motion of sediment. Water Science and Engineering, 7(2), 183-193.

Ashley, R. M., Bertrand-Krajewski, J. L., Hvitved-Jacobsen, T., & Verbanck, M. (Eds.). (2004). Solids in sewers. IWA Publishing.

Soulsby RL (1997). Dynamics of Marine Sands: a manual for practical applications. Thomas Telford, London, England.

Stamou, A. I. (2008). Improving the hydraulic efficiency of water process tanks using CFD models. Chemical Engineering and Processing: Process Intensification, 47(8), 1179-1189.

Stovin, V. R., & Saul, A. J. (1996). Efficiency prediction for storage chambers using computational fluid dynamics. Water Science and Technology, 33(9), 163-170.

Stovin, V. R., & Saul, A. J. (1998). A computational fluid dynamics (CFD) particle tracking approach to efficiency prediction. Water Science and Technology, 37(1), 285-293.

Stovin, V. R., & Saul, A. J. (2000). Computational fluid dynamics and the design of sewage storage chambers. Water and Environment Journal, 14(2), 103-110.

Sumer B.M., and OguzB. (1978). Particle motions near the bottom in turbulent flow in an open channel. Journal of Fluid Mechanics, 86(01), 109-127.

Sumer B.M., and Deigaard R. (1981). Particle motions near the bottom in turbulent flow in an open channel, part 2. Journal of Fluid Mechanics, 109, 311-337.

Sumer, B. M. (1991). Design Of Settling Basins. Journal of Hydraulic Research, 29(1), 136-143.

Takamatsu, M., Barrett, M., & Charbeneau, R. J. (2009). Hydraulic model for sedimentation in storm-water detention basins. Journal of Environmental Engineering, 136(5), 527-534.

Tao, H. F., Qiu, X. Y., & Hao, Y. Z. (2012). The experimental Study of a new sedimentation tank. In Applied Mechanics and Materials (Vol. 178, pp. 582-585). Trans Tech Publications.

Tarpagkou, R., & Pantokratoras, A. (2013). CFD methodology for sedimentation tanks: The effect of secondary phase on fluid phase using DPM coupled calculations. Applied Mathematical Modelling, 37(5), 3478-3494.

Temam, R. (Ed.). (2006). Turbulence and Navier Stokes equations: proceedings of the conference held at the University of Paris-Sud, Orsay, June 12-13, 1975 (Vol. 565). Springer.

Vanoni,V.A.,1946. Transportation of Suspended Sediment by Water, Trans. A.S.C.E., Vol.III.

Vanoni, V.A., 1984. Fifty Years of Sedimentation. Journal of Hydraulic Engineering, Vol.110, No. 8 ASCE.

Van Rijn L (1984). Sediment transport, Part I: bed load transport. Journal of Hydraulic Engineering, ASCE, 110(10), p.1431-1455.

Van Rijn, L. C. (1984). Sediment Transport, Part II: Suspend load Transport. Hydr. Engrg., ASCE, 110(11), 1613-1641.

Verbanck, M. (1989) L'épuration des eaux à Bruxelles : caratérisation des charges polluantes. Actes du Forum 'Quelles solutions pour les eaux usées à Bruxelles ?', Forum A.Ir.Br.-V.Ir.Br., Bruxelles, Belgique, 31 May, 15-26 .

Verstraeten, G., & Poesen, J. (2000). Estimating trap efficiency of small reservoirs and ponds: methods and implications for the assessment of sediment yield. Progress in Physical Geography, 24(2), 219-251.

Verstraeten, G., & Poesen, J. (2001). Modelling the long‐term sediment trap efficiency of small ponds. Hydrological Processes, 15(14), 2797-2819.

Versteeg, H. K., & Malalasekera, W. (1995). An introduction to computational fluid dynamics: the finite volume method. Pearson Education.

Vries DE. Application of physical and mathematical models for river problems[J]. IN: GENERAL REPORTS, DISCUSSIONS, LECTURES, VOL. IV, 1973.

Wadell H. Sphericity and roundness of rock particles[J]. (1993).The Journal of Geology, 41(3): 310-331.

Yalin,M.S., (1963).”An Expression for Bed Load Transportation”, ASCE 89, HY3.

Yalin,M.S., (1972). ”Mechanics of Sediment Transport”,Pergamon Press.

Yan H., Lipeme Kouyi G., and Bertrand-Krajewski J.-L. (2011). 3D modeling of flow, solid transport and settling processes in a large stormwater detention basin. Proceedings of 12th International Conference on Urban Drainage, 11th-16th September, Porto Alegre, Brazil, 8 p.

Yan H., Lipeme Kouyi G., Bertrand-Krajewski J.-L. (2011). Modélisation numérique 3D des écoulements turbulents a surface libre charges en polluants particulaires dans un bassin de retenue - décantation des eaux pluviales. La Houille Blanche, 2011(5), 40-44.

Yan, H. (2013). Experiments and 3D modelling of hydrodynamics, sediment transport, settling and resuspension under unsteady conditions in an urban stormwater detention basin(Doctoral dissertation, PhD Thesis, INSA de Lyon).

Yang,C.T., (1972). Unit Stream Power and Sediment Transport, Proc.ASCE,98, HY10, 1805-26.

Yang,C.T.,(1973). Incipient Motion and Sediment Transport, Proc. ASCE99, HY10, 1679-1704.

Yang,C.T, (1996). Sediment Transport: Theory and Practice, MC Graw- Hill, New york.

Widera, P. (2011). Study of sediment transport processes using Reynolds Averaged Navier-Stokes and Large Eddy Simulation (Doctoral dissertation, PhD Thesis, Faculty of Engineering, Vrije Universiteit Brussel, S. 205).

Wong, T. H., Fletcher, T. D., Duncan, H. P., & Jenkins, G. A. (2006). Modelling urban stormwater treatment—a unified approach. Ecological Engineering, 27(1), 58-70.

Wu F.-C. and Chou Y.-J. (2003).Rolling and lifting probabilities for sediment entrainment. Journal of Hydraulic Engineering, 129(2), 110-119.

ZHANG, J. X., & Hua, L. I. U. (2007). A vertical 2-D numerical simulation of suspended sediment transport. Journal of Hydrodynamics, Ser. B, 19(2), 217-224.

Zhang, W., Zou, Z., & Sui, J. (2010). Numerical simulation of a horizontal sedimentation tank considering sludge recirculation. Journal of Environmental Sciences, 22(10), 1534-1538.

Zhang, Z., & Chen, Q. (2007). Comparison of the Eulerian and Lagrangian methods for predicting particle transport in enclosed spaces. Atmospheric Environment, 41(25), 5236-5248.

Yi LIU

Modélisation 3D des écoulements et du transport solide dans un bassin à cavités

Résumé : la recherche sur le transport de sédiments dans les réservoirs vise principalement à optimiser la conception du réservoir dans les réseaux d'assainissement. La structure de l'écoulement, qui fait l'objet de cette recherche, représente le facteur principal de contrôle du mouvement des particules et conditionne leur dépôt. Le travail réalisé s'est basé aussi bien sur les méthodes numériques que les essais expérimentaux. La simulation numérique est traitée en utilisant trois géométries différentes, où un volume de modèle de fluide est appliqué pour le suivi de la surface libre et un modèle de phase discrète est utilisé pour calculer la trajectoire des particules, et une fonction définie par l'utilisateur basée sur la courbe de Shields est implémentée comme condition limite pour augmenter les taux de déposition simulés. Des séries d'expériences sont réalisées dans un réservoir rectangulaire avec une cavité, pour mesurer le champ de vitesses dans différentes conditions d'écoulement, et déterminer les zones de dépôts des sédiments au fond du réservoir. La comparaison entre les simulations numériques et les résultats expérimentaux montre une bonne concordance des résultats obtenus pour la prédiction des écoulements et des dépôts. L'amélioration du dépôt de particules nécessite une modification supplémentaire du modèle de suivi des particules.

Mots clés : Simulation numérique, expérience, transport de sédiments, flux, réservoir, structure, trajectoire des particules

Abstract: The investigation on sediment transport in tanks is mainly for optimizing the design of tank in stormwater system and sewers. The flow pattern is the primary factor controlling the movement of particle. Therefore, the emphasis of this investigation is to determine the flow pattern and estimate the deposition of particle. Both computational fluid dynamics and experimental methods are applied to accomplish the research. Numerical simulation are processed by using three different geometries, where a volume of fluid model is applied for tracking the free-surface and a discrete phase model is used for calculation of particle trajectory, and an user defined function based on Shields curve is implemented to the boundary for improving the simulation on sedimentation. A series of experiments are carried out in a rectangular tank with a cavity, where velocity measurements are finished for experiments under different conditions and the sediment deposition is recorded. The comparison between numerical simulation and experimental results show better agreement in the prediction of flow, the improvement on particle deposition needs further modification in the particle tracking model.

Keywords: numerical simulation, experiment, sediment transport, flow, tank, eddy structure, particle trajectory.